WAVE TRANSFORMATION OVER A SUBMERGED SHOAL

BY

ARUN CHAWLA AND JAMES T. KIRBY

RESEARCH REPORT NO. CACR-96-03

APRIL, 1996

This study was supported by the Delaware Sea Grant Program
Project Numbers R/OE-9 and R/OE-13

CENTER FOR APPLIED COASTAL RESEARCH

Ocean Engineering Laboratory
University of Delaware
Newark, Delaware 19716

TABLE OF CONTENTS

Appendix

LIST OF FIGURES

LIST OF TABLES

ABSTRACT

This report describes a study of wave transformation over a shoal. Numerical modeling has been backed by experimental measurements done in a 2-dimensional wave basin. Two different sets of experiments have been studied here, one which considers monochromatic wave transformation over the shoal with no breaking, and the other which considers irregular waves with directional spreading, breaking on top of the shoal. Experimental data for breaking monochromatic waves have also been gathered, but not studied here.

Numerical modeling has been done for all the experimental test cases with the help of two parabolic refraction-diffraction models that were developed here at the University of Delaware. The accuracy of the models has been tested against the data obtained in the basin, and statistical parameters have also been used for comparisons.

A detailed explanation of how the experiments were conducted is given, and attempts have been made to quantify the physical processes taking place in the basin, particularly in the case of the irregular spectrum tests. The comparisons were good, and the models were found to be quite robust. The results were not so good in the regions where the wave field was highly nonlinear, due to the wave-wave interactions in the data which could not be predicted by the weakly nonlinear models. The results for the irregular breaking wave tests were generally better than those of the monochromatic wave tests.

An exhaustive appendix has been provided which gives the experimental and model results in the forms of tables and plots. The various programs used during this study have also been described in the appendix.

Chapter 1

INTRODUCTION

The aim of this study is to do an experimental analysis of wave transformation over a three dimensional submerged shoal. Such shoals are found in plenty in the ocean particularly close to the coast, and greatly change the form and direction of waves propagating over them.

Wave transformation over irregular bathymetry involves three phenomena; shoaling, refraction and diffraction. All three of them change the wave as it progresses, causing the wave to break in many cases. Wave shoaling leads to increasing wave heights in shallow water (as seen near the beach), and the shoaling coefficient can be obtained quite accurately from conservation of energy flux. Wave refraction leads to changes in the direction of the wave crest, and thus causes changes in wave height distributions (wave heights increase wherever wave crests converge, and decrease wherever they diverge). Wave crests change direction as they move over irregular bathymetry because of changes in the celerity of the wave. A similar phenomenon is observed in optics when light changes direction as it moves through materials with varying density. Diffraction is the phenomenon by which energy spreads laterally, perpendicular to the dominant direction of wave transformation. A particular example of this phenomenon in the sea is seen when waves are traveling perpendicular to a long breakwater with a gap in between. Due to diffraction, wave energy leaks from the gap onto the sheltered waters of the breakwater. Usually, refraction and diffraction occur together in nature, and ignoring either one of them would lead to inaccurate estimates. For example, using classical refraction methods, or ray tracing methods as they are better known (see Section 1.1), would indicate wave convergence with high amounts of wave energy, while in the real ocean energy would leak out to its neighboring regions.

Although a combined refraction diffraction analysis would provide very good estimates of the wave field in the entire domain, such an analysis is by no means trivial, and very little progress was made till the mild slope equation was developed by Berkhoff (1972). The equation was obtained by using a mild slope approximation and vertically integrating the Laplace equation. It is a relatively fast model (compared to the Laplace equation model) and estimates wave heights with reasonable amount of accuracy. Since then a lot of effort has been made to clearly understand all the aspects of the combined refraction diffraction phenomenon, and quite a few models have been developed. A brief overview of these models is given in the following section.

1.1 Literature Review

Over the years many different models have been proposed to determine wave transformation due to refraction and diffraction. Linear ray theory is one of the earliest known methods of tracing the refracting waves as they move over varying depths (Dean and Dalrymple, 1991). Ray theory assumes that wave energy propagates along a ray, and energy flux is conserved between two adjacent rays. The diffraction phenomenon is totally ignored in this method, and the theory breaks down when wave ray crossings occur and along caustics. Although numerical techniques have been proposed to obtain averaged wave amplitudes over ray bundles (Bouws and Battjes, 1982), the models still give inaccurate results wherever diffraction effects become significant.

1.1.1 Mild slope equations

The mild slope equation was first developed by Berkhoff (1972). By performing a weighted integration on the 3D equations of motion, Berkhoff obtained a 2D differential equation which describes the phenomenon of combined refraction and diffraction for simple harmonic waves. Commonly known as the mild slope equation it is given by

$$\nabla_h \cdot (CC_g \nabla_h \phi) + k^2 C_g C \phi = 0 \tag{1.1}$$

where $\phi(x, y)$ is the surface potential and is related to the surface displacement η by

$$\phi = \frac{-ig\eta}{\omega} \tag{1.2}$$

∇_h is the horizontal differential operator C is the wave celerity given by $C = \omega/k$ C_g is the group velocity given by

$$C_g = \frac{C}{2}\left(1 + \frac{2kh}{\sinh 2kh}\right) \tag{1.3}$$

k is the local wave number which is related to the local depth h, and the wave frequency ω, by the dispersion relationship

$$\omega^2 = gk \tanh kh \tag{1.4}$$

The equation is valid for irrotational linear harmonic waves, thus loss of energy due to friction or breaking is not taken into account. In constant depth the equation reduces to the Helmholtz equation, and in the shallow water limit it becomes the linearized shallow water equation. The primary assumption in this model is a slowly varying bathymetry, though good results have been obtained for relatively large local bottom slopes (Booij, 1983). The mild slope equation was further enhanced to include the effects of varying currents by Booij (1981) and Kirby (1984).

One of the primary disadvantages of the mild slope equation is that it is an elliptic type of differential equation and requires the boundary conditions to be prescribed at all the boundaries of the domain. This is not always possible and also requires a huge computational time and storage. However, in many water wave problems wave energy propagates without any considerable amount of backscattering. Making use of this, parabolic models have been developed which essentially approximate the elliptic type mild slope equation to a parabolic type equation. Parabolic equations are numerically easier to solve, because only the initial and lateral boundary conditions are required. The solution is obtained by a marching method, unlike the elliptic equation which needs a simultaneous solution all over the domain.

1.1.2 Parabolic wave equations

Parabolic approximations of elliptic equations were first used by Leontovich and Fock (1965), who applied the method to radio wave propagation in the atmosphere. Radder (1979), was the first person to use parabolic approximations in water waves. He used a splitting matrix technique on the mild slope equation to divide the wave field into a transmitted and reflected field.

$$\phi = \Phi^+ + \Phi^-$$

On neglecting the reflected field (Φ^-), he obtained a parabolic equation for the transmitted field, Φ^+ given by

$$\frac{\partial \Phi^+}{\partial x} = [ik - \frac{1}{2kCC_g}\frac{\partial kCC_g}{\partial x} + \frac{i}{2kCC_g}\frac{\partial}{\partial y}CC_g\frac{\partial}{\partial y}]\Phi^+ \tag{1.5}$$

This equation represents the standard parabolic equation for water waves. It was later enhanced to include waves at angles of up to 45° (Booij 1983). The parabolic equations are approximate equations limited by the fact that they require a preferred direction of motion, and cannot handle wave reflections. Thus they cannot be used in cases where wave reflection is expected to be significant (e.g. waves on a breakwater).

Berkhoff *et al.* (1982) compared three numerical models with experimental data. Their setup consisted of an elliptical shoal on a sloping bottom. The waves were fairly linear (low Ursell number(U_r) on top of the shoal), and the numerical models compared were

1. a refraction model involving averaging over bundles of adjacent rays (Bouws and Battjes, 1982),

2. a linear parabolic model (Radder, 1979), and

3. an elliptic mild slope equation model (Berkhoff, 1972).

The difference between the three models is restricted to the consideration of diffraction. While the mild slope model considers diffraction along both the direction of propagation and the transverse direction, the parabolic model considers diffraction only along the transverse direction, and the refraction model does not consider diffraction at all.

Though a few discrepancies existed, the mild slope model was found to give the best results, while the refraction model performed the worst. The disadvantage of the mild slope model, though, is the intense amount of computations involved, while the parabolic model, while computationaly less intensive, is not as accurate. Thus, there is a trade off between numerical computation and accuracy when making the choice of what model to use. A lot of literature is available on both these types of models, and in this study we concentrate on the faster parabolic models.

In order to develop a more accurate parabolic model, Kirby and Dalrymple (1983) developed a weakly nonlinear parabolic model governing the amplitude of a modulated Stokes wave, using a multiple scale perturbation expansion. The governing equation is given by

$$\begin{aligned} 2ikCC_gA_x + 2k(k-k_o)(CC_g)A + i(kCC_g)_xA + (CC_gA_y)_y \\ -k(CC_g)K'|A|^2A = 0 \end{aligned} \tag{1.6}$$

where A is the Stokes wave amplitude, k_o is a reference wavenumber given by the initial condition of the wave field, and K' is a local constant given by

$$K' = k^3 \frac{C}{C_g} \frac{\cosh 4kh + 8 - 2\tanh kh^2}{8 \sinh kh^4} \tag{1.7}$$

The Stokes wave amplitude A is related to the potential Φ^+ by

$$\Phi^+ = -\frac{ig}{2\omega_0} A(x, y) \exp\left[i(k_0 x - \omega_0 t)\right] \tag{1.8}$$

Simplifying for a constant depth case yields the nonlinear Schrödinger equation for diffraction given by Yue and Mei (1980). Experimental verification of eqn. (1.7) was done by Kirby and Dalrymple (1984) using the data from Berkhoff *et al.* (1982). The comparisons were very good, and it was shown that the discrepancy between the linear models and data was not due to inaccuracies in modeling techniques but due to nonlinear effects which were taken into account in their model.

1.1.3 Spectral models

Although relatively accurate models have been developed to study the evolution of waves over an irregular bottom, all these models have been derived for monochromatic waves only and cannot handle an irregular spectrum directly. This is a point of major concern since the wave field in the ocean is very rarely monochromatic. Coastal engineers all over the world have addressed this problem by approximating an irregular wave field using a monochromatic wave. This has been shown to be highly erroneous by Vincent and Briggs (1989). Their experiments quantified the differences in refraction diffraction patterns of monochromatic and irregular waves having similar statistics, and found vast dissimilarities in the wave fields. Panchang *et al.* (1990) determined the evolution characteristics of an irregular sea spectrum indirectly with the help of a monochromatic wave model. They used a spectral calculation method which consisted of decomposing a spectrum into monochromatic components, determining the wave transformation of each component, and then assembling the wave components by linear superposition. The numerical results were reasonably accurate compared to the data of Vincent and Briggs (1989). Thus, monochromatic wave models can still be used to study the evolution of irregular spectra. The advantage of this method lies in its simplicity, which allows for reasonable estimates of the spectrum to be made without having to develop another complicated model. The main assumption in this kind of analysis is that linear decomposition and superposition of a spectrum is possible with reasonable accuracy. Thus the model will not be able to predict wave-wave interactions of the different wave components, and will give erroneous results wherever these effects are highly significant.

1.2 Present work

In the previous section a brief account of the development of different refraction-diffraction models was given. A detailed review of various wave propagation models can be found in Liu (1990). The emphasis over the past few years has been to obtain accurate parabolic and mild slope models (we limit ourselves to these two types of models), and of late to use these models to obtain spectral estimates of irregular seas (Goda 1985, Vincent and Briggs 1989, Panchang *et al.* 1990). In this study, the evolution patterns of waves from two large-angle parabolic models (a monochromatic wave model and a spectral wave model) will be studied and compared with experimental data. The spectral wave model was developed by Özkan and Kirby (1993), and determines the spectral characteristics using a monochromatic wave model, similar to what was done by Panchang *et al.* (1990). The basic governing equation for both the models is an enhanced version of eqn. (1.7), and a brief outline of these models is given in Chapter 2. The monochromatic wave model has been extensively studied before (Kirby and Dalrymple 1984, Kirby 1986a, Kirby 1986b), and has been analysed here for completeness. The emphasis here is more on the spectral model, which has not been rigorously tested yet. The spectral model of Panchang *et al.* (1990) was based on the linear parabolic model (Radder, 1979), while the present spectral model is based on the more accurate nonlinear, large-angle parabolic equation obtained by Kirby (1986b). The aim is to see how well a spectral calculation method estimates the wave field for a range of breaking wave conditions.

The study has been divided into two parts. The first part consisting of the experimentation is explained in detail in Chapter 3. The experiments include both monochromatic wave tests and irregular spectra with directional spreading. A vast data set consisting of breaking wave tests has been amassed which can be used for study with shallow water wave models (e.g. Boussinesq models). For a qualitative analysis of the wave field, a video camera has been used to film the waves on top of and behind the shoal. In the second part the experimental results have been used to test the limitations and accuracy of two numerical models, **Ref/Dif 1** (Kirby and Dalrymple, 1993), and **Ref/Dif S** (Kirby and Özkan, 1994) . The data analysis has been carried out in detail in Chapter 4, and the Appendices provide detailed information about the software used, the instrumentation, and the raw data files.

Chapter 2

THEORETICAL MODELS

2.1 Introduction

Two models have been analysed in this study, a monochromatic model known as **Ref/Dif 1** (Kirby 1986a, Kirby and Dalrymple 1993), and a spectral model known as **Ref/Dif S** (Özkan and Kirby 1993, Kirby and Özkan 1994). A brief account of the two models is given here, with emphasis on some of the changes that were made in the spectral model for this study.

Both the models are based on a parabolic Stokes wave model (eqn. (1.7)), which was further enhanced by Kirby (1986a) to include strong currents using a wide angle approximation. The governing equation is given by

$$
\begin{aligned}
&(C_{gn}+U)(A_n)_x - 2\Delta_1 V (A_n)_y + i(\bar{k}_n - a_0 k_n)(C_{gn}+U)A_n \\
&+\left\{\frac{\sigma_n}{2}\left(\frac{C_{gn}+U}{\sigma_n}\right)_x - \Delta_1\sigma_n\left(\frac{V}{\sigma_n}\right)_y\right\}A_n + i\Delta_n'\left[\left((CC_g)_n - V^2\right)\left(\frac{A_n}{\sigma_n}\right)_y\right]_y \\
&-i\Delta_1\left\{\left[UV\left(\frac{A_n}{\sigma_n}\right)_y\right]_x + \left[UV\left(\frac{A_n}{\sigma_n}\right)_x\right]_y\right\} + \alpha A_n \\
&+\frac{-b_1}{k_n}\left\{\left[\left((CC_g)_n - V^2\right)\left(\frac{A_n}{\sigma_n}\right)_y\right]_{yx} + 2i\left(\sigma_n V\left(\frac{A_n}{\sigma_n}\right)_y\right)_x\right\} \\
&+b_1\beta_n\left\{2i\omega_n U\left(\frac{A_n}{\sigma_n}\right)_x + 2i\sigma_n V\left(\frac{A_n}{\sigma_n}\right)_y - 2UV\left(\frac{A_n}{\sigma_n}\right)_{xy}\right. \\
&\left.+\left[\left((CC_g)_n - V^2\right)\left(\frac{A_n}{\sigma_n}\right)_y\right]_y\right\} - \frac{i}{k_n}b_1\left\{(\omega_n V)_y + 3(\omega_n U)_x\right\}\left(\frac{A_n}{\sigma_n}\right)_x \\
&-\Delta_2\left\{\omega_n U\left(\frac{A_n}{\sigma_n}\right)_x + \frac{1}{2}\omega_n U_x\left(\frac{A_n}{\sigma_n}\right)\right\} + ik\omega_n U(a_0-1)\left(\frac{A_n}{\sigma_n}\right) = 0 \qquad (2.1)
\end{aligned}
$$

where

$$\begin{aligned}
\beta_n &= \frac{(k_n)_x}{k_n^2} + \frac{\left(k_n\left((CC_g)_n - U^2\right)\right)_x}{2k_n^2\left((CC_g)_n - U^2\right)} \\
\Delta_1 &= a_1 - b_1 \\
\Delta_2 &= 1 + 2a_1 - 2b_1 \\
\Delta_n' &= a_1 - b_1\frac{\bar{k}_n}{k_n}
\end{aligned} \tag{2.2}$$

The coefficients a_0, a_1 and b_1 depend upon the specific minimax approximation (Kirby 1986b). The choices

$$\begin{aligned}
a_0 &= 1 \\
a_1 &= -0.75 \\
b_1 &= -0.25
\end{aligned} \tag{2.3}$$

recover the Padé approximant of Booij (1981), while

$$\begin{aligned}
a_0 &= 0.994733 \\
a_1 &= -0.890065 \\
b_1 &= -0.451641
\end{aligned} \tag{2.4}$$

gives a minimax approximation with a maximum angular range of $\pm 70°$ (Kirby, 1986b).

In the coming sections some of the characteristics of the models have been explained with their limitations. One of the biggest limitations of these two models is that they are based on a Stokes wave expansion theory, and are thus valid only in the regime where this theory does not break down. The validity of the Stokes solution can determined with the help of the Ursell number (U_r) defined by

$$U_r = \frac{|A|}{h(kh)^2}$$

Where U_r approaches or is greater than unity, the theory breaks down. This occurs in shallow water, and care needs to be taken to avoid this. In any case both the models issue a warning if the above condition is violated.

2.2 Ref/Dif 1

Ref/Dif 1 is an enhanced wave current interaction model developed by a Stokes wave perturbation expansion, for monochromatic waves. Since no approximations have been made on the size of the currents, the model can handle strong currents. The model also allows for dissipation due to boundary layers, porous bottom and wave breaking, and uses the Padé approximant coefficients given in eqn. (2.3). The solution is sought by using a finite difference Crank-Nicolson scheme, which computes the complex amplitudes for all grid points at a grid level, before marching on to the next grid level. A damping algorithm is also provided which reduces the high-wavenumber noise that can propagate into the computational domain (Kirby, 1986a).

A few points about the **Ref/Dif 1** model that should be kept in mind are

- The model has been derived assuming a mildly varying bathymetry, though Booij (1983) has shown that the mild slope approximation works even for slopes as steep as 1:3.

- The model is based on a Stokes perturbation expansion, and is valid only in the regions where the Stokes waves are valid. For shallow water, a heuristic dispersion relation (Hedges, 1976), given by

$$\sigma^2 = gk \tanh(kh(1 + \frac{|A|}{h})) \tag{2.5}$$

  is used with a model that patches it to a Stokes wave dispersion relation in deep water. Due to the different dispersion relationships available, **Ref/Dif 1** has three options; (a) a linear model, (b) a Stokes-to-Hedges nonlinear model (Kirby and Dalrymple, 1986b) and (c) a Stokes model.

- The wave direction is confined to a sector $\pm 45°$ to the assumed principle wave direction.

- The model is primarily for studying the evolution characteristics of monochromatic waves, but is not restricted to that only. A directional spectrum for a particular frequency can also be specified, though being at a single frequency it is not strictly the modeling of a directional spectrum. That is done with the help of **Ref/Dif S**.

The lateral boundary conditions can be either open (transmitting) or closed (reflecting), and for our cases a closed boundary condition (simulating the side walls of the wave basin) has been used. For further details on the theoretical model the reader is referred to Kirby (1986a), while the working of the model is explained in Kirby and Dalrymple (1993).

2.3 Ref/Dif S

Ref/Dif S is a spectral model, and simulates the evolution of random waves as they propagate forward. Based on the spectral distribution method, a two dimensional energy spectrum is discretized into bins, with the energy at each bin being represented by an individual wave component, having the frequency and angle of that particular bin. Thus, a discretized spectrum in the form of monochromatic wave components forms the input for **Ref/Dif S**. The model has a preprocessor **Specgen** which discretizes the energy spectrum into bins and prepares the input data files. Binning can be done in two ways by **Specgen**; An equal energy method, which divides the spectrum into bins of equal energy, and an equal width bin, which divides the spectrum into bins of equal widths. Of the two methods, the equal energy method is more preferred since it does not create a large number of wave components in regions of the spectrum where the energy density is small. Since they represent only part of the energy of the spectrum, the amplitudes of individual wave components are small compared to the significant wave height represented by the spectrum.

Ref/Dif S computes the parabolic models for each wave component just like the monochromatic model **Ref/Dif 1** and stores the results at each step in space. The governing equation for **Ref/Dif S** uses the same Padé approximant as **Ref/Dif 1** does. Though in actual computation of wave characteristics **Ref/Dif S** works quite similarly to **Ref/Dif 1**, a few differences are present:

- Instead of using the complex amplitude in Hedges dispersion relation (eqn. (2.5)), the significant wave height is used for the composite model.

- A statistical breaking model by Thornton and Guza (1983) is used for wave breaking.

- The output is in terms of the statistical quantities at each grid point instead of complex amplitudes.

Except for the few differences shown above, and some input characteristics, **Ref/Dif S** essentially works in the same fashion as **Ref/Dif 1**. Again, for further details about the input requirements and the working of the model, refer to Kirby and Özkan (1994).

2.3.1 Statistical Analysis

Ref/Dif S, as stated earlier, determines wave characteristics for each wave component. These are then statistically superposed to obtain the spectral characteristics at the grid points. The model was developed by Özkan and Kirby (1993) to predict significant wave height ($H_{1/3}$) in the domain. During this study, the model was further modified to obtain other statistical quantities like the frequency spectrum ($S(f)$), the directional spectrum ($S(f,\theta)$) and the average angle ($\bar{\theta}$).

Assuming a Raleigh distribution of the wave heights, the significant wave height is given by

$$H_{1/3} = 4\sqrt{m_0} \tag{2.6}$$

where m_0 is an estimate of the energy summed over all the wave components given by

$$m_0 = \sum_{i=1}^{n} \frac{|A_i|^2}{2},$$

and A_i is the complex wave amplitude of a single wave component.

The frequency spectrum is obtained by summing up the energy of all the wave components with the same frequencies having different directions. Energy is then obtained as a function of frequency, and the spectrum is obtained by scaling the energy with the corresponding bin widths for the frequencies (obtained during the binning of the input spectrum by **Specgen**). The frequency spectrum is thus given by

$$S(f) = \frac{\sum_{i=1}^{n_\theta} |A(f, \theta_i)|^2}{2\delta f} \tag{2.7}$$

where δf is the bin width for frequency f, and can be different for different frequencies, specially if an equal area method is used for binning the input spectrum, and n_θ is the number of directional components at frequency f. It is usually the same for all the frequencies.

Instead of determining the energy for each frequency and angle, estimates of the directional spectrum is done in a slightly different manner. The angular axis from $\theta = -92.5°$ to $\theta = 92.5°$, is divided into 37 bins with a bin width of 5°. For each frequency the wave components are sorted into the different bins based on their directions. The energy is then summed for each bin, and again scaled by the frequency bin width and the angle bin width to obtain the energy density. The representative angle of each angular bin is taken as the mean angle of that bin (e.g. angle for the bin $\theta = 42.5°$ to $\theta = 47.5°$ is given by $\theta = 45°$). The directional spectrum is given by

$$S(f, \theta) = \frac{\sum_{i=1}^{n_b} |A(f, \theta_i)|^2}{2\delta f \delta\theta} \tag{2.8}$$

where n_b is the number of wave components in each angular bin.

It should be kept in mind that the directional spectrum is estimated with a $\delta\theta = 5°$, and this defines the limit of accuracy of the predictions.

An average angle estimate at each grid point is also made to determine the mean angle of the spectrum, with the help of the radiation stress terms. Radiation stress for a monochromatic wave is defined here as the depth-integrated wave averaged stress due to the wave. The value of the radiation stress terms for each wave component moving at an angle θ to the $x-$axis can be determined easily for linear theory (Mei, 1992). The total radiation stress at any point in the field then is the sum total radiation stresses of all the wave components at that point, and is given by

$$\begin{aligned}
S_{xx} &= \frac{1}{2}\sum_{i=1}^{n}|A_i|^2\left[n_i\left(1-\cos^2\theta_i\right)-\frac{1}{2}\right] \\
S_{yy} &= \frac{1}{2}\sum_{i=1}^{n}|A_i|^2\left[n_i\left(1-\sin^2\theta_i\right)-\frac{1}{2}\right] \\
S_{xy} &= \frac{1}{4}\sum_{i=1}^{n}|A_i|^2 n_i\sin(2\theta_i) \qquad (2.9)
\end{aligned}$$

where S_{xx} is the radiation stress acting on the $x-$plane along the $x-$direction, S_{yy} is the radiation stress acting on the $y-$plane along the $y-$direction, S_{xy} is the radiation stress acting on the $y-$plane along the $x-$direction (due to the symmetry of the stress tensor $S_{yx} = S_{xy}$), and n_i is the ratio of the group velocity C_g to the phase velocity C. It is given in terms of wave number (k_i) and the water depth (h), by

$$n_i = \frac{1}{2}\left(1 + \frac{2k_ih}{\sinh(2k_ih)}\right)$$

It is important to note that the radiation stress terms defined in eqn. (2.9) and used in the model are scaled by a constant factor of ρg, where ρ is the density of water and g the acceleration due to gravity.

The average angle at any particular point in the field is defined as the angle that represents the total radiation stress at that point (eqn. (2.9)), for the peak frequency and significant wave height at the same point. Thus the angle is given by

$$\bar{\theta} = \frac{1}{2} \arcsin \left(\frac{32 S_{xy}}{(n_p H_{1/3}^2)} \right) \tag{2.10}$$

where S_{xy} is the radiation stress given by eqn. (2.9), $H_{1/3}$ is the significant wave height, $\bar{\theta}$ is the average angle, and n_p is the ratio of the group velocity to the phase velocity for the peak frequency.

2.3.2 Remarks

Apart from the modifications made to obtain extra statistical information from **Ref/Dif S**, a couple of other changes have also been made in the model. The model has been adapted to spatially average statistical quantities over subgrids in the $y-$direction. The angle at each grid point is given by

$$\theta_i = \arctan \left(\frac{A_i k_y}{A_i k_x + \bar{k}} \right) \tag{2.11}$$

The earlier version of the model computed angle values using a forward difference scheme in the $y-$direction in eqn. (2.11). For a completely symmetrical wave field with a symmetrical bathymetry the average angles computed from the model should be symmetrical, but that was not the case. The bias was removed when a central difference scheme was used along the $y-$direction in eqn. (2.11).

It has been emphasized before that though the study has been done to test both the monochromatic and the spectral models, the interest is more on how the spectral model will behave. **Ref/Dif S** is a relatively new model and has not yet been put through an extensive set of tests unlike its counterpart **Ref/Dif 1**, which is being used all over the world in coastal engineering applications.

Chapter 3

EXPERIMENTAL SETUP

3.1 Introduction

This chapter describes the conduct of the experiments and the problems encountered. A description of the wave basin and shoal characteristics is given and mention is made of the different sources of noise existing in the wave field. A mathematical model similar to the one obtained by Dalrymple (1989) is derived here to obtain a relation between paddle stroke time series of the wavemaker and the desired wave field in the basin. An explanation of the coordinate system used and a brief step by step procedure followed during data collection is also given here.

The experiments were divided into four sets. The first two sets consisted of monochromatic wave patterns transforming over the shoal. In the first set care was taken that none of the waves were breaking on top of the shoal, so that comparisons could be made with both linear and nonlinear wave models, while in the second set, data for breaking monochromatic waves over the shoal were obtained so as to be able to compare shallow water breaking wave models with experimental data. The third and fourth sets of experiments concentrated on the study of irregular multidirectional waves having a TMA spectral distribution (Bouws *et al.* , 1985) in frequency and a wrapped normal spectral distribution (Borgman, 1984) in direction (see Appendix A.1). Both narrow and broad directional distributions were studied, and the tests varied from none of the waves breaking on top of the shoal, to almost all waves breaking on top of the shoal. The second set of irregular spectral tests were conducted after an error was noticed in the final stages of the first spectral tests (see Appendix A.1).

Apart from measuring data at different points of the basin, a visual recording of all the tests, except for the fourth set of experiments (second set of irregular tests), was done. A video camera was placed behind the wavemaker on a raised platform, pointing down at the shoal. The crests were lit up with the help of a strong, single light source at the water level in front of the shoal, and the wave transformation on top of the shoal were recorded on a super VHS cassette.

3.2 Wave basin

The wave basin is approximately $18m$ long and $18.2m$ wide. It has a three-dimensional wavemaker at one end, which creates the desired wave field, and at the far end there is a stone beach to damp out the waves and minimize reflections. The bottom is flat except for the experimental shoal in the center. A schematic view of the experimental layout, together with gage transect locations (denoted by thick solid lines, see Section 3.4.1), is given in Figure 3.1.

3.2.1 Wavemaker

The three-dimensional wavemaker consists of 34 flap-type paddles, which are individually controlled with the help of servo control motors. A complex arrangement of pulleys and cables convert the rotary servo controller motion to a linear displacement. The paddles are $0.51m$ wide and $1.0m$ high, and are hinged near the bottom (roughly $11.6cm$ above the bottom). A slight clearance of approximately $2.5cm$ exists between the paddles to avoid any wear and tear due to friction between adjoining paddles. This geometrical shape of the paddles (except for the gap between the paddles) has been accounted for in the mathematical model for the stroke time series of the paddles (Section 3.2.2).

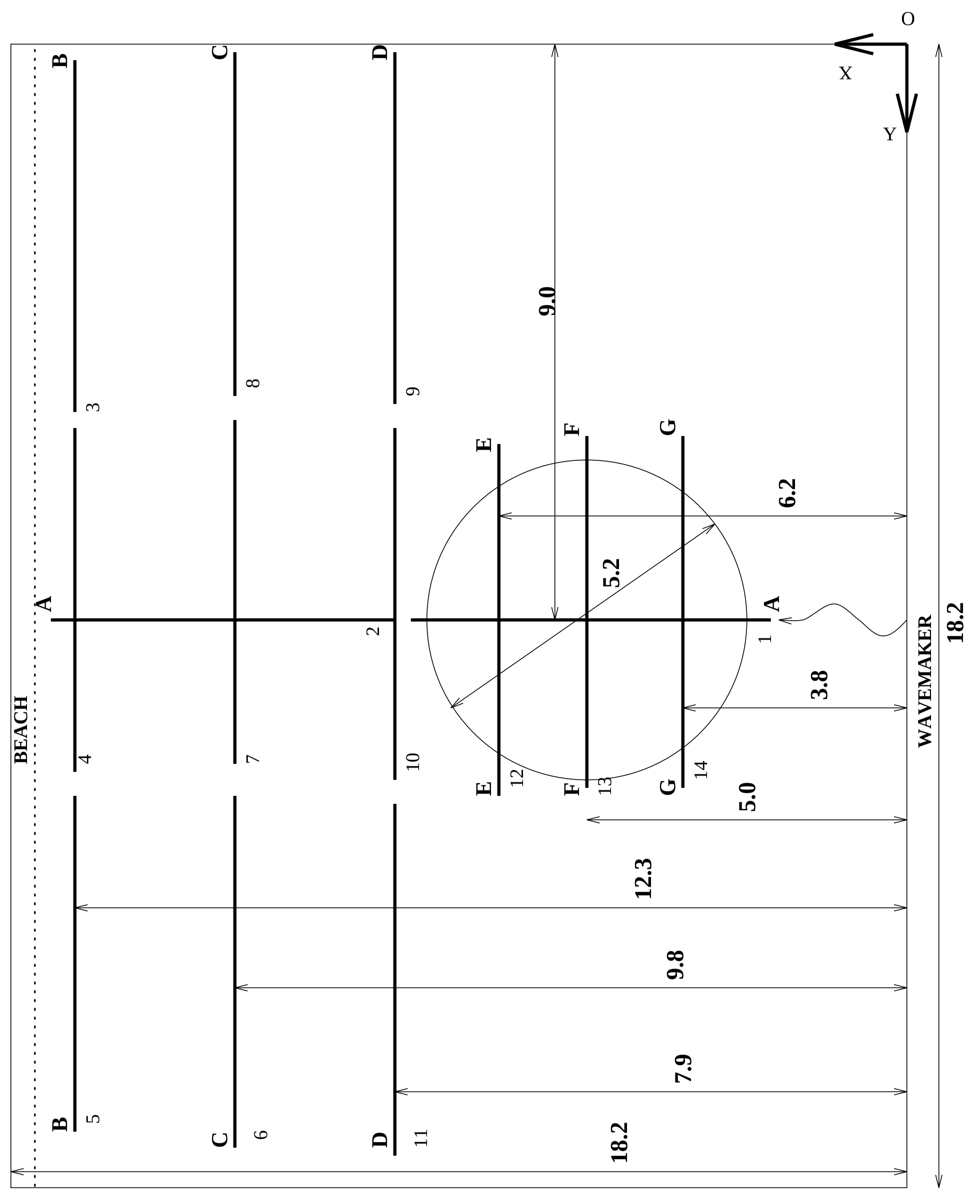

Figure 3.1: Schematic view of the gage transect locations and the experimental setup.

A gap of approximately $30cm$ exists between the back of the paddles and the wave basin wall. During paddle motion, standing waves are formed in this gap, which can have large amplitudes when resonance frequencies are reached. Due to the small clearances provided between the paddles, some of this energy leaks out, and corrupts the wave field being generated by the paddles. To avoid this, a swimming pool lane line was placed behind the paddles, which helped in damping out the standing waves. This problem was more prominent in monochromatic tests, as compared to the irregular tests, where, due to constantly changing stroke and frequency, strong standing wave patterns did not form behind the paddles.

Apart from the noise created by the standing waves behind the paddles, cross waves were also formed at the paddles. These cross wave patterns increased with stroke, and in some cases also broke at the paddles, creating noise in the wave field. Another source of concern was a $15cm$ gap that existed between the last paddle and the wall, adding to the noise in the wave field.

The mathematical model used here is based on the paddles being continuous without any gaps between them, which was not the case in reality. Thus, there was loss of energy through these gaps which the theory did not take into account. Though quite a few sources of error exist in the wave basin, the wave fields obtained during experiments were found to be quite accurate in form. Due to the loss of energy, the wave heights obtained were less than desired, but this problem was overcome by keeping a normalizing gage, which measured the wave field being created by the paddles. The measured wave field at that gage can be used as the input initial condition in numerical models for comparison purposes.

3.2.2 Designer wavemaker theory

One of the problems of studying oblique waves in a closed basin is that the region which is uncorrupted by reflected waves decreases with distance down the basin. Dalrymple (1989) used a splitting technique on the mild slope equation

(Berkhoff, 1972) for determining the stroke of the wave paddles. He makes use of the reflections from the side wall such that an uncorrupted uniform wave field exists across the width of the basin at a specified distance from the wavemaker. This increases the domain over which the desired wave field is obtained. A modified version of that technique has been used in these experiments, and the derivation has been given below for the case of a flat bottom basin such as the one in which the current experiments were conducted.

The assumed water wave motion is taken to be represented by a velocity potential which satisfies the mild slope equation (Berkhoff, 1972). The velocity potential can be given by

$$\Phi(x, y, z, t) = \phi(x, y) f(z) \exp(-i\omega t) \tag{3.1}$$

where

$$f(z) = \frac{\cosh k(h+z)}{\cosh kh} \tag{3.2}$$

is the depth attenuation factor.

The actual domain extends from $y = 0$ to $y = B$, which correspond to the side walls of the wave basin. With the help of a mirror image formulation, the domain is extended from $y = -B$ to $y = B$. The no flux condition at $y = 0$, is satisfied automatically by the method of images, while the no flux condition at $y = B$ gives

$$\frac{\partial \phi}{\partial y} = 0, y = \pm B \tag{3.3}$$

To satisfy the lateral boundary conditions, we seek

$$\phi(x, y) = \sum_n \hat{\phi}_n(x) a_n \cos \lambda_n y \tag{3.4}$$

where

$$\lambda_n = \frac{n\pi}{B} \tag{3.5}$$

The reduced wave potential $\hat{\phi}_n$ consists of waves propagating in the positive direction (ϕ_n^+) and waves propagating in the negative direction (ϕ_n^-). Thus splitting

$\hat{\phi}_n$ in eqn. (3.4), substituting in the mild slope equation given in Chapter 1 (eqn. (1.1)), and solving for ϕ by neglecting the waves in the negative direction, we get

$$\phi(x,y) = \sum_n \acute{a}_n \exp\left(i(\sqrt{k^2-\lambda_n^2})x\right)\cos(\lambda_n y) \tag{3.6}$$

or,

$$\Phi(x,y,t) = \sum_n \acute{a}_n \exp\left(i(\sqrt{k^2-\lambda_n^2})x\right)\cos(\lambda_n y) f(z)\exp\left(-i\omega t\right) \tag{3.7}$$

Seeking

$$\eta = \sum_n A_n \exp\left(i(\sqrt{k^2-\lambda_n^2})x\right)\cos(\lambda_n y)\exp\left(-i\omega t\right) \tag{3.8}$$

we obtain from the free surface boundary condition,

$$\Phi(x,y,t) = \sum_n \frac{-igA_n}{\omega} \exp\left(i(\sqrt{k^2-\lambda_n^2})x\right)\cos\lambda_n y f(z)\exp\left(-i\omega t\right) \tag{3.9}$$

If the desired wave field at a distance $x = x_m$, from the wavemaker, is a uniform plane wave across the width of the basin, at an angle θ, with an amplitude a, then

$$\eta = a\exp\left(i\lambda|y|\right)\exp\left(i\sqrt{(k^2-\lambda^2)(x-x_m)-\omega t-\epsilon}\right) \tag{3.10}$$

where

$$\lambda = k\sin\theta \tag{3.11}$$

Since we are looking for a uniform wave field at $x = x_m$, matching eqns. (3.8) and (3.10), at that point and using orthoganality condition gives

$$A_n = \frac{a}{B[1+\delta(n)]}\left(\int_{-B}^{B}\exp(i\lambda|y|)\cos(\lambda_n y)dy\right)\exp\left(-i[\epsilon+(\sqrt{k^2-\lambda_n^2})x_m]\right) \tag{3.12}$$

where $\delta(n)$ is a delta function given by

$$\delta(n) = \begin{cases} 1 & \text{if } n = 0 \\ 0 & \text{if } n \neq 0 \end{cases}$$

For the initial boundary condition, the wavemaker stroke motion is assumed to be a snake like motion along the $y-$direction, and the stroke is represented by

$$X = \sum S_n g(z) \cos(n\lambda y) \exp(-i\omega t) \tag{3.13}$$

where $g(z)$ is the vertical dependence of the paddle motion over the water depth, and for a flap-type wavemaker is given by

$$g(z) = \begin{cases} 1 + \frac{z}{h-d_b} & -(h-d_b) < z < 0 \\ 0 & -h < z < -(h-d_b) \end{cases}$$

d_b is the distance from the floor to the bottom of the paddle. Matching the horizontal velocities obtained from eqns. (3.13) and (3.9) at $x = 0$, and using the orthogonality condition, we obtain

$$S_n = \frac{ig}{\omega^2} \frac{\int_{-h}^{0} f^2(z)dz}{\int_{-h}^{0} g(z)f(z)dz} A_n \sqrt{k^2 - \lambda_n^2} \tag{3.14}$$

Combining eqns. (3.12), (3.13) and (3.14), we get

$$X = \sum \frac{iga\sqrt{k^2 - \lambda_n^2}}{B[1+\delta(n)]\omega^2} \left(\frac{\int_{-h}^{0} f^2(z)dz}{\int_{-h}^{0} g(z)f(z)dz} \right) \left(\int_{-B}^{B} \exp(i\lambda|y|)\cos(\lambda_n y)dy \right) \exp\left(-i[\epsilon + (\sqrt{k^2-\lambda_n^2})x_m] \right) g(z)\cos(n\lambda y)\exp(-i\omega t) \tag{3.15}$$

which gives a relationship between the stroke of the wave paddle, and the wave amplitude of the design plane wave, such that a uniform wave field exists at $x = x_m$. Note that for a normally incident design wave, $x_m = 0$, since the wave field is uniform over the entire basin, while for an oblique wave changing x_m affects only the phase of the stroke X in eqn. (3.16), and not its absolute value.

The model that has been derived here, strictly speaking, is valid only for plane monochromatic waves. But as we have said in the beginning of this chapter, one of the purposes of the experiments is to study spectral sea states in the wave basin, and for this reason it is important to be able to simulate a random directional sea state. This is done indirectly by breaking up the desired sea spectrum into energy bins, which are represented by monochromatic plane waves. The model is then used to obtain the stroke for each individual wave, and the final paddle stroke time series for the spectral sea is obtained by a linear superposition. The reader is referred to Appendix A.1, for an explanation of the program used to obtain the paddle time series.

3.3 Coordinate system

The coordinate system used here is a right handed coordinate system, with the origin as shown in Figure 3.1. This coincides with the coordinate system used in the models referred to in Chapter 2, and the coordinate axes are defined as follows

- The $x-$coordinate axis is perpendicular to the wavemaker, increasing as we move away from the paddles towards the beach, with $x = 0$ defining the paddle locations.

- The $y-$coordinate axis lies along the paddles, with $y = 0$ and $y = 18.2$, defining the two boundary walls of the basin.

- The $z-$coordinate axis is perpendicular to the still water surface, with $z = 0$ at the still water surface, and increasing upwards.

3.3.1 Shoal

A circular shoal made out of sand and concrete has been used for the experiments. It has a wooden skeletal framework which helped hold the shape while concrete was poured in. The center of the shoal is placed at $x = 5m$ and $y = 8.98m$ (Figure 3.1). A schematic view of the shoal is given in Figure 3.2.

Geometrically the shoal is the top cut off portion of a sphere of radius $9.1m$. The equation for the perimeter is given by

$$(x - 5)^2 + (y - 8.98)^2 = 2.57^2 \tag{3.16}$$

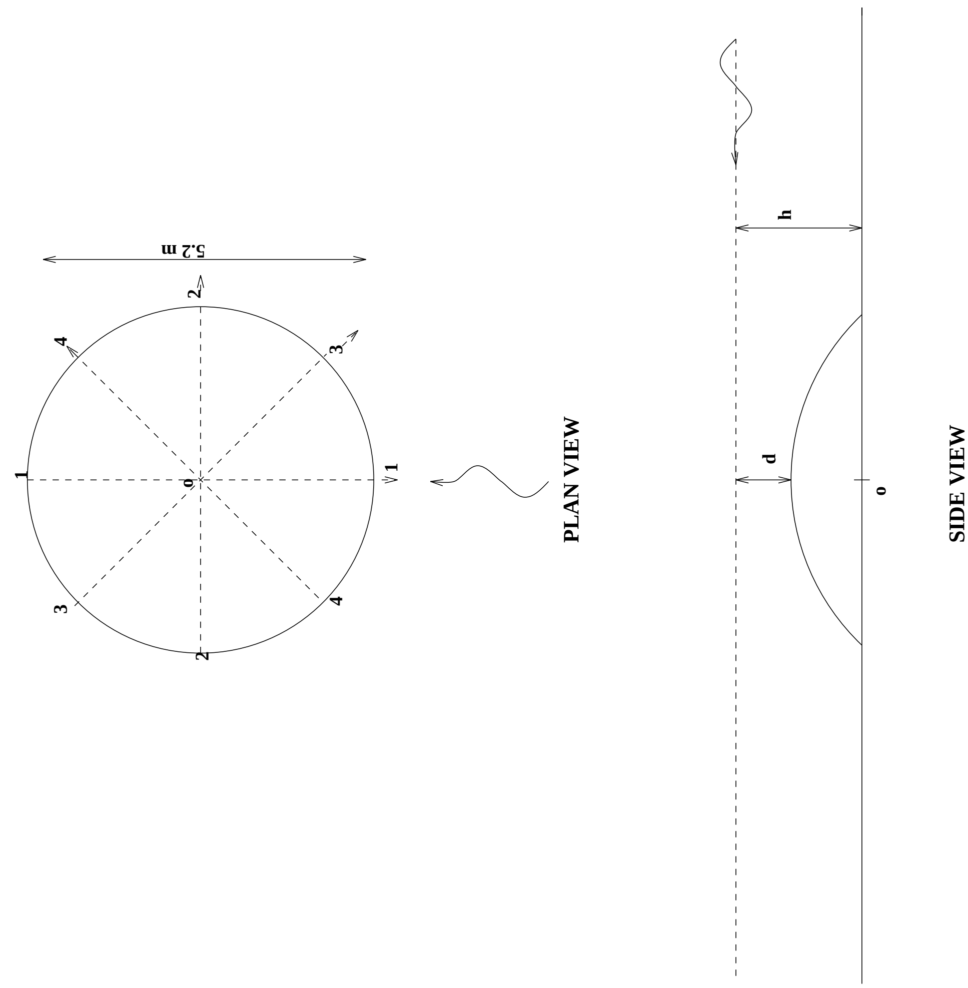

Figure 3.2: Schematic view of the shoal.

The bathymetry is given by

$$z = -h + \sqrt{82.81 - (x-5)^2 - (y-8.98)^2} - 8.73 \tag{3.17}$$

where h is the water depth away from the shoal. The coordinate system used in these equations is the global coordinate system explained in Section 3.3.

3.3.2 Shoal and basin survey

To check the validity of the mathematical equation used to determine the bathymetry of the shoal, a survey of the shoal was done. In all 25 measuring points were taken along four transects (Figure 3.2). Figure 3.3 shows a comparison between the measured depth and the computed depth. All distances have been measured with respect to the center of the shoal along the respective transects, with the positive direction along each transect being marked by an arrow in Figure 3.2. The comparisons are quite good except at a few points. To be certain that these slight variations did not affect the numerical results, the models were also run using a bathymetry obtained by fitting a surface over the measured depths. The results were found to be consistent with the two different bathymetries, and it is safe to say that eqn. (3.17) describes the bathymetry quite accurately. A survey of the basin floor was also done and variations of up to $2cm$ were found. There were variations of up to $5mm$ in the region used to monitor the depth of the water. This is quite crucial since now the depth on top of the shoal is uncertain to $5mm$.

3.4 Gages

Capacitance gages were used during the entire experiments. These gages output a voltage which increases as water level at the gage wire increases. Calibration curves from voltage to cms were found to be linear with the slope not changing much over the day. A detailed account of how calibration was done is given in Appendix A together with the procedure for collecting data.

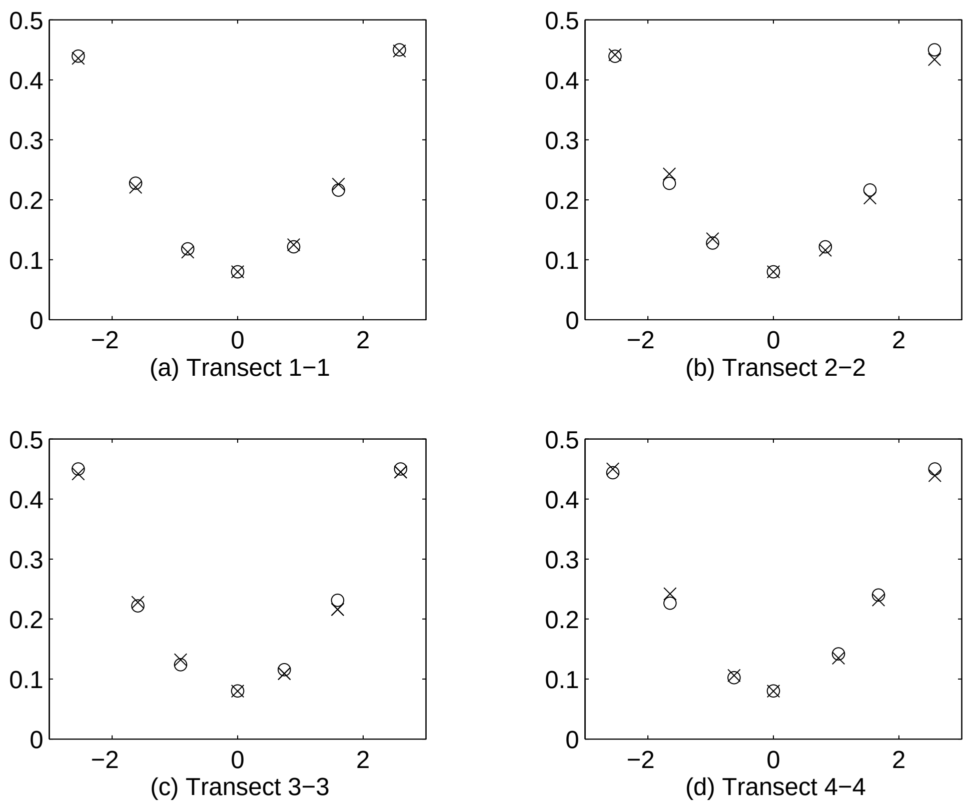

Figure 3.3: Comparisons between surveyed depth (x) and computed depth (o).

Electrical noise is another problem with data collection. For most of the gages this was quite low compared to the data signal, except gage 10. A considerable amount of noise was found at this gage and test cases with very small amplitudes had to be discarded all together.

3.4.1 Gage locations

A total of ten gages were used for data collection. Of these, nine gages were placed on an array which was then placed at different locations to encompass the wave field in the entire basin. The tenth was used as a normalizing gage and was kept at a fixed location (see Section 3.2.1). This was also useful in performing repeatability tests for the monochromatic waves. A schematic view of the gage locations and the experimental setup is given in Figure 3.1, with the gage array being denoted by a thick line. In all 14 different array positions were used (these are identified by their position numbers) leading to a total of 126 different measuring points for each set of experiments.

The exact location of the gages in the basin are dependent upon two factors. The location of the gages on the array, and the location of the array position in the basin. Of these two the former is fixed since the same gage array is used for all the experiments. Gage 1 has been used as the reference gage for fixing the gage coordinates, and the spacings of the other gages with respect to it on the array are given in Table C.1. The coordinates of all the gages for the different experimental sets are given in subsequent tables in Appendix C. The orientation of the different gage arrays are as given below

- Array positions 1 and 2 are oriented perpendicular to the $y-$axis, with gage 1 being closest to the axis.

- Array positions 3 to 14 are oriented perpendicular to the $x-$axis, with gage 1 being the farthest from the axis.

Depending upon their orientation, one or more array positions form a transect along which comparisons are made during data analysis. These are also shown in Figure 3.1. There is one cross shore (or longitudinal) transect (A-A) going right over the shoal, three along shore (or transversal) transects (B-B,C-C,D-D) behind the shoal, and three along shore transects (E-E,F-F,G-G) on top of the shoal. In all these seven transects map the entire wave basin where the wave field is changing due to the presence of the shoal.

3.5 Problems

The capacitance gages were quite sturdy, and most of the time trouble free. The problematic gages were gage 1, and gage 10, on the array. The sensor wire on gage 1 had to be changed a couple of times during the experiments. During the monochromatic breaking wave tests gage 1 tended to become loose, and shift from its measured position, thus some caution must be used during data analysis of this experimental set. The data from gage 10 was quite noisy, and in certain cases where the noise could not be filtered without affecting the wave data, the results had to be discarded. Gage 5 was thrown out of calibration during one of the irregular wave tests (Test 8, position 13), and had to be corrected.

The expected linearity of the calibration curves (Appendix A.4) made it easy to identify the problematic gages. Also during data collection if any of the gages were thrown out of calibration, or were sitting at too high a voltage level, they would transmit a steady voltage to the output, thus the time series were all regularly checked to confirm that the gages were in good working condition.

3.6 Test procedures

The test procedure for each of the experimental sets was as follows:

- The gages were moved to the particular position, corresponding to the position number in the experiment layout, and the coordinate positions of gage 1 were noted down.

- The gages were then calibrated to ensure that none of the gages were damaged during the transportation.

- The different test conditions were then run, and data was collected at the required frequency. A little waiting time was provided between tests to allow the water level to become still.

- The time series from the gages were then converted from volts to cm via the calibration curves, and plotted out to check if the gages were functioning properly during the tests.

- The gages were then moved to the next position, and the whole cycle repeated again.

In this Chapter a brief account of how the experiments were conducted has been given. Data analysis has been carried out on the monochromatic waves with no breaking and the second set of irregular experiments, and is described in detail in Chapter 4. Before proceeding on the reader should go through Appendix A, where some of the programs used in the experiments have been explained in greater detail, and which will help obtain a clearer picture of the experiments.

Chapter 4

DATA ANALYSIS AND COMPARISONS

4.1 Introduction

All the data analysis presented in this study has been carried out for two sets of experiments. Thus, this chapter has been divided into two broad sections. The first section is an analysis of the monochromatic tests with no breaking waves, while the second section concentrates on the second set of irregular wave experiments.

The main objective of the analysis is to compare wave height distributions over the entire domain with numerical model results. However, the analysis is not just limited to comparisons between data and model, and in certain cases, like testing the repeatability of the wave field, or looking at the evolution of directional spectra in the domain, attention has been paid only to one or the other.

Model comparisons have been carried out with the help of **Ref/Dif 1**, for the monochromatic waves, and **Ref/Dif S** for the irregular waves. A brief discussion of these models is given in Chapter 2. Results from the data have been tabulated in Appendix C, and the remaining sets of plots that are not shown in this chapter are available in Appendices D and E. The reader is referred to them for extra details.

4.2 Monochromatic wave tests

Monochromatic wave tests were carried out in $45cm$ water depth. Four tests were conducted with two different wave heights and wave periods. Being corrupted by noise (see Section 3.5), data from Test 3 was not used. The test particulars for the remaining three tests are given in Table 4.1. The Ursell parameter has been

Table 4.1: Test particulars for monochromatic waves.

Test no.	H (m)	T_p (sec)	h (mts)	d (mts)
1	0.0195	0.75	0.45	0.08
2	0.04	0.75	0.45	0.08
4	0.0233	1.0	0.45	0.08

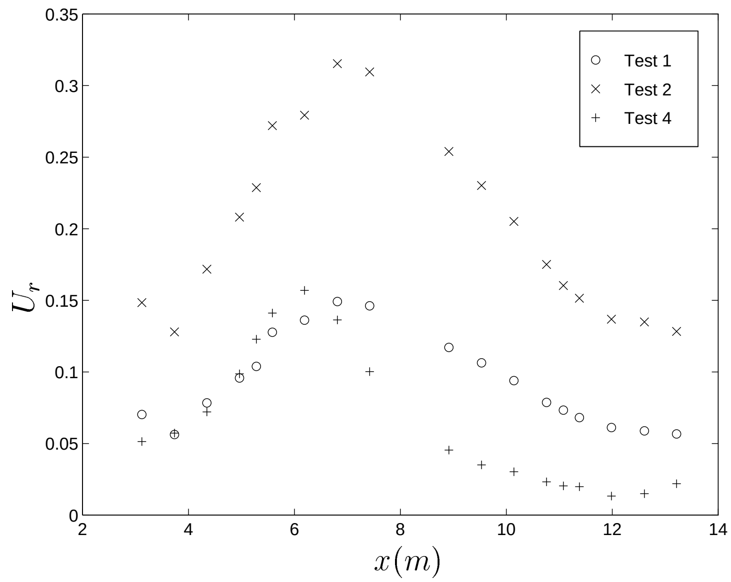

Figure 4.1: U_r values along transect A-A for monochromatic wave tests.

determined from the data for the three tests and Figure 4.1 gives these values along the center line of the shoal (transect A-A). In the figure the shoal extends from $x = 2.5m$ to $x = 7.6m$, with minimum depth at $x = 5.0m$. Maximum values of U_r for these tests still lie within the regime of Stokes wave theory (see Chapter 2).

Since the model predicts the wave heights for the primary harmonics only, the data set was first filtered through a Butterworth fifth-order band pass filter, to filter out all the noise and the higher harmonics. Wave heights before filtering (H) and after filtering (H_f) are given in Tables C.5, C.6 and C.7, together with the gage coordinates. The actual data has a lot of higher harmonics as can be seen from the

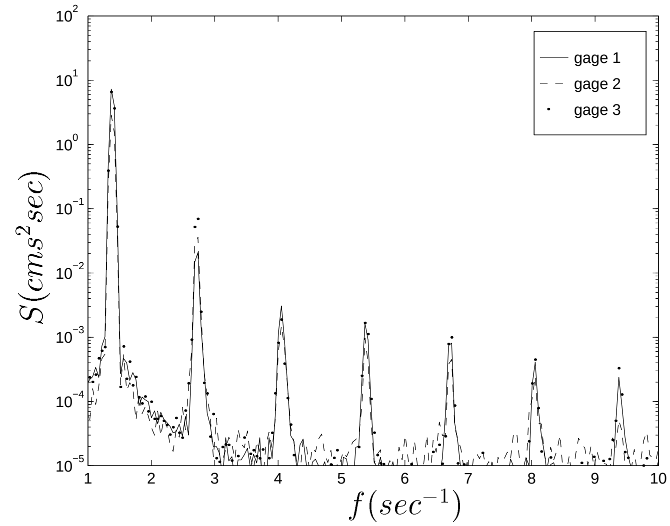

Figure 4.2: Frequency spectra along position 1 for monochromatic wave test 2 (gages 1 to 3).

frequency spectra plots shown in Figures 4.2 − 4.4 along position 1 (longitudinal transect) for Test 2, with gage 5 lying on top of the shoal, and the waves focusing somewhere between gage 7 and 8. These higher harmonics are consistent with Stokes wave theory.

Wave height measurements from the data were obtained using the zero-upcrossing method. To avoid reflections from the beach corrupting the data, it is important to determine the wave heights before the reflected waves can reach the gages. In order to do this data collection was done from a cold start, and the wave envelope function was determined from the causal function of the time series. Since the input signal has a ten second ramp up to supress long wave transients in the basin, the envelope function for each time series shows a monotonic increase before becoming constant. As these were monochromatic waves with a constant wave height, it was necessary to average them over a few wave periods only. Thus, as soon as the envelope function reached a constant value, the wave heights were

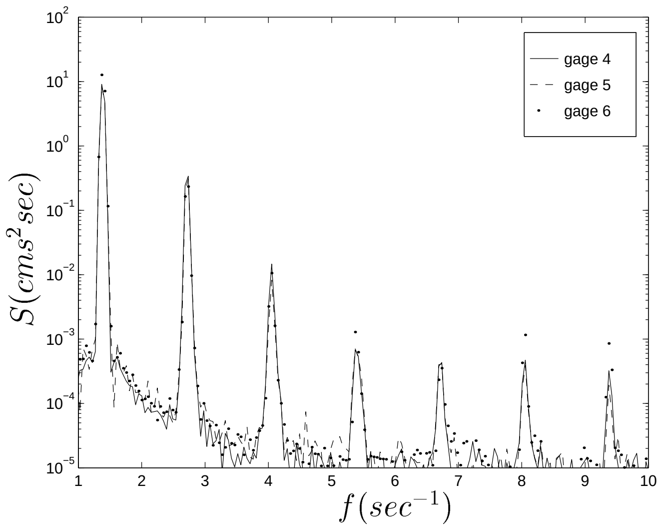

Figure 4.3: Frequency spectra along position 1 for monochromatic wave test 2 (gages 4 to 6).

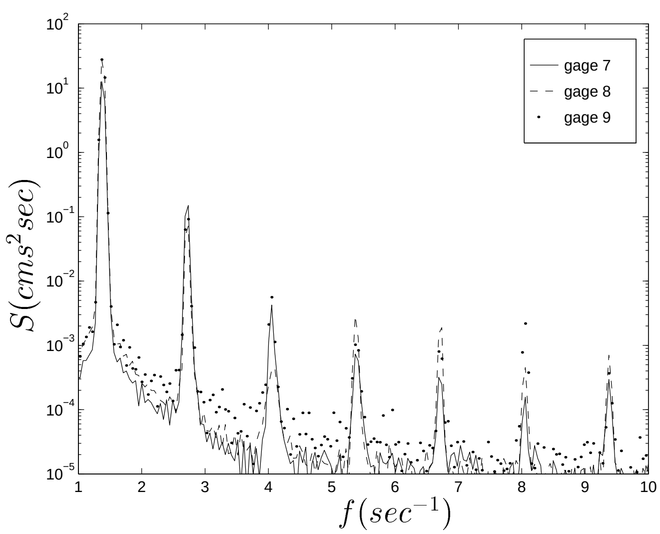

Figure 4.4: Frequency spectra along position 1 for monochromatic wave test 2 (gages 7 to 9).

obtained by averaging over 500 sample points or 10 wave periods. A small section of the time series on top of the shoal is seen in Figure 4.5 for the monochromatic tests, together with the envelope function for the filtered time series. Since on top of the shoal most of the higher harmonics are generated, discrepancy between the filtered and unfiltered time series would be maximum here. In all the cases, the filtered and unfiltered time series are both periodic waves with the same period, but for Test 2 and Test 4 the unfiltered time series have a slight setup due to the higher harmonics. The discrepancy between the two time series is quite limited, thus, the filtered time series is used for all further analysis on monochromatic waves.

4.2.1 Repeatability

Before any kinds of comparisons are made between the data and the model, it is important to look at the repeatability of the tests. The periodic nature of the waves can be seen from Figure 4.5, but it remains to be seen how the wave heights vary for different runs. As has been stated in Section 3.6, the tests were run for 14 different positions, during which only gage 10 (the normalizing gage) remained stationary. Thus, an idea about the repeatability of the tests can be obtained from the wave heights at gage 10 for the different runs. A percentage variation of the wave height from its mean value, for Test 1 is given in Figure 4.6. There is a $\pm$ 10 % variation in the wave heights which is also seen in the other tests. The standard deviation of the wave heights at gage 10 are given in Table 4.2.1, while the wave height and period distributions at gage 10, for the 14 different runs, are given in Tables C.2, C.3 and C.4.

The input wave heights for Tests 1 and 2 have been determined from the mean wave height at gage 10. Since it is uncertain whether variations in the wave heights at gage 10 are due to instabilities within the tank, or due to instabilities between different runs, in this analysis we assume that the wave form is stable within the tank and that the variations arise due to instabilities within runs. Thus,

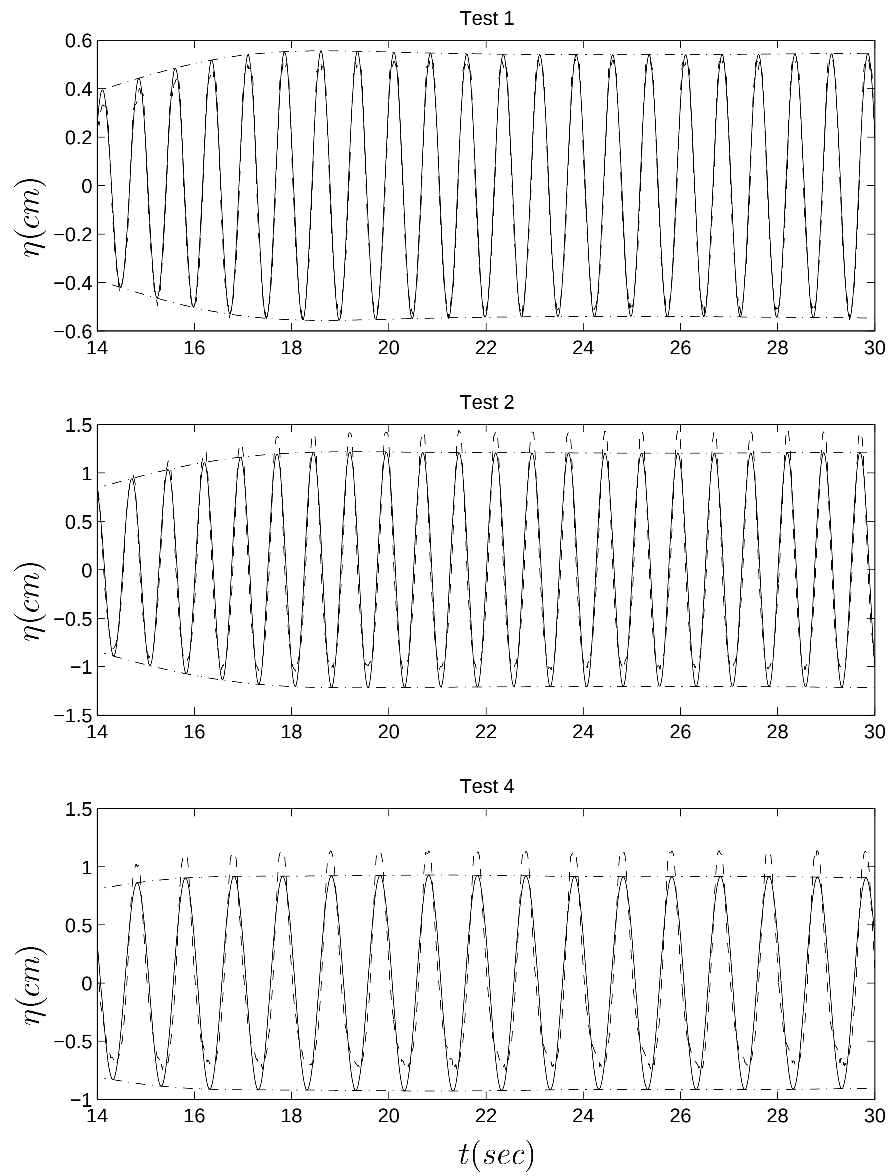

Figure 4.5: Time series for monochromatic wave tests on top of the shoal, '- ' filtered time series, '-.' envelope function ,'- -' unfiltered time series.

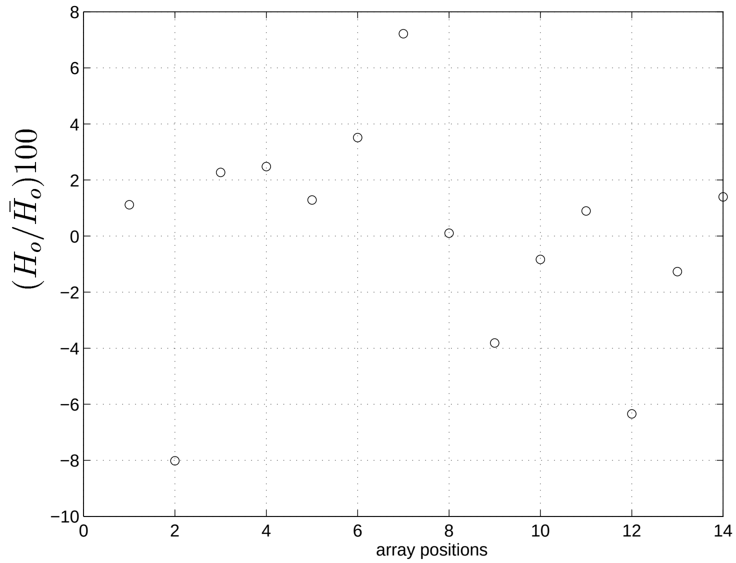

Figure 4.6: Percentage variations of wave heights from mean value, at gage 10, for Test 1.

Table 4.2: Standard deviation at gage 10 for monochromatic wave tests.

Test	σ_d
1	0.0008
2	0.0014
4	0.0014

in the model to data wave height comparisons, the wave heights at the gages for a particular run are normalized by the wave height at gage 10 for that particular run, while the wave heights for the model results are normalized by the input wave height.

The same method could not be used for Test 4 because the input wave height was found to be too low. Thus for the case of Test 4, the input wave height was obtained by averaging the wave heights along position 14. A linear shoaling coefficient is used to remove the inverse shoaling effects that are observed at the gages at position 14. The input wave height is thus obtained by

$$H_0 = \bar{H}_1(\sqrt{\bar{C}_{1g}/C_{0g}}) \tag{4.1}$$

where $\bar{H}_1$ is the wave height at position 14, averaged over the 9 gages, $\bar{C}_{1g}$ is the group velocity at position 14, averaged over the 9 gages, C_{0g} is the input group velocity, and H_0 is the input wave height. In this case the wave height distributions for both the model and the data are normalized by the input wave height.

4.2.2 Depth sensitivity

Before looking at data to model comparisons, it is important to look at the sensitivity of the models to variations in water depth on top of the shoal, since an error of $5mm$ exist in the recording of depth on top of the shoal (Section 3.3.2). A sensitivity test was done for the three tests, by running the models for two different depths. The results for Test 4 are shown both in the transverse section (Figures 4.9 and 4.10), and the longitudinal section (Figures 4.7 and 4.8). Compared to the data these variations are not too bad, and thus the model predictions can be accepted with reasonable amount of confidence. However it must be kept in mind that for the transverse directions, there is a very slight shift in the peaks of the wave height distributions, which could give vast differences in the model and data comparisons

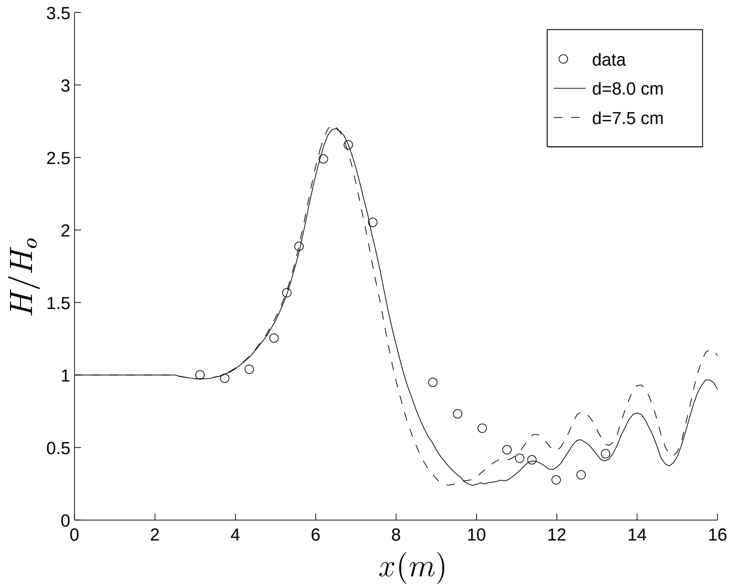

Figure 4.7: Depth sensitivity test for monochromatic wave test 4, (linear model) along transect A-A.

because of the sharp crests and troughs formed by these distributions. In the horizontal direction the gage positions were determined accurately within $1cm$.

4.2.3 Comparisons

The waves in these tests lie within the Stokes wave regime, and thus, the data is compared with both the linear version and the Stokes version of the **Ref/Dif 1** model (see Chapter 2). Dissipation due to boundary layers was ignored.

Contour plots for Test 4 are shown in Figures 4.11, 4.12 and 4.13. The contour plot for data in Figure 4.13 has been obtained in **Matlab** by using an inverse distance method routine between gage measurements. One has to be very careful before coming to any conclusions from them, since the gages are not spaced closely enough to resolve the wave height distributions reasonably well. From a comparison of the three figures we see that qualitatively the data and the models tend to be similar in the sense that in all the cases a focusing of the waves is seen

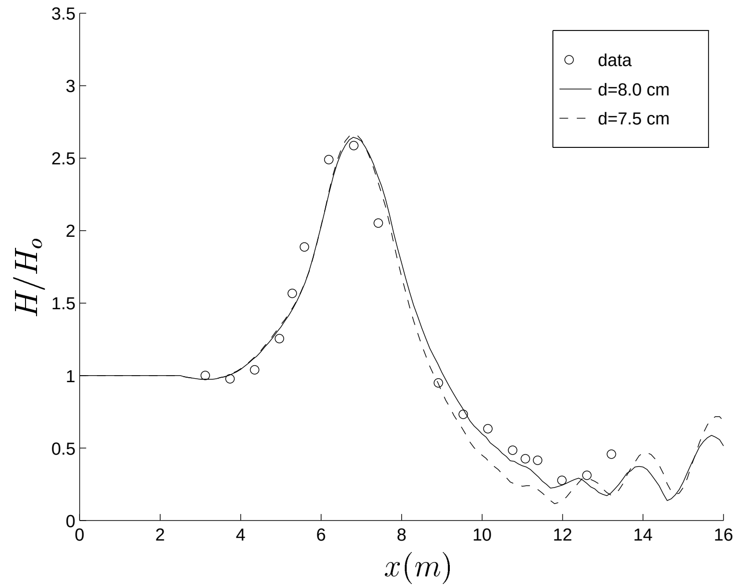

Figure 4.8: Depth sensitivity test for monochromatic wave test 4, (Stokes model) along transect A-A.

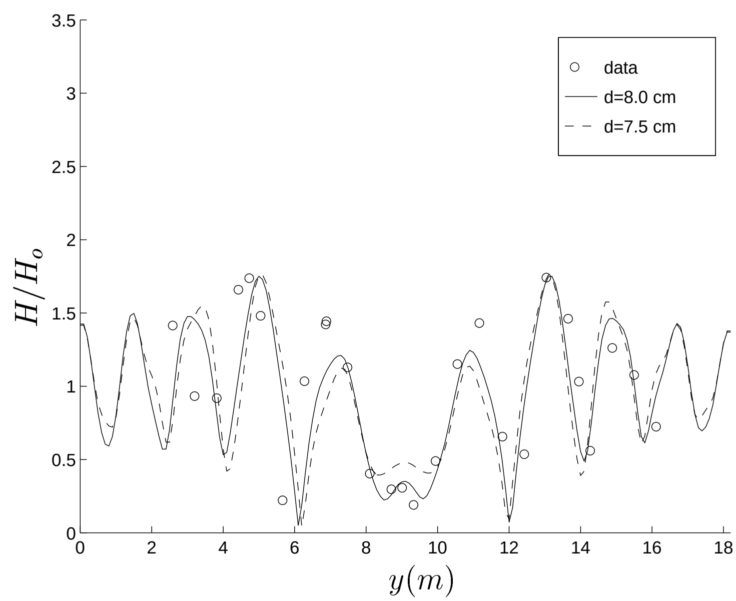

Figure 4.9: Depth sensitivity test for monochromatic wave test 4, (linear model) along transect B-B.

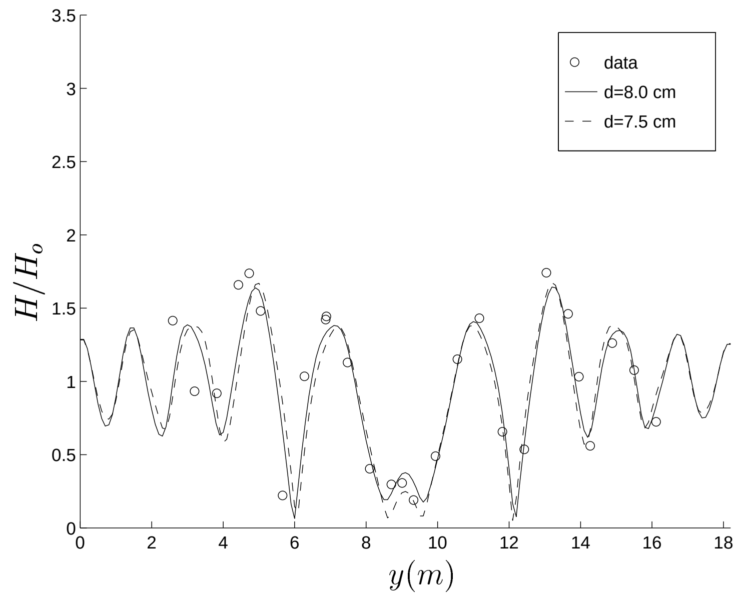

Figure 4.10: Depth sensitivity test for monochromatic wave test 4, (Stokes model) along transect B-B.

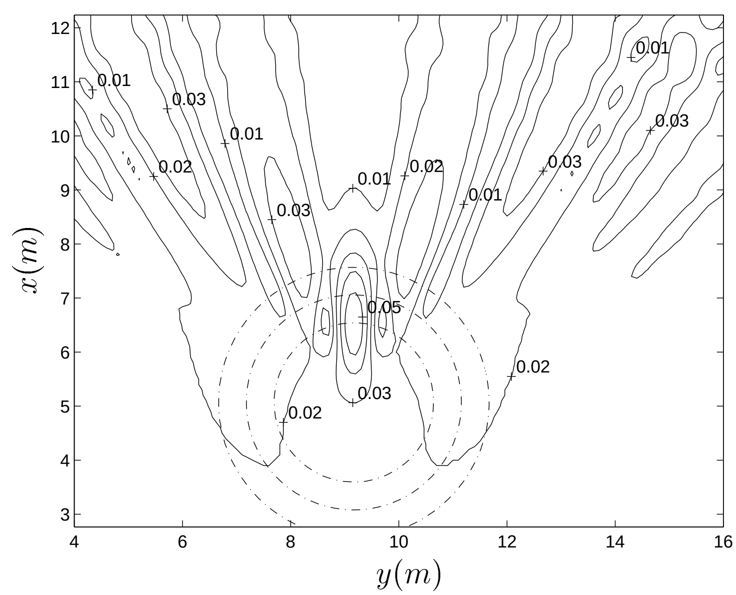

Figure 4.11: Contour plot of linear model for monochromatic wave test 4.

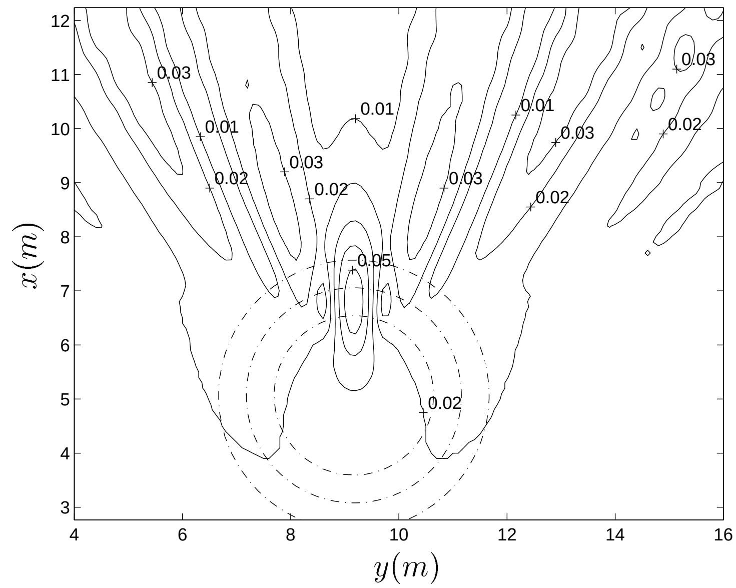

Figure 4.12: Contour plot of Stokes model for monochromatic wave test 4.

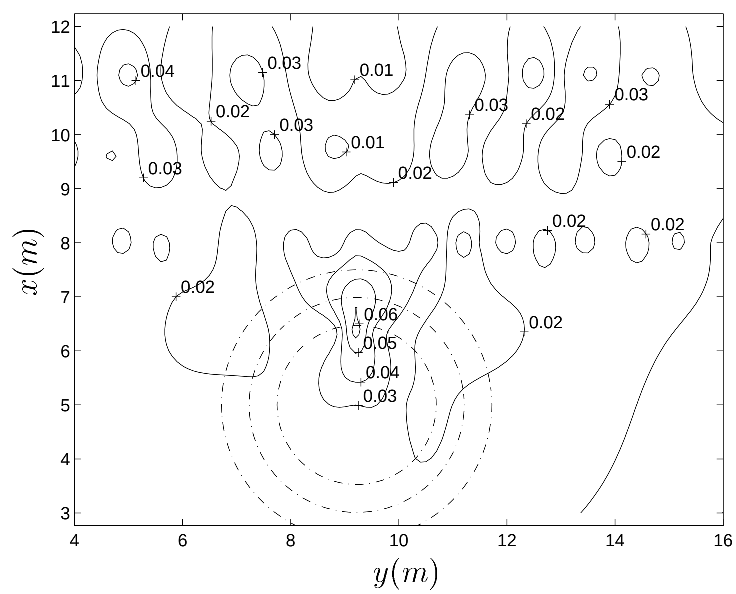

Figure 4.13: Contour plot of data for monochromatic wave test 4.

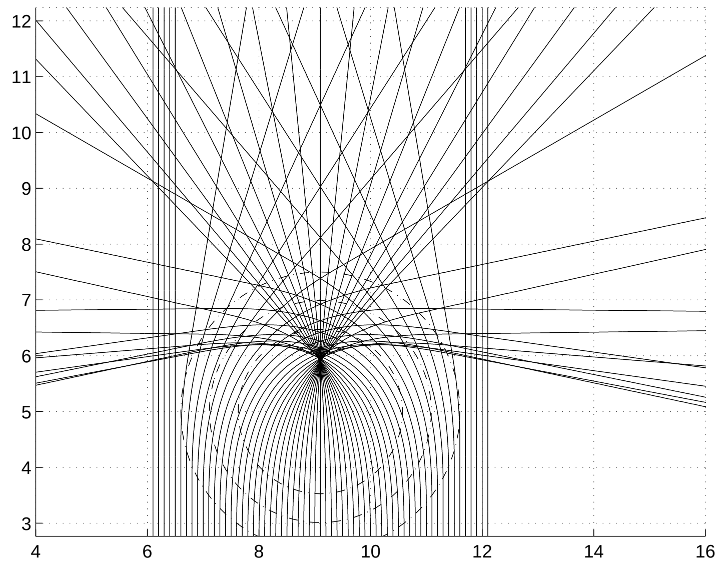

Figure 4.14: Wave ray diagram corresponding to monochromatic wave test 4 (T = 1.0 sec).

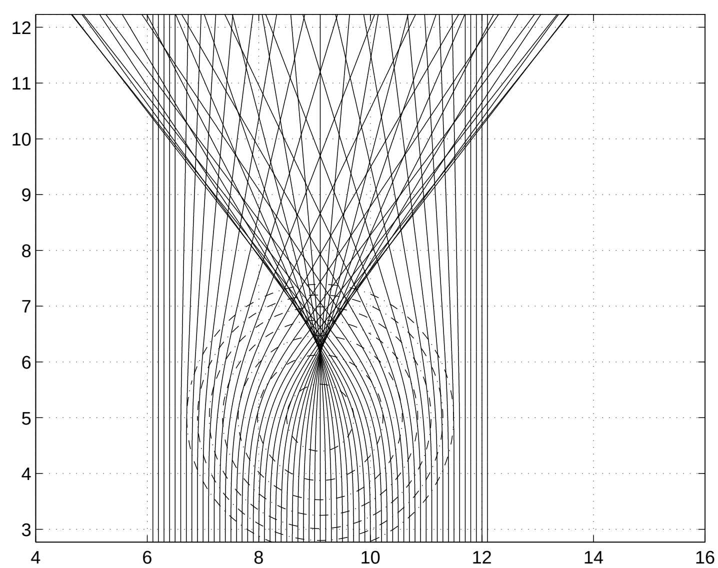

Figure 4.15: Wave ray diagram corresponding to monochromatic wave tests 1 and 2 (T = 0.75 sec).

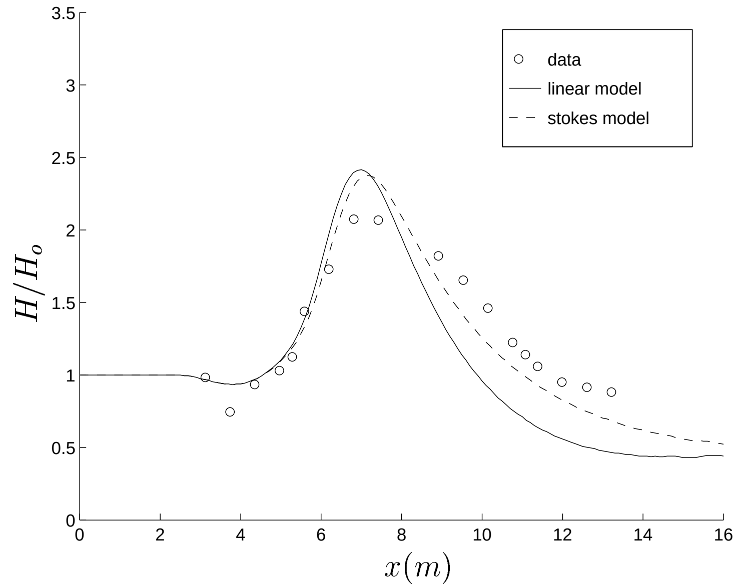

Figure 4.16: Data to model comparisons for monochromatic waves along transect A-A (Test 1).

behind the shoal, with a shadow region behind the focusing point where the wave heights are quite small, with alternating regions of large and small waveheights in the alongshore direction. However, to obtain a clearer picture comparisons need to be made between data at gage positions and model results along different transects (Section 3.4.1).

Before passing on to wave height comparisons along individual transects, it is worthwhile to look at the refraction patterns for the given bathymetry. Refraction patterns can be obtained with the help of wave rays (Mei, 1992) which are computed here using

$$\frac{d}{dx}\left[\frac{ky'}{\sqrt{1+y'^2}}\right] = \sqrt{1+y'^2}\frac{\partial k}{\partial y} \tag{4.2}$$

where $y = y(x)$ represents the wave ray, $k = k(x, y(x))$ is the wavenumber, and $y' = \tan\theta$ represents the slope of the curve. For larger angles ($y' \to \infty$) wave rays

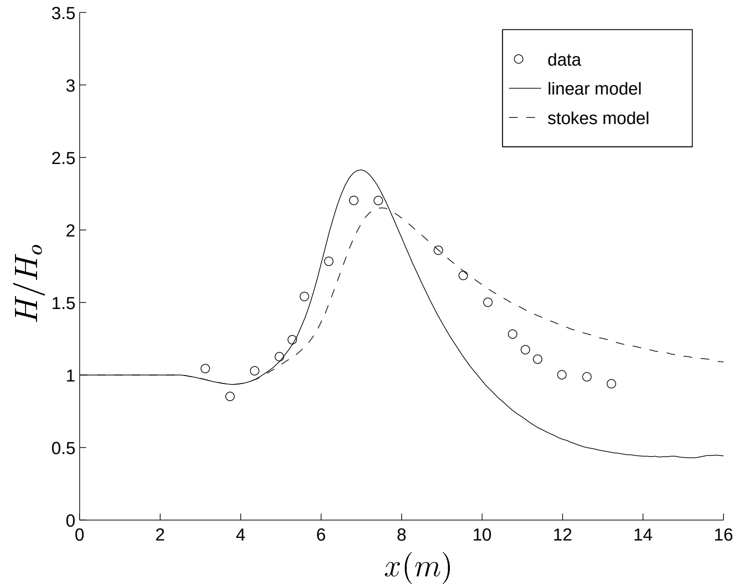

Figure 4.17: Data to model comparisons for monochromatic waves along transect A-A (Test 2).

can be represented by $x = x(y)$, and are computed using

$$\frac{d}{dy}\left[\frac{kx'}{\sqrt{1+x'^2}}\right] = \sqrt{1+x'^2}\frac{\partial k}{\partial x} \tag{4.3}$$

Figures 4.14 and 4.15 show the refraction patterns obtained from eqns. (4.2) and (4.3). We see that the focusing is quite severe, occuring almost on top of the shoal. This is unlike the earlier experiments of Berkhoff *et al.* (1982), where the focusing occurs downwave of the shoal. Such a sharp focus seems to indicate that wave height distributions behind the region of focus will have considerable variations, and which is really the case as shall be seen in the wave height comparisons along different transects. Comparing with the model results for similar conditions (Figure 4.11), we see that the focus in the model is slightly delayed, probably due to diffraction effects.

A statistical parameter has been used to quantify the accuracy of the models. This statistical parameter, also known as an index of agreement (d_i), was proposed

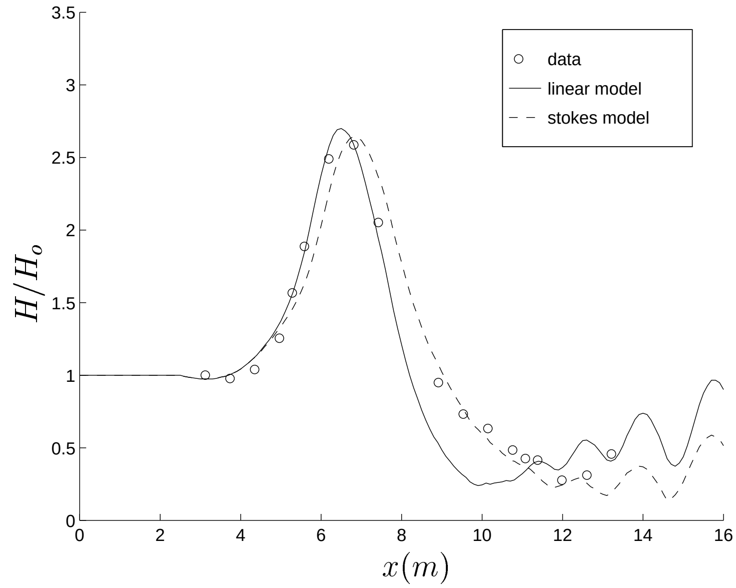

Figure 4.18: Data to model comparisons for monochromatic waves along transect A-A (Test 4).

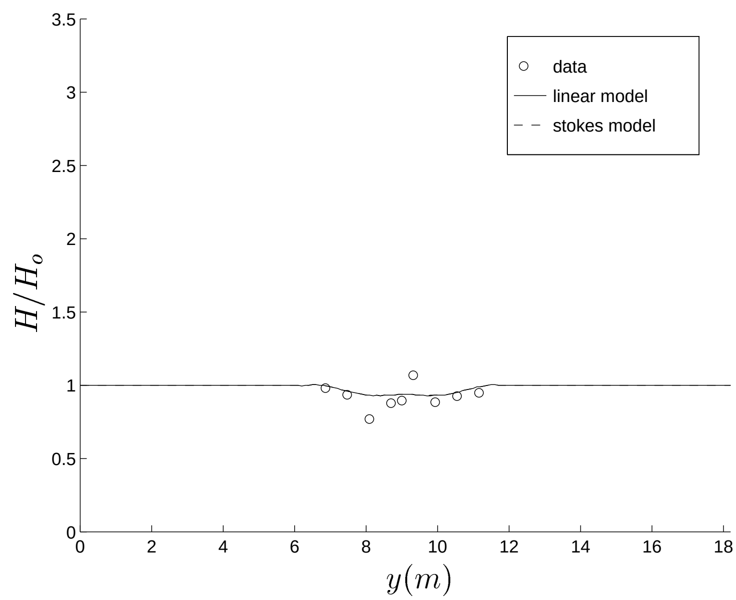

Figure 4.19: Data to model comparisons for monochromatic waves along transect G-G (Test 1).

by Wilmott (1981). This index of agreement varies between $d_i = 1$ (perfect agreement) and $d_i = 0$ (complete disagreement), and is defined as

$$d_i = 1 - \frac{\sum_{i=1}^{n}(y(i) - x(i))^2}{\sum_{i=1}^{n}(|y(i) - \bar{x}| + |x(i) - \bar{x}|)^2} \tag{4.4}$$

where $x(i)$ are the measured data, $y(i)$ are the predicted values from the model, and $\bar{x}$ is the data mean. The index of agreement values for the monochromatic waves along the different transects are given in Table 4.2.3. Apart from this the data to model wave height comparisons are also shown (Figures 4.16 $-$ 4.36). Along transect A-A we see from the index of agreement values that the Stokes model performs better than the linear model for all the three test cases. In all the three tests, the linear model gives a better prediction before the focusing, while the Stokes model performs better in predicting the wave height at the focus as well as behind the focus region (Figures 4.16 $-$ 4.18). The focusing in all cases occurs around $x = 8m$, and the wave height increases quite rapidly as compared to the Berkhoff *et al.* data (1982). The focusing is predicted quite well by the model in that the region of focus, and the wave height distribution there compare very well with the data. The models perform better as we move from transect G-G to transect E-E, with the linear model faring better than the Stokes model (Figures 4.19 $-$ 4.27). These transects lie in front of the region of focus, and the initial discrepancy between data and the nonlinear model results could be due to the failure of the approximate equations to focus rapidly enough (Kirby and Dalrymple, 1984). Along transect D-D we see that the data shows considerable amount of variations in the wave height distribution for Test 4 as compared to Tests 1 or 2, and the models are unable to predict these sharp variations (Figures 4.28 $-$ 4.30). This discrepancy is due to the severe focus seen in Figures 4.14 and 4.15. In Test 4 we see that right behind the shoal near transect D-D we have rays moving almost perpendicular to the basin walls. But the parabolic model has a maximum angular range of $\pm 45°$ only, and thus does not give good results along transect D-D. For Tests 1 and 2 we observe

Table 4.3: Index of Agreement (d_i) for monochromatic waves.

	Test 1		Test 2		Test 4	
Transect	linear	Stokes	linear	Stokes	linear	Stokes
A-A	0.8748	0.9649	0.8677	0.9172	0.9838	0.9904
G-G	0.4173	0.4173	0.5225	0.5153	0.6659	0.6659
F-F	0.8371	0.8275	0.9371	0.898	0.9658	0.9671
E-E	0.9017	0.9207	0.8835	0.9142	0.9193	0.9278
D-D	0.9144	0.9346	0.8817	0.9037	0.5056	0.7687
C-C	0.6478	0.8109	0.5705	0.7981	0.8003	0.8480
B-B	0.5455	0.6509	0.5578	0.7750	0.8557	0.9435

that the focusing is downward compared to Test 4, and not so severe. As a result the comparisons are better along transect D-D. In general, from the index of agreement table (Table 4.2.3), we see that the Stokes model performs much better than the linear model.

4.3 Irregular waves

In this section model runs from **Ref/Dif S** are compared with the experimental data of the second set of irregular experiments. The experiments were conducted in a water depth of $40cms$, with a depth of $3cm$ on top of the shoal, and consisted of four different test runs (Test 3, Test 4, Test 5 and Test 6). The energy variance of Test 3 and Test 4 are lower than that of Test 5 and Test 6. In all four tests the waves break on top of the shoal (roughly 1/3 of the waves breaking for Tests 3 and 4, and about 2/3 of the waves breaking for Tests 5 and 6). The four cases also have two different directional spreadings, with a mean angle normal to the wavemaker ($\theta_m = 0°$). Tests 3 and 5 have a narrow directional spread ($\pm 11°$), while, Tests 4 and 6 have a broad directional spread ($\pm 45°$).

Ref/Dif S requires a spectrum to be given as input. While input frequency spectrum was obtained from averaging the frequency spectrum along the gages at

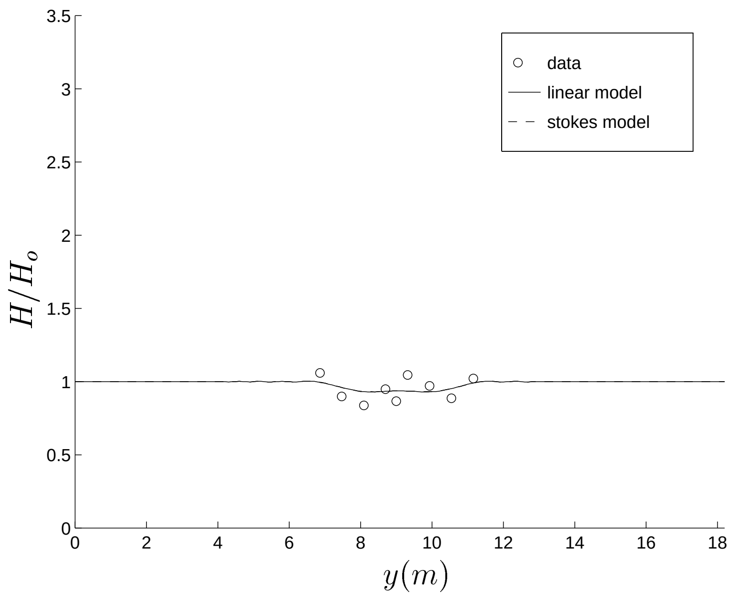

Figure 4.20: Data to model comparisons for monochromatic waves along transect G-G (Test 2).

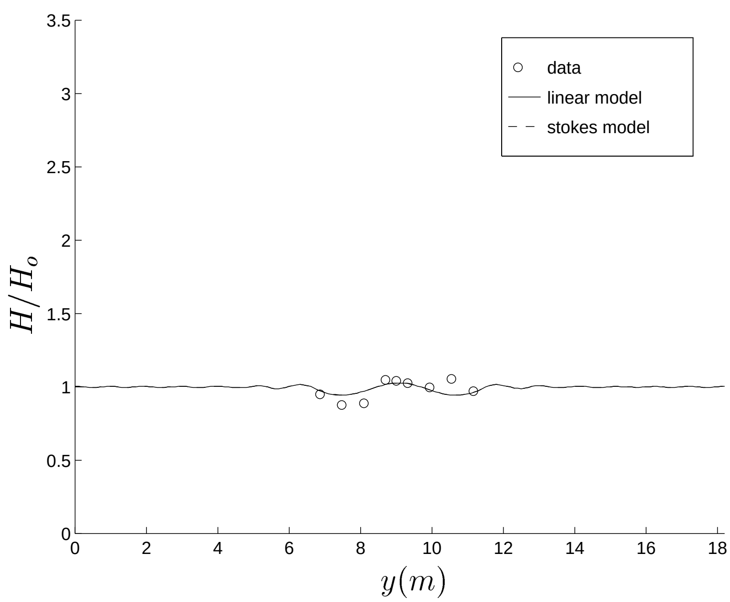

Figure 4.21: Data to model comparisons for monochromatic waves along transect G-G (Test 4).

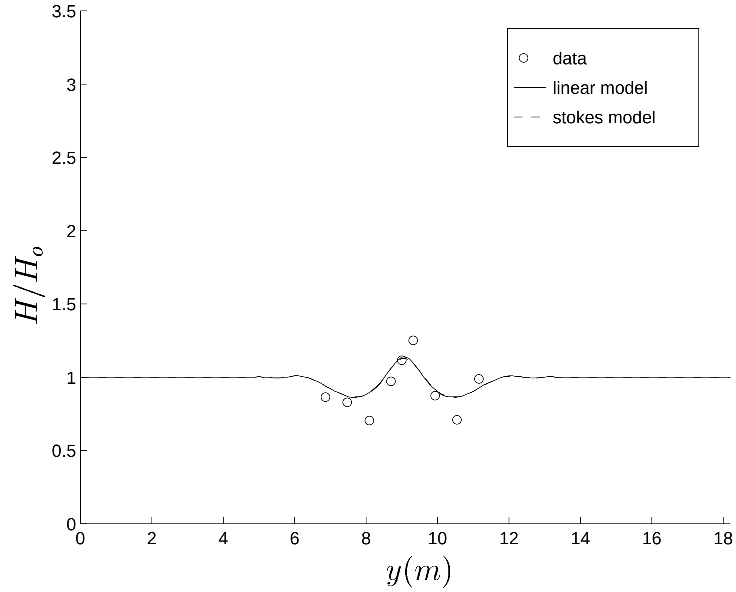

Figure 4.22: Data to model comparisons for monochromatic waves along transect F-F (Test 1).

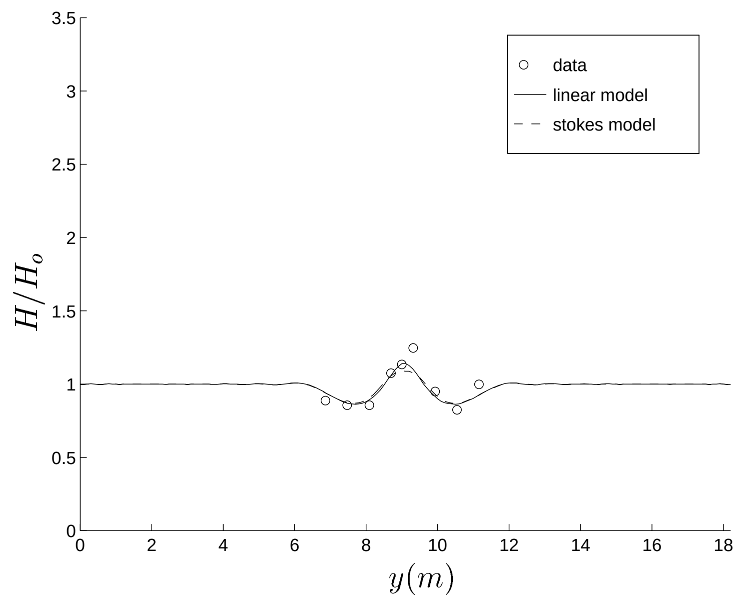

Figure 4.23: Data to model comparisons for monochromatic waves along transect F-F (Test 2).

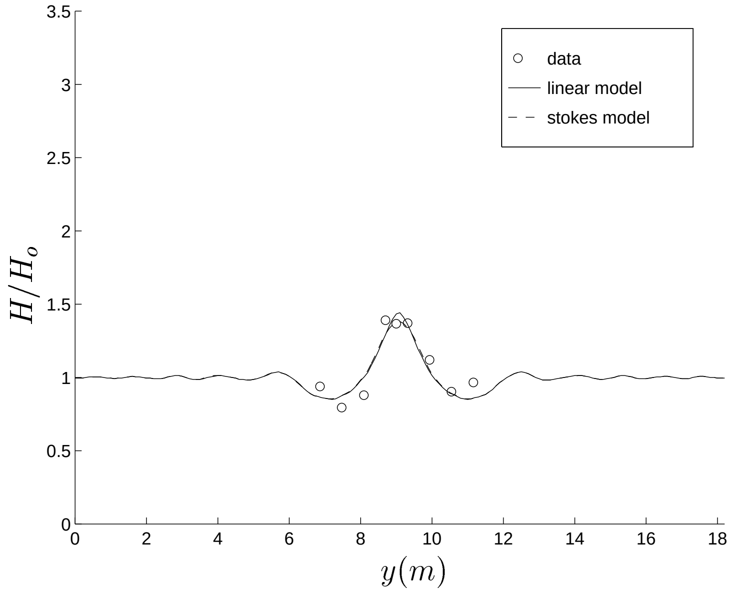

Figure 4.24: Data to model comparisons for monochromatic waves along transect F-F (Test 4).

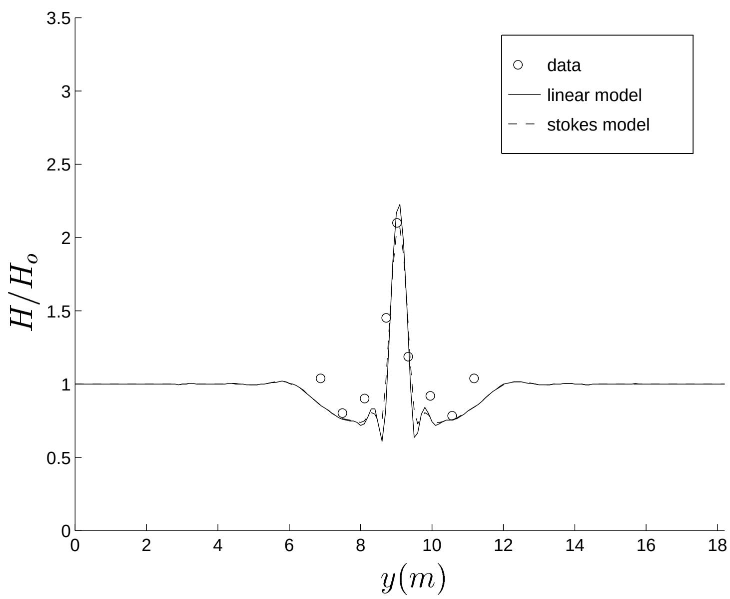

Figure 4.25: Data to model comparisons for monochromatic waves along transect E-E (Test 1).

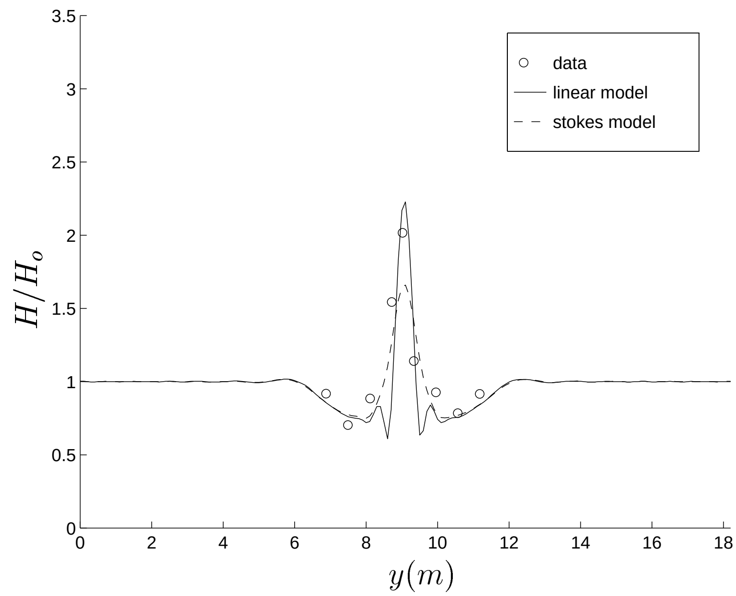

Figure 4.26: Data to model comparisons for monochromatic waves along transect E-E (Test 2).

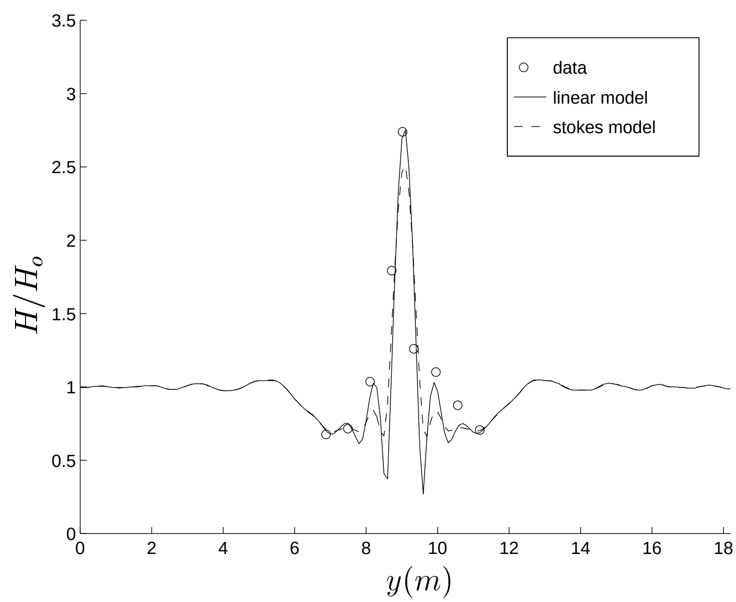

Figure 4.27: Data to model comparisons for monochromatic waves along transect E-E (Test 4).

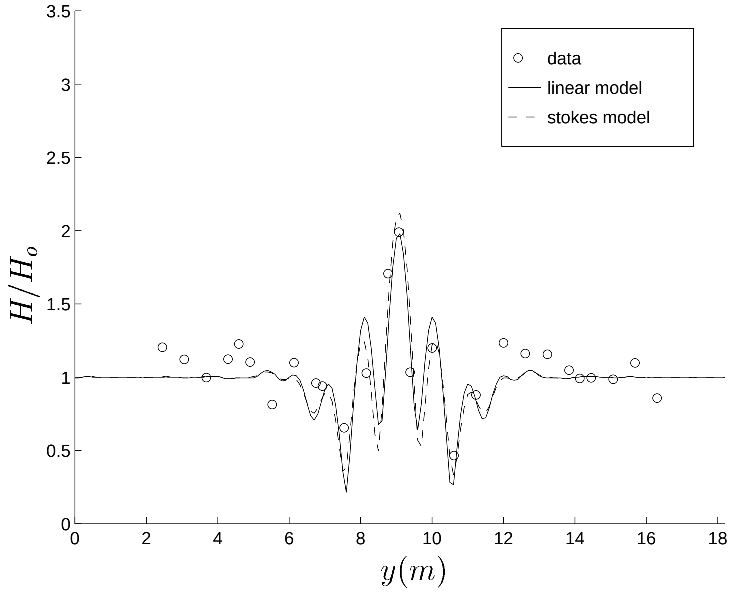

Figure 4.28: Data to model comparisons for monochromatic waves along transect D-D (Test 1).

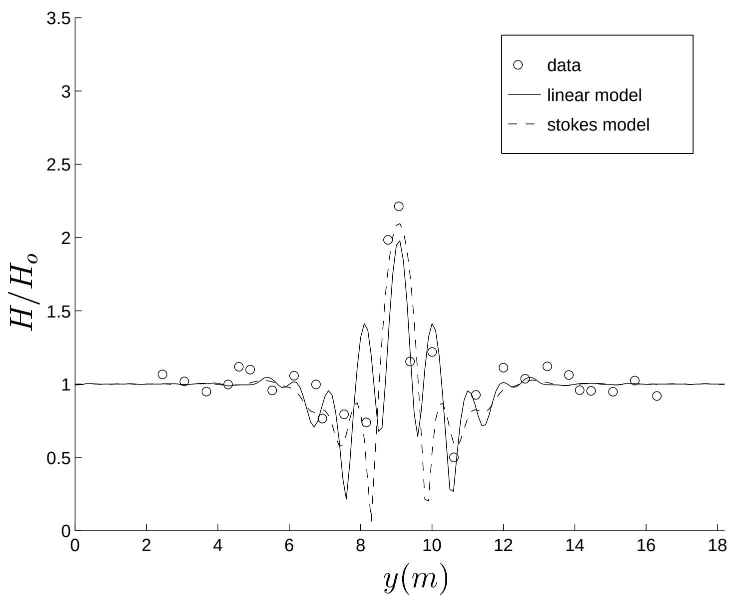

Figure 4.29: Data to model comparisons for monochromatic waves along transect D-D (Test 2).

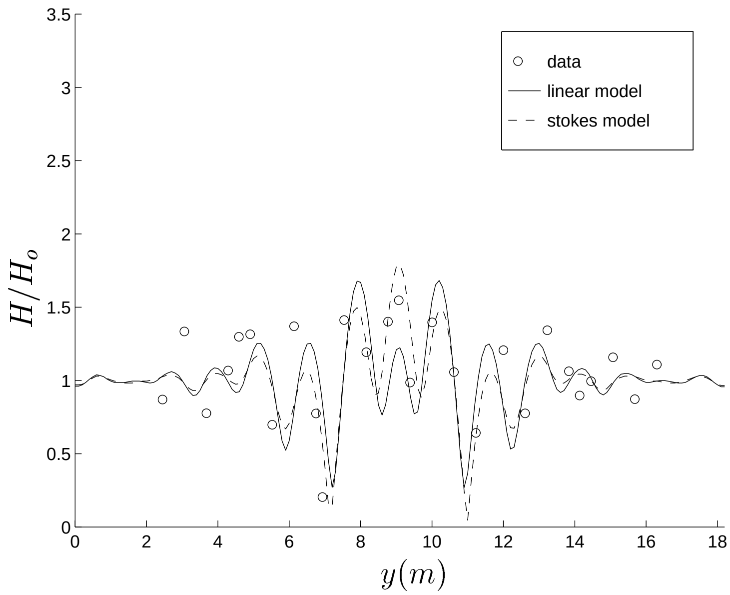

Figure 4.30: Data to model comparisons for monochromatic waves along transect D-D (Test 4).

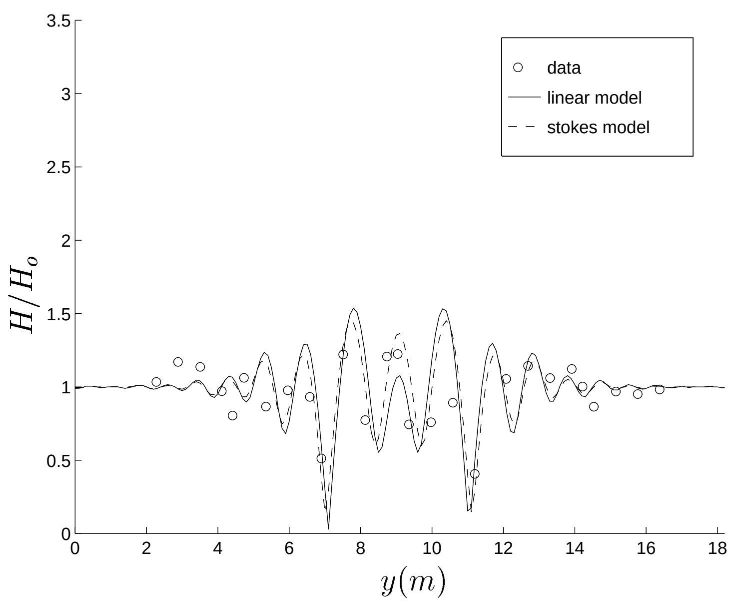

Figure 4.31: Data to model comparisons for monochromatic waves along transect C-C (Test 1).

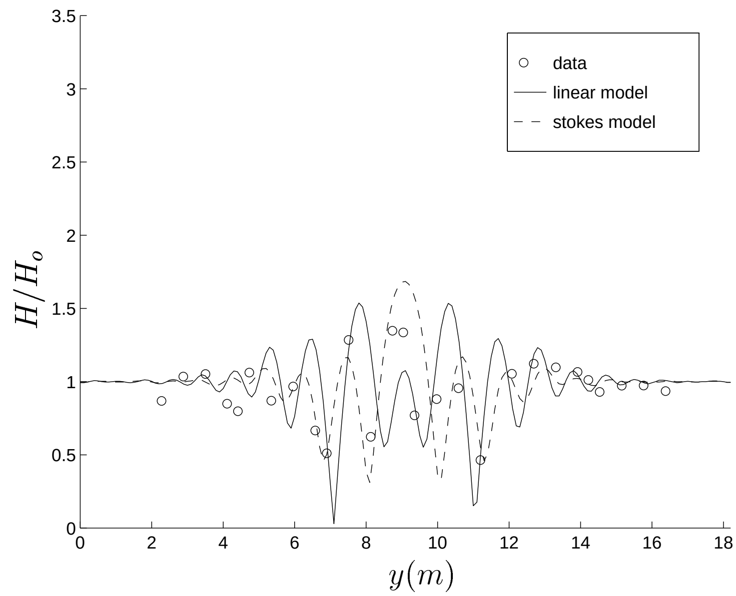

Figure 4.32: Data to model comparisons for monochromatic waves along transect C-C (Test 2).

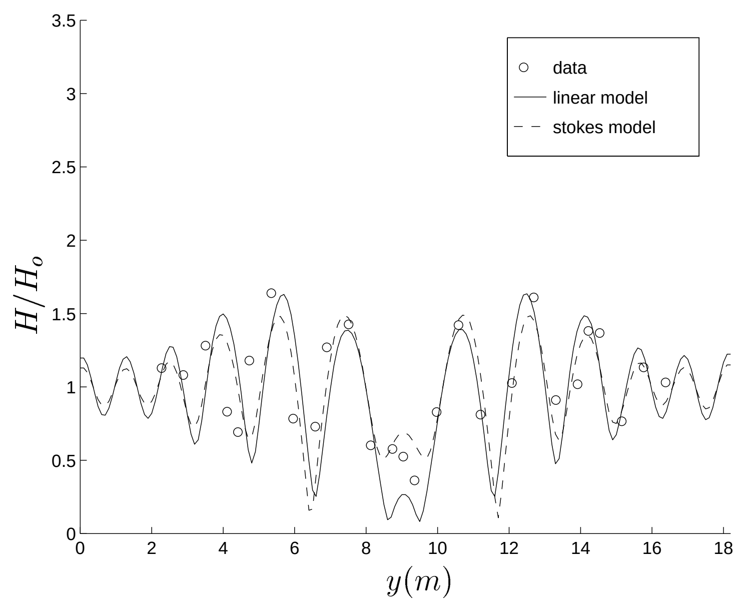

Figure 4.33: Data to model comparisons for monochromatic waves along transect C-C (Test 4).

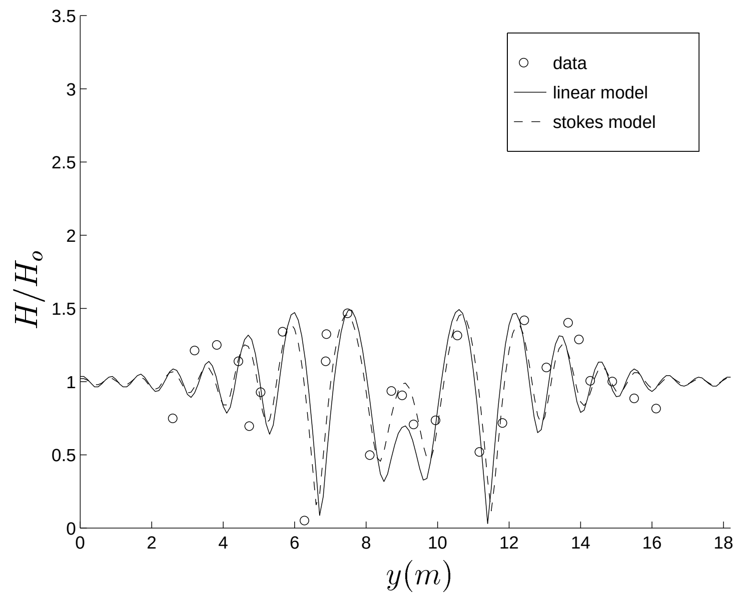

Figure 4.34: Data to model comparisons for monochromatic waves along transect B-B (Test 1).

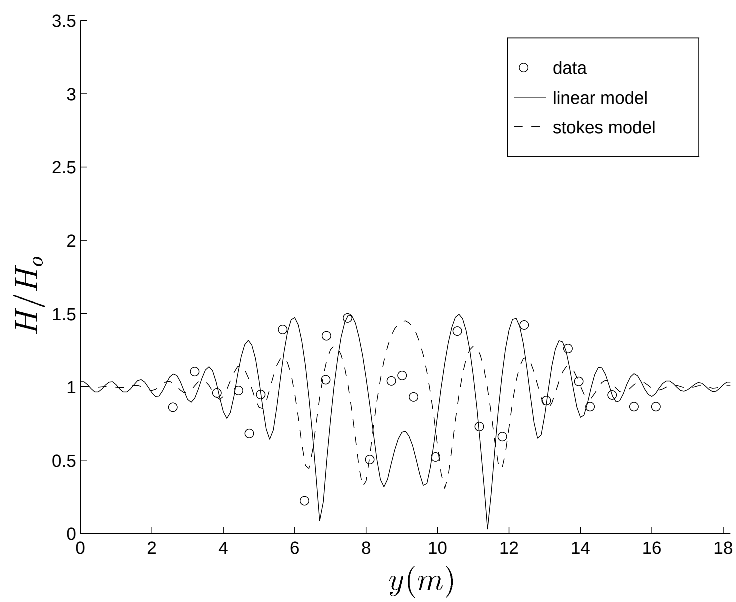

Figure 4.35: Data to model comparisons for monochromatic waves along transect B-B (Test 2).

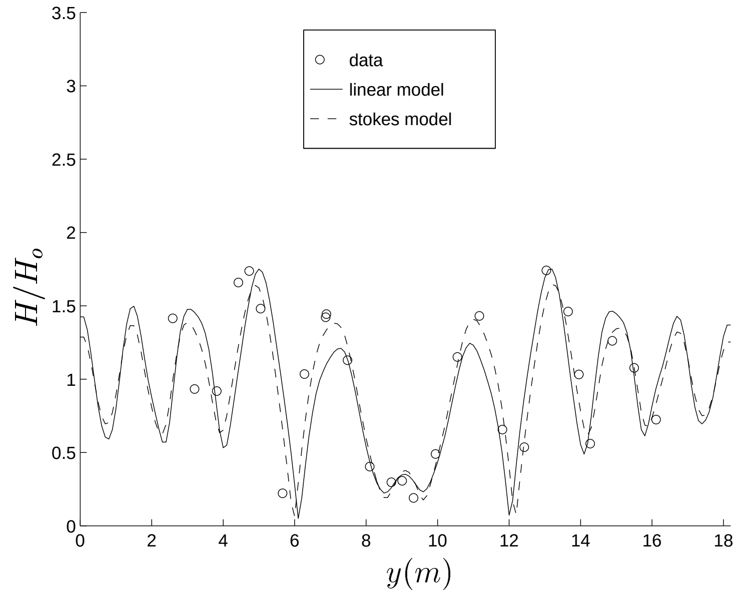

Figure 4.36: Data to model comparisons for monochromatic waves along transect B-B (Test 4).

position 14, the directional spread was obtained by the help of a wrapped normal directional spreading function (Borgman, 1984) given by,

$$D(\theta) = \frac{1}{2\pi} + \frac{1}{\pi}\sum_{j=1}^{J} \exp\left[-\frac{(j\sigma_m)^2}{2}\right] \cos j\,(\theta - \theta_m) \tag{4.5}$$

where θ_m = mean wave direction = $0°$, J = number of terms in the series chosen as 50 in the numerical calculations, and σ_m is a parameter which determines the width of the directional spectrum

In accordance with the spectral method used in **Ref/Dif S** (see Chapter 2), the entire spectrum was divided into equal energy bins to obtain 900 monochromatic waves (each bin representing one monochromatic wave) which were given as input to the model. All this is done with the help of a preprocessor called **Specgen** (see Chapter 2). A similar directional spectrum was used to obtain the paddle time series from designer wavemaker theory (Appendix A.1). By using the same spreading for the model, the assumption has been made that while energy losses in the wave field reduce the desired wave heights, the direction of the waves remain unchanged. Ideally the input directional spectrum for the model would be determined from the wave field, but this is not possible since the wave field is inhomogeneous, and estimates of directional spectrum from a gage array require a homogeneous wave field.

Data from gage 10 has not been used here to determine the initial wave conditions because the energy that was obtained at this gage was found to be inconsistently low compared to the remainder of the measuring sites. This was probably due to the fact that the gage was placed along the centerline of the shoal, close to the wall for these experiments, where there was a lot of wave interference caused by energy propagating away from the shoal. This can be seen more clearly from the wave ray diagram given in Figure 4.39, where a lot of energy is seen propagating perpendicular to the wall. Reflections from the wall would lead to standing wave patterns and gage 10 might have been sitting at a node. The exact nature is not very clear, but because of this inconsistency, gage 10 has not been used in the following analysis. Input frequency spectra for the different test cases was obtained by averaging the data spectra along position 14. The wave heights obtained after rebinning, using **Specgen**, were multiplied by an inverse shoaling coefficient similar to the one used for monochromatic Test 4, except that now the peak frequency was used to determine the group velocity (see Section 4.2). The particulars for the four different test cases are given in Table 4.4, in the form of the the input wave height, the peak period (T_p), the mean angle (θ_m), and the directional spreading parameter (σ_m).

4.3.1 Depth sensitivity

As before a depth sensitivity test has been carried out on the model. Since the water depth on top of the shoal is much less now, the model is expected to be

Table 4.4: Test particulars for irregular waves.

Test no.	$H_{0s}(m)$	$T_p(sec)$	θ_m	σ_m
3	0.0139	0.73	0	5
4	0.0156	0.73	0	20
5	0.0233	0.73	0	5
6	0.0249	0.71	0	20

more sensitive to changes in water depth as compared to the monochromatic tests. The model was run for depths of $d = 2.5cm$, $d = 3.0cm$ and $d = 3.5cm$, on top of the shoal. As in the case of the monochromatic tests, an index of agreement comparison was carried out to determine at which depth the model gives best agreement with data (Tables C.12, C.13, C.14 and C.15). The data lies within the predictions of the model for the three different depths (Figures 4.37 and 4.38), with the index of agreement analysis showing that the results are not very good for the case of $d = 2.5cm$. But since it cannot be said clearly whether the results are better for $d = 3.0cm$ or $d = 3.5cm$, all analysis has been carried out assuming a depth of $3cm$ on top of the shoal.

4.3.2 Wave height distributions

Similar to what was done for the monochromatic cases, a model to data comparison of significant wave heights is shown here for the seven different transects. The significant wave heights at the gages have been determined with the help of a zero-up crossing method on the entire time series (unlike the monochromatic tests, where it was applied on only part of the time series). Reflections from the beach are a matter of concern, but have been ignored here. Also no filtering is done on the data since we are studying breaking wave patterns, and the effects of higher harmonics become important here. As the model works on a superposition principle (see Chapter 2), the wave heights of individual wave components are very small,

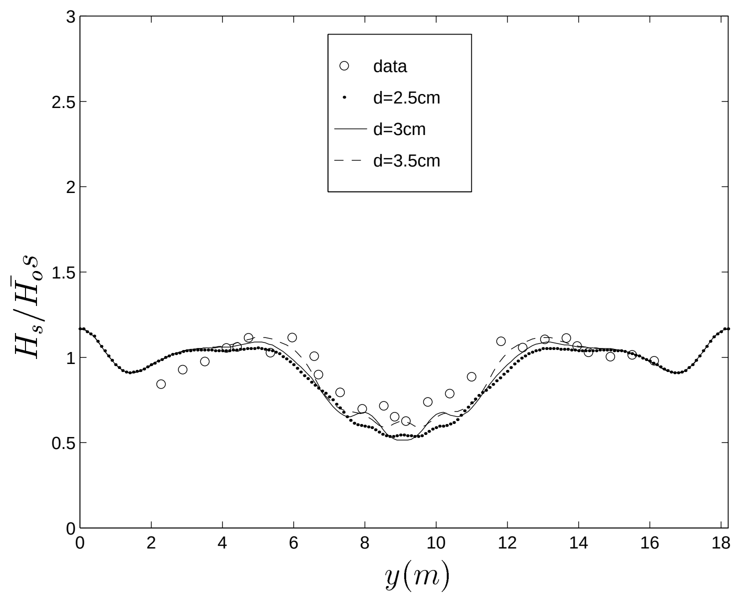

Figure 4.37: Depth sensitivity comparisons for irregular waves along transect C-C (Test 5).

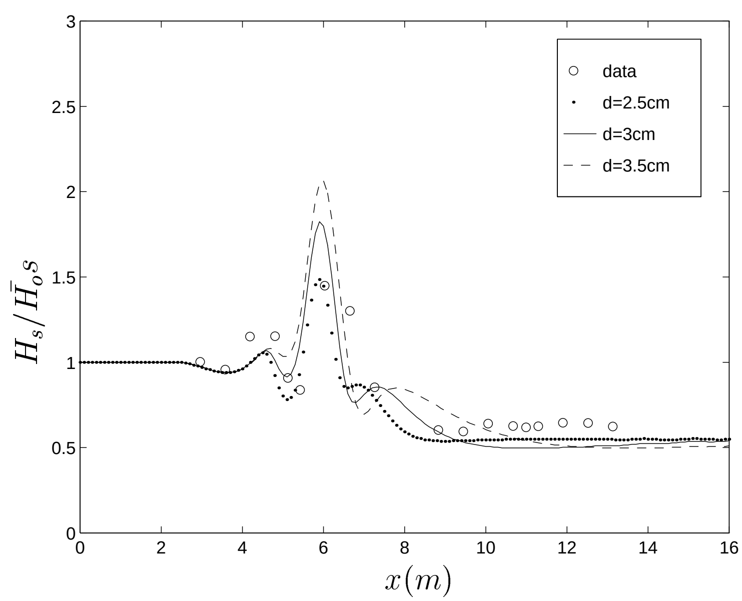

Figure 4.38: Depth sensitivity comparisons for irregular waves along transect A-A (Test 5).

and the results from the linear and Stokes model are the same. Thus results only from the linear model runs are shown here. All the significant wave heights have been normalized with the input significant wave height.

Again modeling eqns. (4.2) and (4.3) for these test cases, we find that the refraction patterns focus more rapidly than for the monochromatic tests (Figure 4.39). This is not unusual since the water depth on top of the shoal for the irregular wave tests is less compared to the monochromatic test cases. From Figure 4.39 we also see that as we go from $f = 1Hz$ to $f = 1.45Hz$ (which more or less represents the range of frequencies in the spectrum), the focusing becomes less severe, although the region of focus does not move much, and lies between $x = 5m$ and $x = 6m$.

Data to model comparisons along transect A-A (Figures 4.40 $-$ 4.43), show that the results are quite good in all four test cases, except for the estimation at the region of focus, where the model always overestimates the significant wave height. This is probably because wave focusing is taking place in and around the surf zone where the model does not perform so well (see Section 4.3.3).

In all the along shore (transverse) transects we see that the model predicts large wave heights at the side walls, for all the test cases. This is because of the boundary conditions at the side wall, which due to its no flux nature makes all the waves form an antinode at that point. These when superimposed to obtain the significant wave heights lead to large values at the side wall boundaries. The comparisons along transect G-G (Figures 4.44 $-$ 4.47) are quite good for all the cases, and not surprisingly since the wave heights along this transect are used to obtain the input wave conditions for the model runs. On top of the shoal where the waves are breaking (Figures 4.48 $-$ 4.51), the predictions are not good, while along transect E-E (Figures 4.52 $-$ 4.55) the shapes of the distribution are predicted quite well with a slight overprediction of energy content. An explanation for this disparity is given in Section 4.3.3. An interesting thing to note is that the distribution is more

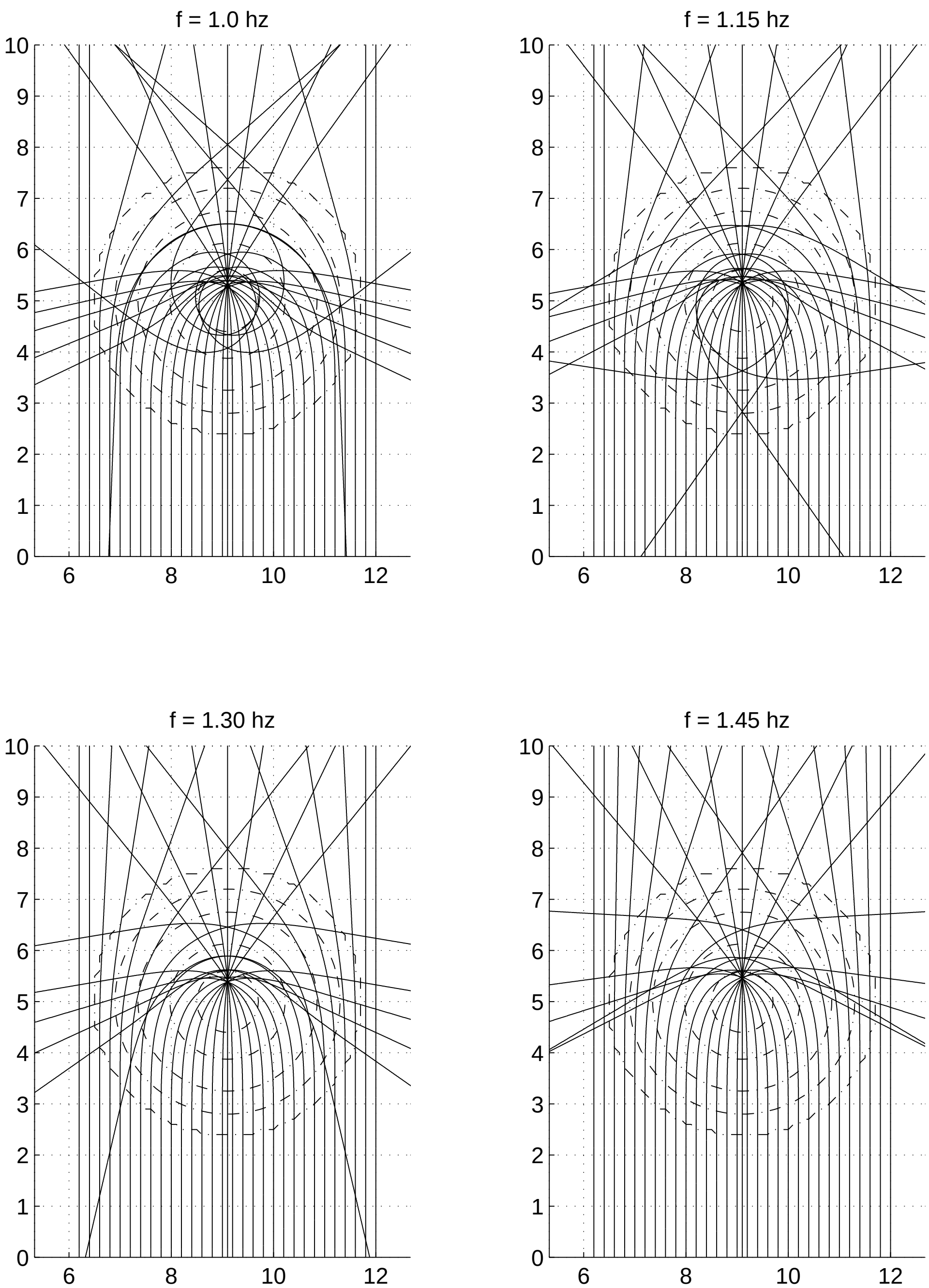

Figure 4.39: Wave ray diagram for bathymetry of irregular wave tests.

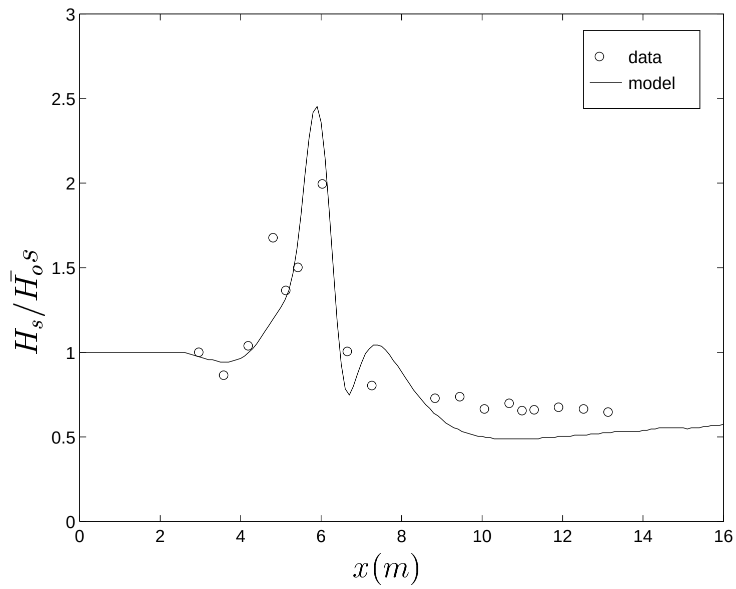

Figure 4.40: Data to model comparisons for irregular waves along transect A-A (Test 3).

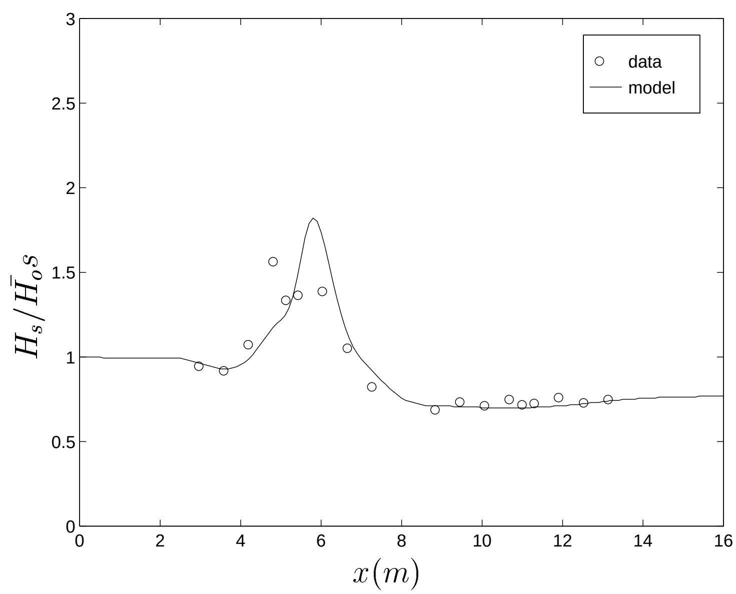

Figure 4.41: Data to model comparisons for irregular waves along transect A-A (Test 4).

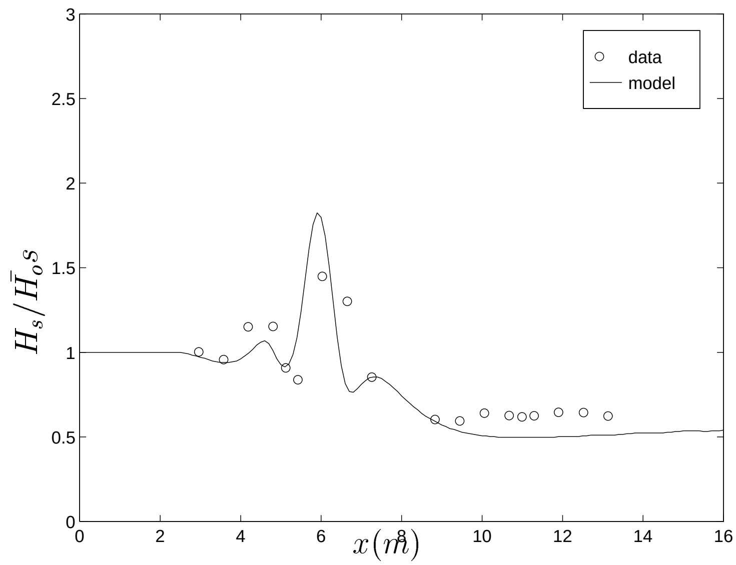

Figure 4.42: Data to model comparisons for irregular waves along transect A-A (Test 5).

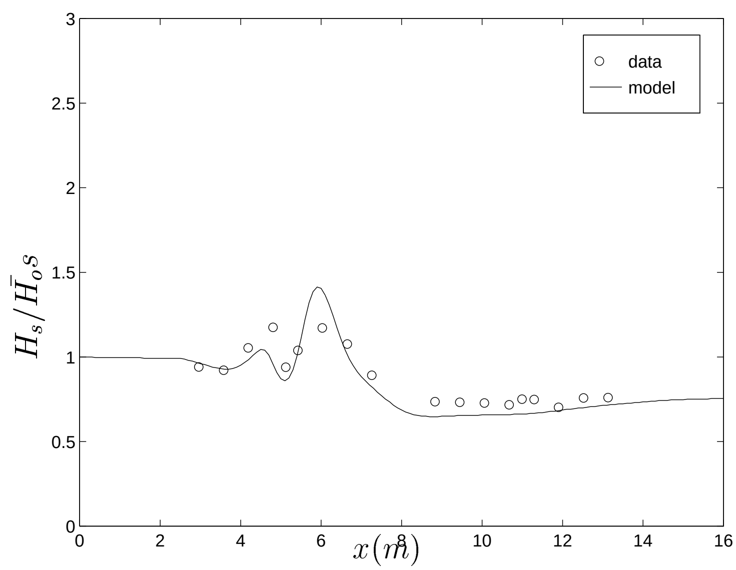

Figure 4.43: Data to model comparisons for irregular waves along transect A-A (Test 6).

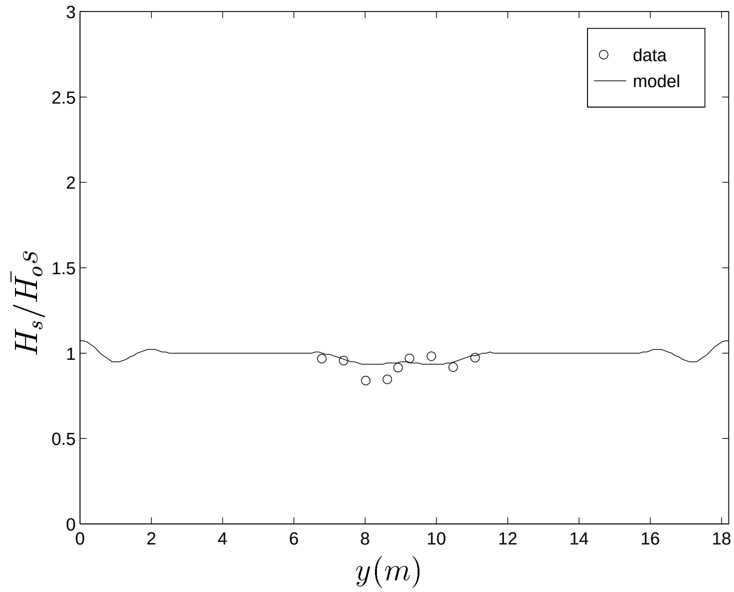

Figure 4.44: Data to model comparisons for irregular waves along transect G-G (Test 3).

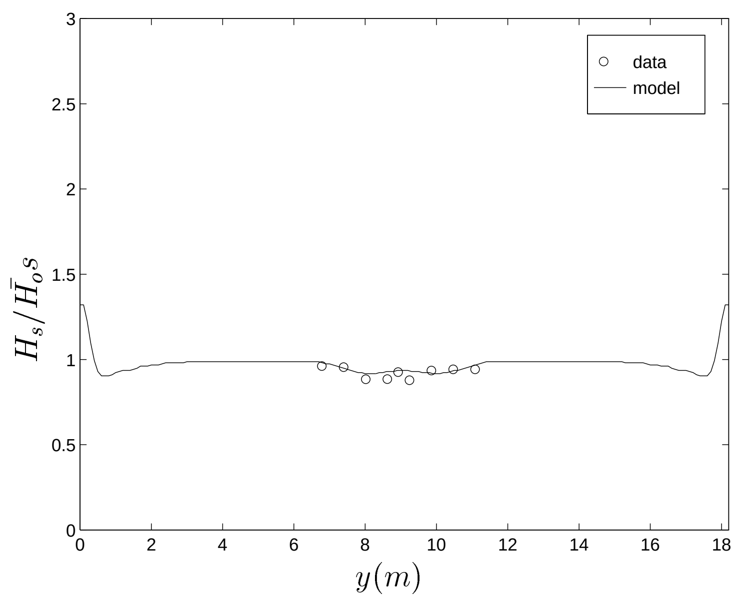

Figure 4.45: Data to model comparisons for irregular waves along transect G-G (Test 4).

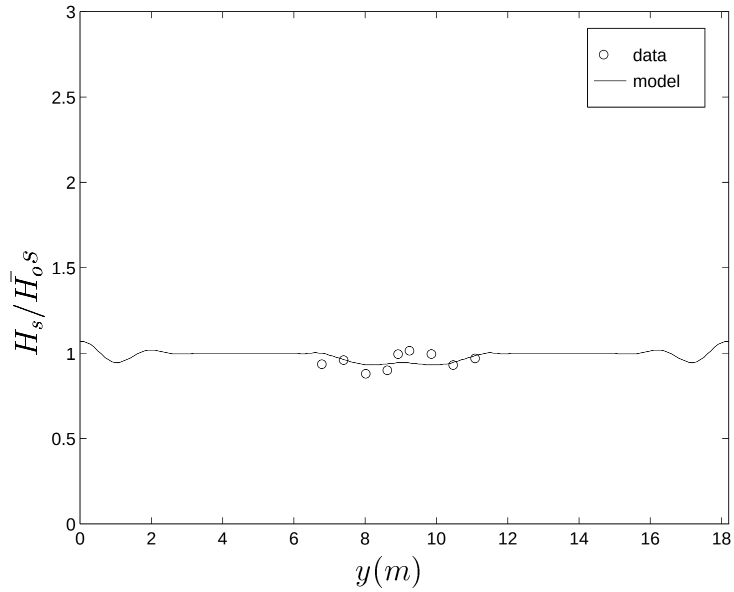

Figure 4.46: Data to model comparisons for irregular waves along transect G-G (Test 5).

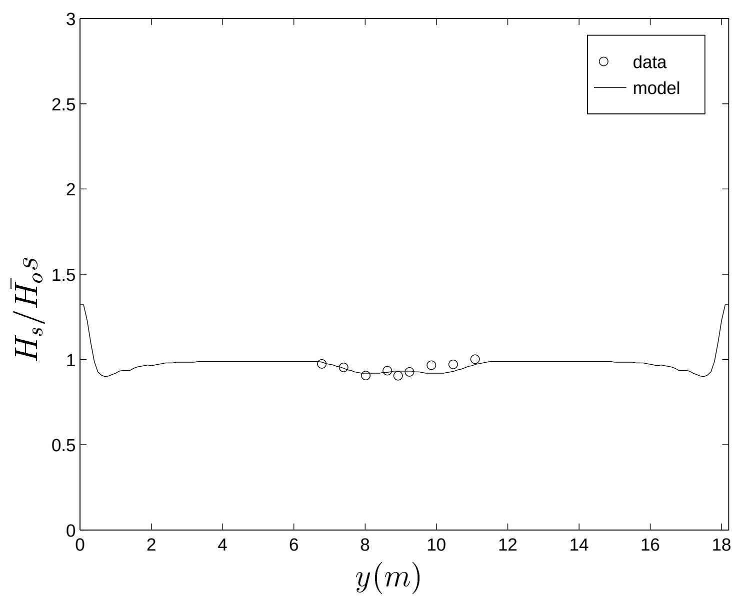

Figure 4.47: Data to model comparisons for irregular waves along transect G-G (Test 6).

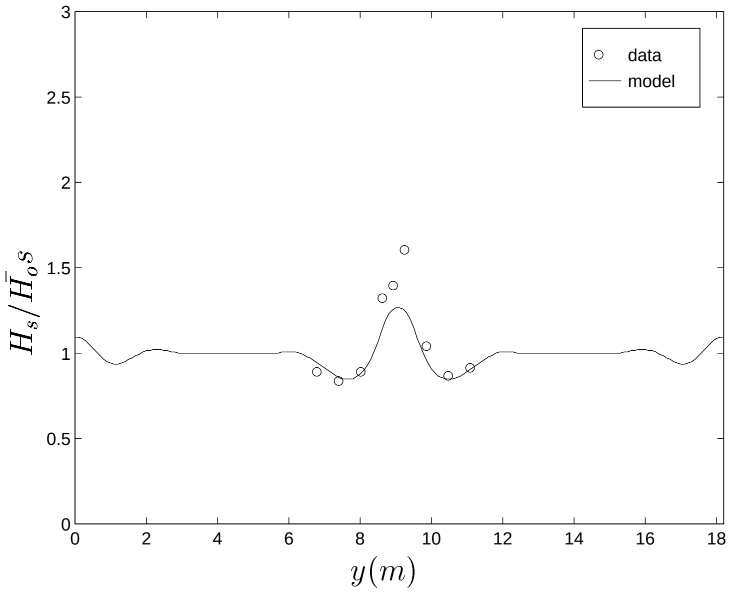

Figure 4.48: Data to model comparisons for irregular waves along transect F-F (Test 3).

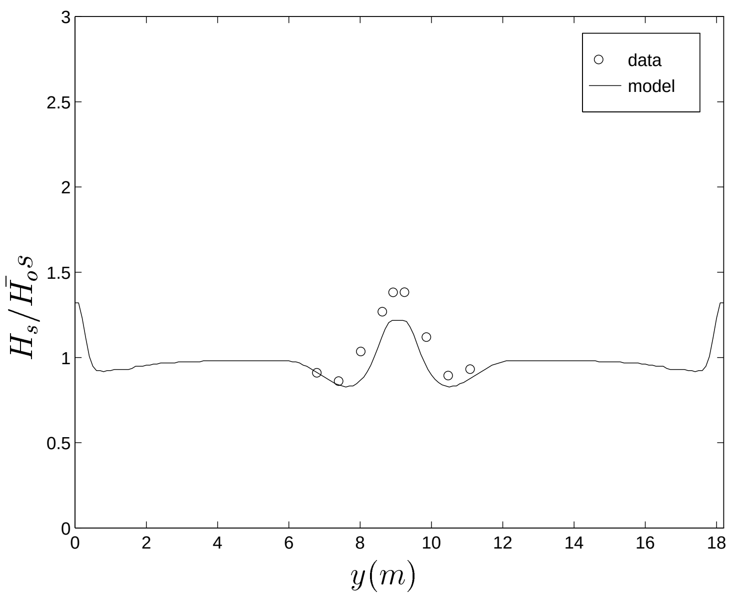

Figure 4.49: Data to model comparisons for irregular waves along transect F-F (Test 4).

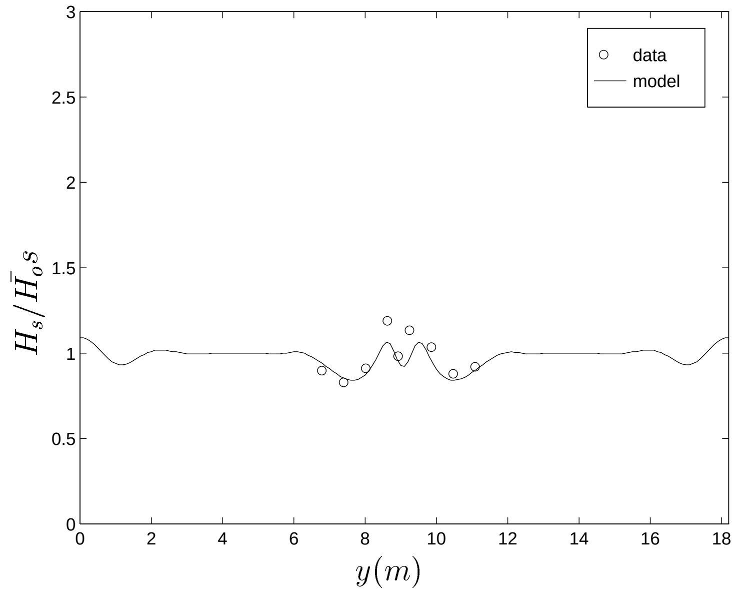

Figure 4.50: Data to model comparisons for irregular waves along transect F-F (Test 5).

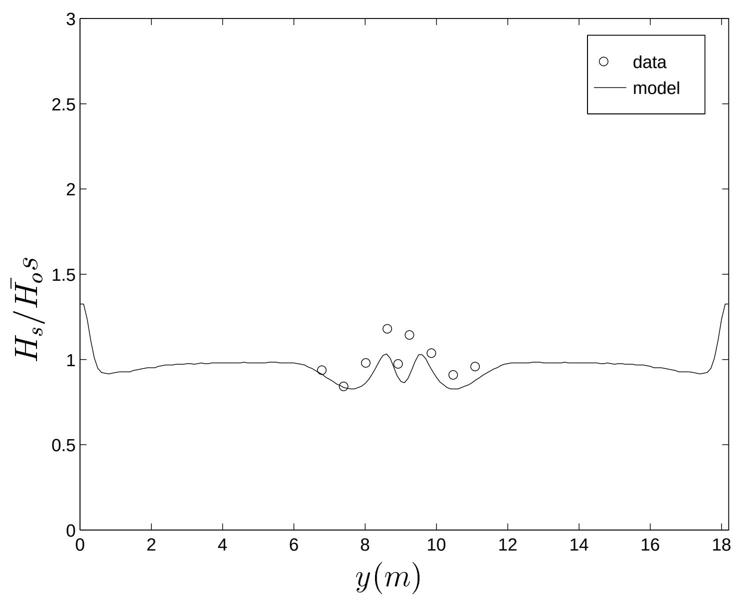

Figure 4.51: Data to model comparisons for irregular waves along transect F-F (Test 6).

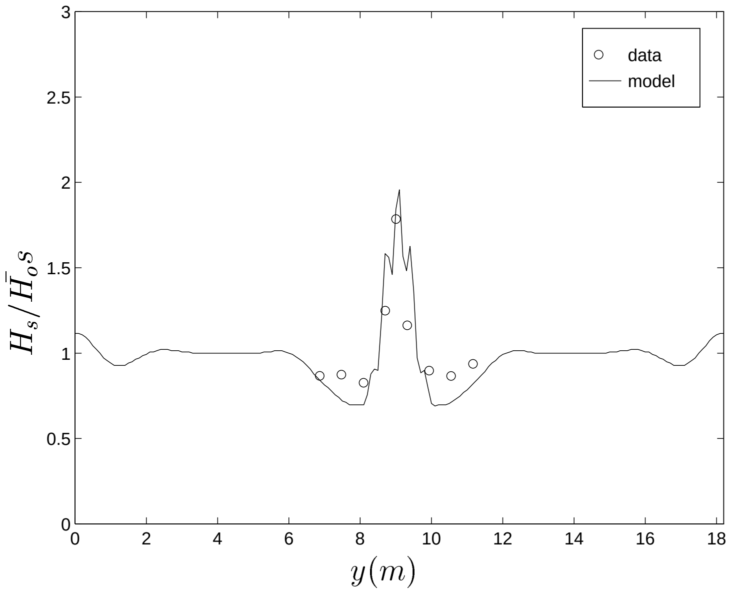

Figure 4.52: Data to model comparisons for irregular waves along transect E-E (Test 3).

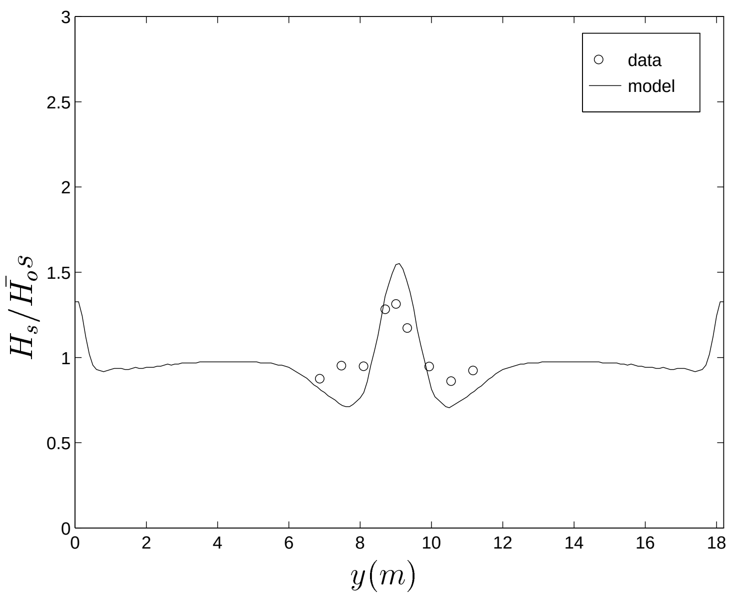

Figure 4.53: Data to model comparisons for irregular waves along transect E-E (Test 4).

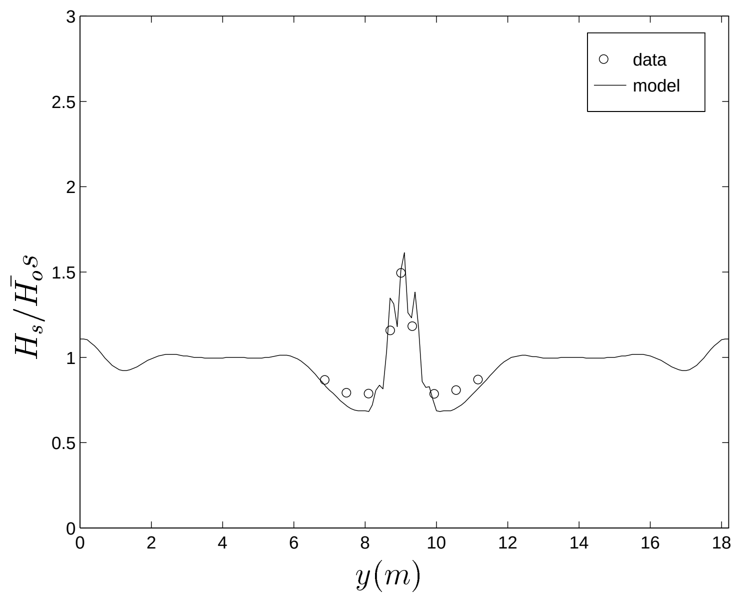

Figure 4.54: Data to model comparisons for irregular waves along transect E-E (Test 5).

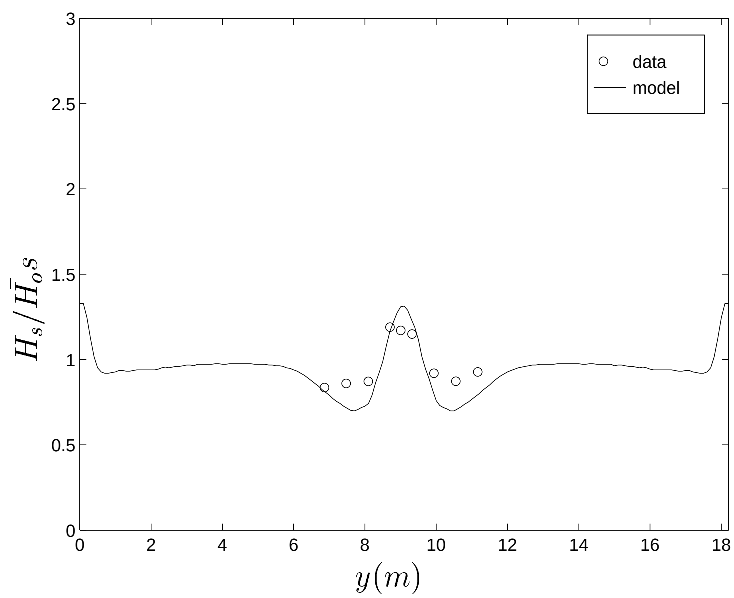

Figure 4.55: Data to model comparisons for irregular waves along transect E-E (Test 6).

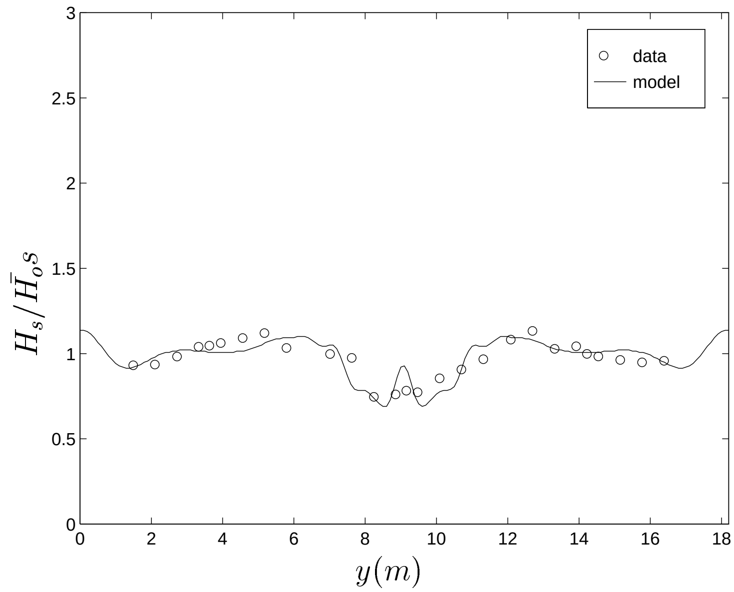

Figure 4.56: Data to model comparisons for irregular waves along transect D-D (Test 3).

smoothed out for the broad directional spectra (Figures 4.53 and 4.55), as compared to the peaky distribution for the narrow spectra (Figures 4.52 and 4.54). Thus the wave height distribution is more dependent on the kind of directional spectrum.

Comparisons behind the shoal are given in Figures 4.56 − 4.67, and the same smoothing can be seen for the broad directional spectra cases. The comparisons in this region show an excellent agreement between data and model, specially for the broad spectral cases. There is some disagreement along transect D-D, in the shadow of the shoal ($y = 7.5m$ to $y = 11.6m$), for the narrow directional distributions. Also from the model runs we find that the wave height distributions tend to be more uniformly spread for the broad directional spectra, than for the narrow ones.

4.3.3 Frequency spectra

One of the drawbacks of the **Ref/Dif S** model is that it is unable to model wave-wave interactions. In nature these interactions lead to the formation of higher

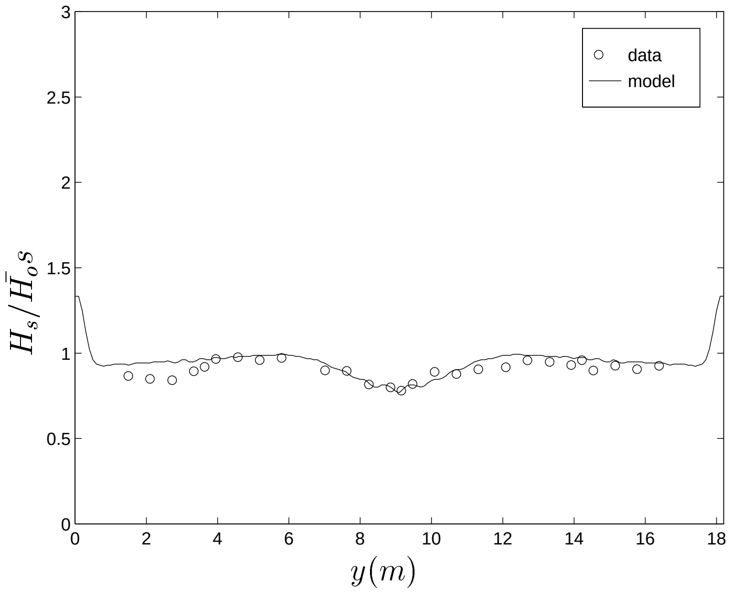

Figure 4.57: Data to model comparisons for irregular waves along transect D-D (Test 4).

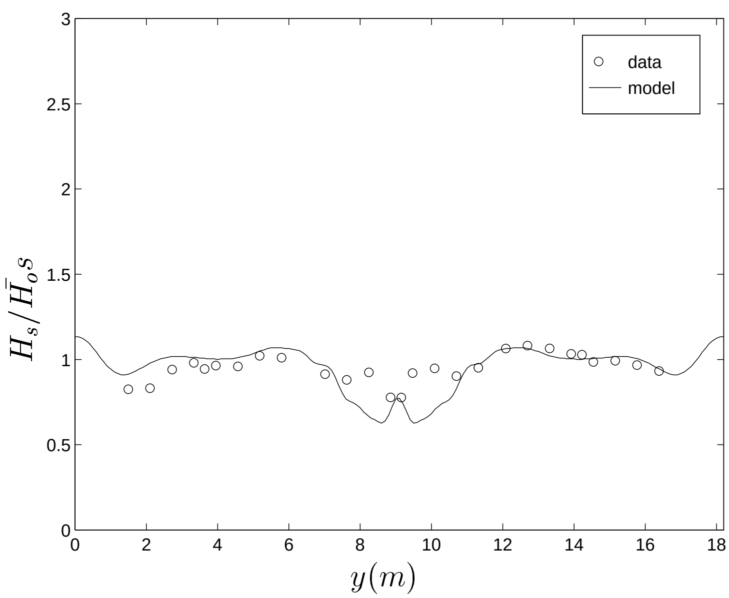

Figure 4.58: Data to model comparisons for irregular waves along transect D-D (Test 5).

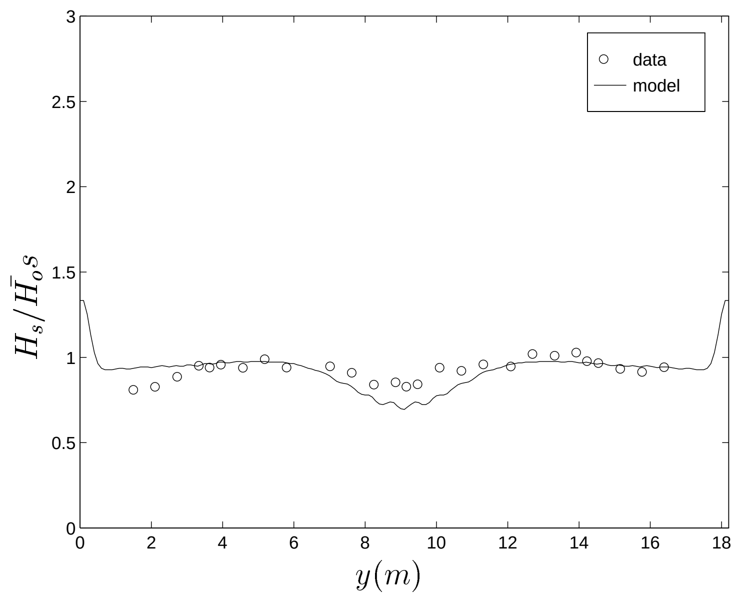

Figure 4.59: Data to model comparisons for irregular waves along transect D-D (Test 6).

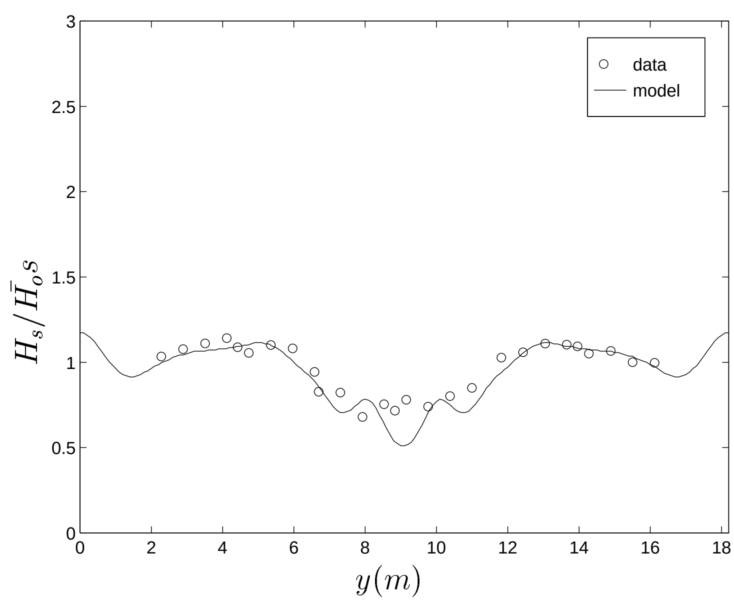

Figure 4.60: Data to model comparisons for irregular waves along transect C-C (Test 3).

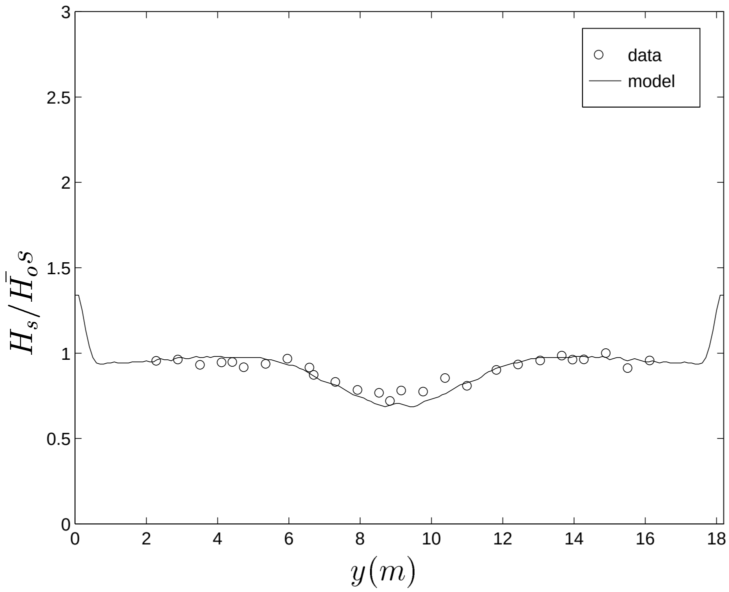

Figure 4.61: Data to model comparisons for irregular waves along transect C-C (Test 4).

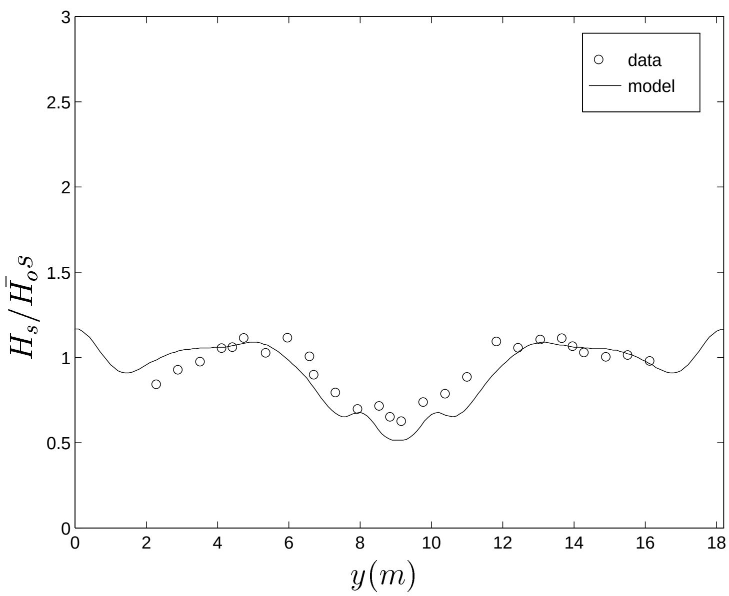

Figure 4.62: Data to model comparisons for irregular waves along transect C-C (Test 5).

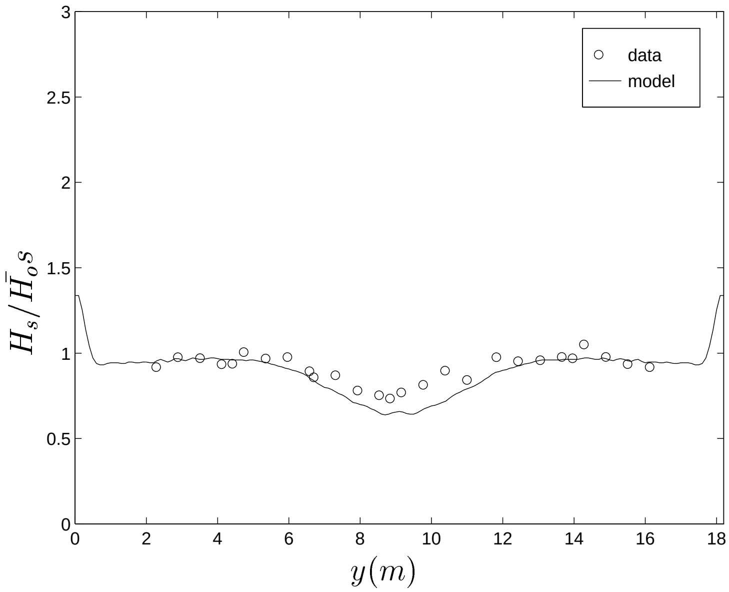

Figure 4.63: Data to model comparisons for irregular waves along transect C-C (Test 6).

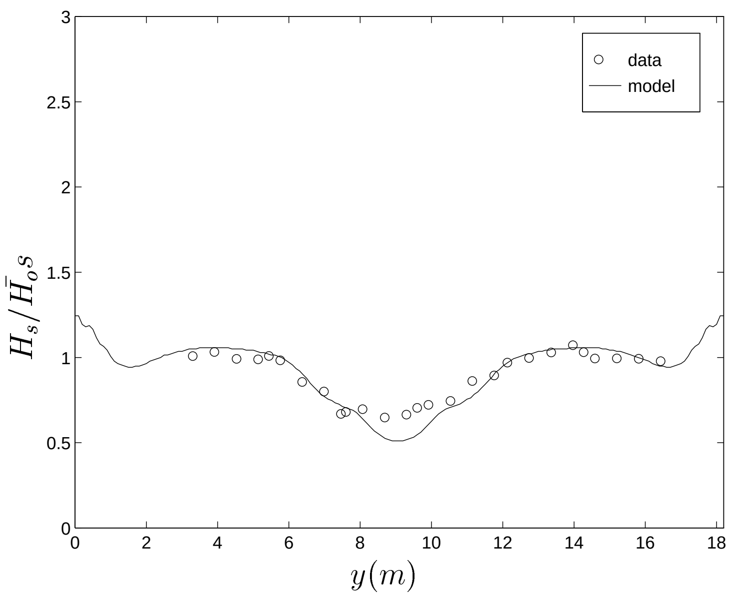

Figure 4.64: Data to model comparisons for irregular waves along transect B-B (Test 3).

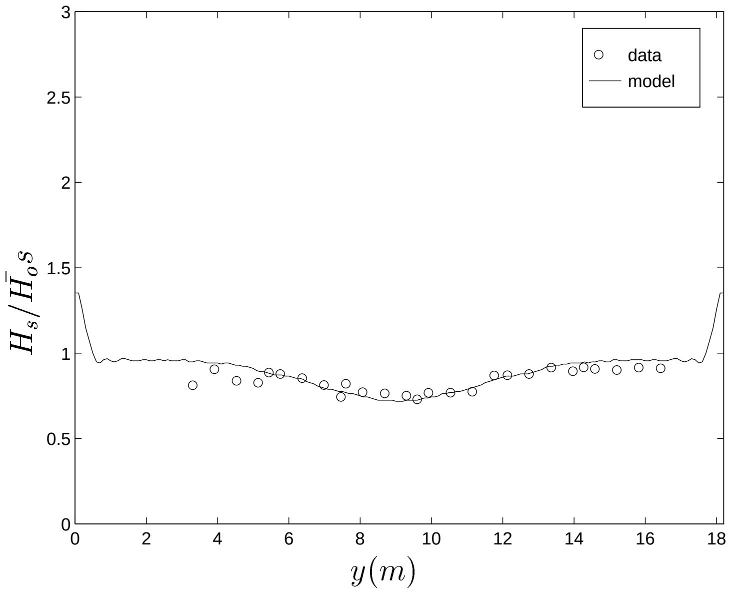

Figure 4.65: Data to model comparisons for irregular waves along transect B-B (Test 4).

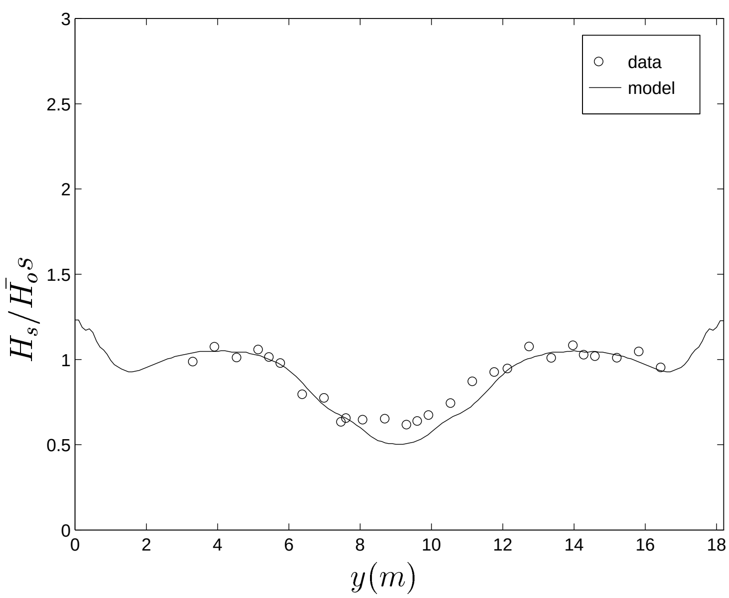

Figure 4.66: Data to model comparisons for irregular waves along transect B-B (Test 5).

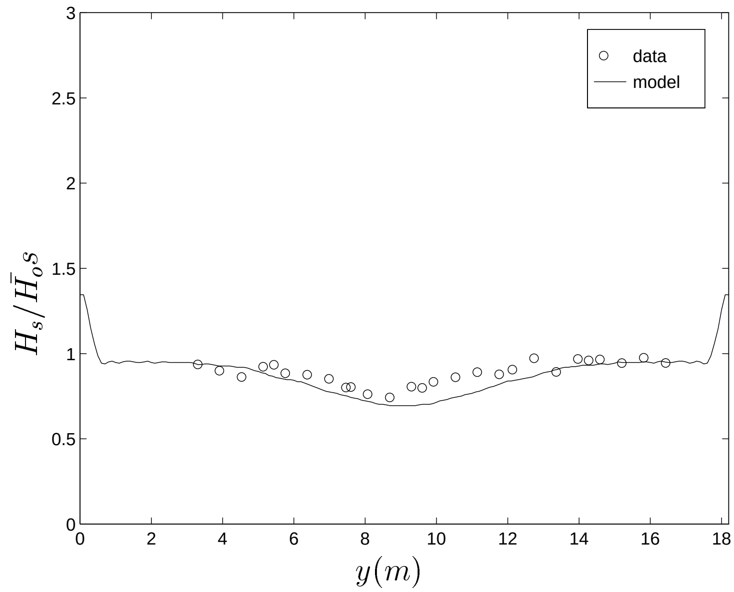

Figure 4.67: Data to model comparisons for irregular waves along transect B-B (Test 6).

harmonics, which grow with increasing nonlinearity in the wave field. A comparison of frequency spectra on top of the shoal (the wave field being highly nonlinear here), shows this disparity very clearly (Figure 4.68). The higher harmonics (second peak) in the data have almost as much energy as the primary wave field, and thus cannot be ignored. The inability of the model to predict these interactions are an important reason why comparisons around the top of the shoal and in the surf zone are not so good. A fairly good picture of the growth and development of these higher harmonics can be obtained from the frequency spectra plots of the data given in Appendix D.

4.3.4 Angle distributions

All mention that is made of directional spectral distribution in this section refer to the spectra obtained from the model, since as stated earlier no angle estimates can be made from the data.

For all the four spectral tests, the directional spectrum initially has a mean

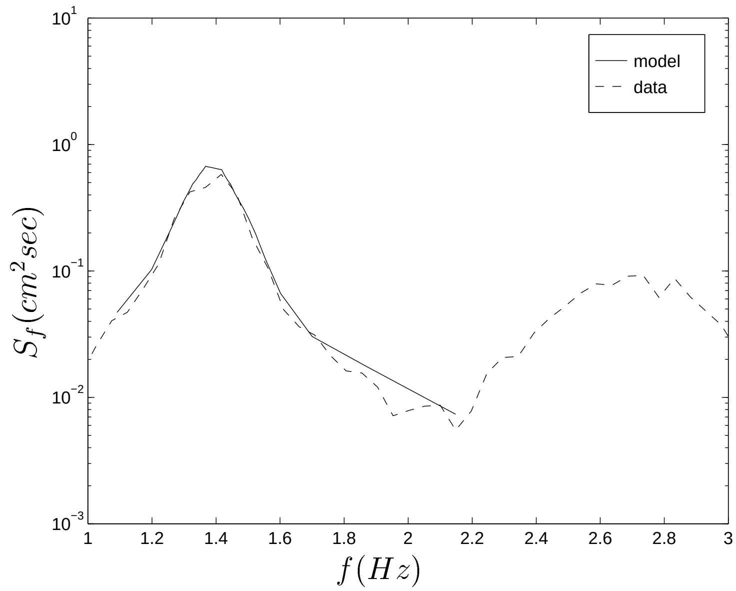

Figure 4.68: Spectrum comparison on top of the shoal (position 13, gage 5) for Test 3.

angle normal to the wavemaker ($\theta_m = 0°$). Thus, the average angle (given by eqn. (2.10)) should be 0° everywhere if the shoal is not present. Due to refraction effects from the shoal, the average angle deviates from 0°, and a plot of that, together with the gage array locations, shows this effect (Figure 4.69). A similar pattern was found for all four cases, showing that the average angle distribution does not depend on either the energy in the spectrum or the directional spreading of the spectrum.

The average angle refers to the mean angle of the directional spectrum, and thus, as the mean angle shifts so does the spectrum. When the average angles from both sides of the shoal cross each other, as is seen along transect E-E (behind the top of the shoal), there is a superposition of two different directional spectra leading to a very complicated spectrum (Figure 4.71), as compared to the relatively clean spectrum on top of the shoal (Figure 4.70).

The directional spectra plots for the four cases are given in Appendix E. The mean angle reaches a maximum value of ±30°, which means that for a broad

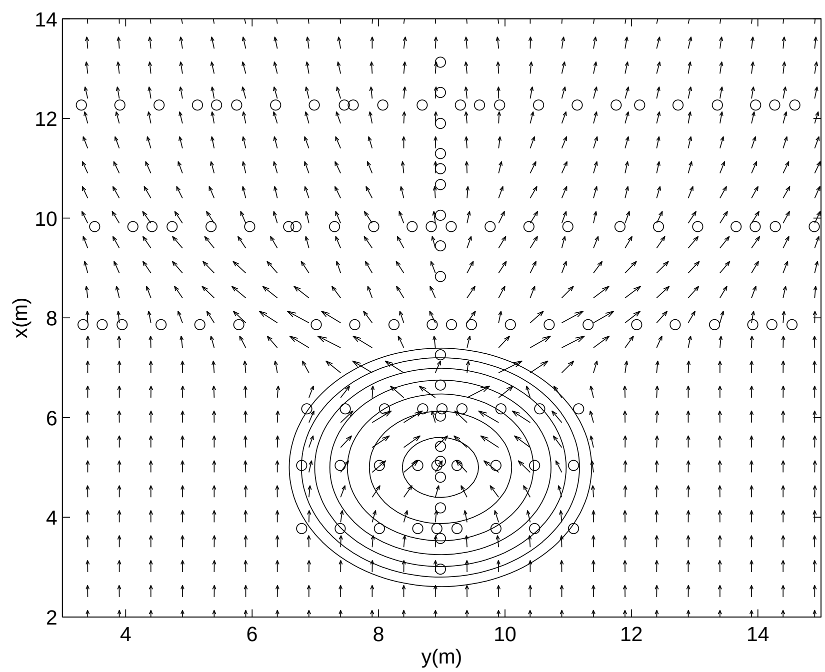

Figure 4.69: Mean angle distribution with gage locations ('o') for irregular spectra.

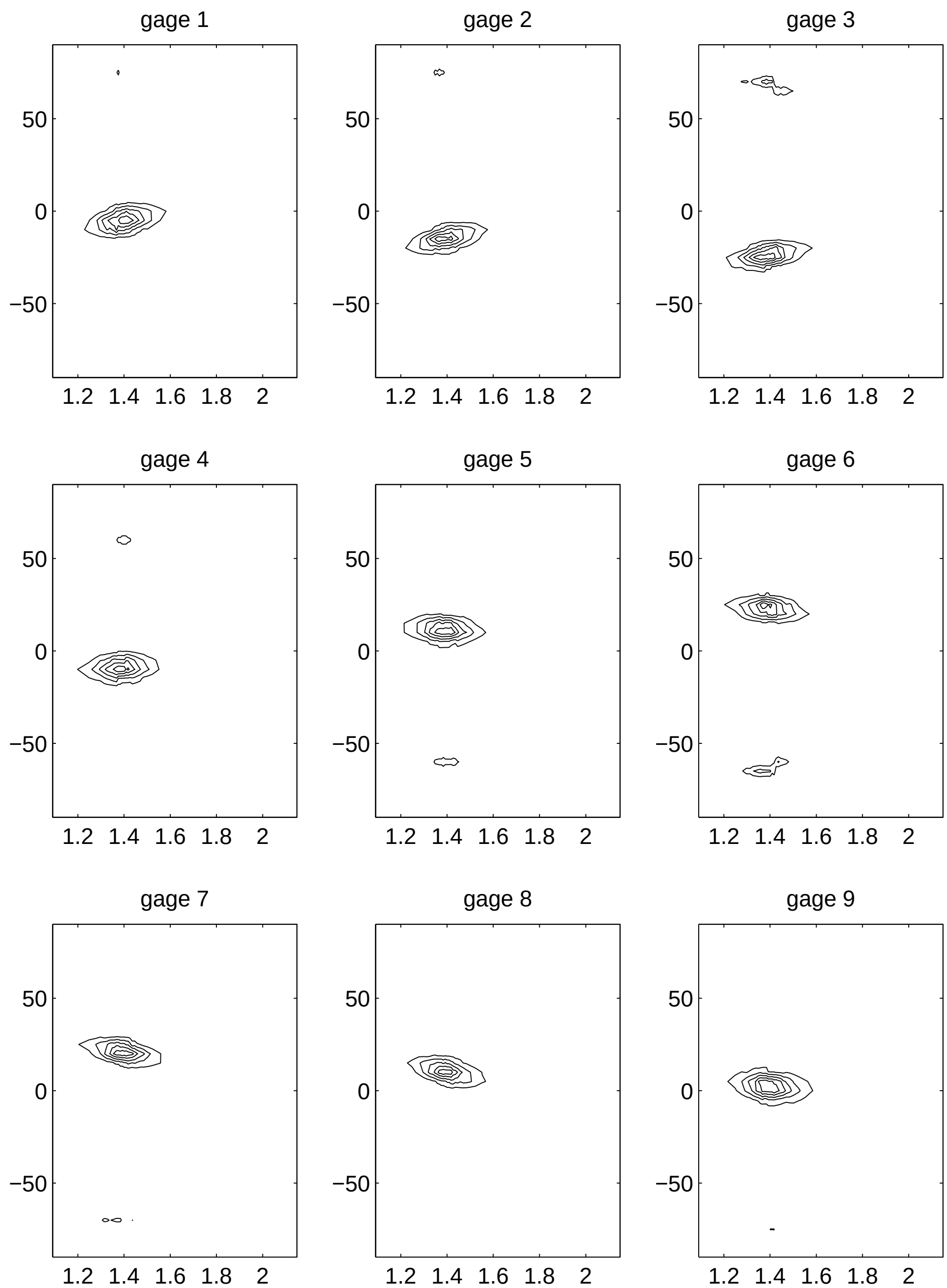

Figure 4.70: Directional spectra for Test 3 along transect F-F.

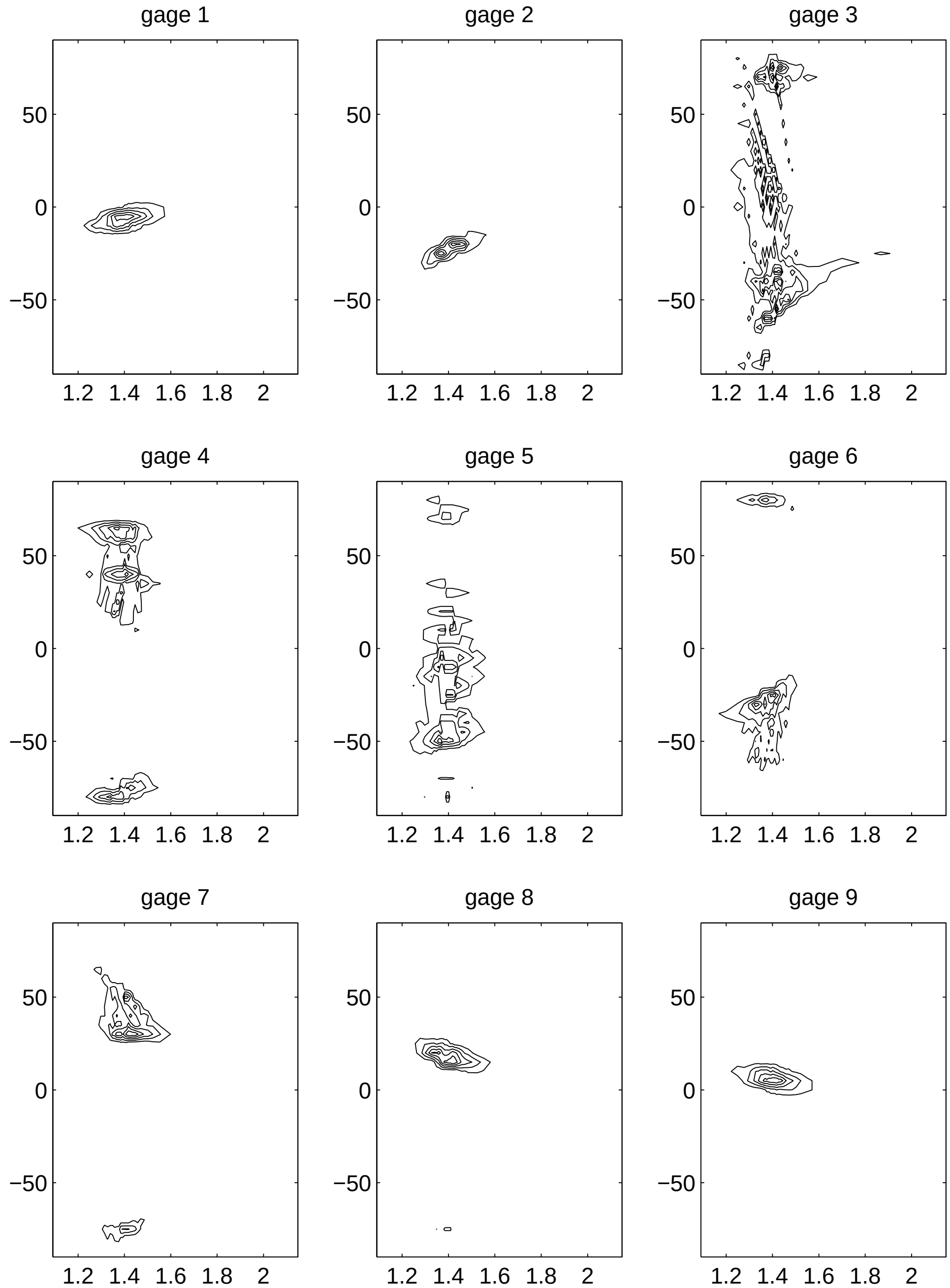

Figure 4.71: Directional spectra for Test 3 along transect E-E.

spectrum, there are waves moving at angles of $\pm 75°$, which is much beyond the stated limits of the model (see Chapter 2). The excellent data to model comparisons even with waves of such large angles shows that the model works very well even for large directional spreadings.

Chapter 5

CONCLUSIONS AND SUGGESTIONS

The aim of this report has been to study the effects of refraction and diffraction on waves transforming over a submerged shoal. Numerical modeling has been accompanied by an extensive experimental study. The work has concentrated on two types of wave conditions, nonbreaking monochromatic waves propagating normal to the wavemaker, and irregular waves with directional spreading. Numerical analysis has been carried out with the help of two weakly nonlinear large-angle parabolic models. **Ref/Dif 1** is the monochromatic model, while **Ref/Dif S** is the spectral model.

For the monochromatic tests, the model was run for two different dispersion relations, a linear dispersion and a nonlinear (Stokes) dispersion. Comparisons with data have shown that the Stokes dispersion works much better in predicting the wave heights at the point of focus and after that, while the linear dispersion gives better results in the regions before focus. The initial discrepancy between the Stokes dispersion model and the data could be due to the failure of the approximate equations to focus rapidly enough (Kirby and Dalrymple, 1984). The comparisons though reasonably good were not as good as the results obtained by Kirby and Dalrymple (1984), when they tested the model with the data of Berkhoff *et al.* (1982). This is due to two reasons. The focusing in these experiments is very rapid, with a lot of variations in the wave height distributions. The numerical models are limited to $\theta = \pm 45°$, and are unable to predict waves moving at larger angles. Also depth sensitivity test shows that the peaks in the wave height distribution change with slight changes in the water depth, and since the water depth was not monitored very accurately, some discrepancy exists between the data and model results. It remains to be seen wether the discrepancies in the data are due to experimental errors, or if a model with no limitation on the range of angles will be able to make better predictions of the wave height distributions.

Model comparisons with the irregular wave data gave excellent results. The wave height distribution behind the shoal is much more smoothed out as compared to the monochromatic wave field, with the smoothing increasing with increasing directional spreading. The wave height distribution behind the shoal is more a function of the directional spread of the input wave condition, rather than a function of the energy content. Around the top of the shoal the model to data comparisons are not very good. The drawback of the model has been its inability to handle wave-wave interactions. In the cases of highly nonlinear wave fields, such as the ones tested in the experiments, these interactions become important, leading to the formation of higher harmonics with about as much energy as the peak frequency. Studies of the frequency spectrum has shown the presence of such harmonics in the data, which the model has been unable to reproduce. This is a big factor responsible for any disparity between the data and the model. The advantage of using a spectral distribution method, such as the one that has been used here in the spectral model, is that a sea spectrum can be simulated quite accurately with considerable ease. Such a method cannot be used to determine wave-wave interactions, and it will be interesting to see how a model, capable of simulating such a phenomenon will compare with the data.

At first look it may seem a little surprising that the monochromatic wave results are not as good as the irregular spectral wave results, even though the spectral waves are breaking on top of the shoal. But it must be kept in mind that in the case of the spectral waves a lot of averaging is taking place, which smoothes the wave height distribution and hides a lot of errors, while for the monochromatic cases there is a lot of variation in the distribution. Infact considering the rapid focusing on top of the shoal, the monochromatic model actually performs quite well. Thus, we find that due to the tendency of the waves to smooth out the wave height distributions in random directional seas, wave height predictions in these cases tend to be quite accurate, even if the counterpart monochromatic models do not fare so well. This is quite important since in nature waves are irregular, and being able to simulate them accurately is very helpful. Another important point to note is that the monochromatic wave field after focusing looks very different from an irregular spectral wave field, and thus, approximating a spectral wave field by a monochromatic wave field would lead to incorrect results.

REFERENCES

Berkhoff, J.C.W. (1972) "Computation of combined refraction diffraction", *Proceedings of the* 13^{th} *International Coastal Engineering Conference*, ASCE, Vancouver

Berkhoff, J.C.W., Booij, N and Radder, A.C. (1982) "Verification of numerical wave propagation models for simple harmonic linear water waves", *Coastal Engineering*, 6, pp 255-279

Booij, N. (1981) "Gravity waves on water with non uniform depth and current", *Communication on Hydraulics*, Dept. of Civil Engrg., Delft University of Technology, Netherlands, Report No. 81-1

Booij, N. (1983) "A note on the accuracy of the mild slope equation", *Coastal Engineering*, 7, pp 191-203

Borgman, L.E. (1984) "Directional spectrum estimation for the S_{xy} gages", *Technical Report*, Coastal Engrg. Res. Center, Vicksburg, 1-104

Bouws, E. and Battjes, J.A. (1982) "A monte carlo approach to the computation of refraction of water waves", *J. Geophys. Res.*, 87 (8), pp 5718-5722

Bouws, E., Gunther, H., Rosenthal, W. and Vincent, C. (1985) "Similarity of the wind wave spectrum in finite depth water", *J. Geophys. Res.*, 90(C1), 975-986

Dean, R.G. and Dalrymple, R.A. (1991) "Water wave mechanics for Engineers and Scientists", *World Scientific*, New Jersey

Hedges, T.S. (1976) "An empirical modification to linear wave theory", *Proc Inst Civ Engrg*, Part 2, 612, pp 575-579

Karpman, V.I. (1975) "Nonlinear waves in dispersive media", *Pergamon press*, New York

Kirby, J.T. (1984) “A note on linear surface wave-current interaction over slowly varying topography”, *J. Geophys. Res.*, 89, pp 745-747

Kirby, J.T. (1986a) “Higher-order approximations in the parabolic equation for water waves”, *J. Geophys. Res.* , 91, pp 933-952

Kirby, J.T. (1986b) “Rational approximations in the parabolic equation method for water waves”, *Coastal Engineering* , 10, pp 355-378

Kirby, J.T. and Dalrymple, R.A. (1983) “A parabolic equation for combined refraction diffraction of stokes waves by mildly varying topography”, *J. Fluid Mech (1983)*, vol 136, pp 453-466

Kirby, J.T. and Dalrymple, R.A. (1984) “A verification of a parabolic equationfor propagation of weakly nonlinear waves”, *Coastal Engineering*, 8, pp 219-221

Kirby, J.T. and Dalrymple, R.A. (1986a) “Modelling waves in surf zones and around islands”, *J. Waterways, Port, Coastal and Ocean Engrg.*, 112(1), pp 78-93

Kirby, J.T. and Dalrymple, R.A. (1986b) “An approximate model for nonlinear dispersion in monochromatic wave propagation models”, *Coastal Engineering* , 9, pp 545-561

Kirby, J.T. and Dalrymple, R.A. (1993) “Combined Refraction/Diffraction model”, *Documentation and User's Manual*, Dept. of Civil Engrg., University of Delaware, Report no. CACR-92-04

Kirby, J.T. and Özkan, T.H. (1994) “Combined Refraction/Diffraction model for spectral wave conditions”, *Documentation and User's Manual*, Dept. of Civil Engrg., University of Delaware, Report no. CACR-92-06

Leontovich, M.A. and Fock, V.A. (1965) “Solution of the problem of propagation of electromagnetic waves along the earth's surface by the method of parabolic equations”, *Electromagentic diffraction and propagation problems, Pergamon press*, New York

Liu, P.L.F. (1986a) “Viscous effects on the evolution of Stokes waves”, *J. Waterways, Port, Coastal and Ocean Engrg.*, 112(1), pp 55-63

Liu, P.L.F. (1990) “Wave Transformation”, *The Sea, vol 9 part A, John Wiley and Sons inc*, New York, pp 27-63

Mei, C.C. (1992) “The Applied Dynamics of Ocean Surface Waves”, *World Scientific*, New Jersey

Ozkan, H.T. and Kirby, J.T. (1993) “Evolution of breaking directional spectral waves in the nearshore zone”, *Proceedings of the Second International Symposium*, New Orleans, pp 849-863

Panchang, V.G., Wei, G., Pearce, B.R. and Briggs, M.J. (1990) “Numerical simulation of irregular wave propagation over shoal”, *J. Waterways, Port, Coastal and Ocean Engrg.*, 116, pp 324-340

Radder, A.C. (1979) “On the parabolic equation method for water wave propagation”, *J. Fluid Mech (1979)*, vol 95, part 1, pp 159-176

Thornton, E.B. and Guza, R.T. (1983) “Transformations of wave height distribution”, *J. Geophys. Res.*, 88, pp 5925-5938

Vincent, C.L. and Briggs, M.J. (1989) “Refraction-diffraction of irregular waves over a mound”, *J. Waterways, Port, Coastal and Ocean Engrg.*, 115(2), pp 269-284

Wilmott, C.J. (1981) “On the validation of models”, *Physical Geography*, 2(2), pp 219-232

Yue, D.K.P. and Mei, C.C. (1980) “Forward diffraction of stokes waves by a thin wedge”, *J. Fluid Mech (1980)*, vol 99, pp 33-52

Appendix A

PROGRAM DESCRIPTIONS

During the entire experimentation four different programs were used. These were **Deswave_keep** to obtain the paddle stroke time series for the desired wave field, **Waves** to actually control the wavemaker and make the paddles move, **Gcal1** to calibrate the gages between gage runs, and **Take_data** to collect data during gage runs. Of these four programs, **Waves** was written in **C**, while the other three were written in **FORTRAN**. A Concurrent 7200 system has been used to control the wavemaker and obtain data from the gages. In this appendix a brief outline of each of these programs has been given.

A.1 Paddle time series

Deswave_keep is the designer wavemaker program which converts the specified wave field into the time series of the paddles based on the theory given in Section 3.2.2. The mathematical model given by eqn(3.16), theoretically requires the modes to be summed to infinity, but in reality summation need be done only till

$$k^2 \geq \lambda_n^2$$

. Beyond that the modes become evanescent and exponentially decay away from the paddles. **Deswave_keep** sums up to a maximum limit of 100 modes, which can be changed.

The theory has been developed for monochromatic progressive waves, but a paddle stroke time series for a spectral sea can also be obtained. The desired spectra is broken down into separate bins, and each bin is represented by a monochromatic wave. Based on the wave height and angle for each monochromatic wave, **Deswave_keep** then determines a paddle stroke frequency spectrum for each paddle , which is inverse transformed to obtain the paddle stroke time series. For the irregular tests a spectral sea state was obtained by using the directional spreading function given by eqn (4.5) (Borgman, 1984) for direction, and a TMA spreading function for frequency (Bouws *et al.*, 1985), given by

$$\begin{aligned} E(f,h) &= \alpha g^2 (2\pi)^{-4} f^{-5} \exp(-5/4(f/f_p)^{-4}) \\ &\exp\left[\ln(\gamma)\exp(-(f-f_p)^2/2\sigma^2 f_p^2)\right]\Phi(\omega) \end{aligned} \tag{A.1}$$

where f_p is the peak frequency, ω the angular frequency is

$$\omega = 2\pi f,$$

α is a linear constant which can be scaled to obtain the desired variance, γ is a factor which determines how broad the spectrum is (for our experiments we have taken $\gamma = 10$), σ depends on the frequency f

$$\sigma = \begin{cases} 0.07 & f \le f_p \\ 0.09 & f \ge f_p \end{cases}$$

and Φ is given by

$$\Phi = \begin{cases} 0.5\omega^2 & \omega \le 1 \\ 1.0 & \omega \ge 2 \\ 1 - 0.5(2-\omega)^2 & \text{otherwise} \end{cases}$$

It should be noted that for model simulations by **Ref/Dif S**, the input directional spectrum was obtained by using the same directional spreading function (eqn. (4.5

)), while the frequency spread was determined from the data, and not from the TMA function used to describe the desired wave field in eqn (A.1). The assumption here is that due to energy losses in the basin (see Chapter 3), the actual wave field obtained by the wavemaker may differ in energy characteristics from the desired wave field, the directionality is reproduced exactly. This is an important assumption, and though seems quite reasonable, extensive tests need to be carried out with the wavemaker to check if this is really true.

Input to **Deswave_keep** is specified in an **indat.dat** file in the form of the number of waves and the characteristics of each wave (the period, amplitude, angle and the phase). Apart from the input via **indat.dat**, the user specifies the following input online to **Deswave_keep**

- the name of the file in which paddle time series is to be saved,
- the water depth in cm,
- distance from the paddles where a uniform wave field across the basin is desired, specified by the variable X_m(this is important only for oblique waves),
- the desired time step for the paddle series, and,
- the corresponding length of the time series.

The paddles have been calibrated to obtain the voltage to displacement response curve. The response curve was found to be linear, and the slope of each paddle response curve was noted in a file called **gain.dat** . **Deswave_keep** uses this gain information to determine the time series of the paddle displacement in voltages, which can then be sent to the motor controls. The paddles have a physical limit of ±6.5 volts, and any signal that exceeds it is physically cut off to this value, with a warning by **Deswave_keep**

An error was noted in the **Deswave_keep** program during data analysis. Due to a bug, whenever the number of modes over which the paddle displacements are summed over exceeded the maximum limit before the evanescent modes, the paddle stroke contribution at that frequency was set to zero. Thus, all the high frequency contributions beyond a particular frequency were cut off. This resulted in the irregular wave trains having a very narrow frequency spectrum, and thus being very groupy. This bug was unfortunately not noticed earlier, because the testing of the program was done at a lower frequency, where the maximum limit of the number of modes was not reached. The bug was later removed and Figure A.1 compares the power spectra of the paddle time series, both before the bug was removed, and after the bug was removed, to the desired power spectra. Since the bug was removed after the spectra tests were completed, another set of irregular spectral wave experiments had to be conducted. Thus, there are two sets of spectral experiments, one with a peaky frequency spectrum, and the other with a broader frequency spectrum.

A.2 Instrumentation

Once the time series has been created, the signals have to be sent to the paddles at the required frequency to obtain the desired paddle motion. As has already been mentioned in Section 3.2.1 the paddle motions are controlled by the help of servo controller motors. Each paddle has its own servo controller with a feedback mechanism, such that each paddle can be moved independent of the other. The feedback mechanism ensures that the servo controller motor moves to the desired voltage before the next signal arrives. The motors run on analog signals, and it is thus necessary to convert the digital time series to an analog signal. This is done with the help of 3 16-channel D/A boards (VMIVME 4100), that are mounted on the Concurrent 7200 computer system. As the name suggests these boards convert the digital signals to the analog signals and then feed them to the Servo controller motors at the desired frequency. The Concurrent 7200 computer system, which is a data

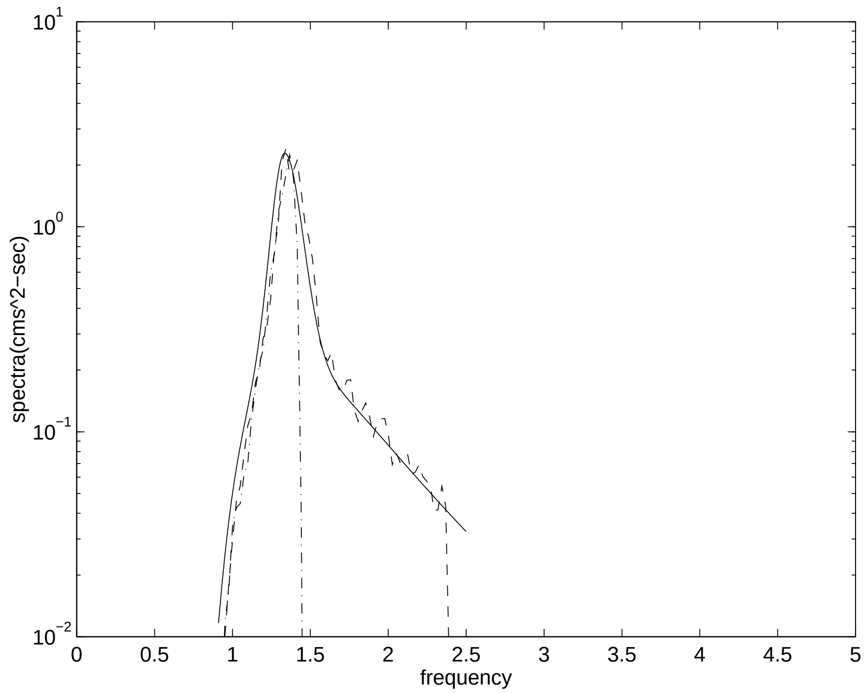

Figure A.1: Comparison between desired spectra (-), old spectra (-.) and new spectra (- -).

acquisition device has 4 D/A channels of its own, but since the number of paddles far exceeds this, the VMIVME 4100 boards had to be installed. These boards do not have an internal clock of their own, and use one of the D/A clocks of the computer system. There are a total of 48 D/A channels, but only 34 paddles. Thus, the last 14 channels are physically sent a zero signal. This facility is incorporated in **Deswave_keep** when it is creating the data file for the paddle time series.

A program called **Waves** provides a simple user interface with the D/A boards. **Waves** reads the time series data from a data file, sorts it and sends the time series of each paddle to the respective channels on the D/A boards. The D/A boards then convert these signals and sends them to the paddles at the frequency specified by **Waves**. **Waves** also ramps up the signal, so that the paddles are not subjected to large motions at cold start. This reduces the load acting on the paddles quite considerably, and consequently, the mechanical wear and tear over the long run. There is also an option by which, the user can either make **Waves** cycle through the data file and thus send a periodic signal to the D/A boards, or can make it stop at reaching the end of the data file. The format for running **Waves** is as follows

Waves *file_name mode frequency amplifier*

file_name Name of the data file created by **Deswave_keep**, containing the time series for each individual paddle.

mode This can either be *one_shot* (the program goes through the data file once and stops) or *cycle* (the program continues to cycle through the data file indefinitely).

frequency The required frequency at which the signals have to be sent to the Servo Controller motors. The system is designed to run at around 300 Hz, but can run as well at higher or lower frequencies. Below 50 Hz the waiting period between two signals is too high, leading to discrete paddle motions, while close to 1000 Hz the system is unable to keep pace. The frequency specified is equal to the inverse of the time step specified in **Deswave_keep** for generating the paddle time series.

amplifier This is an optional multiplication factor that can be specified. It must always be greater than 0 and has a default value of 1.

The **Waves** program can be killed by pressing 'CTRL - C'. This terminates the signal being sent to the D/A boards, and consequently the motors come to a stop. The motors can then be brought back to their zero volts position, by sending a zero data file, via **Waves**.

A.3 Data Collection

Data collection from the gages is done by the same Concurrent 7200 computer system, that sends out a time series signal to the wavemaker motors. In this case, the intent is to convert the analog signals coming from the gages, to digital signals and store them in data files.

The Concurrent system contains eighty A/D channels, numbered from 0 to 79. Channel 0 to 15 are the AD12V26 A/D convertor channels, while channels 16 to 79 are the SH12V26 Sample and Hold channels. The main difference between the A/D converter channels and the Sample and Hold channels is that, the Sample and Hold channels can collect data from all the gages at the same instant in time. Thus, data collection is always at the same time step in all the gages. Due to this major advantage, the Sample and Hold channels have been used for all the data collection in these experiments.

A Fortran program called **Take_data** provides an interface for the user to interact with the A/D channels. Via the program, the user tells the computer how many data points to be sampled per gage, the sampling frequency, the number of gages, and the channel number at which data collection is done for the first gage. (The program assumes that all the other gages will be connected in increasing order to successive channels, so care must be taken to ensure that). In the beginning of the source code for **Take_data** there are two parameter statements, **'MAXIMUM'** and **'WAIT_TIME'**. These specify the maximum number of points the program will allow for sampling, and the total waiting time for the sampling, respectively. The two things that the user must ensure before running this program are

- The total number of samples (i.e. number of samples per gage x number of gages), must be **less than** what is specified by **MAXIMUM**.
- The total time taken (i.e. number of samples per gage x sampling rate), must be **less than** what is specified by**WAIT_TIME**.

If the parameter statements in the source code are changed then the source code can be compiled again by the following statement

f77 -o take_data take_data.f -lmr

Where -lmr connects the program with the mr library routines for data acquisition, that are present in the Concurrent system, and are used by **Take_data**. The program uses the internal A/D clocks of the system.

A.4 Calibration

The raw data that is collected from the gages is in volts, which has to be converted to *cm* to obtain the time series for the data. For this reason the wave gages have to be calibrated. Calibration can be done in two ways. Either the water level can be changed and the wave gage kept fixed, or the wave gages can be moved up and down and the water level kept still. The latter obviously makes more sense, and for this reason stepper motors are attached to the gages. The stepper motor controls have a switch which allows the motors to be switched from a manual control to a computer control. Calibration is done with the help of a program called **Gcal1**, which serves a two way purpose.

- To move the motors during calibration, and,
- To collect data at each calibration point, in the same way as **Take_data** does.

To move the motors, **Gcal1** uses three A/D clocks of the Concurrent computer systems. One of the clocks moves the motors through the specified distance between calibration points, Another clock collects data at the calibration point, while a third clock changes the direction of the motors, when the total number of calibration points in a particular direction (as specified by the user) have been completed. Although the distance between calibration points is specified by the user in the form of number of stepper motor steps; the program uses $1cm$ as the distance between calibration points, and thus a value of 151 steps (which corresponds to $1cm$) was specified for calibration during the experiments. A 100 samples at a 100 hz were collected at each calibration point, and the average value taken as the reading at that point. All the readings were taken with reference to the mean water level reading, and a linear regression analysis was done. The results were plotted in three data files, **'calg.dat'**, **'regr.dat'** and **'lin.dat'**. These data files were then used by a matlab routine, **calib.m**, to obtain the linear calibration curves, of volts to *cm*, for all the ten gages, with the respective slope and the intercept. A sample of these curves is shown in Figure A.2

The linear curves were found to fit very well with all the calibration points. Most of the time the slope was found to remain relatively unchanged, making excessive calibration unnecessary. Changes in water temperatures affected the calibration curves slightly, and for consistency calibration was required to be done atleast once a day. For the experiments, the calibration was done everytime the gage array was moved to a new location, so as to ensure that the gages were functioning properly, and had not been damaged or disconnected during the transportation. Thus, for the monochromatic waves, calibration was done about three to four times a day, and for the irregular wave tests, calibration was done about once a day. Calibration on top of the shoal was not always possible, particularly for the shallow water cases, because of lack of enough water level to obtain a large number of calibration points.

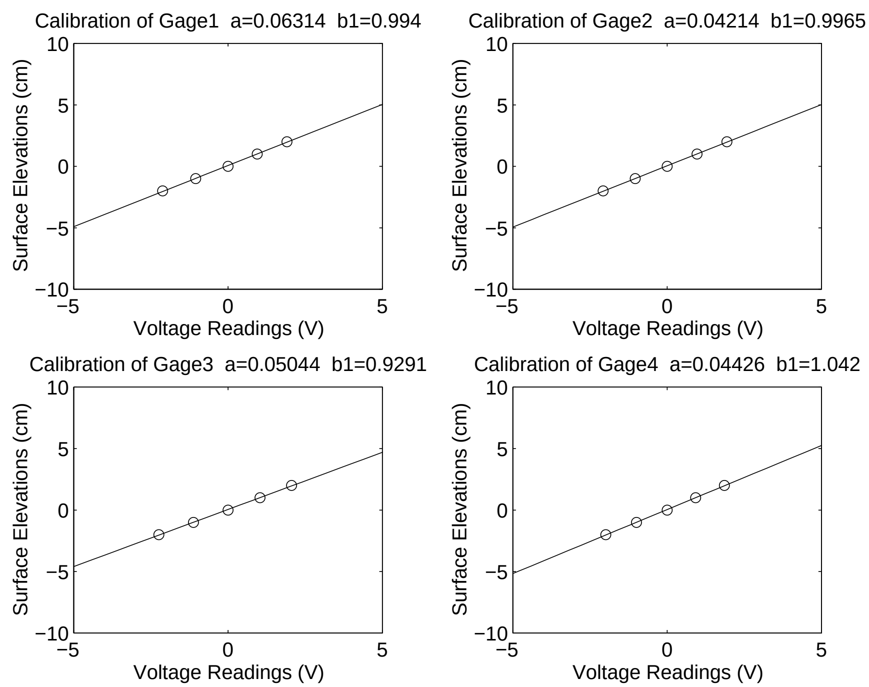

Figure A.2: Sample plot of the gage calibration curves.

In such cases calibration curves of the previous position were used.

Appendix B

DATA FILES

B.1 Raw Data

The gages output the data in the form of a voltage time series. This data has been converted into surface elevations in centimetres with the help of the calibration curves and stored in data files.

In the data set for monchromatic wave tests, each time series consists of 4096 samples, and the sampling rate is $50Hz$. Data collection was started from a cold start so the data can be used with time domain models also. The reference water level can be determined from the initial part of the time series when no wave is seen. The mean therefore does not have to be zeroed out, and certain characterisitics like the wave setup or setdown can be determined.

The irregular wave test data sets consist of much longer time series (32768 samples), which are also sampled at $50Hz$. The long time series have been chosen such that they correspond to one cycle of the paddle time series, to maintain the irregular nature of the waves. Unfortunately due to the larger size of these data files, data collection could not be started from a cold start. Information about the initial water level is stored in seperate data files which were sampled in still water. This has only been done for the second set of irregular wave tests, and for the first set the mean will have to be subtracted out from the time series.

B.2 Naming convention

The naming convention used for the data files is as follows *[name]_[gage number]*.**t**_*[test number]***p**_*[position number]*, where

name is a three character word signifying what kind of experiment the data is from.
'lin' is for monochromatic linear tests,
'bre' is for monochromatic non linear tests,
'irr' is for the first set of irregular spectra tests, and
'nir' is for the second set of irregular spectra tests.

gage number is a two digit number specifying which gage it is.

test number is a two digit number specifying which test it is in the particular set of experiments. The particulars about the test numbers are given in the tables.

position number is a two digit number specifying the position of the gage array (see Figure 3.1).

Appendix C

WAVE DATA

Table C.1: Gage distances on array, with respect to gage 1.

Gage no.	distance (mts)
2	0.626
3	1.228
4	1.884
5	2.1615
6	2.464
7	3.07
8	3.691
9	4.3

Table C.2: Wave characteristics at gage 10 for Test 1 (monochromatic waves).

Array pos.	H	H_f	T_p
1.0000000e+00	2.1989800e-02	1.9689200e-02	7.5006600e-01
2.0000000e+00	1.9315400e-02	1.7911300e-02	7.4949100e-01
3.0000000e+00	2.1446400e-02	1.9913400e-02	7.4946700e-01
4.0000000e+00	2.1617100e-02	1.9954100e-02	7.4895900e-01
5.0000000e+00	2.2237900e-02	1.9722200e-02	7.5029600e-01
6.0000000e+00	2.1988300e-02	2.0155400e-02	7.5026100e-01
7.0000000e+00	2.2980500e-02	2.0877300e-02	7.4908300e-01
8.0000000e+00	2.1535500e-02	1.9491900e-02	7.4972500e-01
9.0000000e+00	2.0480400e-02	1.8729500e-02	7.4910100e-01
1.0000000e+01	2.1828500e-02	1.9309000e-02	7.4975400e-01
1.1000000e+01	2.1642400e-02	1.9645700e-02	7.5080700e-01
1.2000000e+01	2.0756300e-02	1.8236900e-02	7.4938000e-01
1.3000000e+01	2.1755100e-02	1.9225100e-02	7.5024900e-01
1.4000000e+01	2.3013200e-02	1.9744200e-02	7.5031700e-01

Table C.3: Wave characteristics at gage 10 for Test 2 (monochromatic waves).

Array pos.	H	H_f	T_p
1.0000000e+00	4.0011000e-02	3.9153800e-02	7.5034900e-01
2.0000000e+00	3.9470800e-02	3.8084000e-02	7.5040100e-01
3.0000000e+00	4.1322100e-02	4.0404000e-02	7.4980500e-01
4.0000000e+00	4.3352100e-02	4.0800900e-02	7.5000600e-01
5.0000000e+00	4.2780600e-02	4.0668800e-02	7.4999000e-01
6.0000000e+00	4.0357600e-02	4.0442100e-02	7.4973000e-01
7.0000000e+00	4.5763900e-02	4.3307700e-02	7.4993200e-01
8.0000000e+00	4.3300000e-02	4.0823300e-02	7.5030000e-01
9.0000000e+00	4.0017700e-02	3.8572700e-02	7.5014400e-01
1.0000000e+01	3.8923500e-02	3.7623200e-02	7.5071600e-01
1.1000000e+01	4.0905500e-02	4.0500300e-02	7.5037300e-01
1.2000000e+01	4.1230900e-02	3.8866100e-02	7.5073900e-01
1.3000000e+01	4.1792000e-02	4.0011300e-02	7.4965200e-01
1.4000000e+01	4.2034200e-02	4.0494600e-02	7.4946000e-01

Table C.4: Wave characteristics at gage 10 for Test 4 (monochromatic waves).

Array pos.	H	H_f	T_p
1.0000000e+00	2.3283300e-02	2.1083600e-02	9.9902600e-01
2.0000000e+00	2.5174000e-02	2.3145100e-02	9.9934700e-01
3.0000000e+00	2.0850100e-02	2.0717900e-02	1.0007000e+00
4.0000000e+00	2.4271100e-02	2.2117200e-02	1.0016800e+00
5.0000000e+00	2.3684600e-02	2.2344100e-02	1.0013700e+00
6.0000000e+00	2.1541700e-02	2.0473100e-02	1.0006800e+00
7.0000000e+00	2.5959100e-02	2.3230500e-02	1.0027500e+00
8.0000000e+00	2.3413400e-02	2.2139300e-02	1.0015400e+00
9.0000000e+00	2.1390100e-02	1.9844400e-02	1.0008300e+00
1.0000000e+01	2.2039100e-02	2.0809100e-02	1.0012400e+00
1.1000000e+01	1.8888200e-02	1.8020400e-02	1.0012100e+00
1.2000000e+01	2.2243100e-02	2.0804400e-02	1.0018800e+00
1.3000000e+01	2.3693100e-02	2.1582700e-02	1.0027400e+00
1.4000000e+01	2.0826000e-02	1.9532900e-02	1.0012300e+00

Table C.5: Wave height characteristics for TEST 1 (monochromatic waves).

Array pos.	Gage no.	x (mts)	y (mts)	H (mts)	H_f (mts)
1	1	3.1200	8.9800	0.0182	0.0194
1	2	3.7360	8.9800	0.0144	0.0147
1	3	4.3480	8.9800	0.0175	0.0184
1	4	4.9640	8.9800	0.0197	0.0203
1	5	5.2815	8.9800	0.0213	0.0221
1	6	5.5840	8.9800	0.0271	0.0283
1	7	6.1900	8.9800	0.0328	0.0341
1	8	6.8110	8.9800	0.0393	0.0408
1	9	7.4200	8.9800	0.0384	0.0407
2	1	8.9150	8.9800	0.0328	0.0326
2	2	9.5310	8.9800	0.0301	0.0296
2	3	10.1430	8.9800	0.0263	0.0262
2	4	10.7590	8.9800	0.0222	0.0219
2	5	11.0765	8.9800	0.0209	0.0204
2	6	11.3790	8.9800	0.0195	0.0190
2	7	11.9850	8.9800	0.0174	0.0170
2	8	12.6060	8.9800	0.0168	0.0164
2	9	13.2150	8.9800	0.0168	0.0158
3	1	11.1200	6.8900	0.0256	0.0264
3	2	11.1200	6.2740	0.0019	0.0010
3	3	11.1200	5.6620	0.0269	0.0267
3	4	11.1200	5.0460	0.0185	0.0185
3	5	11.1200	4.7285	0.0143	0.0139
3	6	11.1200	4.4260	0.0228	0.0227
3	7	11.1200	3.8200	0.0256	0.0249
3	8	11.1200	3.1990	0.0247	0.0242
3	9	11.1200	2.5900	0.0152	0.0149
4	1	11.1200	11.1700	0.0112	0.0104
4	2	11.1200	10.5540	0.0272	0.0262
4	3	11.1200	9.9420	0.0151	0.0147
4	4	11.1200	9.3260	0.0144	0.0141
4	5	11.1200	9.0085	0.0192	0.0181
4	6	11.1200	8.7060	0.0203	0.0187
4	7	11.1200	8.1000	0.0099	0.0100
4	8	11.1200	7.4790	0.0295	0.0293
4	9	11.1200	6.8700	0.0230	0.0227
5	1	11.1200	16.1150	0.0166	0.0161
5	2	11.1200	15.4990	0.0179	0.0175
5	3	11.1200	14.8870	0.0208	0.0197
5	4	11.1200	14.2710	0.0207	0.0198

5	5	11.1200	13.9535	0.0260	0.0254
5	6	11.1200	13.6510	0.0281	0.0277
5	7	11.1200	13.0450	0.0221	0.0216
5	8	11.1200	12.4240	0.0284	0.0280
5	9	11.1200	11.8150	0.0157	0.0142
6	1	9.6500	16.3800	0.0200	0.0198
6	2	9.6500	15.7640	0.0193	0.0192
6	3	9.6500	15.1520	0.0199	0.0195
6	4	9.6500	14.5360	0.0182	0.0174
6	5	9.6500	14.2185	0.0205	0.0202
6	6	9.6500	13.9160	0.0228	0.0226
6	7	9.6500	13.3100	0.0221	0.0214
6	8	9.6500	12.6890	0.0230	0.0230
6	9	9.6500	12.0800	0.0214	0.0212
7	1	9.6500	11.2000	0.0086	0.0085
7	2	9.6500	10.5840	0.0177	0.0186
7	3	9.6500	9.9720	0.0155	0.0159
7	4	9.6500	9.3560	0.0161	0.0155
7	5	9.6500	9.0385	0.0242	0.0256
7	6	9.6500	8.7360	0.0239	0.0252
7	7	9.6500	8.1300	0.0160	0.0162
7	8	9.6500	7.5090	0.0248	0.0255
7	9	9.6500	6.9000	0.0107	0.0107
8	1	9.6500	6.5750	0.0183	0.0182
8	2	9.6500	5.9590	0.0199	0.0190
8	3	9.6500	5.3470	0.0172	0.0169
8	4	9.6500	4.7310	0.0213	0.0207
8	5	9.6500	4.4135	0.0155	0.0157
8	6	9.6500	4.1110	0.0189	0.0189
8	7	9.6500	3.5050	0.0222	0.0222
8	8	9.6500	2.8840	0.0231	0.0228
8	9	9.6500	2.2750	0.0206	0.0202
9	1	7.9950	6.7700	0.0185	0.0180
9	2	7.9950	6.1540	0.0211	0.0206
9	3	7.9950	5.5420	0.0155	0.0152
9	4	7.9950	4.9260	0.0215	0.0207
9	5	7.9950	4.6085	0.0225	0.0230
9	6	7.9950	4.3060	0.0216	0.0210
9	7	7.9950	3.7000	0.0186	0.0187
9	8	7.9950	3.0790	0.0213	0.0210
9	9	7.9950	2.4700	0.0232	0.0226
10	1	7.9950	11.2300	0.0183	0.0170
10	2	7.9950	10.6140	0.0093	0.0090

10	3	7.9950	10.0020	0.0229	0.0232
10	4	7.9950	9.3860	0.0199	0.0200
10	5	7.9950	9.0685	0.0388	0.0384
10	6	7.9950	8.7660	0.0334	0.0330
10	7	7.9950	8.1600	0.0206	0.0199
10	8	7.9950	7.5390	0.0137	0.0126
10	9	7.9950	6.9300	0.0191	0.0181
11	1	7.9950	16.3000	0.0173	0.0168
11	2	7.9950	15.6840	0.0221	0.0216
11	3	7.9950	15.0720	0.0196	0.0194
11	4	7.9950	14.4560	0.0203	0.0196
11	5	7.9950	14.1385	0.0198	0.0195
11	6	7.9950	13.8360	0.0206	0.0206
11	7	7.9950	13.2300	0.0234	0.0227
11	8	7.9950	12.6090	0.0233	0.0228
11	9	7.9950	12.0000	0.0239	0.0243
12	1	6.3500	11.1800	0.0188	0.0190
12	2	6.3500	10.5640	0.0148	0.0143
12	3	6.3500	9.9520	0.0163	0.0168
12	4	6.3500	9.3360	0.0209	0.0216
12	5	6.3500	9.0185	0.0391	0.0383
12	6	6.3500	8.7160	0.0258	0.0265
12	7	6.3500	8.1100	0.0157	0.0164
12	8	6.3500	7.4890	0.0153	0.0146
12	9	6.3500	6.8800	0.0188	0.0190
13	1	5.0750	11.1600	0.0182	0.0190
13	2	5.0750	10.5440	0.0134	0.0136
13	3	5.0750	9.9320	0.0158	0.0168
13	4	5.0750	9.3160	0.0228	0.0241
13	5	5.0750	8.9985	0.0207	0.0215
13	6	5.0750	8.6960	0.0176	0.0187
13	7	5.0750	8.0900	0.0131	0.0135
13	8	5.0750	7.4690	0.0151	0.0159
13	9	5.0750	6.8600	0.0164	0.0166
14	1	3.8850	11.1600	0.0178	0.0187
14	2	3.8850	10.5440	0.0186	0.0183
14	3	3.8850	9.9320	0.0172	0.0175
14	4	3.8850	9.3160	0.0211	0.0211
14	5	3.8850	8.9985	0.0180	0.0177
14	6	3.8850	8.6960	0.0167	0.0173
14	7	3.8850	8.0900	0.0150	0.0152
14	8	3.8850	7.4690	0.0187	0.0185
14	9	3.8850	6.8600	0.0190	0.0194

Table C.6: Wave height characteristics for TEST 2 (monochromatic waves).

Array pos.	Gage no.	x (mts)	y (mts)	H (mts)	H_f (mts)
1	1	3.1200	8.9800	0.0401	0.0409
1	2	3.7360	8.9800	0.0319	0.0334
1	3	4.3480	8.9800	0.0395	0.0403
1	4	4.9640	8.9800	0.0454	0.0441
1	5	5.2815	8.9800	0.0493	0.0487
1	6	5.5840	8.9800	0.0606	0.0604
1	7	6.1900	8.9800	0.0694	0.0698
1	8	6.8110	8.9800	0.0851	0.0863
1	9	7.4200	8.9800	0.0845	0.0862
2	1	8.9150	8.9800	0.0696	0.0708
2	2	9.5310	8.9800	0.0626	0.0642
2	3	10.1430	8.9800	0.0557	0.0572
2	4	10.7590	8.9800	0.0474	0.0488
2	5	11.0765	8.9800	0.0433	0.0447
2	6	11.3790	8.9800	0.0417	0.0423
2	7	11.9850	8.9800	0.0384	0.0382
2	8	12.6060	8.9800	0.0371	0.0376
2	9	13.2150	8.9800	0.0349	0.0358
3	1	11.1200	6.8900	0.0532	0.0545
3	2	11.1200	6.2740	0.0097	0.0090
3	3	11.1200	5.6620	0.0546	0.0562
3	4	11.1200	5.0460	0.0365	0.0383
3	5	11.1200	4.7285	0.0268	0.0276
3	6	11.1200	4.4260	0.0383	0.0394
3	7	11.1200	3.8200	0.0372	0.0387
3	8	11.1200	3.1990	0.0432	0.0446
3	9	11.1200	2.5900	0.0339	0.0348
4	1	11.1200	11.1700	0.0285	0.0298
4	2	11.1200	10.5540	0.0546	0.0563
4	3	11.1200	9.9420	0.0204	0.0213
4	4	11.1200	9.3260	0.0364	0.0380
4	5	11.1200	9.0085	0.0425	0.0440
4	6	11.1200	8.7060	0.0410	0.0424
4	7	11.1200	8.1000	0.0209	0.0206
4	8	11.1200	7.4790	0.0587	0.0600
4	9	11.1200	6.8700	0.0413	0.0428
5	1	11.1200	16.1150	0.0337	0.0352
5	2	11.1200	15.4990	0.0340	0.0352
5	3	11.1200	14.8870	0.0365	0.0384
5	4	11.1200	14.2710	0.0340	0.0352

5	5	11.1200	13.9535	0.0407	0.0422
5	6	11.1200	13.6510	0.0492	0.0513
5	7	11.1200	13.0450	0.0356	0.0369
5	8	11.1200	12.4240	0.0557	0.0578
5	9	11.1200	11.8150	0.0268	0.0269
6	1	9.6500	16.3800	0.0360	0.0378
6	2	9.6500	15.7640	0.0379	0.0394
6	3	9.6500	15.1520	0.0379	0.0393
6	4	9.6500	14.5360	0.0361	0.0376
6	5	9.6500	14.2185	0.0397	0.0409
6	6	9.6500	13.9160	0.0413	0.0431
6	7	9.6500	13.3100	0.0426	0.0444
6	8	9.6500	12.6890	0.0435	0.0454
6	9	9.6500	12.0800	0.0412	0.0426
7	1	9.6500	11.2000	0.0196	0.0201
7	2	9.6500	10.5840	0.0394	0.0414
7	3	9.6500	9.9720	0.0371	0.0381
7	4	9.6500	9.3560	0.0317	0.0333
7	5	9.6500	9.0385	0.0552	0.0579
7	6	9.6500	8.7360	0.0565	0.0584
7	7	9.6500	8.1300	0.0259	0.0270
7	8	9.6500	7.5090	0.0540	0.0556
7	9	9.6500	6.9000	0.0213	0.0221
8	1	9.6500	6.5750	0.0259	0.0272
8	2	9.6500	5.9590	0.0380	0.0395
8	3	9.6500	5.3470	0.0343	0.0355
8	4	9.6500	4.7310	0.0420	0.0434
8	5	9.6500	4.4135	0.0313	0.0326
8	6	9.6500	4.1110	0.0331	0.0347
8	7	9.6500	3.5050	0.0414	0.0430
8	8	9.6500	2.8840	0.0402	0.0422
8	9	9.6500	2.2750	0.0336	0.0355
9	1	7.9950	6.7700	0.0371	0.0385
9	2	7.9950	6.1540	0.0396	0.0408
9	3	7.9950	5.5420	0.0354	0.0369
9	4	7.9950	4.9260	0.0412	0.0424
9	5	7.9950	4.6085	0.0408	0.0431
9	6	7.9950	4.3060	0.0371	0.0385
9	7	7.9950	3.7000	0.0352	0.0366
9	8	7.9950	3.0790	0.0381	0.0393
9	9	7.9950	2.4700	0.0398	0.0411
10	1	7.9950	11.2300	0.0337	0.0348
10	2	7.9950	10.6140	0.0182	0.0188

10	3	7.9950	10.0020	0.0439	0.0459
10	4	7.9950	9.3860	0.0414	0.0434
10	5	7.9950	9.0685	0.0814	0.0832
10	6	7.9950	8.7660	0.0731	0.0746
10	7	7.9950	8.1600	0.0274	0.0278
10	8	7.9950	7.5390	0.0288	0.0299
10	9	7.9950	6.9300	0.0280	0.0288
11	1	7.9950	16.3000	0.0354	0.0372
11	2	7.9950	15.6840	0.0400	0.0415
11	3	7.9950	15.0720	0.0369	0.0384
11	4	7.9950	14.4560	0.0369	0.0386
11	5	7.9950	14.1385	0.0374	0.0388
11	6	7.9950	13.8360	0.0411	0.0430
11	7	7.9950	13.2300	0.0440	0.0454
11	8	7.9950	12.6090	0.0403	0.0420
11	9	7.9950	12.0000	0.0427	0.0450
12	1	6.3500	11.1800	0.0342	0.0356
12	2	6.3500	10.5640	0.0298	0.0305
12	3	6.3500	9.9520	0.0339	0.0360
12	4	6.3500	9.3360	0.0421	0.0443
12	5	6.3500	9.0185	0.0770	0.0784
12	6	6.3500	8.7160	0.0570	0.0600
12	7	6.3500	8.1100	0.0323	0.0344
12	8	6.3500	7.4890	0.0270	0.0273
12	9	6.3500	6.8800	0.0339	0.0357
13	1	5.0750	11.1600	0.0389	0.0400
13	2	5.0750	10.5440	0.0318	0.0330
13	3	5.0750	9.9320	0.0363	0.0380
13	4	5.0750	9.3160	0.0497	0.0499
13	5	5.0750	8.9985	0.0464	0.0454
13	6	5.0750	8.6960	0.0424	0.0430
13	7	5.0750	8.0900	0.0335	0.0342
13	8	5.0750	7.4690	0.0325	0.0343
13	9	5.0750	6.8600	0.0346	0.0355
14	1	3.8850	11.1600	0.0398	0.0414
14	2	3.8850	10.5440	0.0341	0.0359
14	3	3.8850	9.9320	0.0377	0.0393
14	4	3.8850	9.3160	0.0410	0.0423
14	5	3.8850	8.9985	0.0336	0.0351
14	6	3.8850	8.6960	0.0360	0.0384
14	7	3.8850	8.0900	0.0329	0.0339
14	8	3.8850	7.4690	0.0353	0.0364
14	9	3.8850	6.8600	0.0412	0.0429

Table C.7: Wave height characteristics for TEST 4 (monochromatic waves).

Array pos.	Gage no.	x (mts)	y (mts)	H (mts)	H_f (mts)
1	1	3.1200	8.9800	0.0220	0.0233
1	2	3.7360	8.9800	0.0219	0.0228
1	3	4.3480	8.9800	0.0235	0.0242
1	4	4.9640	8.9800	0.0297	0.0292
1	5	5.2815	8.9800	0.0375	0.0365
1	6	5.5840	8.9800	0.0455	0.0440
1	7	6.1900	8.9800	0.0571	0.0580
1	8	6.8110	8.9800	0.0593	0.0603
1	9	7.4200	8.9800	0.0471	0.0478
2	1	8.9150	8.9800	0.0237	0.0221
2	2	9.5310	8.9800	0.0183	0.0171
2	3	10.1430	8.9800	0.0156	0.0148
2	4	10.7590	8.9800	0.0117	0.0113
2	5	11.0765	8.9800	0.0109	0.0099
2	6	11.3790	8.9800	0.0099	0.0097
2	7	11.9850	8.9800	0.0074	0.0065
2	8	12.6060	8.9800	0.0082	0.0073
2	9	13.2150	8.9800	0.0104	0.0107
3	1	11.1200	6.8900	0.0331	0.0336
3	2	11.1200	6.2740	0.0259	0.0241
3	3	11.1200	5.6620	0.0060	0.0052
3	4	11.1200	5.0460	0.0321	0.0345
3	5	11.1200	4.7285	0.0388	0.0405
3	6	11.1200	4.4260	0.0378	0.0387
3	7	11.1200	3.8200	0.0194	0.0214
3	8	11.1200	3.1990	0.0248	0.0217
3	9	11.1200	2.5900	0.0322	0.0330
4	1	11.1200	11.1700	0.0314	0.0333
4	2	11.1200	10.5540	0.0258	0.0268
4	3	11.1200	9.9420	0.0111	0.0114
4	4	11.1200	9.3260	0.0064	0.0044
4	5	11.1200	9.0085	0.0094	0.0072
4	6	11.1200	8.7060	0.0084	0.0069
4	7	11.1200	8.1000	0.0085	0.0094
4	8	11.1200	7.4790	0.0270	0.0263
4	9	11.1200	6.8700	0.0335	0.0331
5	1	11.1200	16.1150	0.0155	0.0169
5	2	11.1200	15.4990	0.0257	0.0251
5	3	11.1200	14.8870	0.0271	0.0294
5	4	11.1200	14.2710	0.0170	0.0131

5	5	11.1200	13.9535	0.0262	0.0240
5	6	11.1200	13.6510	0.0330	0.0340
5	7	11.1200	13.0450	0.0380	0.0406
5	8	11.1200	12.4240	0.0152	0.0125
5	9	11.1200	11.8150	0.0174	0.0153
6	1	9.6500	16.3800	0.0234	0.0240
6	2	9.6500	15.7640	0.0229	0.0264
6	3	9.6500	15.1520	0.0180	0.0178
6	4	9.6500	14.5360	0.0307	0.0319
6	5	9.6500	14.2185	0.0305	0.0322
6	6	9.6500	13.9160	0.0229	0.0237
6	7	9.6500	13.3100	0.0214	0.0212
6	8	9.6500	12.6890	0.0348	0.0375
6	9	9.6500	12.0800	0.0219	0.0239
7	1	9.6500	11.2000	0.0184	0.0189
7	2	9.6500	10.5840	0.0324	0.0331
7	3	9.6500	9.9720	0.0182	0.0193
7	4	9.6500	9.3560	0.0101	0.0084
7	5	9.6500	9.0385	0.0128	0.0122
7	6	9.6500	8.7360	0.0138	0.0134
7	7	9.6500	8.1300	0.0152	0.0140
7	8	9.6500	7.5090	0.0325	0.0332
7	9	9.6500	6.9000	0.0289	0.0296
8	1	9.6500	6.5750	0.0160	0.0170
8	2	9.6500	5.9590	0.0185	0.0183
8	3	9.6500	5.3470	0.0359	0.0382
8	4	9.6500	4.7310	0.0257	0.0275
8	5	9.6500	4.4135	0.0161	0.0161
8	6	9.6500	4.1110	0.0184	0.0194
8	7	9.6500	3.5050	0.0293	0.0299
8	8	9.6500	2.8840	0.0236	0.0252
8	9	9.6500	2.2750	0.0250	0.0263
9	1	7.9950	6.7700	0.0180	0.0181
9	2	7.9950	6.1540	0.0311	0.0319
9	3	7.9950	5.5420	0.0175	0.0163
9	4	7.9950	4.9260	0.0302	0.0307
9	5	7.9950	4.6085	0.0291	0.0302
9	6	7.9950	4.3060	0.0247	0.0249
9	7	7.9950	3.7000	0.0189	0.0181
9	8	7.9950	3.0790	0.0293	0.0311
9	9	7.9950	2.4700	0.0207	0.0203
10	1	7.9950	11.2300	0.0146	0.0150
10	2	7.9950	10.6140	0.0238	0.0246

10	3	7.9950	10.0020	0.0313	0.0325
10	4	7.9950	9.3860	0.0241	0.0230
10	5	7.9950	9.0685	0.0357	0.0361
10	6	7.9950	8.7660	0.0327	0.0327
10	7	7.9950	8.1600	0.0278	0.0278
10	8	7.9950	7.5390	0.0316	0.0329
10	9	7.9950	6.9300	0.0053	0.0048
11	1	7.9950	16.3000	0.0243	0.0258
11	2	7.9950	15.6840	0.0221	0.0203
11	3	7.9950	15.0720	0.0259	0.0270
11	4	7.9950	14.4560	0.0227	0.0232
11	5	7.9950	14.1385	0.0206	0.0209
11	6	7.9950	13.8360	0.0247	0.0248
11	7	7.9950	13.2300	0.0300	0.0313
11	8	7.9950	12.6090	0.0188	0.0181
11	9	7.9950	12.0000	0.0271	0.0281
12	1	6.3500	11.1800	0.0159	0.0164
12	2	6.3500	10.5640	0.0206	0.0204
12	3	6.3500	9.9520	0.0248	0.0257
12	4	6.3500	9.3360	0.0287	0.0293
12	5	6.3500	9.0185	0.0620	0.0638
12	6	6.3500	8.7160	0.0408	0.0418
12	7	6.3500	8.1100	0.0235	0.0241
12	8	6.3500	7.4890	0.0167	0.0167
12	9	6.3500	6.8800	0.0156	0.0158
13	1	5.0750	11.1600	0.0215	0.0225
13	2	5.0750	10.5440	0.0209	0.0210
13	3	5.0750	9.9320	0.0256	0.0261
13	4	5.0750	9.3160	0.0321	0.0319
13	5	5.0750	8.9985	0.0319	0.0318
13	6	5.0750	8.6960	0.0323	0.0324
13	7	5.0750	8.0900	0.0196	0.0205
13	8	5.0750	7.4690	0.0181	0.0185
13	9	5.0750	6.8600	0.0215	0.0219
14	1	3.8850	11.1600	0.0218	0.0226
14	2	3.8850	10.5440	0.0241	0.0246
14	3	3.8850	9.9320	0.0227	0.0232
14	4	3.8850	9.3160	0.0238	0.0239
14	5	3.8850	8.9985	0.0235	0.0243
14	6	3.8850	8.6960	0.0233	0.0244
14	7	3.8850	8.0900	0.0201	0.0207
14	8	3.8850	7.4690	0.0198	0.0204
14	9	3.8850	6.8600	0.0211	0.0221

Table C.8: Wave height characteristics for TEST 3 (irregular waves).

Array pos.	Gage no.	x (mts)	y (mts)	H_s (mts)	T_s (mts)
1	1	2.9600	8.9800	0.013911	0.730482
1	2	3.5760	8.9800	0.012023	0.732678
1	3	4.1880	8.9800	0.014435	0.742379
1	4	4.8040	8.9800	0.023313	0.744445
1	5	5.1215	8.9800	0.018989	0.694797
1	6	5.4240	8.9800	0.020879	0.736012
1	7	6.0300	8.9800	0.027735	0.740200
1	8	6.6510	8.9800	0.013976	0.660253
1	9	7.2600	8.9800	0.011176	0.680917
2	1	8.8300	8.9800	0.010125	0.732373
2	2	9.4460	8.9800	0.010262	0.730967
2	3	10.0580	8.9800	0.009252	0.726249
2	4	10.6740	8.9800	0.009717	0.728338
2	5	10.9915	8.9800	0.009113	0.726268
2	6	11.2940	8.9800	0.009183	0.731553
2	7	11.9000	8.9800	0.009386	0.735858
2	8	12.5210	8.9800	0.009253	0.728958
2	9	13.1300	8.9800	0.008991	0.724647
3	1	12.2700	7.6000	0.009461	0.737459
3	2	12.2700	6.9840	0.011125	0.730824
3	3	12.2700	6.3720	0.011906	0.731693
3	4	12.2700	5.7560	0.013668	0.725915
3	5	12.2700	5.4385	0.014026	0.726411
3	6	12.2700	5.1360	0.013752	0.737767
3	7	12.2700	4.5300	0.013787	0.726499
3	8	12.2700	3.9090	0.014349	0.737288
3	9	12.2700	3.3000	0.014016	0.730770
4	1	12.2700	11.7600	0.012433	0.718891
4	2	12.2700	11.1440	0.011985	0.731649
4	3	12.2700	10.5320	0.010360	0.731481
4	4	12.2700	9.9160	0.010038	0.729260
4	5	12.2700	9.5985	0.009790	0.728298
4	6	12.2700	9.2960	0.009237	0.723435
4	7	12.2700	8.6900	0.009007	0.729648
4	8	12.2700	8.0690	0.009682	0.737456
4	9	12.2700	7.4600	0.009300	0.726769
5	1	12.2700	16.4300	0.013598	0.734129
5	2	12.2700	15.8140	0.013802	0.733856
5	3	12.2700	15.2020	0.013828	0.740067
5	4	12.2700	14.5860	0.013819	0.730109

5	5	12.2700	14.2685	0.014330	0.734908
5	6	12.2700	13.9660	0.014904	0.736070
5	7	12.2700	13.3600	0.014313	0.726824
5	8	12.2700	12.7390	0.013856	0.724946
5	9	12.2700	12.1300	0.013483	0.729362
6	1	9.8300	16.1200	0.013854	0.732052
6	2	9.8300	15.5040	0.013910	0.736015
6	3	9.8300	14.8920	0.014821	0.735909
6	4	9.8300	14.2760	0.014608	0.738785
6	5	9.8300	13.9585	0.015201	0.728698
6	6	9.8300	13.6560	0.015338	0.737524
6	7	9.8300	13.0500	0.015423	0.728587
6	8	9.8300	12.4290	0.014719	0.717463
6	9	9.8300	11.8200	0.014278	0.725548
7	1	9.8300	10.9950	0.011815	0.718786
7	2	9.8300	10.3790	0.011145	0.713835
7	3	9.8300	9.7670	0.010287	0.723568
7	4	9.8300	9.1510	0.010849	0.727244
7	5	9.8300	8.8335	0.009958	0.725895
7	6	9.8300	8.5310	0.010480	0.734162
7	7	9.8300	7.9250	0.009445	0.731781
7	8	9.8300	7.3040	0.011429	0.722430
7	9	9.8300	6.6950	0.011496	0.719153
8	1	9.8300	6.5800	0.013114	0.719172
8	2	9.8300	5.9640	0.015029	0.728261
8	3	9.8300	5.3520	0.015304	0.732714
8	4	9.8300	4.7360	0.014664	0.733855
8	5	9.8300	4.4185	0.015128	0.735168
8	6	9.8300	4.1160	0.015866	0.734579
8	7	9.8300	3.5100	0.015440	0.731574
8	8	9.8300	2.8890	0.014975	0.737749
8	9	9.8300	2.2800	0.014370	0.729740
9	1	7.8650	5.7900	0.014361	0.732465
9	2	7.8650	5.1740	0.015578	0.739656
9	3	7.8650	4.5620	0.015168	0.740819
9	4	7.8650	3.9460	0.014764	0.740064
9	5	7.8650	3.6285	0.014551	0.737890
9	6	7.8650	3.3260	0.014455	0.738782
9	7	7.8650	2.7200	0.013663	0.733621
9	8	7.8650	2.0990	0.013010	0.734226
9	9	7.8650	1.4900	0.012954	0.741516
10	1	7.8650	11.3150	0.013440	0.725825
10	2	7.8650	10.6990	0.012606	0.721510

10	3	7.8650	10.0870	0.011886	0.707658
10	4	7.8650	9.4710	0.010752	0.697588
10	5	7.8650	9.1535	0.010878	0.725668
10	6	7.8650	8.8510	0.010570	0.722822
10	7	7.8650	8.2450	0.010376	0.710556
10	8	7.8650	7.6240	0.013555	0.714878
10	9	7.8650	7.0150	0.013863	0.723946
11	1	7.8650	16.3850	0.013311	0.735886
11	2	7.8650	15.7690	0.013184	0.739072
11	3	7.8650	15.1570	0.013379	0.739626
11	4	7.8650	14.5410	0.013669	0.733466
11	5	7.8650	14.2235	0.013878	0.737878
11	6	7.8650	13.9210	0.014498	0.737548
11	7	7.8650	13.3150	0.014288	0.730262
11	8	7.8650	12.6940	0.015750	0.731543
11	9	7.8650	12.0850	0.015043	0.736908
12	1	6.1750	11.1650	0.013025	0.728189
12	2	6.1750	10.5490	0.012044	0.741365
12	3	6.1750	9.9370	0.012478	0.750383
12	4	6.1750	9.3210	0.016162	0.732653
12	5	6.1750	9.0035	0.024814	0.737387
12	6	6.1750	8.7010	0.017359	0.724207
12	7	6.1750	8.0950	0.011489	0.733776
12	8	6.1750	7.4740	0.012154	0.740646
12	9	6.1750	6.8650	0.012056	0.730170
13	1	5.0400	11.0850	0.012704	0.730021
13	2	5.0400	10.4690	0.012054	0.727830
13	3	5.0400	9.8570	0.014471	0.748794
13	4	5.0400	9.2410	0.022313	0.749090
13	5	5.0400	8.9235	0.019402	0.727093
13	6	5.0400	8.6210	0.018377	0.744698
13	7	5.0400	8.0150	0.012381	0.745758
13	8	5.0400	7.3940	0.011625	0.731787
13	9	5.0400	6.7850	0.012377	0.729384
14	1	3.7750	11.0850	0.013533	0.731655
14	2	3.7750	10.4690	0.012764	0.735587
14	3	3.7750	9.8570	0.013647	0.732390
14	4	3.7750	9.2410	0.013469	0.735539
14	5	3.7750	8.9235	0.012718	0.730226
14	6	3.7750	8.6210	0.011768	0.733980
14	7	3.7750	8.0150	0.011665	0.730828
14	8	3.7750	7.3940	0.013295	0.729504
14	9	3.7750	6.7850	0.013456	0.732909

Table C.9: Wave height characteristics for TEST 4 (irregular waves).

Array pos.	Gage no.	x (mts)	y (mts)	H_s (mts)	T_s (mts)
1	1	2.9600	8.9800	0.014740	0.735742
1	2	3.5760	8.9800	0.014320	0.744972
1	3	4.1880	8.9800	0.016740	0.745723
1	4	4.8040	8.9800	0.024388	0.747306
1	5	5.1215	8.9800	0.020820	0.696133
1	6	5.4240	8.9800	0.021281	0.723430
1	7	6.0300	8.9800	0.021638	0.739119
1	8	6.6510	8.9800	0.016404	0.729874
1	9	7.2600	8.9800	0.012845	0.721493
2	1	8.8300	8.9800	0.010727	0.728162
2	2	9.4460	8.9800	0.011442	0.726070
2	3	10.0580	8.9800	0.011107	0.729988
2	4	10.6740	8.9800	0.011675	0.728911
2	5	10.9915	8.9800	0.011187	0.730503
2	6	11.2940	8.9800	0.011310	0.727351
2	7	11.9000	8.9800	0.011860	0.736663
2	8	12.5210	8.9800	0.011363	0.734332
2	9	13.1300	8.9800	0.011680	0.730486
3	1	12.2700	7.6000	0.012810	0.731243
3	2	12.2700	6.9840	0.012687	0.736418
3	3	12.2700	6.3720	0.013312	0.735966
3	4	12.2700	5.7560	0.013693	0.732275
3	5	12.2700	5.4385	0.013822	0.734982
3	6	12.2700	5.1360	0.012898	0.729006
3	7	12.2700	4.5300	0.013071	0.727308
3	8	12.2700	3.9090	0.014123	0.732631
3	9	12.2700	3.3000	0.012658	0.731845
4	1	12.2700	11.7600	0.013560	0.731084
4	2	12.2700	11.1440	0.012081	0.730370
4	3	12.2700	10.5320	0.011983	0.727286
4	4	12.2700	9.9160	0.011982	0.725271
4	5	12.2700	9.5985	0.011375	0.733718
4	6	12.2700	9.2960	0.011715	0.734933
4	7	12.2700	8.6900	0.011917	0.729204
4	8	12.2700	8.0690	0.012035	0.730719
4	9	12.2700	7.4600	0.011605	0.730478
5	1	12.2700	16.4300	0.014211	0.735688
5	2	12.2700	15.8140	0.014280	0.733935
5	3	12.2700	15.2020	0.014061	0.735474
5	4	12.2700	14.5860	0.014160	0.736787

5	5	12.2700	14.2685	0.014296	0.735002
5	6	12.2700	13.9660	0.013945	0.735877
5	7	12.2700	13.3600	0.014277	0.734297
5	8	12.2700	12.7390	0.013697	0.733792
5	9	12.2700	12.1300	0.013586	0.740158
6	1	9.8300	16.1200	0.014937	0.733841
6	2	9.8300	15.5040	0.014229	0.741485
6	3	9.8300	14.8920	0.015604	0.743864
6	4	9.8300	14.2760	0.015034	0.739466
6	5	9.8300	13.9585	0.015006	0.734505
6	6	9.8300	13.6560	0.015372	0.737716
6	7	9.8300	13.0500	0.014933	0.739192
6	8	9.8300	12.4290	0.014565	0.730330
6	9	9.8300	11.8200	0.014072	0.732933
7	1	9.8300	10.9950	0.012616	0.726119
7	2	9.8300	10.3790	0.013327	0.728330
7	3	9.8300	9.7670	0.012088	0.733199
7	4	9.8300	9.1510	0.012190	0.725436
7	5	9.8300	8.8335	0.011230	0.724562
7	6	9.8300	8.5310	0.011981	0.728620
7	7	9.8300	7.9250	0.012243	0.729573
7	8	9.8300	7.3040	0.012975	0.729866
7	9	9.8300	6.6950	0.013610	0.727877
8	1	9.8300	6.5750	0.014286	0.725811
8	2	9.8300	5.9590	0.015099	0.733565
8	3	9.8300	5.3470	0.014625	0.732498
8	4	9.8300	4.7310	0.014311	0.735190
8	5	9.8300	4.4135	0.014791	0.727445
8	6	9.8300	4.1110	0.014754	0.734390
8	7	9.8300	3.5050	0.014536	0.731108
8	8	9.8300	2.8840	0.015023	0.737622
8	9	9.8300	2.2750	0.014895	0.734156
9	1	7.8650	5.7950	0.015169	0.735513
9	2	7.8650	5.1790	0.014960	0.735891
9	3	7.8650	4.5670	0.015233	0.733032
9	4	7.8650	3.9510	0.015067	0.734227
9	5	7.8650	3.6335	0.014350	0.738732
9	6	7.8650	3.3310	0.013948	0.737956
9	7	7.8650	2.7250	0.013125	0.734326
9	8	7.8650	2.1040	0.013246	0.734004
9	9	7.8650	1.4950	0.013514	0.738509
10	1	7.8650	11.3150	0.014120	0.731334
10	2	7.8650	10.6990	0.013696	0.722987

10	3	7.8650	10.0870	0.013894	0.719325
10	4	7.8650	9.4710	0.012787	0.724315
10	5	7.8650	9.1535	0.012172	0.722990
10	6	7.8650	8.8510	0.012472	0.734431
10	7	7.8650	8.2450	0.012739	0.722168
10	8	7.8650	7.6240	0.013984	0.728256
10	9	7.8650	7.0150	0.014027	0.721816
11	1	7.8650	16.3850	0.014448	0.733770
11	2	7.8650	15.7690	0.014130	0.736803
11	3	7.8650	15.1570	0.014460	0.742369
11	4	7.8650	14.5410	0.014015	0.737634
11	5	7.8650	14.2235	0.014956	0.743454
11	6	7.8650	13.9210	0.014514	0.742468
11	7	7.8650	13.3150	0.014800	0.738034
11	8	7.8650	12.6940	0.014940	0.742469
11	9	7.8650	12.0850	0.014312	0.731592
12	1	6.1750	11.1650	0.014410	0.736615
12	2	6.1750	10.5490	0.013441	0.731349
12	3	6.1750	9.9370	0.014781	0.739314
12	4	6.1750	9.3210	0.018302	0.740154
12	5	6.1750	9.0035	0.020499	0.743458
12	6	6.1750	8.7010	0.020015	0.738616
12	7	6.1750	8.0950	0.014800	0.734581
12	8	6.1750	7.4740	0.014851	0.733904
12	9	6.1750	6.8650	0.013663	0.728071
13	1	5.0400	11.0850	0.014532	0.733377
13	2	5.0400	10.4690	0.013943	0.743406
13	3	5.0400	9.8570	0.017472	0.750724
13	4	5.0400	9.2410	0.021574	0.729609
13	5	5.0400	8.9235	0.021566	0.740551
13	6	5.0400	8.6210	0.019791	0.742082
13	7	5.0400	8.0150	0.016151	0.745990
13	8	5.0400	7.3940	0.013439	0.737274
13	9	5.0400	6.7850	0.014201	0.732970
14	1	3.7750	11.0850	0.014701	0.741581
14	2	3.7750	10.4690	0.014704	0.736657
14	3	3.7750	9.8570	0.014585	0.737737
14	4	3.7750	9.2410	0.013708	0.740788
14	5	3.7750	8.9235	0.014443	0.737764
14	6	3.7750	8.6210	0.013798	0.734194
14	7	3.7750	8.0150	0.013796	0.737354
14	8	3.7750	7.3940	0.014898	0.735314
14	9	3.7750	6.7850	0.014998	0.732347

Table C.10: Wave height characteristics for TEST 5 (irregular waves).

Array pos.	Gage no.	x (mts)	y (mts)	H_s (mts)	T_s (mts)
1	1	2.9600	8.9800	0.023363	0.732306
1	2	3.5760	8.9800	0.022305	0.735304
1	3	4.1880	8.9800	0.026819	0.742971
1	4	4.8040	8.9800	0.026871	0.745350
1	5	5.1215	8.9800	0.021155	0.713590
1	6	5.4240	8.9800	0.019525	0.684645
1	7	6.0300	8.9800	0.033759	0.751916
1	8	6.6510	8.9800	0.030327	0.730755
1	9	7.2600	8.9800	0.019894	0.699136
2	1	8.8300	8.9800	0.014049	0.722492
2	2	9.4460	8.9800	0.013848	0.719118
2	3	10.0580	8.9800	0.014927	0.726227
2	4	10.6740	8.9800	0.014602	0.730384
2	5	10.9915	8.9800	0.014424	0.725884
2	6	11.2940	8.9800	0.014558	0.737329
2	7	11.9000	8.9800	0.015052	0.732240
2	8	12.5210	8.9800	0.015008	0.731226
2	9	13.1300	8.9800	0.014535	0.724681
3	1	12.2700	7.6000	0.015286	0.728620
3	2	12.2700	6.9840	0.018050	0.715157
3	3	12.2700	6.3720	0.018554	0.727816
3	4	12.2700	5.7560	0.022815	0.725478
3	5	12.2700	5.4385	0.023636	0.725712
3	6	12.2700	5.1360	0.024672	0.733883
3	7	12.2700	4.5300	0.023571	0.723917
3	8	12.2700	3.9090	0.025045	0.727291
3	9	12.2700	3.3000	0.023018	0.732653
4	1	12.2700	11.7600	0.021586	0.718828
4	2	12.2700	11.1440	0.020318	0.718357
4	3	12.2700	10.5320	0.017334	0.715155
4	4	12.2700	9.9160	0.015710	0.732860
4	5	12.2700	9.5985	0.014894	0.734080
4	6	12.2700	9.2960	0.014394	0.736123
4	7	12.2700	8.6900	0.015207	0.731475
4	8	12.2700	8.0690	0.015074	0.735043
4	9	12.2700	7.4600	0.014787	0.722030
5	1	12.2700	16.4300	0.022226	0.728138
5	2	12.2700	15.8140	0.024410	0.736943
5	3	12.2700	15.2020	0.023543	0.732887
5	4	12.2700	14.5860	0.023757	0.736898

5	5	12.2700	14.2685	0.023952	0.736675
5	6	12.2700	13.9660	0.025247	0.734682
5	7	12.2700	13.3600	0.023525	0.731455
5	8	12.2700	12.7390	0.025083	0.731112
5	9	12.2700	12.1300	0.022076	0.724482
6	1	9.8300	16.1200	0.022830	0.731974
6	2	9.8300	15.5040	0.023634	0.741914
6	3	9.8300	14.8920	0.023387	0.736742
6	4	9.8300	14.2760	0.023986	0.736587
6	5	9.8300	13.9585	0.024845	0.736841
6	6	9.8300	13.6560	0.025946	0.740317
6	7	9.8300	13.0500	0.025752	0.738802
6	8	9.8300	12.4290	0.024633	0.727319
6	9	9.8300	11.8200	0.025495	0.727297
7	1	9.8300	10.9950	0.020647	0.715988
7	2	9.8300	10.3790	0.018344	0.708383
7	3	9.8300	9.7670	0.017208	0.726062
7	4	9.8300	9.1510	0.014605	0.720098
7	5	9.8300	8.8335	0.015194	0.729267
7	6	9.8300	8.5310	0.016682	0.730099
7	7	9.8300	7.9250	0.016272	0.722097
7	8	9.8300	7.3040	0.018516	0.712299
7	9	9.8300	6.6950	0.020940	0.718483
8	1	9.8300	6.5750	0.023459	0.725578
8	2	9.8300	5.9590	0.025998	0.735008
8	3	9.8300	5.3470	0.023934	0.727455
8	4	9.8300	4.7310	0.025972	0.735250
8	5	9.8300	4.4135	0.024714	0.732906
8	6	9.8300	4.1110	0.024581	0.736475
8	7	9.8300	3.5050	0.022740	0.736452
8	8	9.8300	2.8840	0.021631	0.733188
8	9	9.8300	2.2750	0.019639	0.742355
9	1	7.8650	5.7950	0.023541	0.739593
9	2	7.8650	5.1790	0.023808	0.734895
9	3	7.8650	4.5670	0.022347	0.734347
9	4	7.8650	3.9510	0.022472	0.735789
9	5	7.8650	3.6335	0.022012	0.740179
9	6	7.8650	3.3310	0.022845	0.734884
9	7	7.8650	2.7250	0.021927	0.734877
9	8	7.8650	2.1040	0.019381	0.730822
9	9	7.8650	1.4950	0.019225	0.740592
10	1	7.8650	11.3150	0.022176	0.736380
10	2	7.8650	10.6990	0.021030	0.724500

10	3	7.8650	10.0870	0.022090	0.719353
10	4	7.8650	9.4710	0.021437	0.720099
10	5	7.8650	9.1535	0.018111	0.695074
10	6	7.8650	8.8510	0.018128	0.707637
10	7	7.8650	8.2450	0.021545	0.728046
10	8	7.8650	7.6240	0.020518	0.728462
10	9	7.8650	7.0150	0.021301	0.726710
11	1	7.8650	16.3850	0.021724	0.734024
11	2	7.8650	15.7690	0.022535	0.737038
11	3	7.8650	15.1570	0.023123	0.736431
11	4	7.8650	14.5410	0.022972	0.735469
11	5	7.8650	14.2235	0.023951	0.741696
11	6	7.8650	13.9210	0.024068	0.735314
11	7	7.8650	13.3150	0.024814	0.736962
11	8	7.8650	12.6940	0.025188	0.732643
11	9	7.8650	12.0850	0.024802	0.739233
12	1	6.1750	11.1650	0.020268	0.727722
12	2	6.1750	10.5490	0.018825	0.733220
12	3	6.1750	9.9370	0.018311	0.729337
12	4	6.1750	9.3210	0.027552	0.724994
12	5	6.1750	9.0035	0.034833	0.751808
12	6	6.1750	8.7010	0.026977	0.729762
12	7	6.1750	8.0950	0.018353	0.724181
12	8	6.1750	7.4740	0.018468	0.729404
12	9	6.1750	6.8650	0.020218	0.732892
13	1	5.0400	11.0850	0.021450	0.729286
13	2	5.0400	10.4690	0.020480	0.728264
13	3	5.0400	9.8570	0.024114	0.747381
13	4	5.0400	9.2410	0.026417	0.750215
13	5	5.0400	8.9235	0.022885	0.750383
13	6	5.0400	8.6210	0.027714	0.750484
13	7	5.0400	8.0150	0.021228	0.740001
13	8	5.0400	7.3940	0.019310	0.726167
13	9	5.0400	6.7850	0.020914	0.729105
14	1	3.7750	11.0850	0.022582	0.732815
14	2	3.7750	10.4690	0.021666	0.732953
14	3	3.7750	9.8570	0.023181	0.731151
14	4	3.7750	9.2410	0.023624	0.733793
14	5	3.7750	8.9235	0.023165	0.732634
14	6	3.7750	8.6210	0.020959	0.732063
14	7	3.7750	8.0150	0.020492	0.733567
14	8	3.7750	7.3940	0.022355	0.734121
14	9	3.7750	6.7850	0.021786	0.727314

Table C.11: Wave height characteristics for TEST 6 (irregular waves).

Array pos.	Gage no.	x (mts)	y (mts)	H_s (mts)	T_s (mts)
1	1	2.9600	8.9800	0.023435	0.734697
1	2	3.5760	8.9800	0.022952	0.740467
1	3	4.1880	8.9800	0.026235	0.751598
1	4	4.8040	8.9800	0.029261	0.749365
1	5	5.1215	8.9800	0.023395	0.681875
1	6	5.4240	8.9800	0.025864	0.687778
1	7	6.0300	8.9800	0.029177	0.737967
1	8	6.6510	8.9800	0.026808	0.739660
1	9	7.2600	8.9800	0.022207	0.722926
2	1	8.8300	8.9800	0.018325	0.724141
2	2	9.4460	8.9800	0.018236	0.715308
2	3	10.0580	8.9800	0.018129	0.720071
2	4	10.6740	8.9800	0.017854	0.720325
2	5	10.9915	8.9800	0.018697	0.729966
2	6	11.2940	8.9800	0.018637	0.726490
2	7	11.9000	8.9800	0.017498	0.726179
2	8	12.5210	8.9800	0.018873	0.728390
2	9	13.1300	8.9800	0.018925	0.723264
3	1	12.2700	7.6000	0.020021	0.734006
3	2	12.2700	6.9840	0.021213	0.731663
3	3	12.2700	6.3720	0.021827	0.729608
3	4	12.2700	5.7560	0.022029	0.731317
3	5	12.2700	5.4385	0.023266	0.731056
3	6	12.2700	5.1360	0.022988	0.733545
3	7	12.2700	4.5300	0.021490	0.731556
3	8	12.2700	3.9090	0.022409	0.730851
3	9	12.2700	3.3000	0.023326	0.730843
4	1	12.2700	11.7600	0.021865	0.727749
4	2	12.2700	11.1440	0.022184	0.731290
4	3	12.2700	10.5320	0.021457	0.728953
4	4	12.2700	9.9160	0.020780	0.734110
4	5	12.2700	9.5985	0.019889	0.729571
4	6	12.2700	9.2960	0.020065	0.729171
4	7	12.2700	8.6900	0.018491	0.722678
4	8	12.2700	8.0690	0.018970	0.724268
4	9	12.2700	7.4600	0.019954	0.732418
5	1	12.2700	16.4300	0.023543	0.730896
5	2	12.2700	15.8140	0.024288	0.732695
5	3	12.2700	15.2020	0.023511	0.732629
5	4	12.2700	14.5860	0.024041	0.734636

5	5	12.2700	14.2685	0.023907	0.732175
5	6	12.2700	13.9660	0.024113	0.733976
5	7	12.2700	13.3600	0.022223	0.735377
5	8	12.2700	12.7390	0.024215	0.732894
5	9	12.2700	12.1300	0.022566	0.733672
6	1	9.8300	16.1200	0.022867	0.743252
6	2	9.8300	15.5040	0.023298	0.732649
6	3	9.8300	14.8920	0.024340	0.733416
6	4	9.8300	14.2760	0.026174	0.739874
6	5	9.8300	13.9585	0.024154	0.737516
6	6	9.8300	13.6560	0.024354	0.734154
6	7	9.8300	13.0500	0.023877	0.736048
6	8	9.8300	12.4290	0.023730	0.735110
6	9	9.8300	11.8200	0.024307	0.730641
7	1	9.8300	10.9950	0.020982	0.726089
7	2	9.8300	10.3790	0.022351	0.731338
7	3	9.8300	9.7670	0.020276	0.729161
7	4	9.8300	9.1510	0.019175	0.725296
7	5	9.8300	8.8335	0.018280	0.721345
7	6	9.8300	8.5310	0.018764	0.725282
7	7	9.8300	7.9250	0.019448	0.730870
7	8	9.8300	7.3040	0.021680	0.731390
7	9	9.8300	6.6950	0.021370	0.728345
8	1	9.8300	6.5750	0.022259	0.723305
8	2	9.8300	5.9590	0.024327	0.735540
8	3	9.8300	5.3470	0.024115	0.735300
8	4	9.8300	4.7310	0.025050	0.737561
8	5	9.8300	4.4135	0.023356	0.727699
8	6	9.8300	4.1110	0.023280	0.732735
8	7	9.8300	3.5050	0.024168	0.731005
8	8	9.8300	2.8840	0.024311	0.734250
8	9	9.8300	2.2750	0.022864	0.730711
9	1	7.8650	5.7950	0.023408	0.734185
9	2	7.8650	5.1790	0.024635	0.739139
9	3	7.8650	4.5670	0.023373	0.734734
9	4	7.8650	3.9510	0.023826	0.739988
9	5	7.8650	3.6335	0.023412	0.731930
9	6	7.8650	3.3310	0.023670	0.731433
9	7	7.8650	2.7250	0.022068	0.735588
9	8	7.8650	2.1040	0.020598	0.734614
9	9	7.8650	1.4950	0.020164	0.731280
10	1	7.8650	11.3150	0.023871	0.727858
10	2	7.8650	10.6990	0.022940	0.721768

10	3	7.8650	10.0870	0.023396	0.724699
10	4	7.8650	9.4710	0.020971	0.726375
10	5	7.8650	9.1535	0.020614	0.725739
10	6	7.8650	8.8510	0.021263	0.727935
10	7	7.8650	8.2450	0.020911	0.724730
10	8	7.8650	7.6240	0.022654	0.734402
10	9	7.8650	7.0150	0.023589	0.727643
11	1	7.8650	16.3850	0.023455	0.739010
11	2	7.8650	15.7690	0.022779	0.734027
11	3	7.8650	15.1570	0.023222	0.731005
11	4	7.8650	14.5410	0.024064	0.734743
11	5	7.8650	14.2235	0.024352	0.735470
11	6	7.8650	13.9210	0.025593	0.738405
11	7	7.8650	13.3150	0.025147	0.736882
11	8	7.8650	12.6940	0.025387	0.736186
11	9	7.8650	12.0850	0.023575	0.732723
12	1	6.1750	11.1650	0.023086	0.730673
12	2	6.1750	10.5490	0.021731	0.730657
12	3	6.1750	9.9370	0.022896	0.730776
12	4	6.1750	9.3210	0.028615	0.738458
12	5	6.1750	9.0035	0.029161	0.748342
12	6	6.1750	8.7010	0.029630	0.737729
12	7	6.1750	8.0950	0.021715	0.727485
12	8	6.1750	7.4740	0.021421	0.733258
12	9	6.1750	6.8650	0.020819	0.730774
13	1	5.0400	11.0850	0.023862	0.727880
13	2	5.0400	10.4690	0.022649	0.734222
13	3	5.0400	9.8570	0.025836	0.745540
13	4	5.0400	9.2410	0.028488	0.745888
13	5	5.0400	8.9235	0.024265	0.723080
13	6	5.0400	8.6210	0.029376	0.745560
13	7	5.0400	8.0150	0.024393	0.743325
13	8	5.0400	7.3940	0.020967	0.725909
13	9	5.0400	6.7850	0.023346	0.731941
14	1	3.7750	11.0850	0.024952	0.735951
14	2	3.7750	10.4690	0.024186	0.727113
14	3	3.7750	9.8570	0.024056	0.739353
14	4	3.7750	9.2410	0.023097	0.740329
14	5	3.7750	8.9235	0.022527	0.739575
14	6	3.7750	8.6210	0.023260	0.738709
14	7	3.7750	8.0150	0.022558	0.730723
14	8	3.7750	7.3940	0.023747	0.734626
14	9	3.7750	6.7850	0.024250	0.731584

Table C.12: Index of Agreement results for irregular waves (TEST 3).

Transect	$d_i(d = 2.5cm)$	$d_i(d = 3cm)$	$d_i(d = 3.5cm)$
A-A	0.9588	0.9448	0.9436
G-G	0.5434	0.5434	0.5389
F-F	0.8522	0.8845	0.8818
E-E	0.8541	0.9314	0.9390
D-D	0.8848	0.9086	0.8237
C-C	0.9266	0.9355	0.9728
B-B	0.9490	0.9610	0.9520

Table C.13: Index of Agreement results for irregular waves (TEST 4).

Transect	$d_i(d = 2.5cm)$	$d_i(d = 3cm)$	$d_i(d = 3.5cm)$
A-A	0.9367	0.9426	0.9301
G-G	0.6543	0.6896	0.6663
F-F	0.8206	0.8751	0.8847
E-E	0.8970	0.8743	0.8602
D-D	0.8374	0.8577	0.7160
C-C	0.9151	0.9525	0.9605
B-B	0.8978	0.9016	0.8639

Table C.14: Index of Agreement results for irregular waves (TEST 5).

Transect	$d_i(d = 2.5cm)$	$d_i(d = 3cm)$	$d_i(d = 3.5cm)$
A-A	0.9221	0.8954	0.8660
G-G	0.3865	0.3878	0.3878
F-F	0.6130	0.7949	0.8823
E-E	0.9175	0.9712	0.9485
D-D	0.6953	0.7176	0.7048
C-C	0.9028	0.9205	0.9440
B-B	0.9579	0.9653	0.9694

Table C.15: Index of Agreement results for irregular waves (TEST 6).

Transect	$d_i(d = 2.5cm)$	$d_i(d = 3cm)$	$d_i(d = 3.5cm)$
A-A	0.8513	0.9233	0.9422
G-G	0.7479	0.7691	0.7784
F-F	0.4768	0.6414	0.7486
E-E	0.8952	0.8998	0.8923
D-D	0.6446	0.7302	0.8070
C-C	0.8363	0.8793	0.9233
B-B	0.7949	0.8303	0.8776

Appendix D

FREQUENCY SPECTRA PLOTS

The frequency spectra at each gage location, for the second set of irregular spectra experiments, has been plotted here. For each time series, the spectrum was smoothed by a bartlett average over 32 hanning windows, each consisting of 1024 data points. For the sake of clarity the spectrum has been plotted on a log scale.

The spectral plots give a good idea of the growth and propogation of higher harmonics in the wave field. For all four test cases, the generation of secondary harmonics is seen on top of the shoal (position 1, gages 4 to 6; and position 13, gages 4 to 6). The higher harmonics then progress down the tank, moving away from the center and decreasing in strength (position 10, gages 1 to 3 and 7 to 9; and then along position 6 and position 8). Whereas the spectral energy increases due to wave shoaling and focusing behind the shoal, and can be explained to a good degree by linear theory, the generation of higher harmonics are due to wave wave interactions in the wave field, and are caused due to the nonlinear nature of the wave field. In all the four test cases, the secondary harmonics are quite significant, thus showing the prescence of a highly nonlinear physical phenomenon. This is not contrary to expectations as all the cases had wave breaking on top of the shoal.

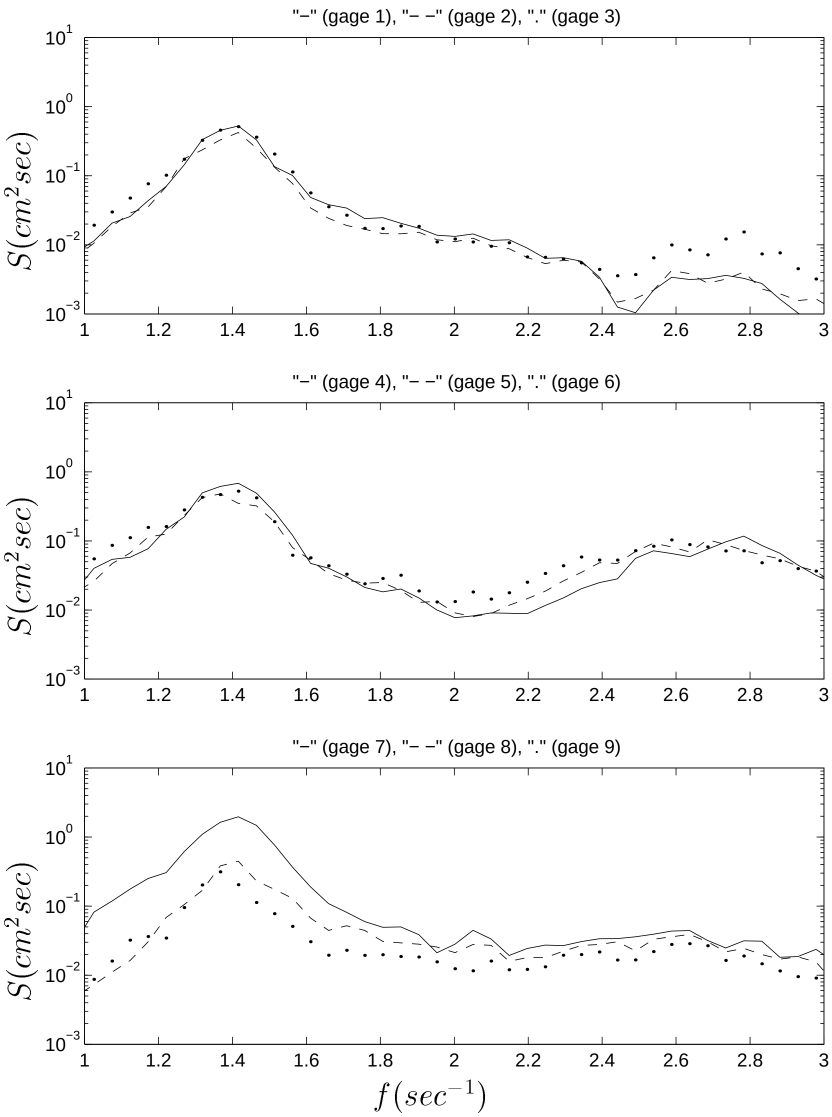

Figure D.1: Frequency spectra for Test 3 (position 1).

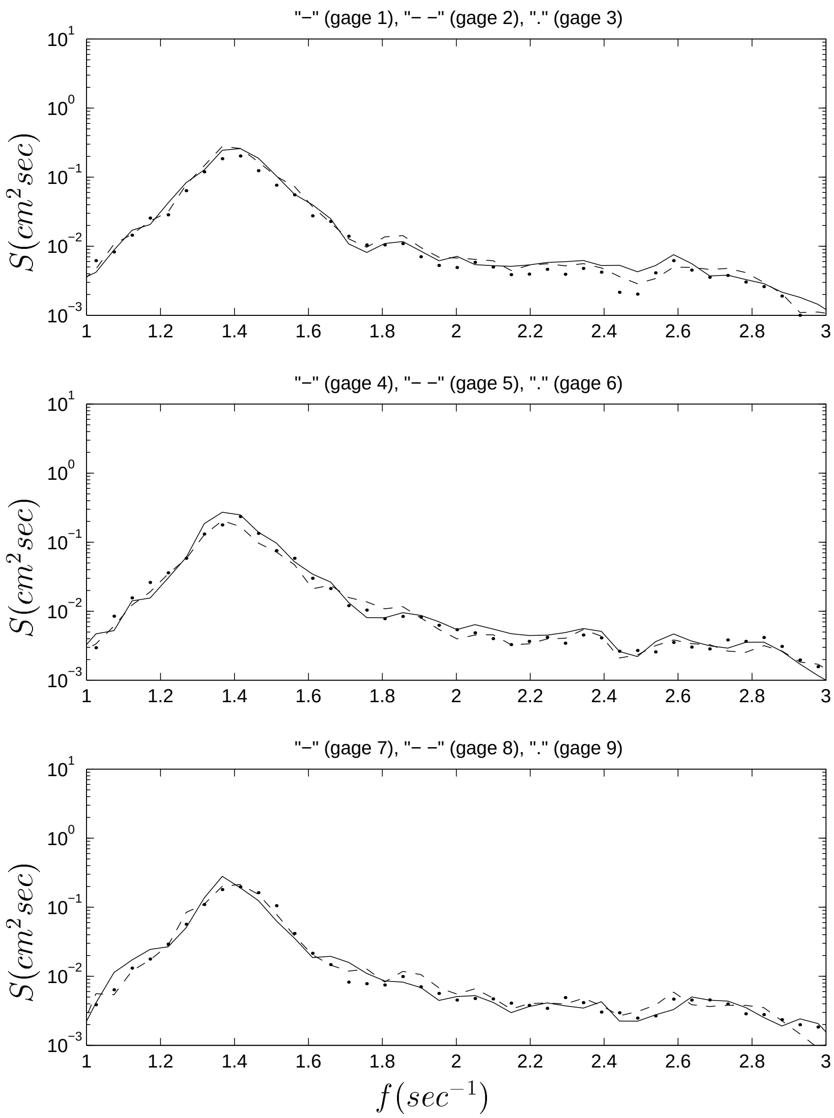

Figure D.2: Frequency spectra for Test 3 (position 2).

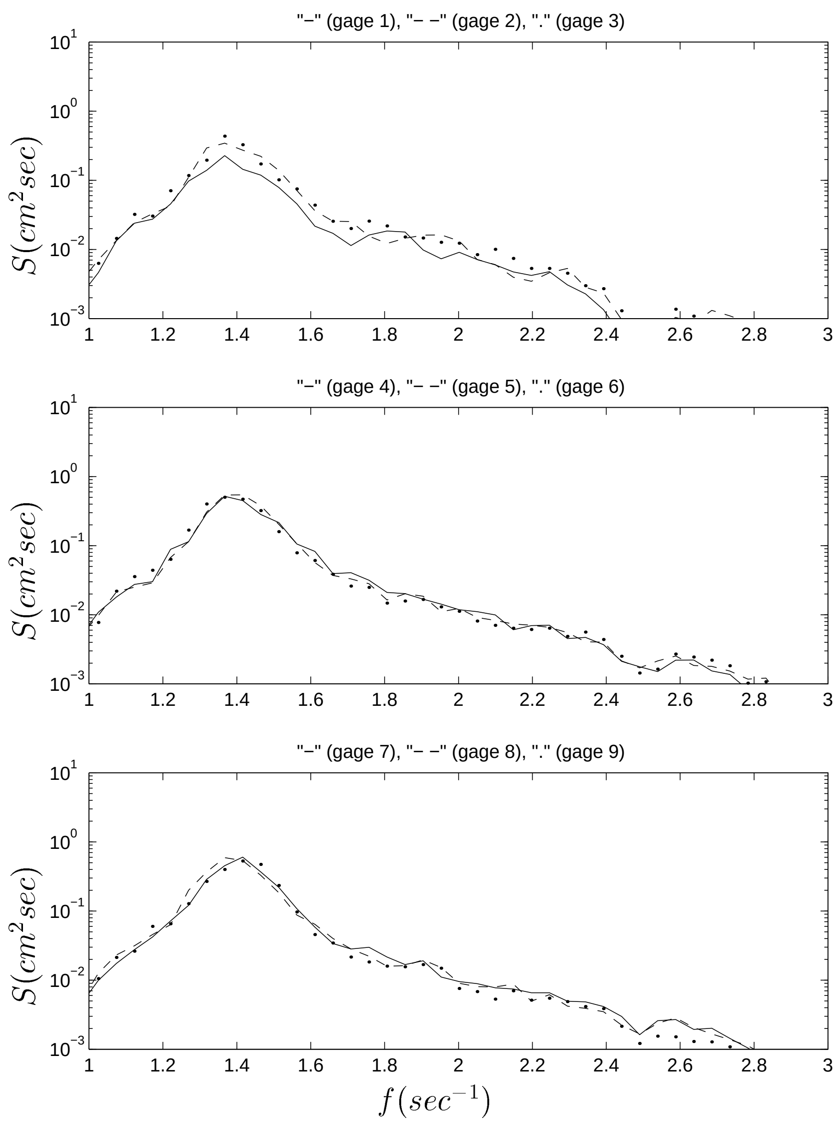

Figure D.3: Frequency spectra for Test 3 (position 3).

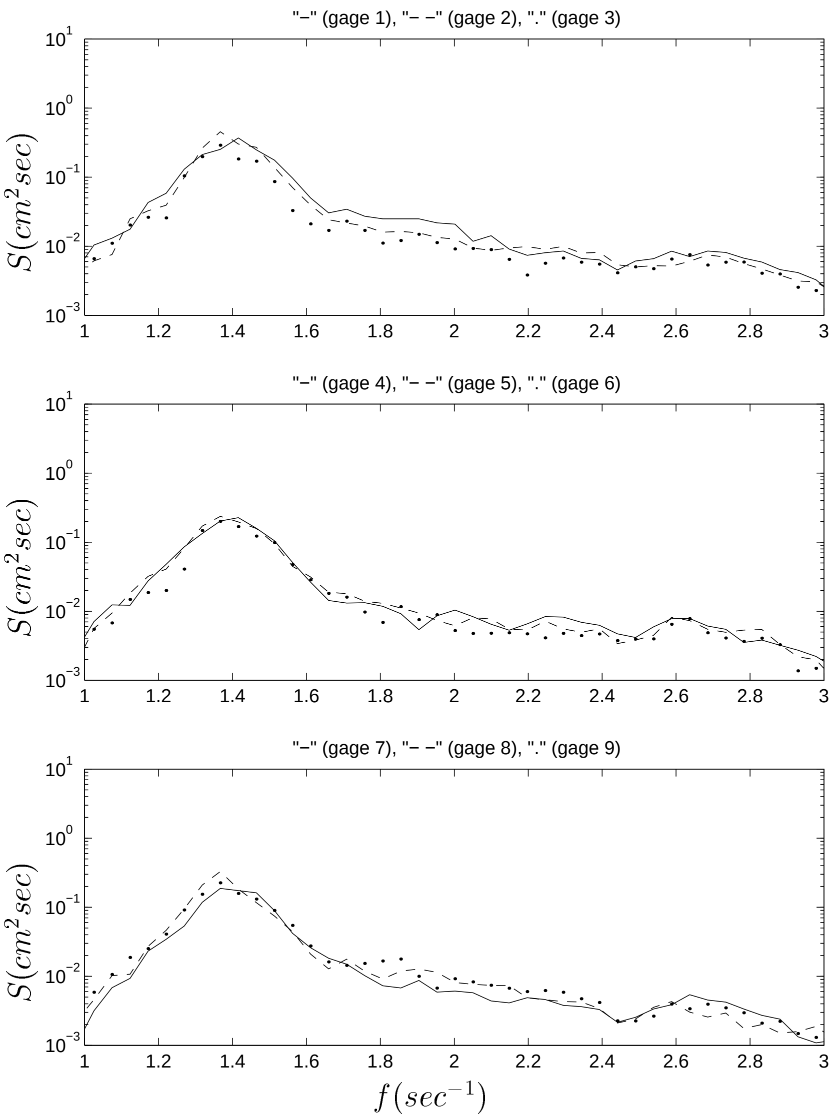

Figure D.4: Frequency spectra for Test 3 (position 4).

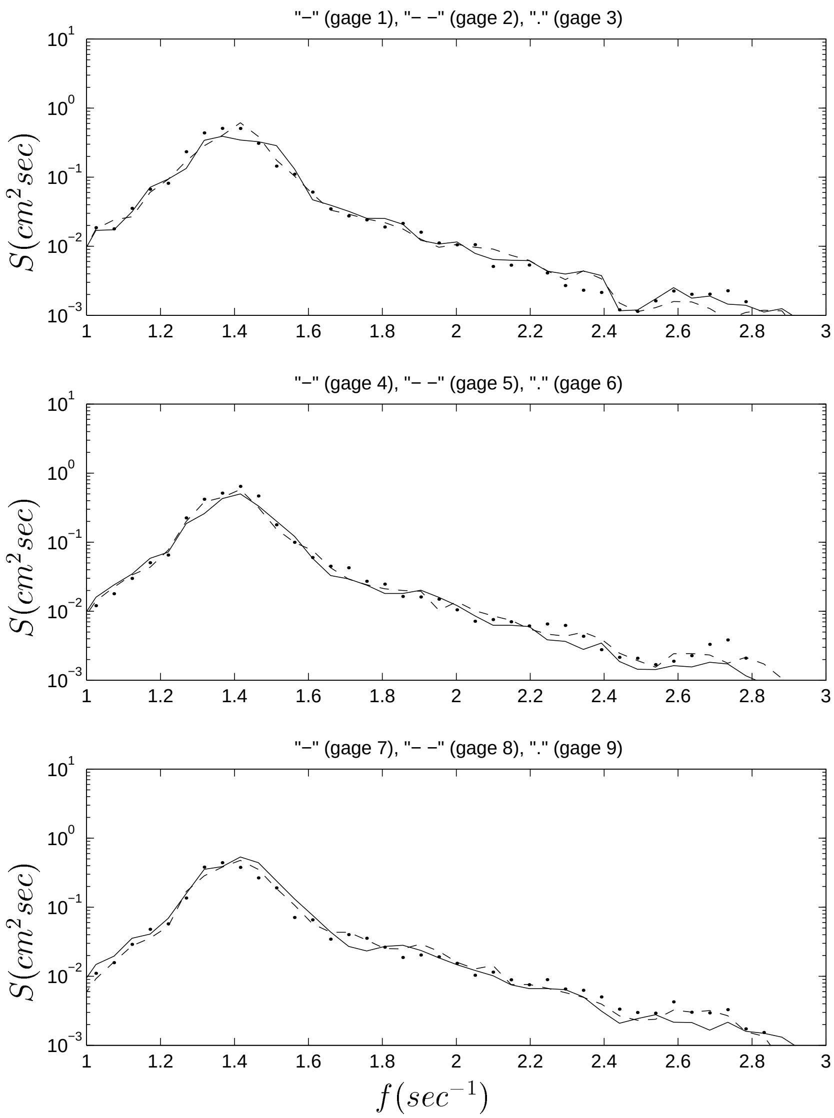

Figure D.5: Frequency spectra for Test 3 (position 5).

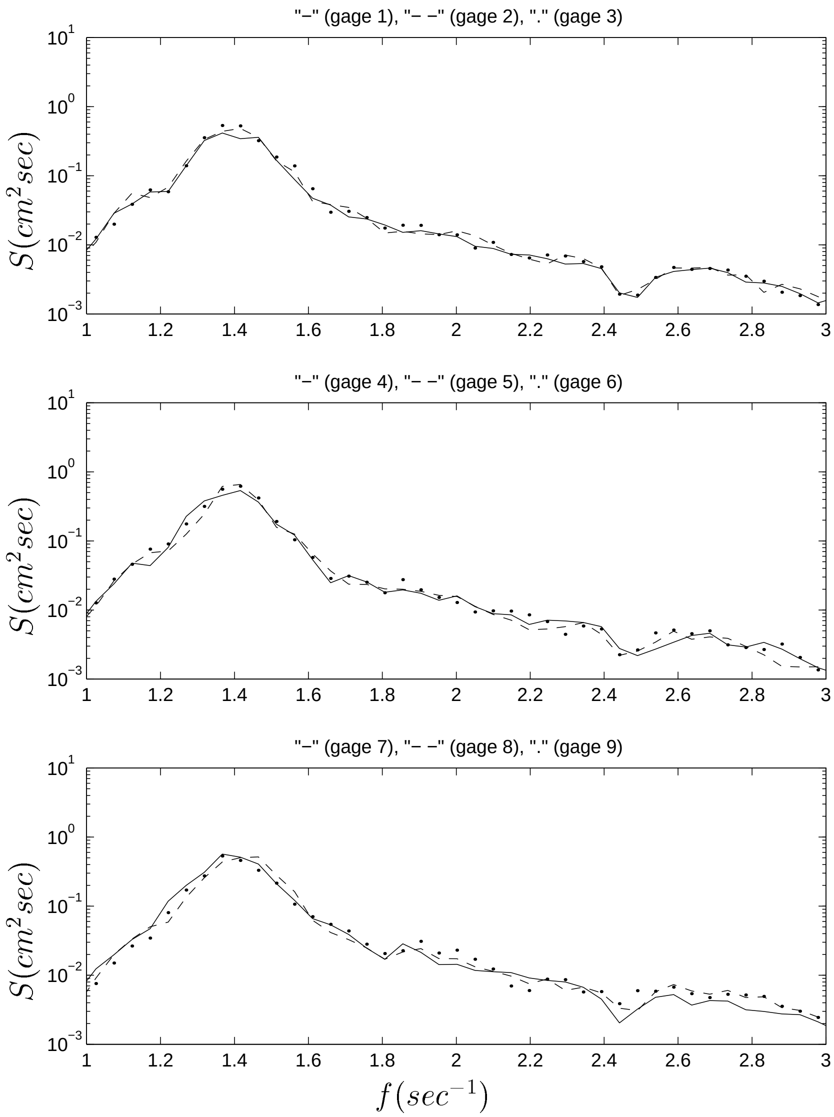

Figure D.6: Frequency spectra for Test 3 (position 6).

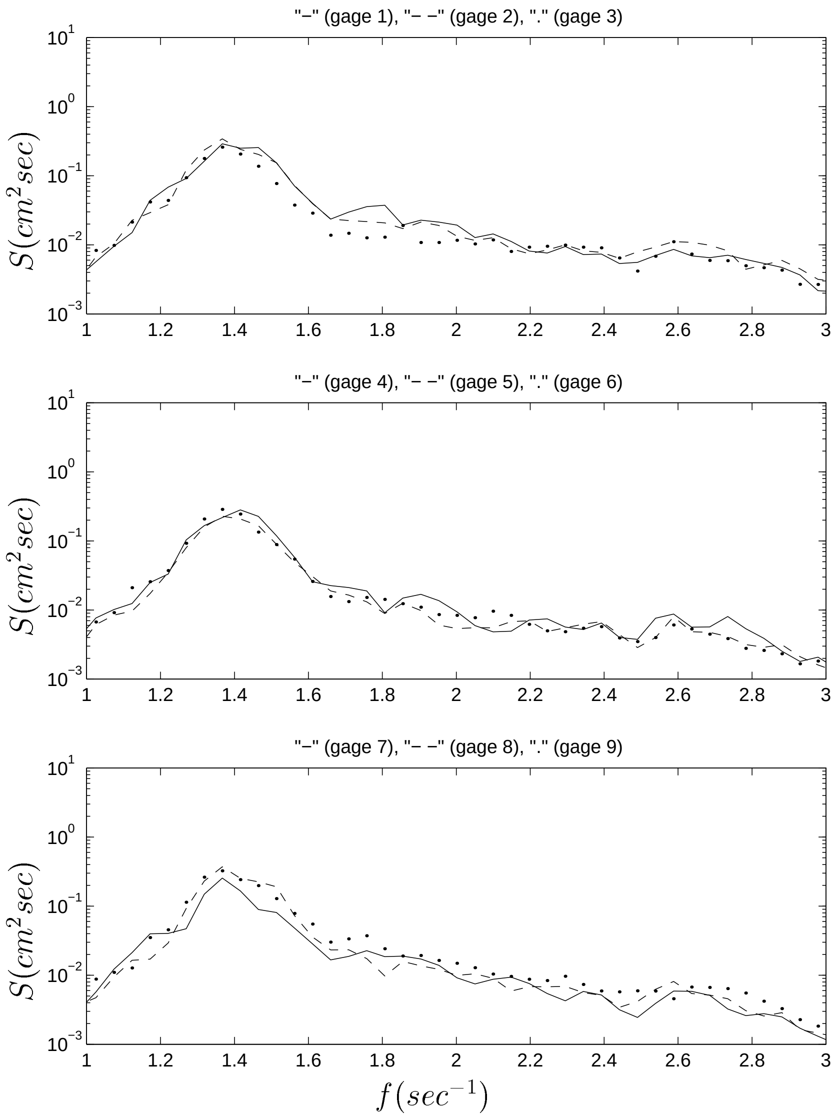

Figure D.7: Frequency spectra for Test 3 (position 7).

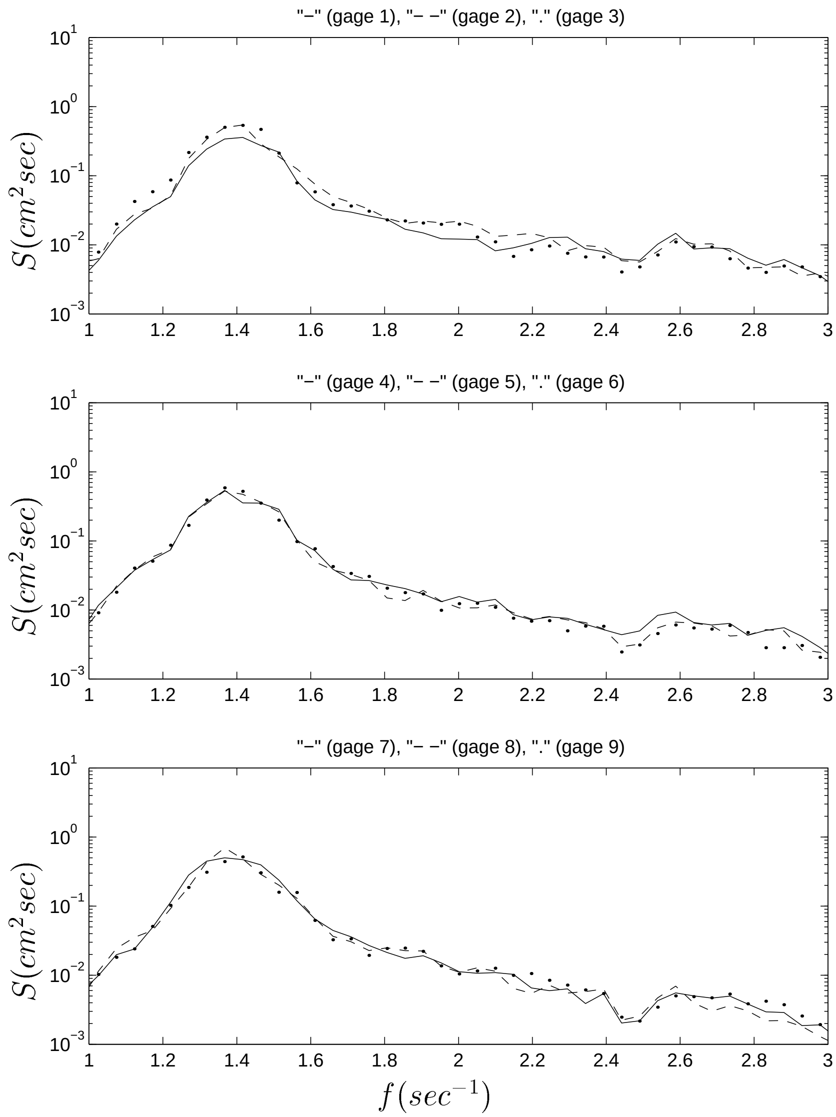

Figure D.8: Frequency spectra for Test 3 (position 8).

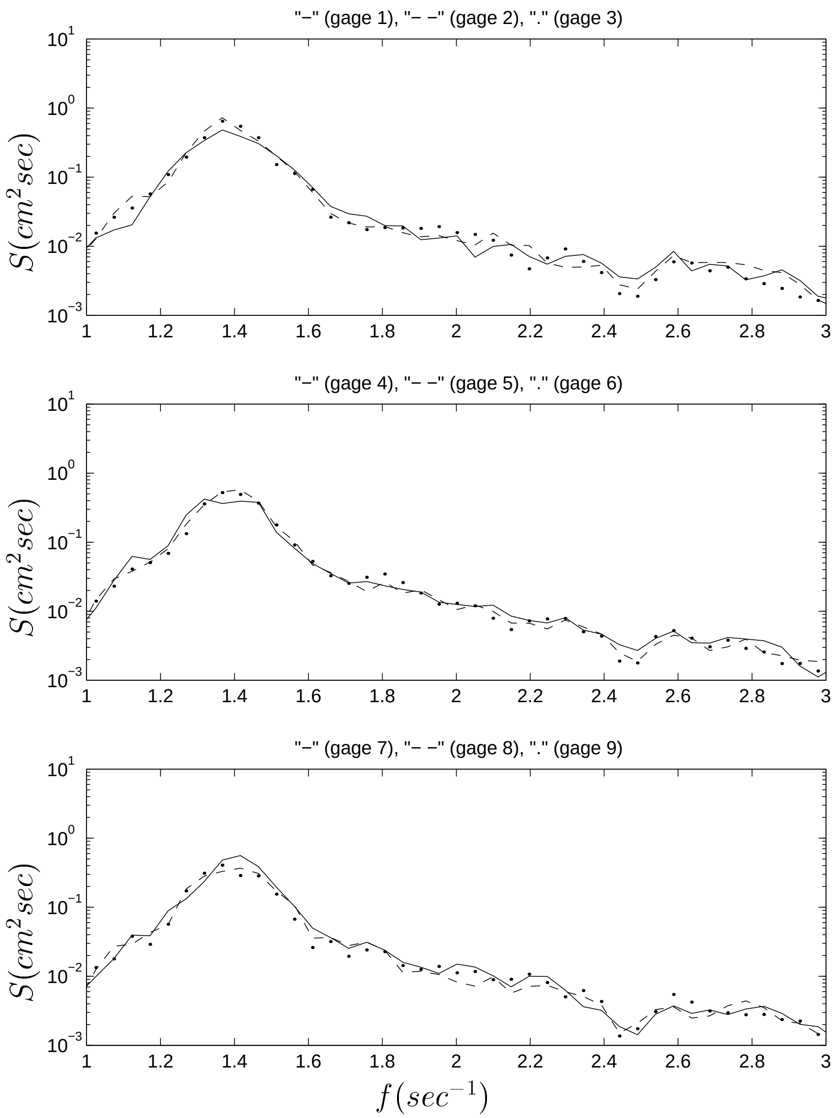

Figure D.9: Frequency spectra for Test 3 (position 9).

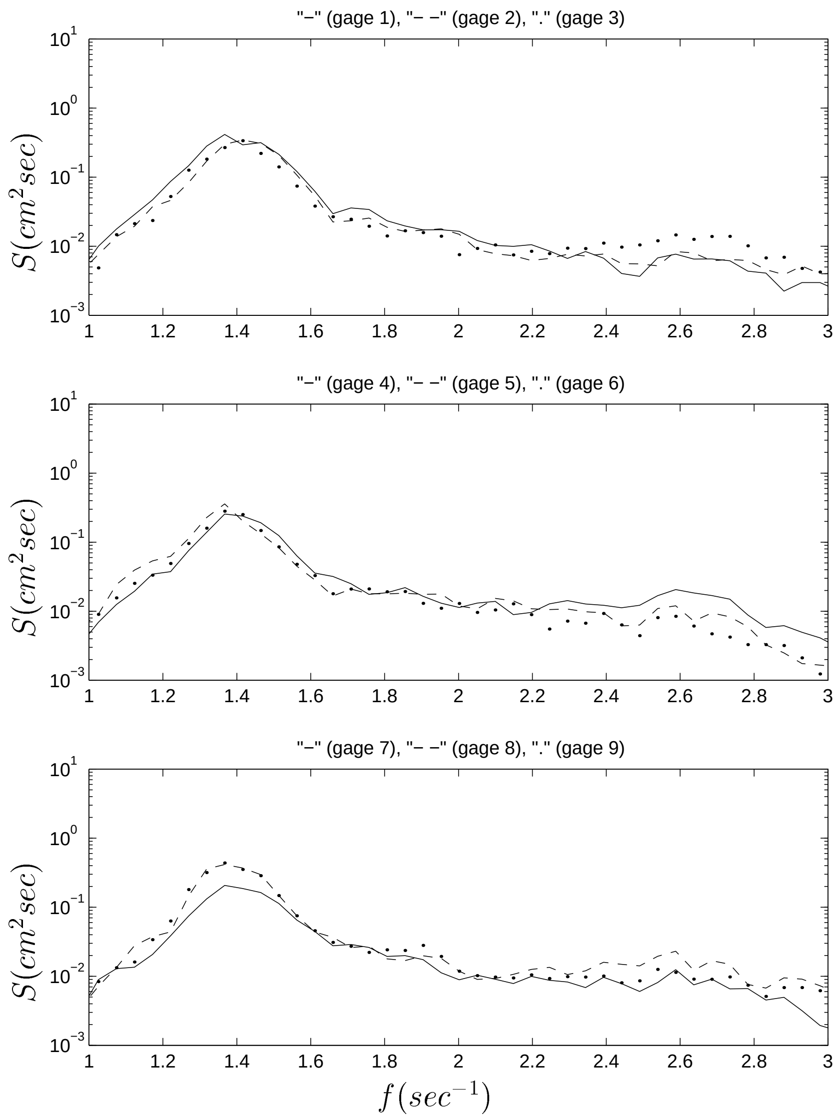

Figure D.10: Frequency spectra for Test 3 (position 10).

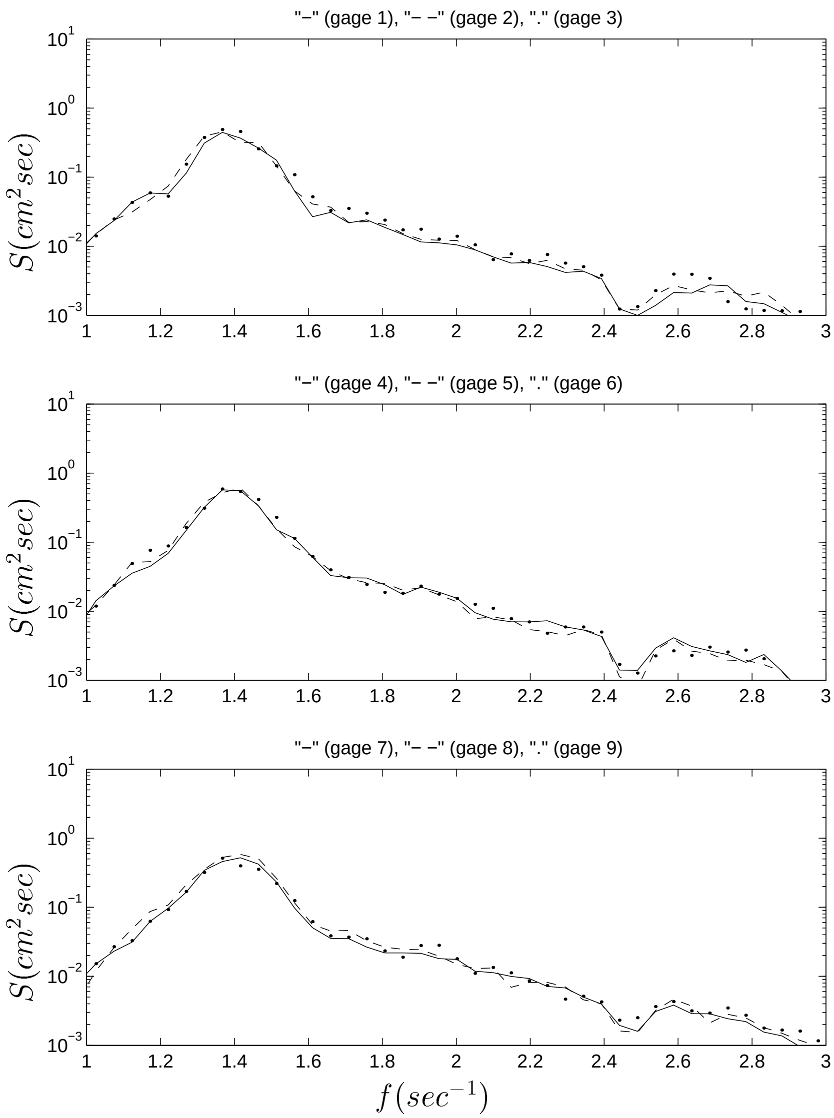

Figure D.11: Frequency spectra for Test 3 (position 11).

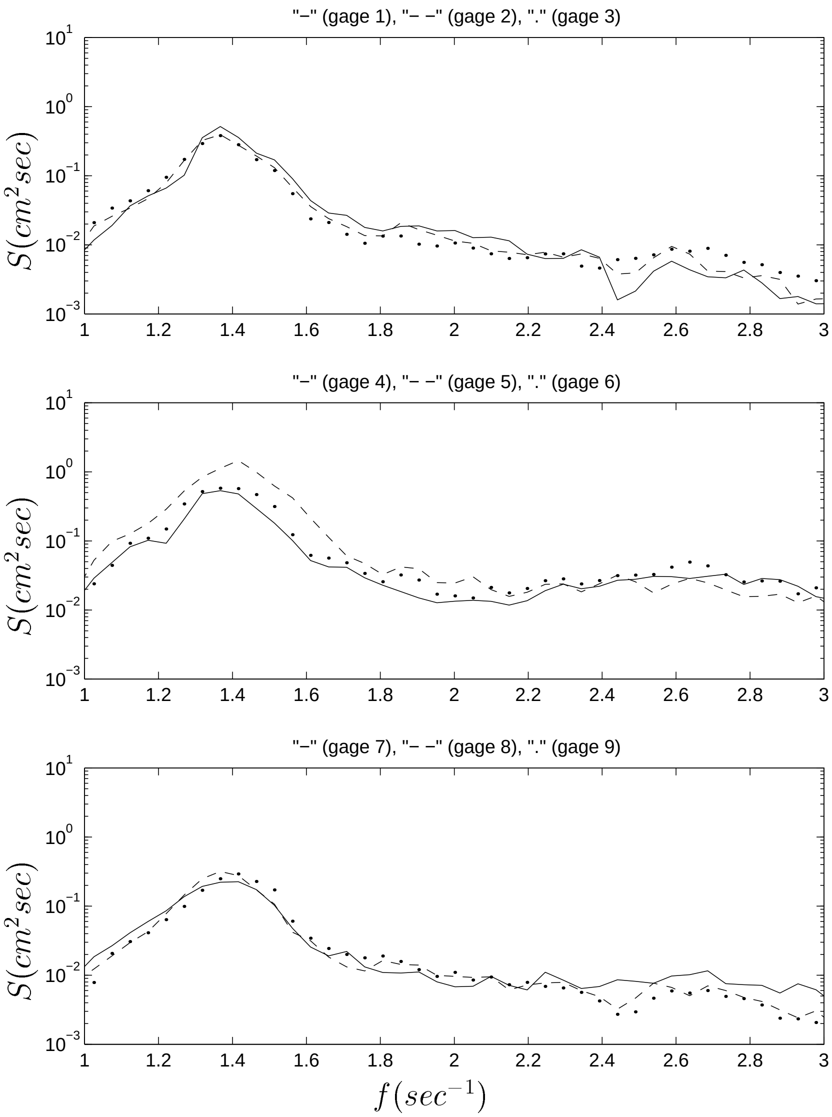

Figure D.12: Frequency spectra for Test 3 (position 12).

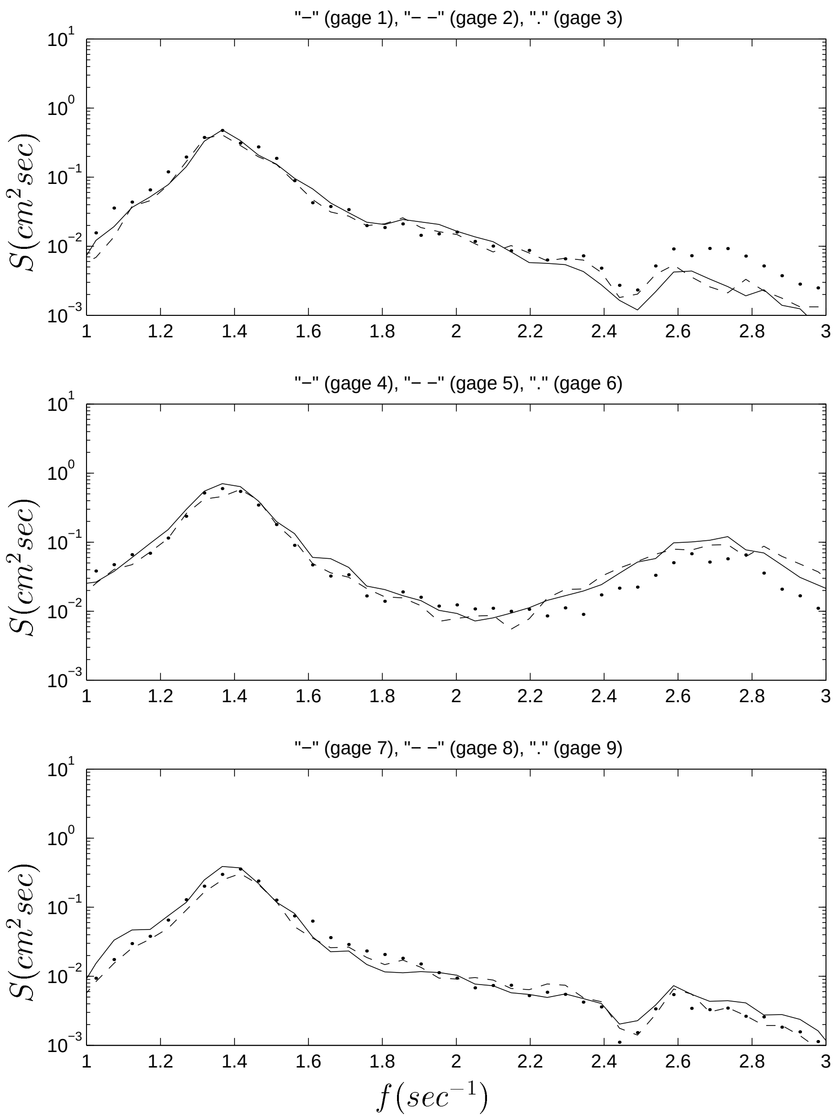

Figure D.13: Frequency spectra for Test 3 (position 13).

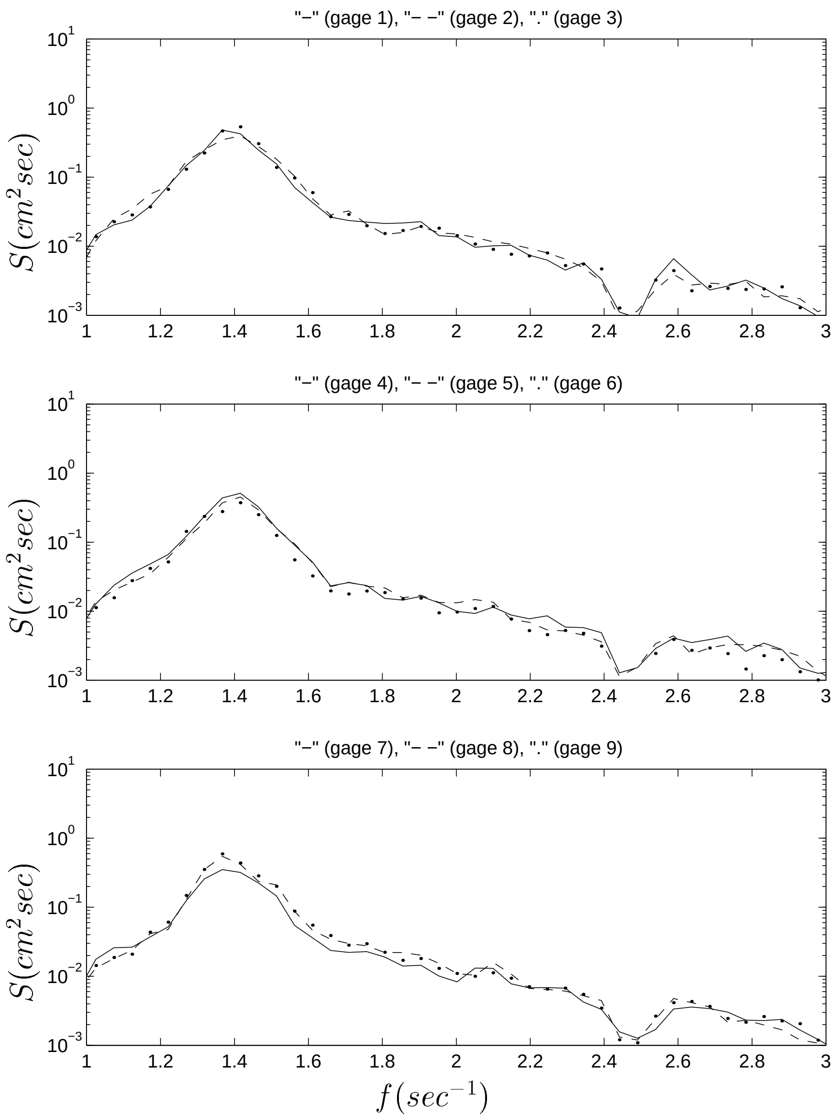

Figure D.14: Frequency spectra for Test 3 (position 14).

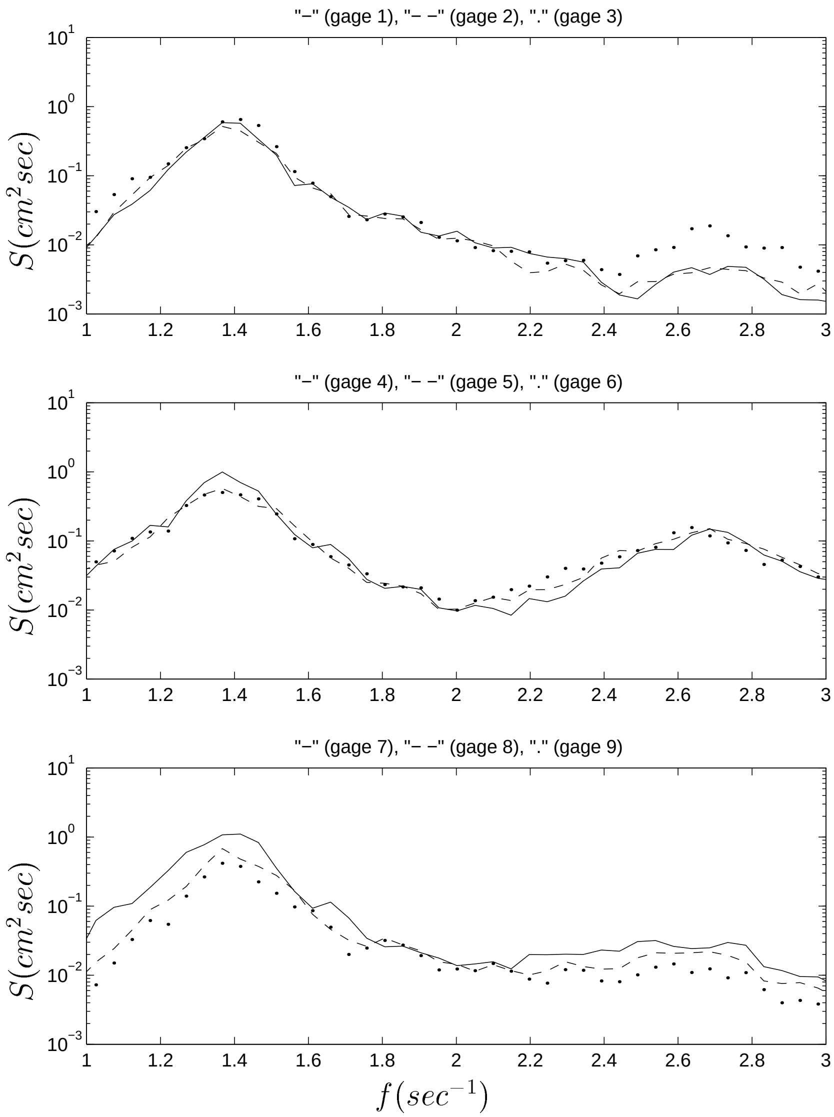

Figure D.15: Frequency spectra for Test 4 (position 1).

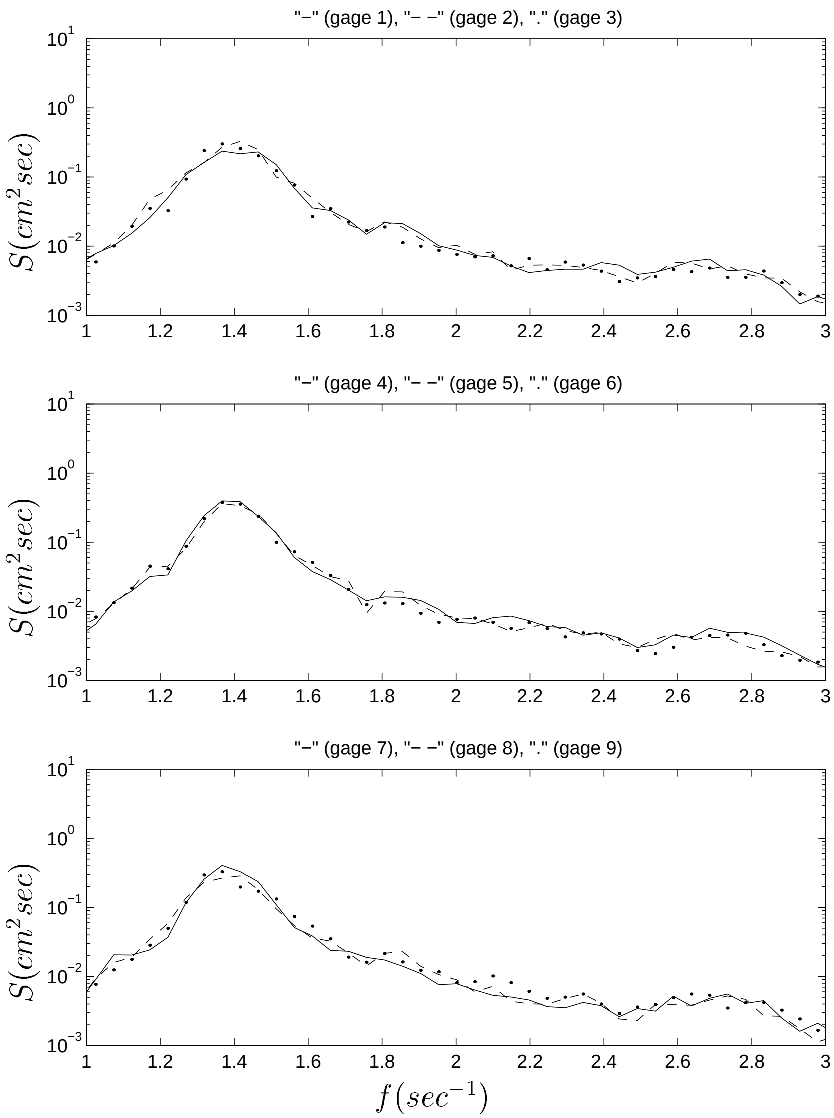

Figure D.16: Frequency spectra for Test 4 (position 2).

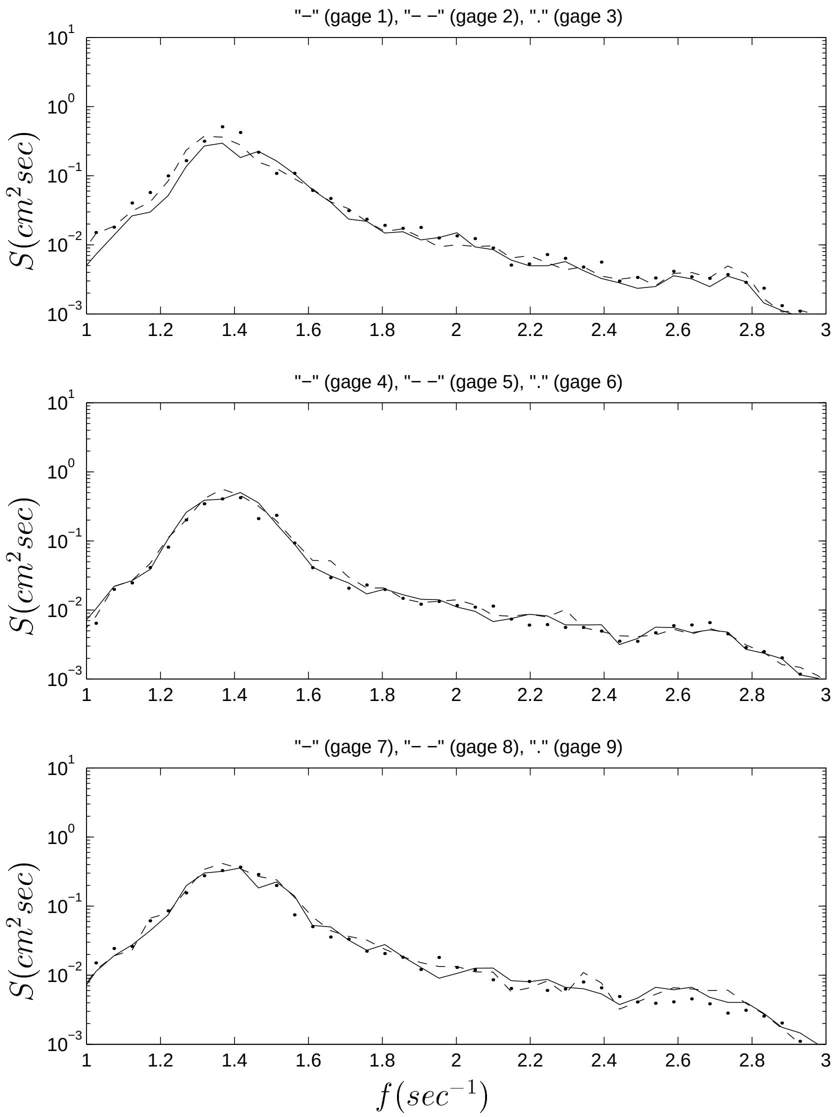

Figure D.17: Frequency spectra for Test 4 (position 3).

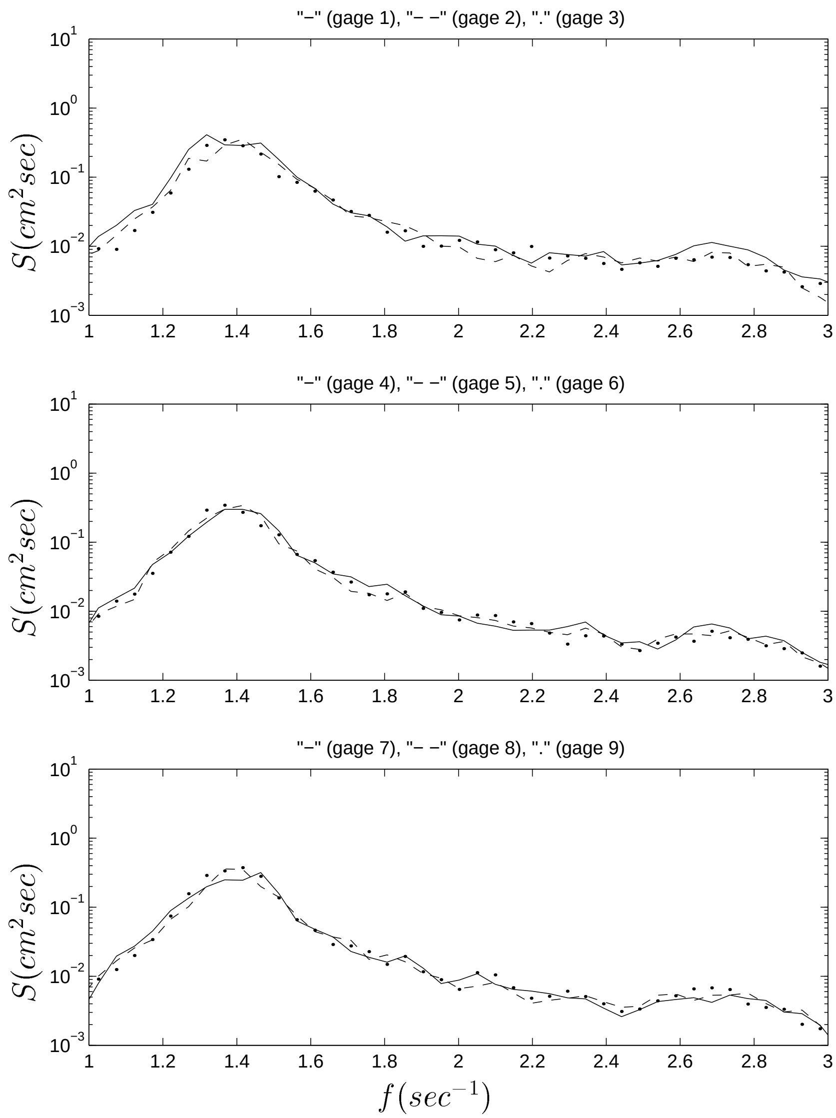

Figure D.18: Frequency spectra for Test 4 (position 4).

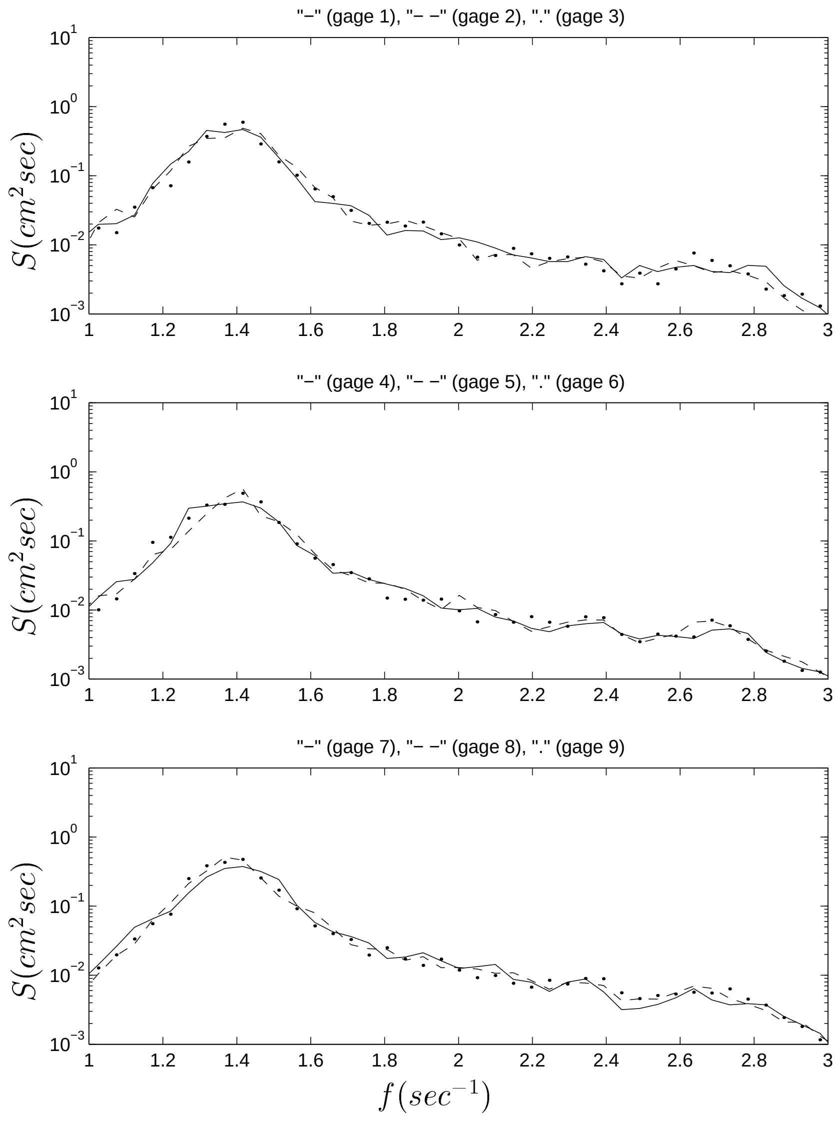

Figure D.19: Frequency spectra for Test 4 (position 5).

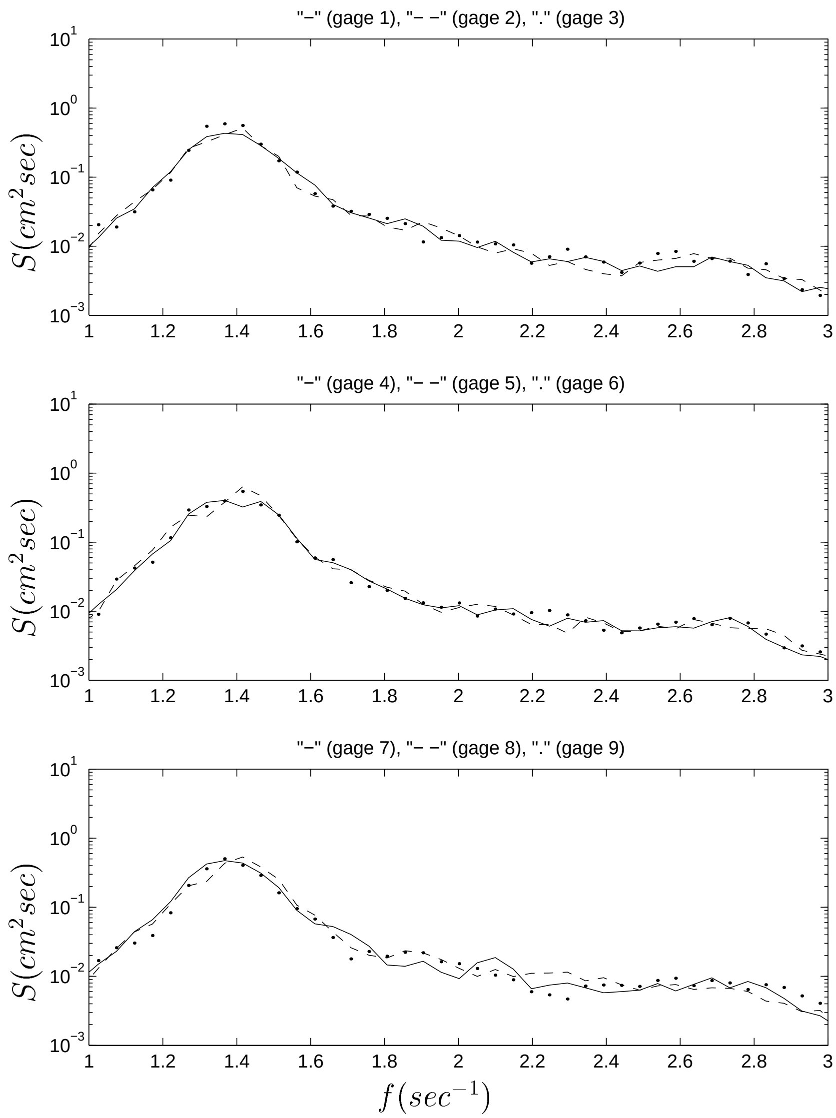

Figure D.20: Frequency spectra for Test 4 (position 6).

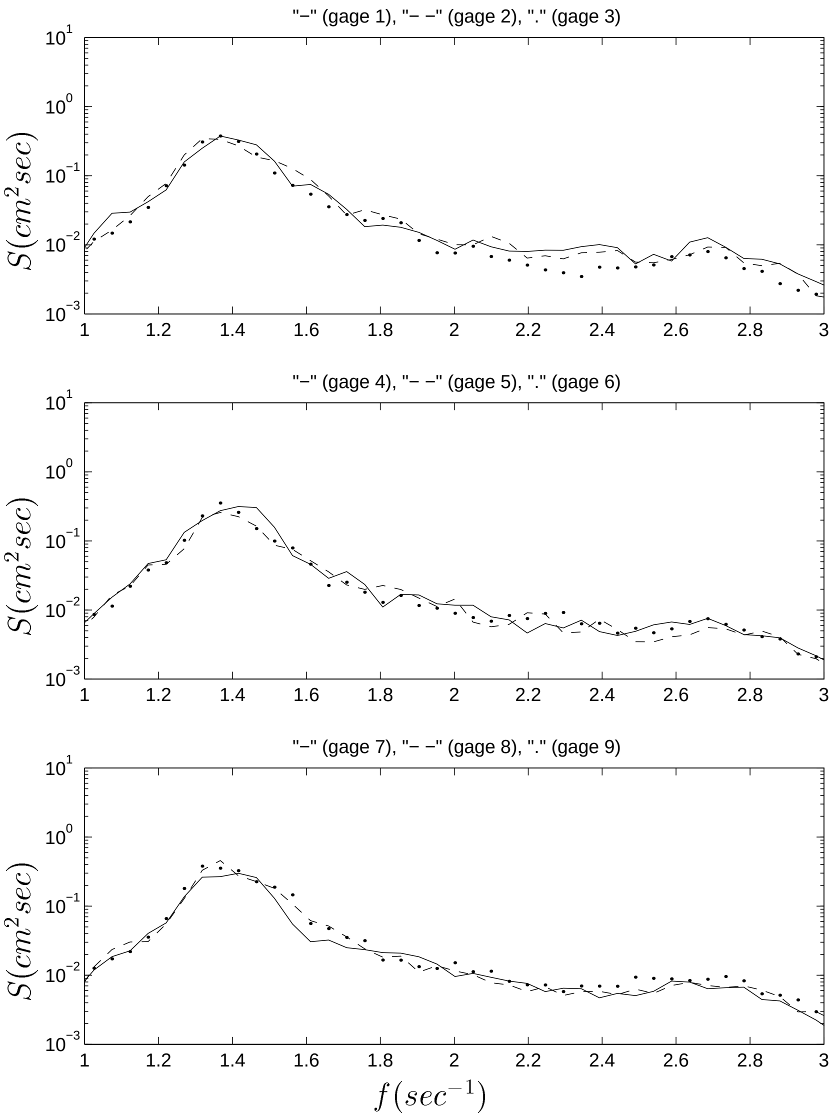

Figure D.21: Frequency spectra for Test 4 (position 7).

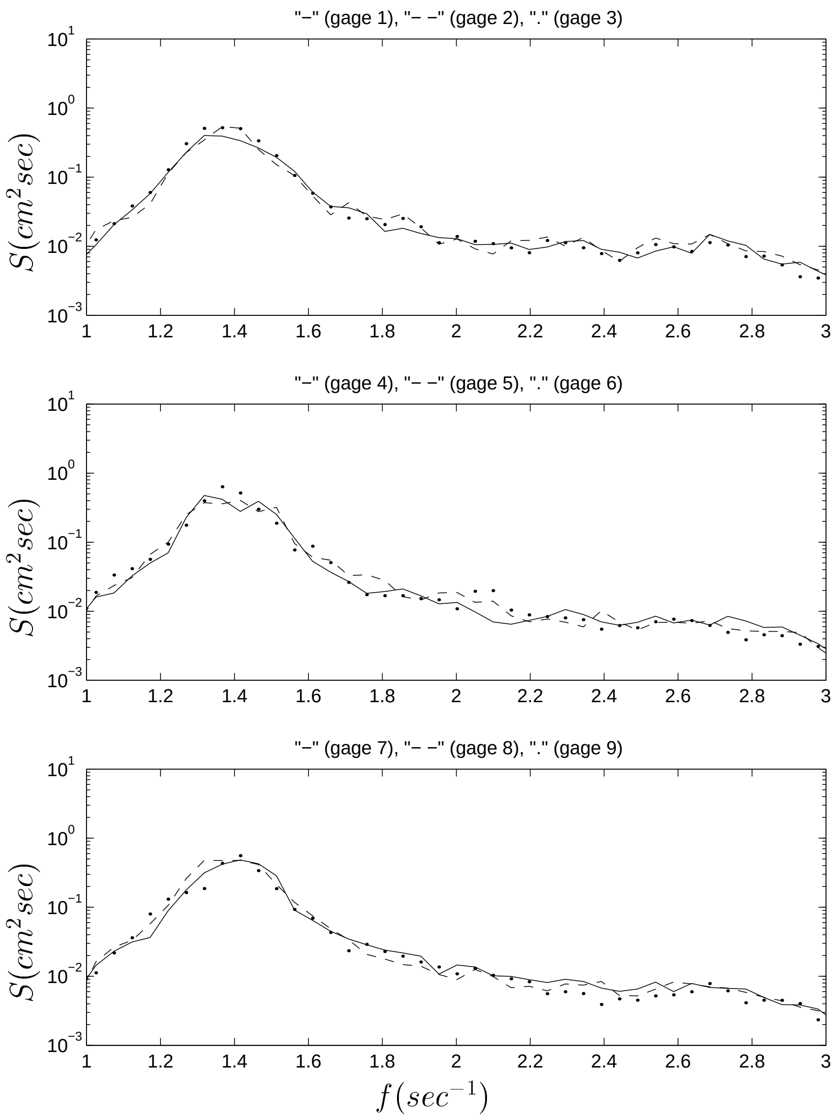

Figure D.22: Frequency spectra for Test 4 (position 8).

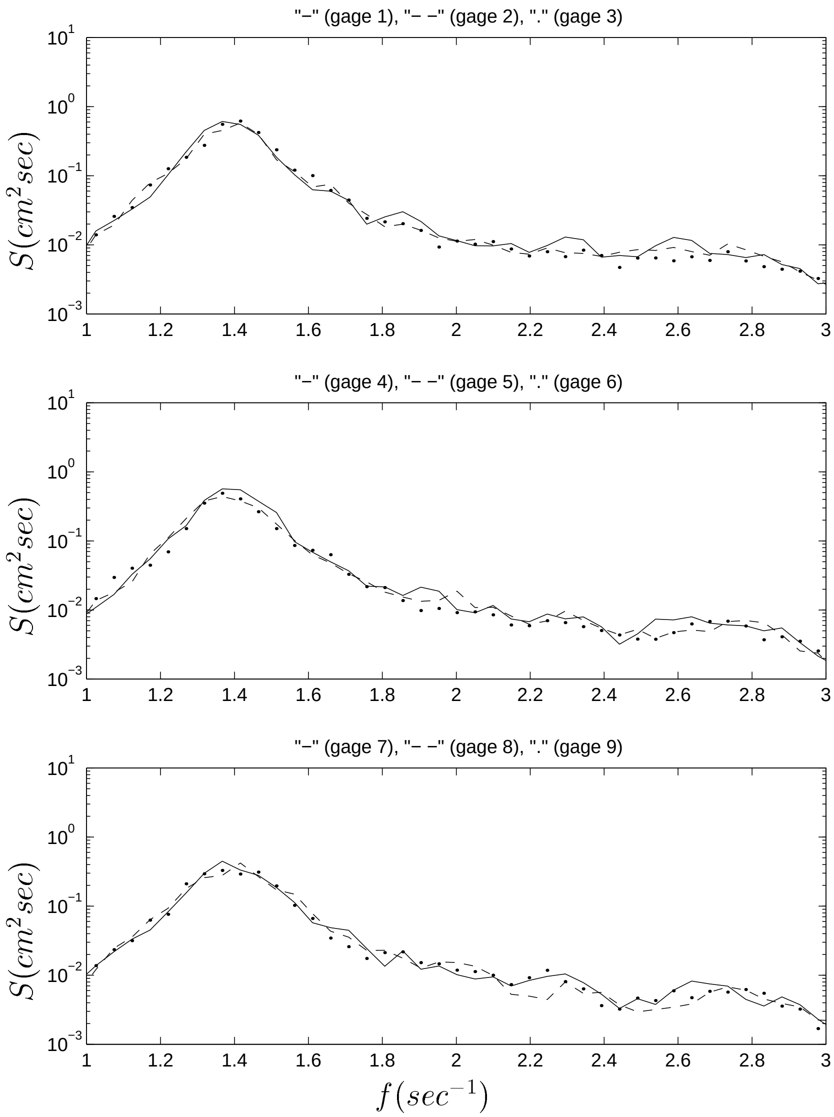

Figure D.23: Frequency spectra for Test 4 (position 9).

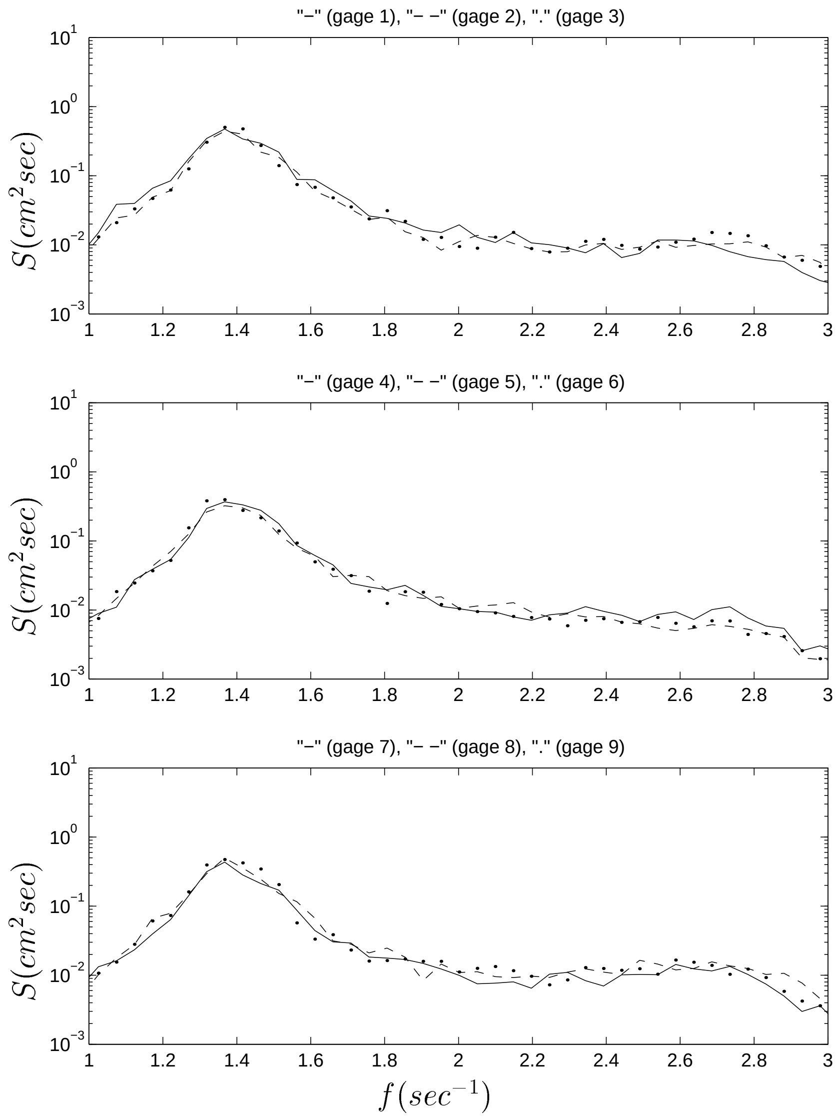

Figure D.24: Frequency spectra for Test 4 (position 10).

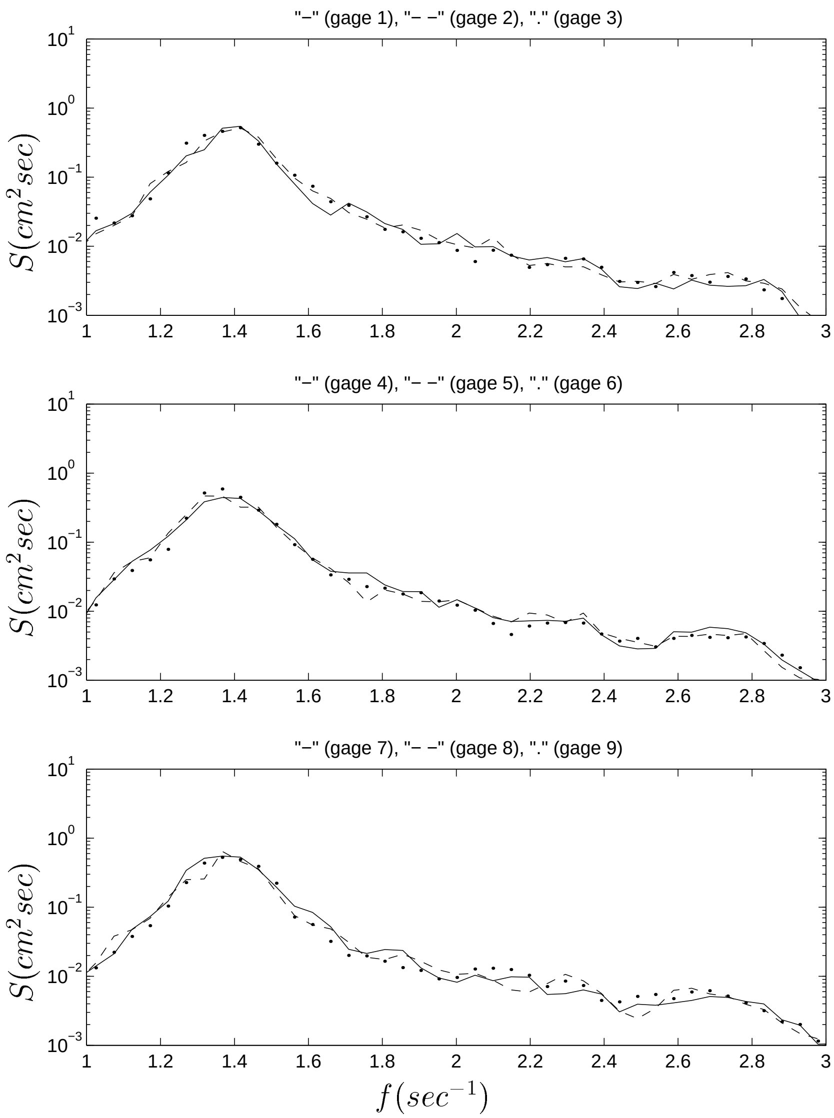

Figure D.25: Frequency spectra for Test 4 (position 11).

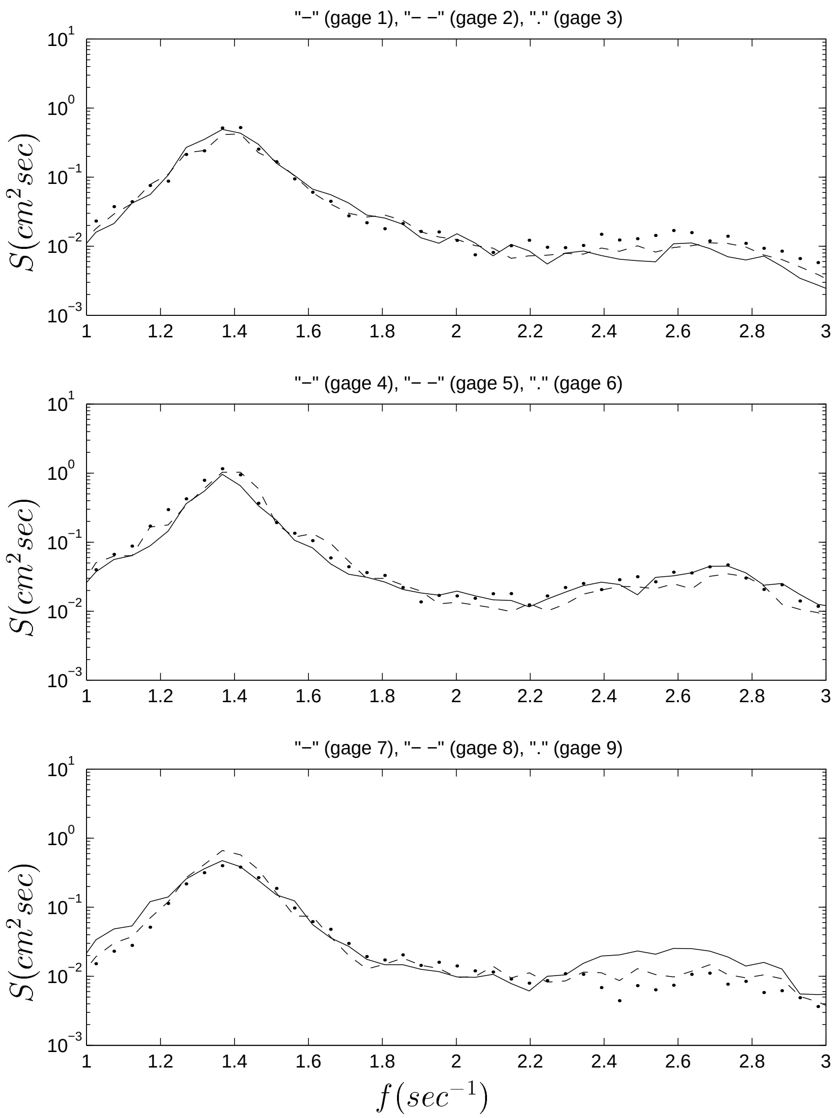

Figure D.26: Frequency spectra for Test 4 (position 12).

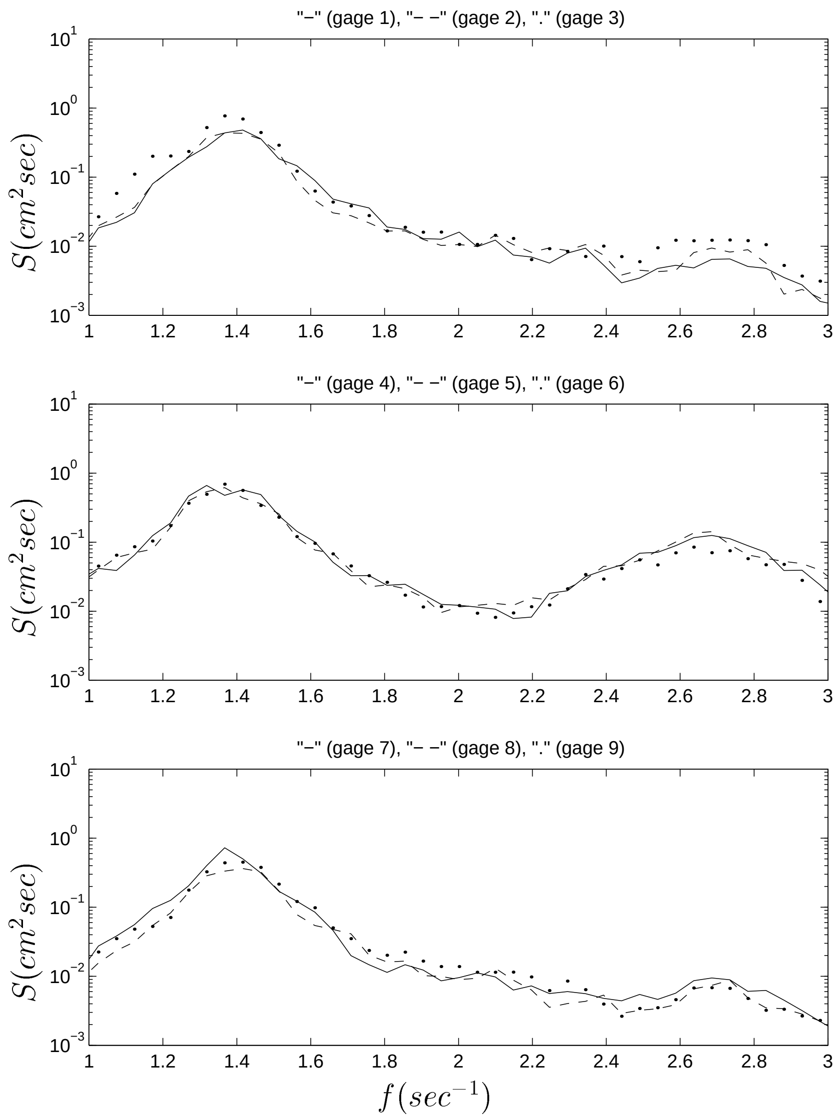

Figure D.27: Frequency spectra for Test 4 (position 13).

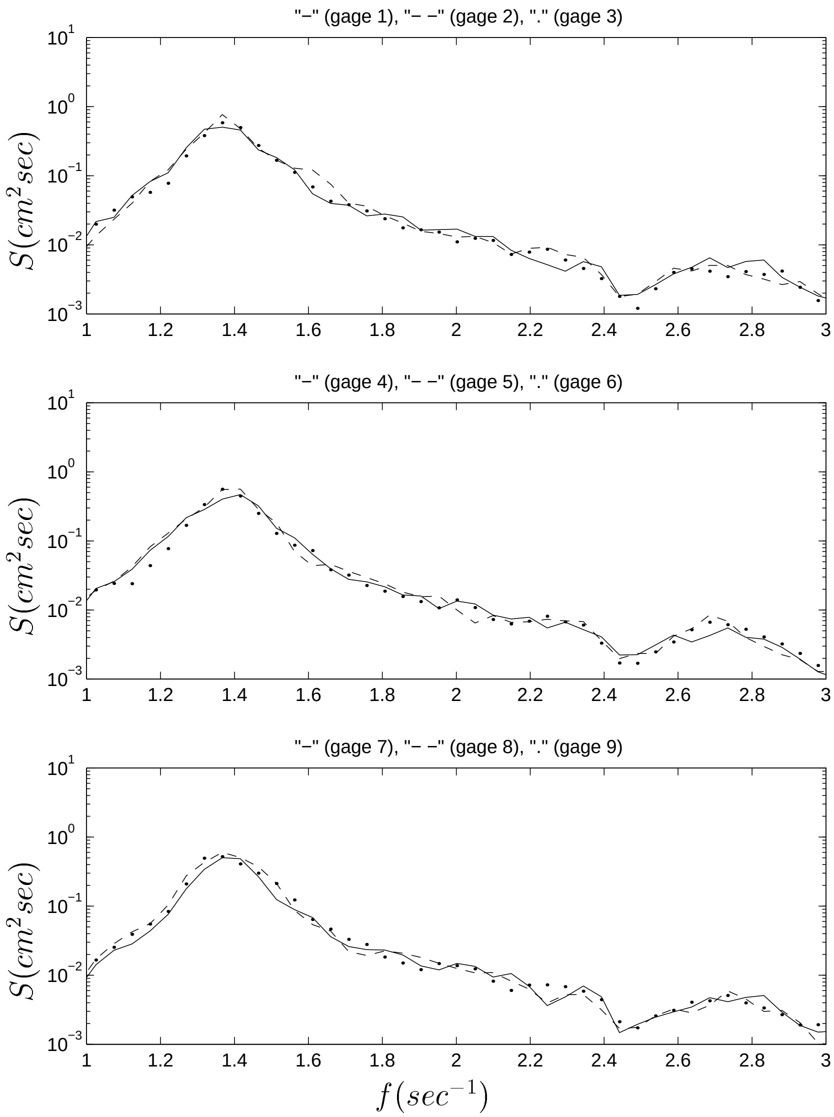

Figure D.28: Frequency spectra for Test 4 (position 14).

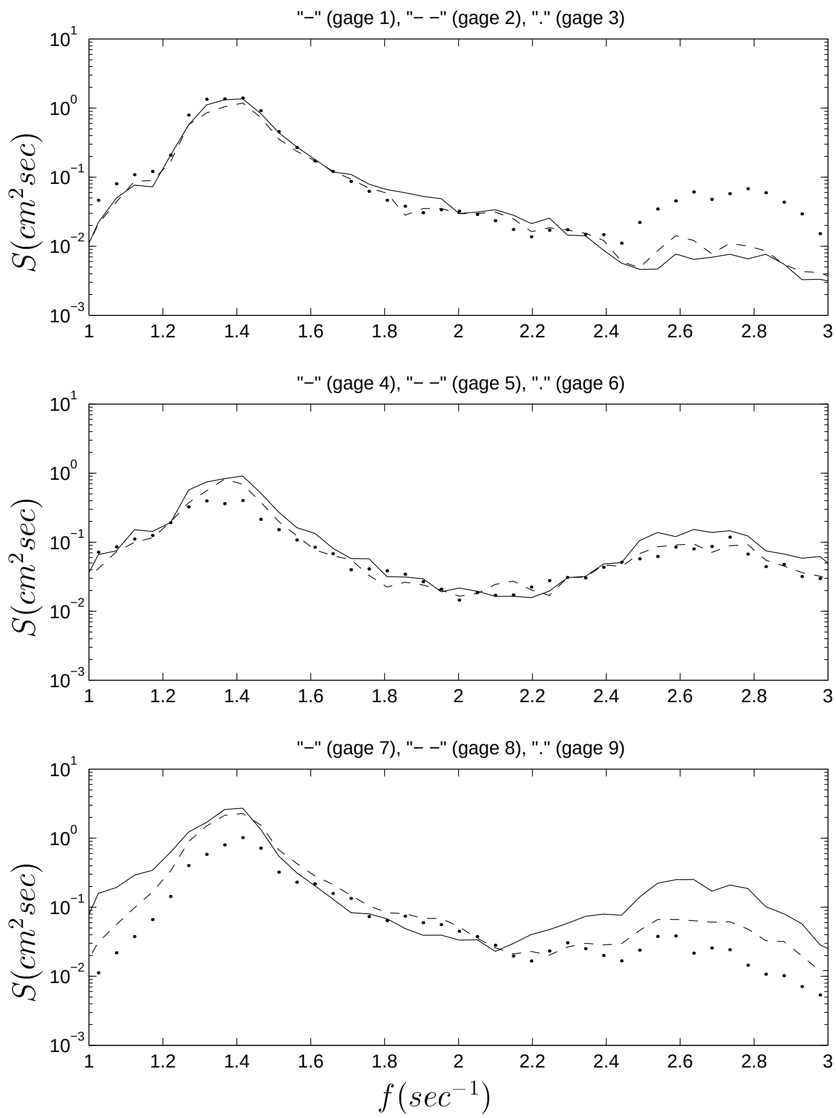

Figure D.29: Frequency spectra for Test 5 (position 1).

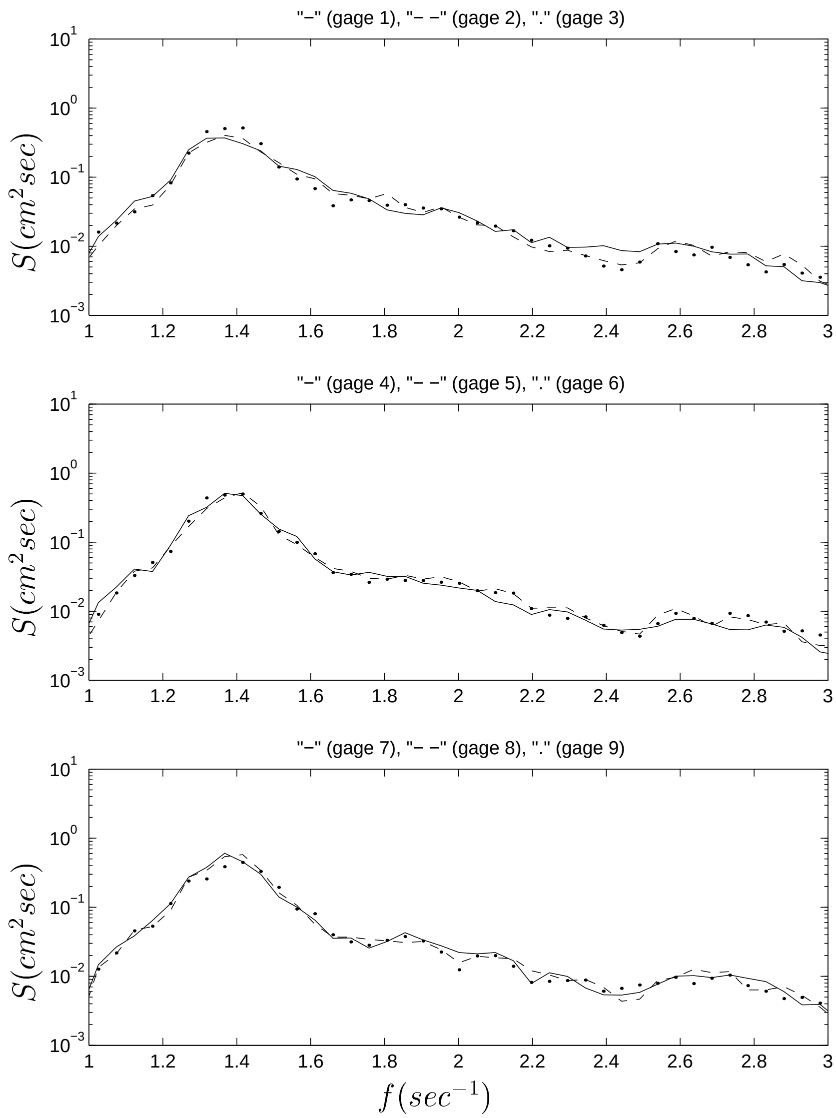

Figure D.30: Frequency spectra for Test 5 (position 2).

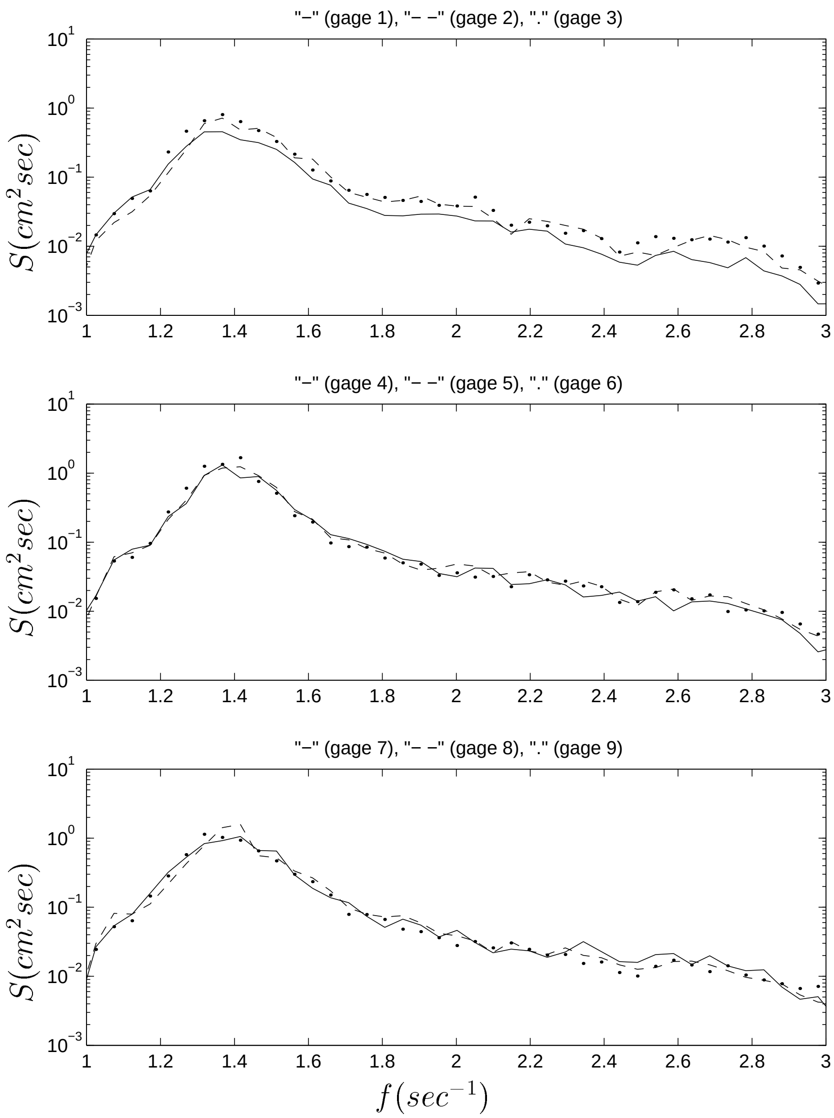

Figure D.31: Frequency spectra for Test 5 (position 3).

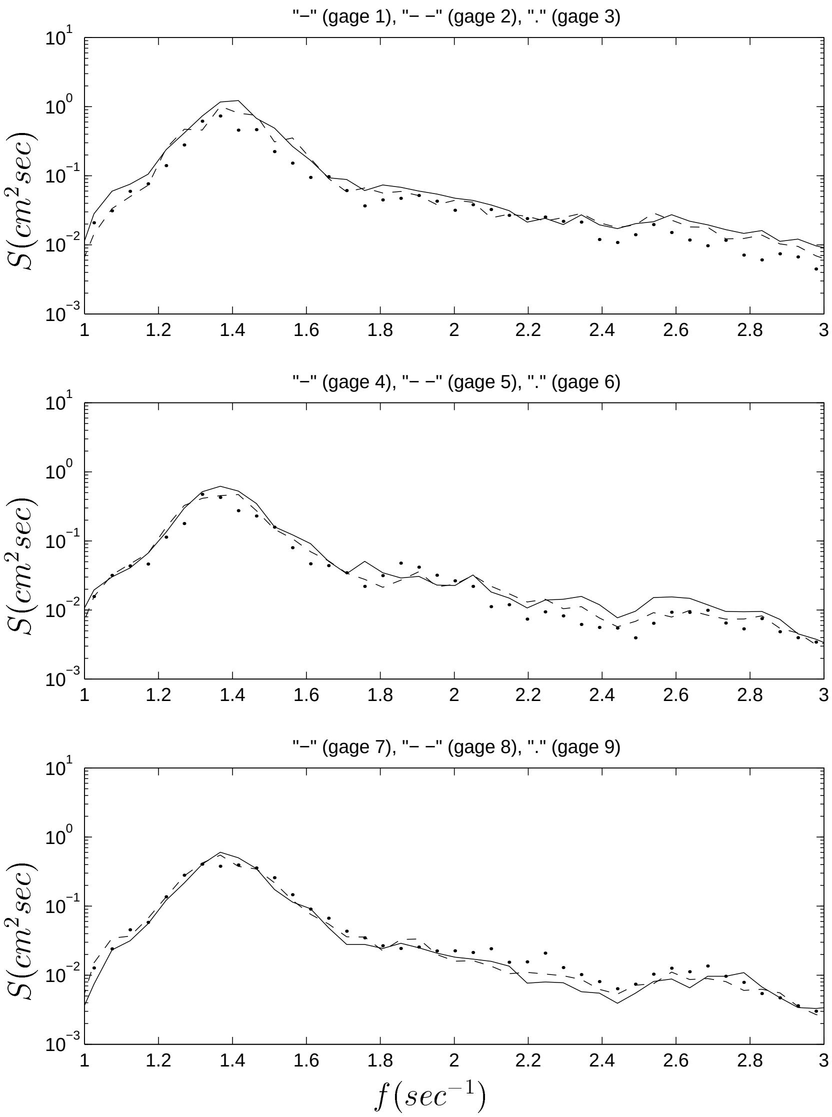

Figure D.32: Frequency spectra for Test 5 (position 4).

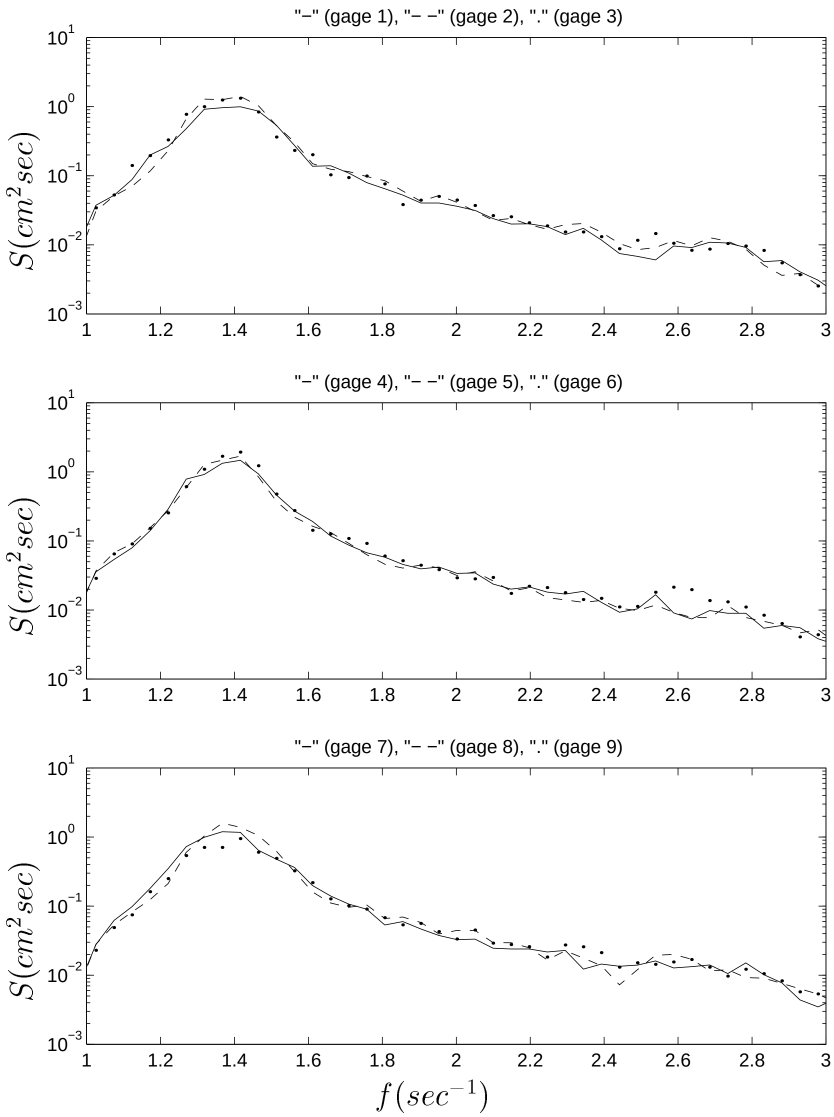

Figure D.33: Frequency spectra for Test 5 (position 5).

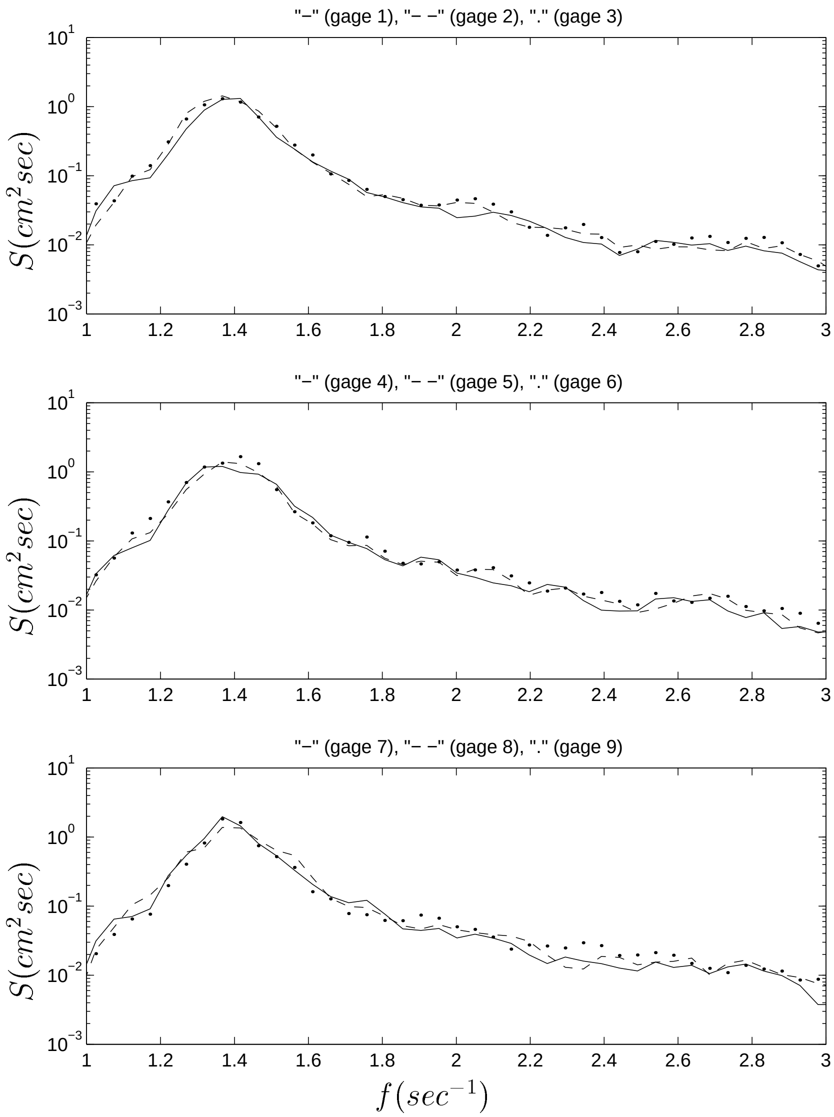

Figure D.34: Frequency spectra for Test 5 (position 6).

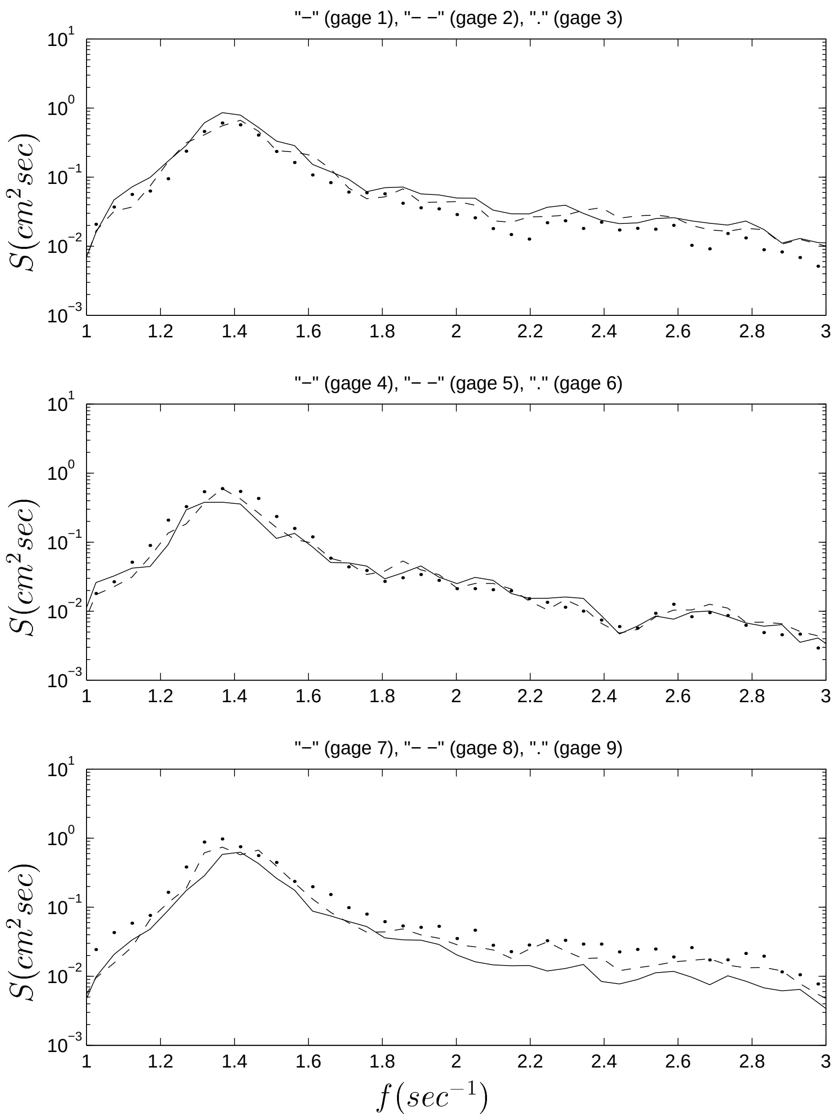

Figure D.35: Frequency spectra for Test 5 (position 7).

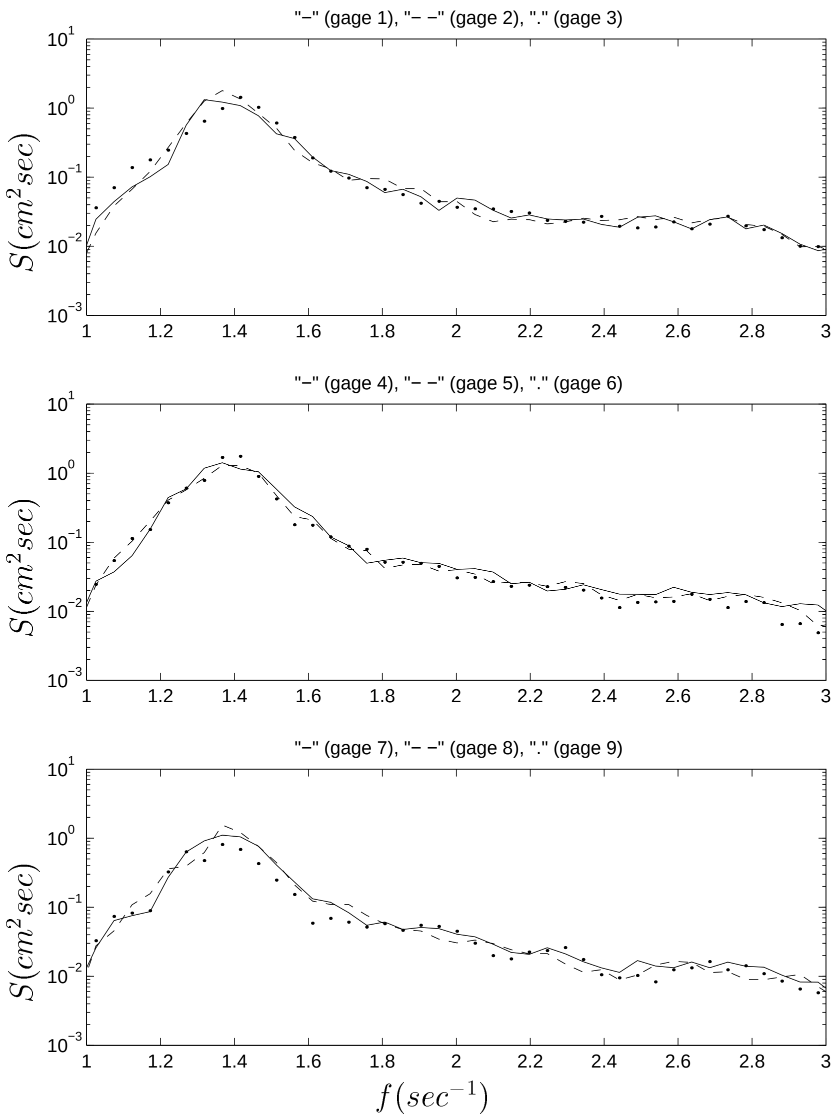

Figure D.36: Frequency spectra for Test 5 (position 8).

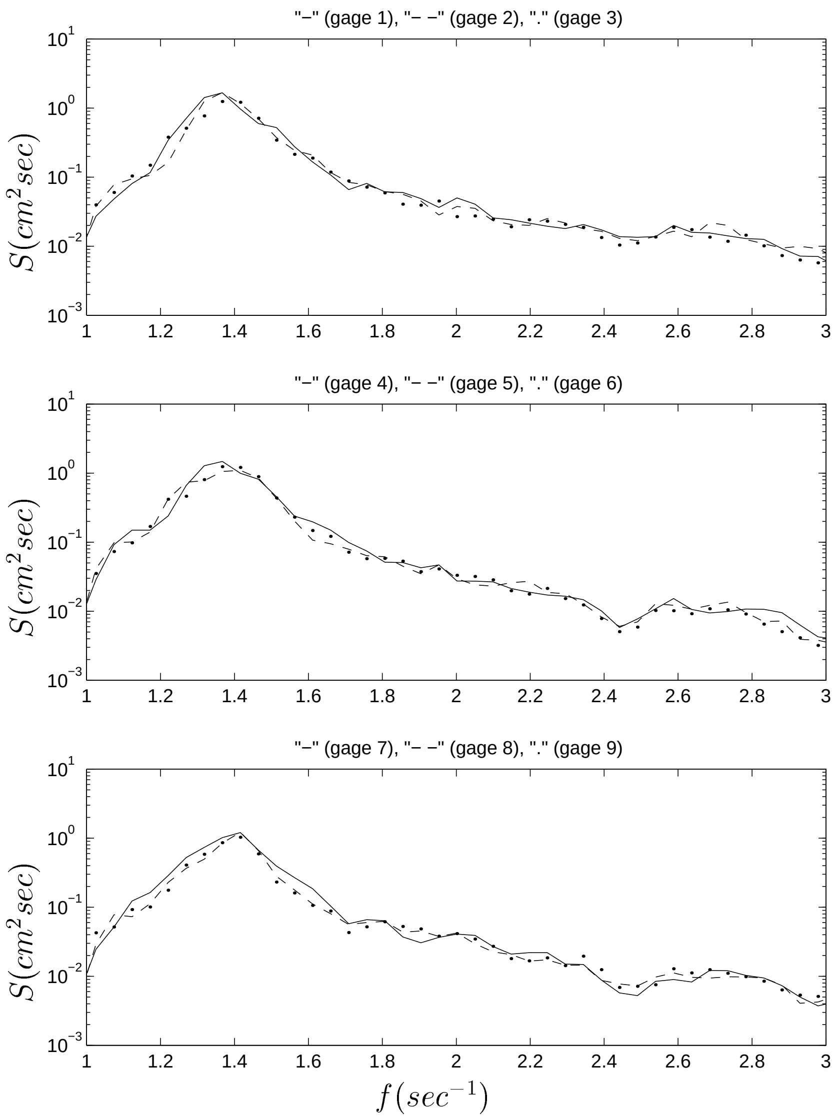

Figure D.37: Frequency spectra for Test 5 (position 9).

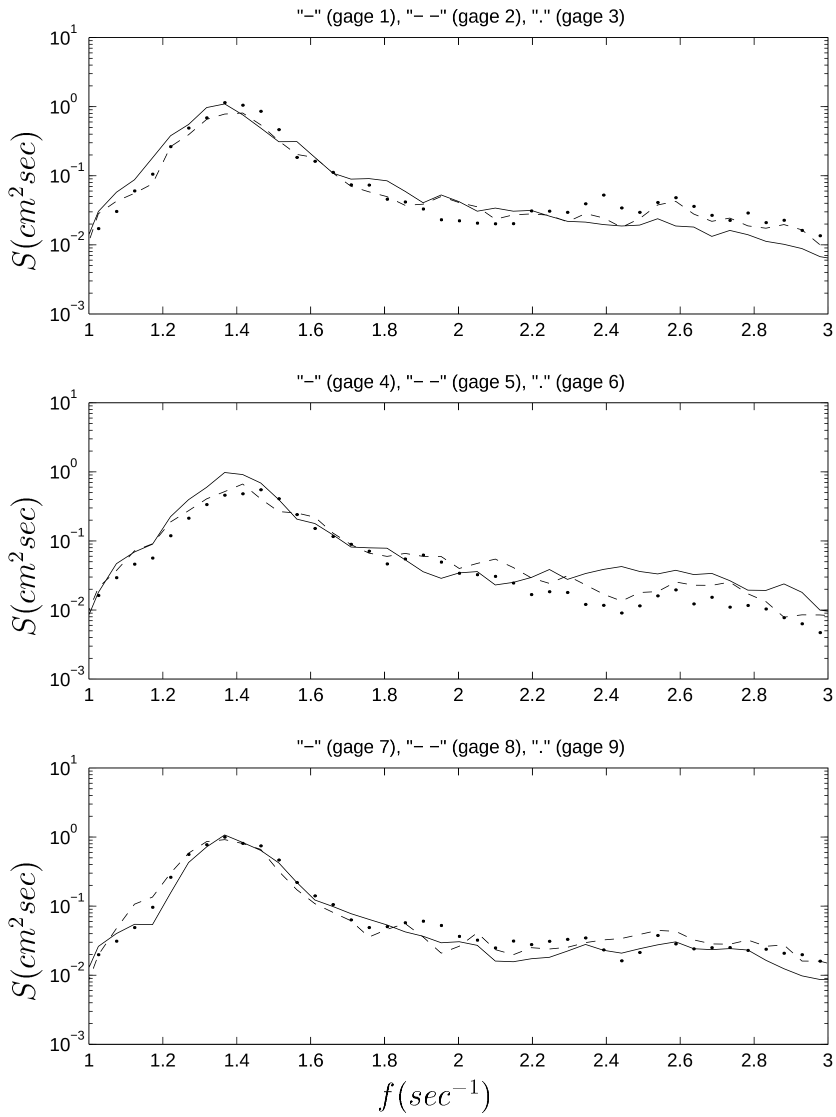

Figure D.38: Frequency spectra for Test 5 (position 10).

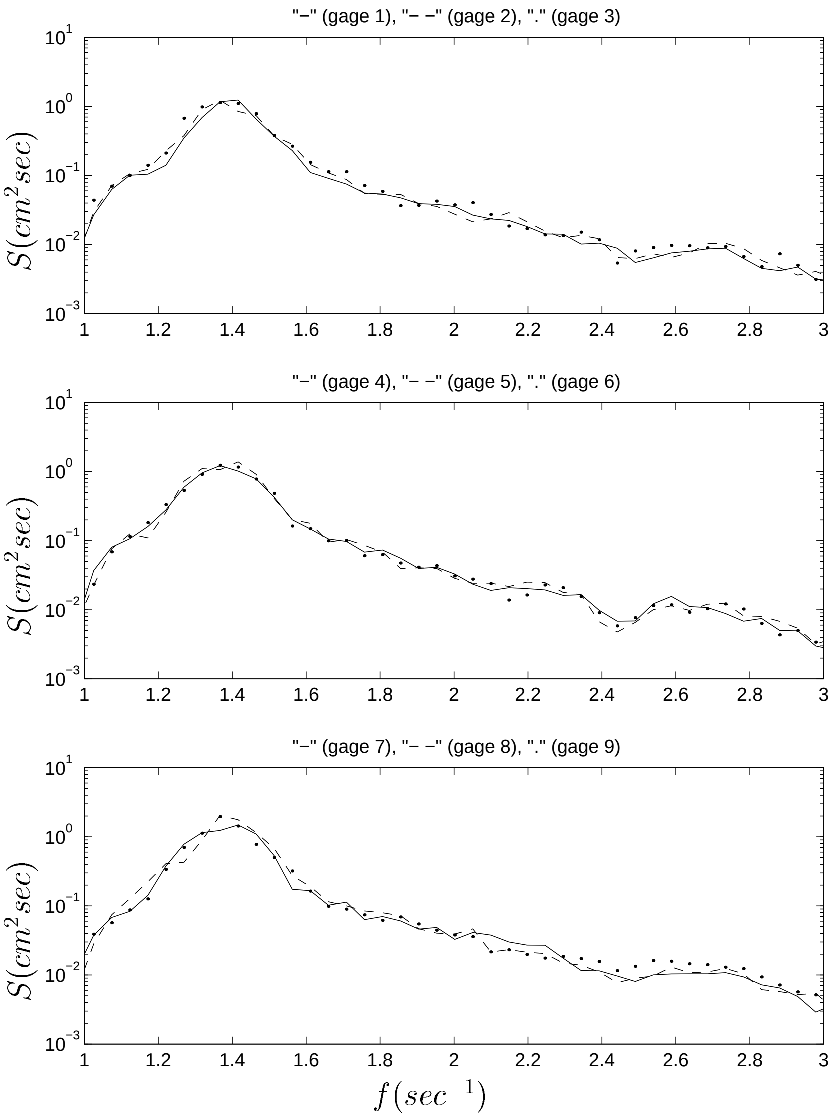

Figure D.39: Frequency spectra for Test 5 (position 11).

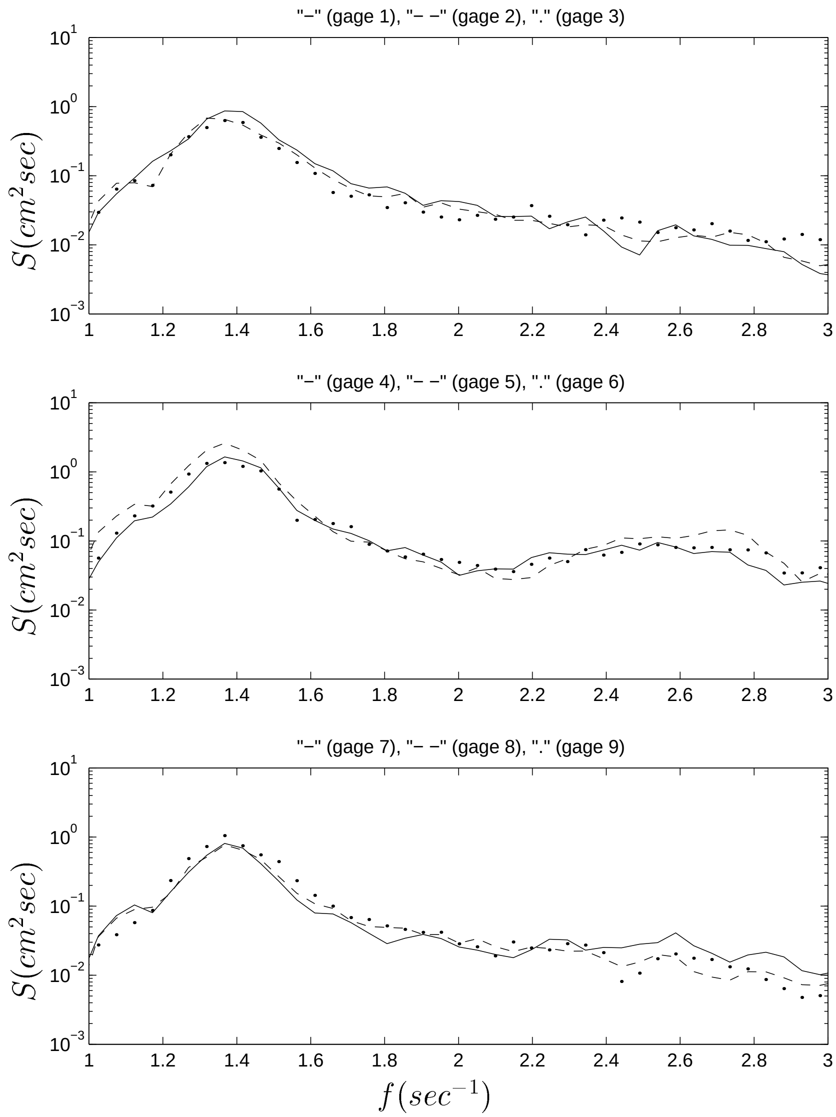

Figure D.40: Frequency spectra for Test 5 (position 12).

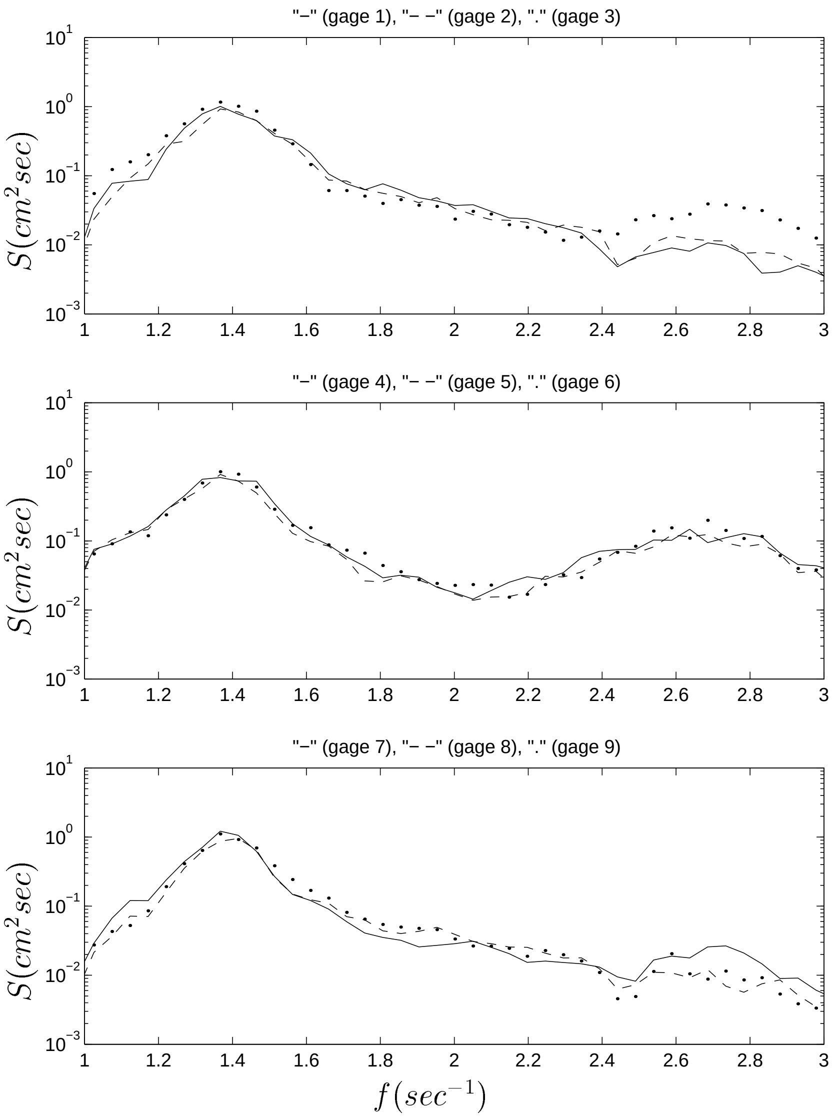

Figure D.41: Frequency spectra for Test 5 (position 13).

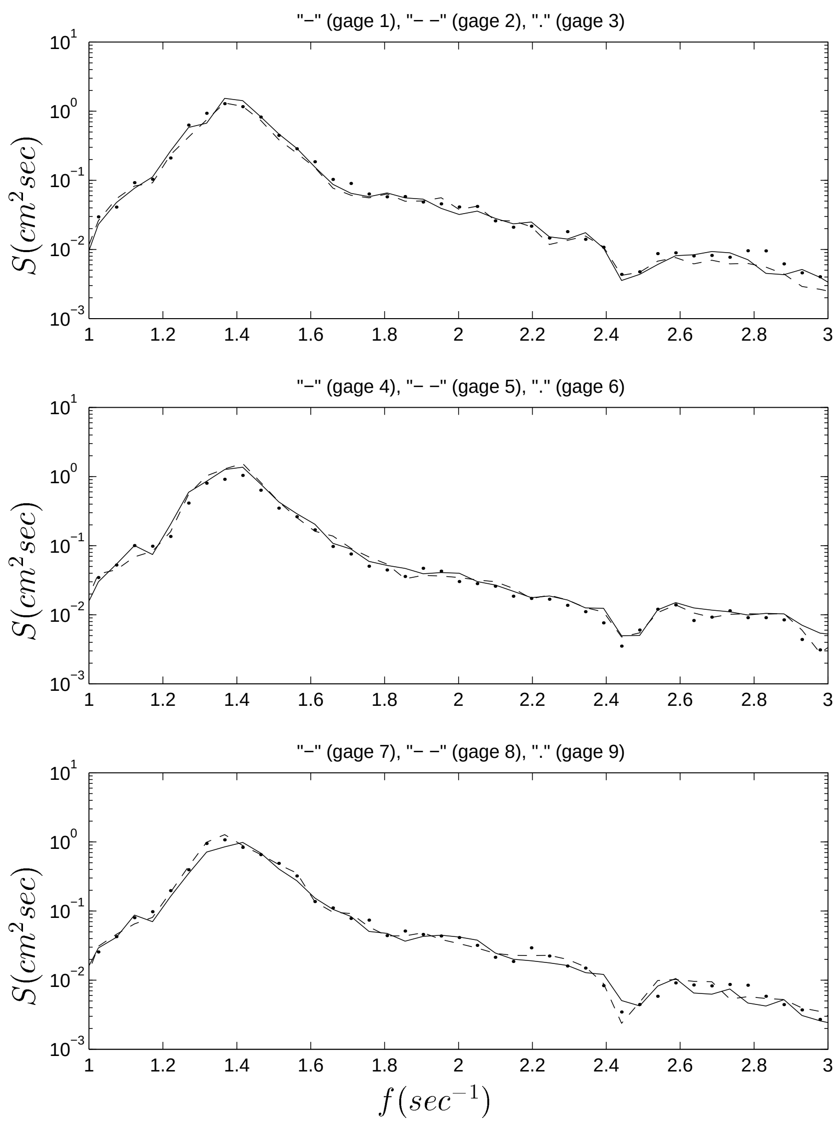

Figure D.42: Frequency spectra for Test 5 (position 14).

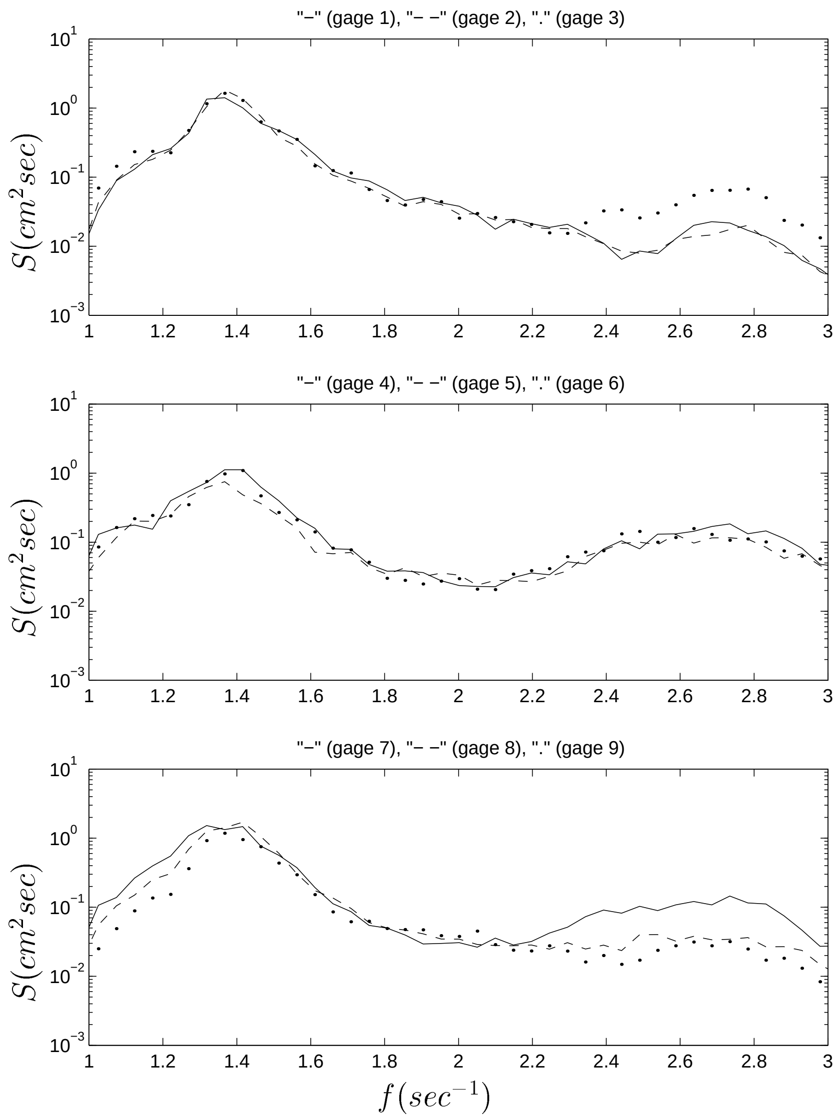

Figure D.43: Frequency spectra for Test 6 (position 1).

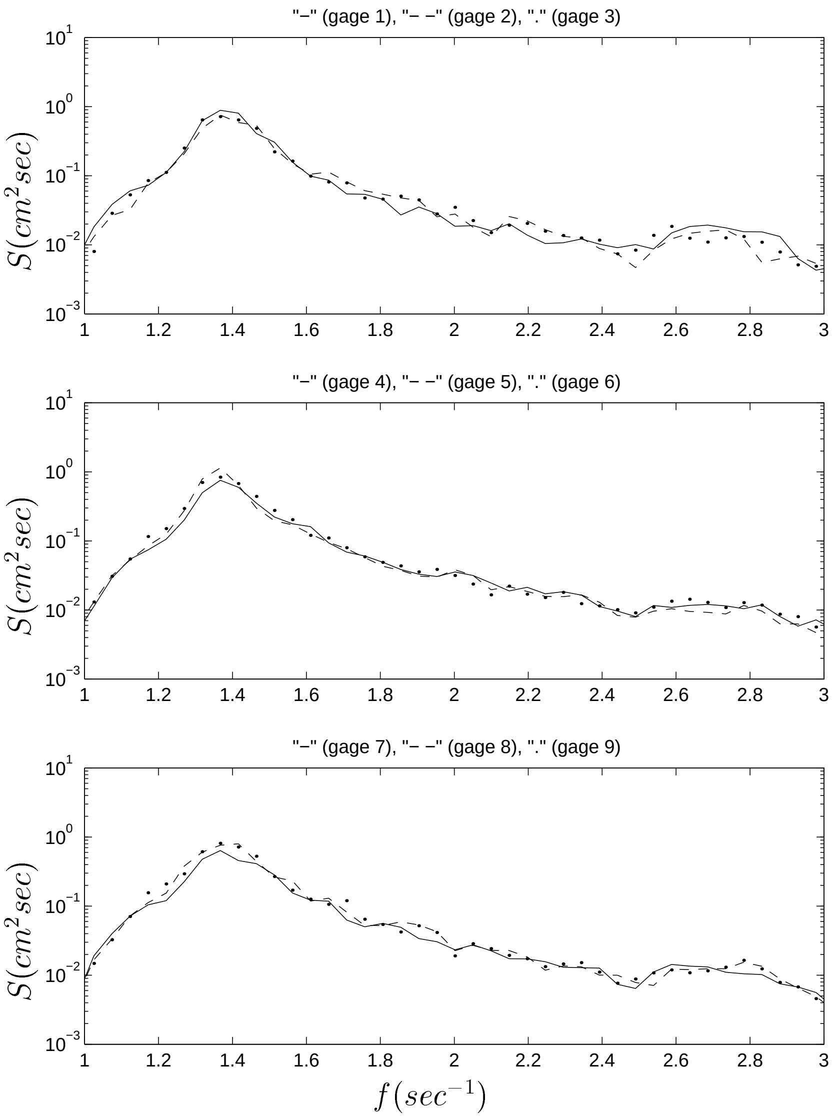

Figure D.44: Frequency spectra for Test 6 (position 2).

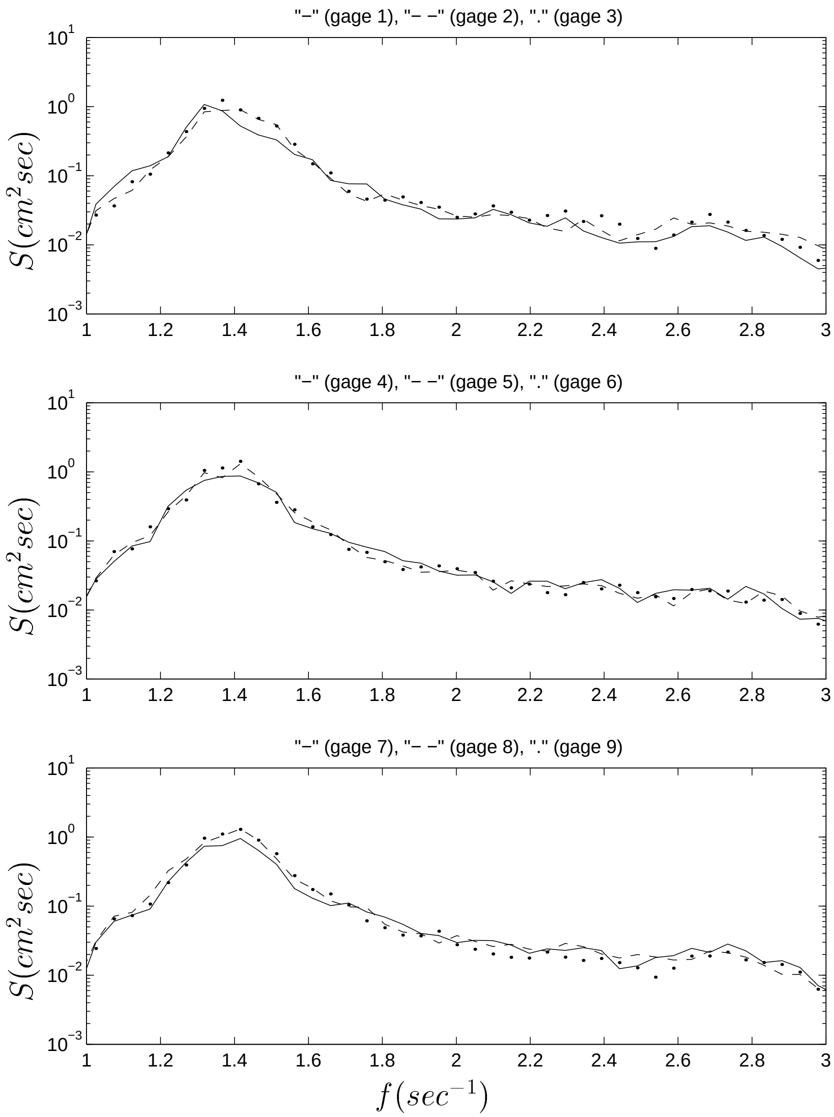

Figure D.45: Frequency spectra for Test 6 (position 3).

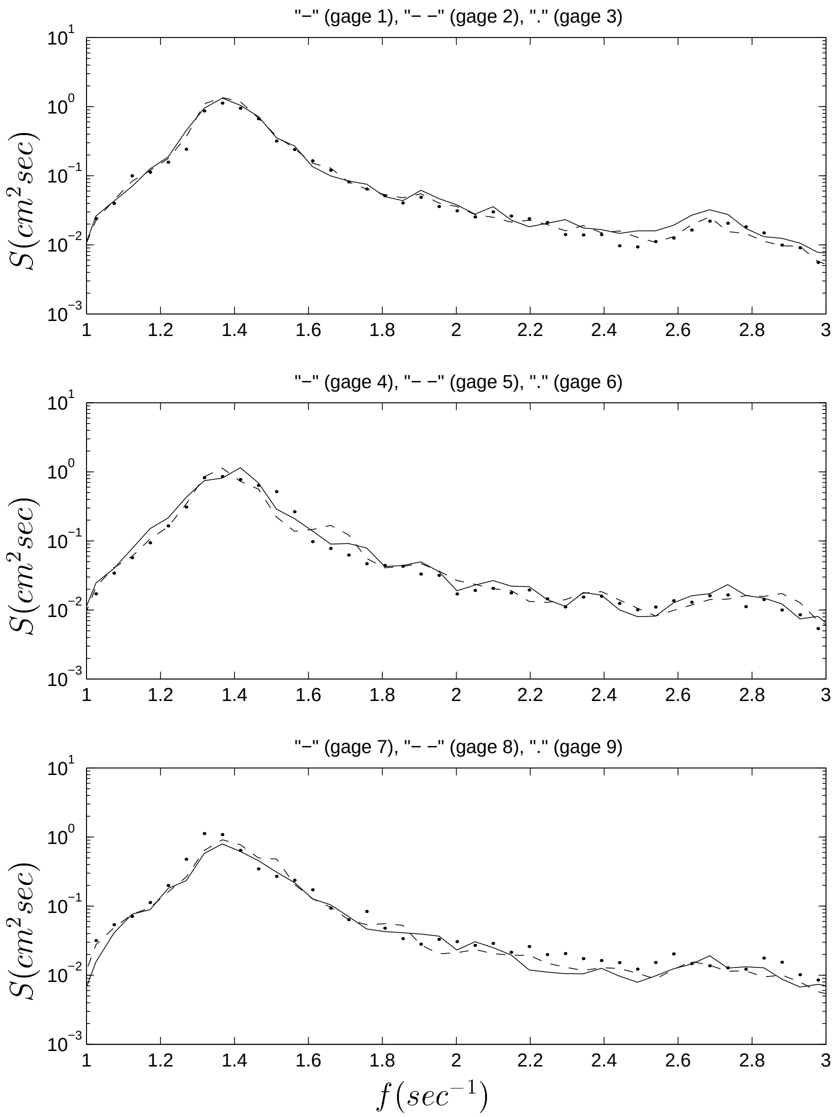

Figure D.46: Frequency spectra for Test 6 (position 4).

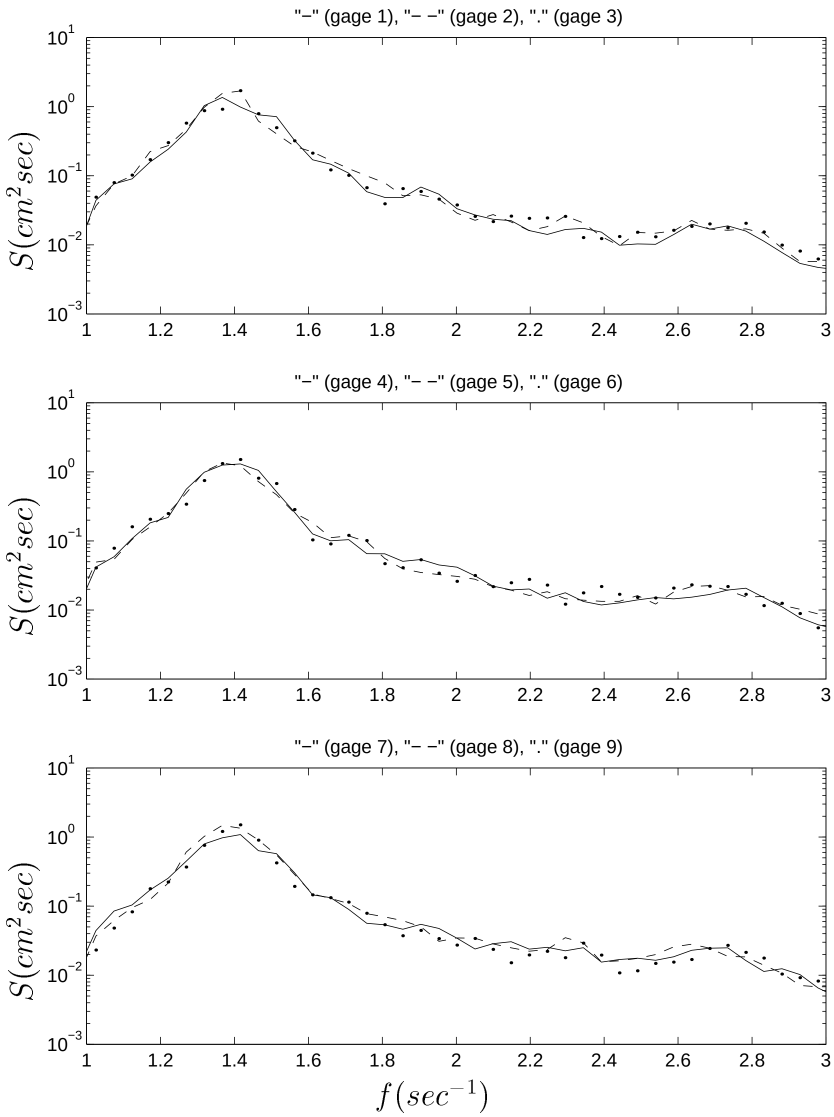

Figure D.47: Frequency spectra for Test 6 (position 5).

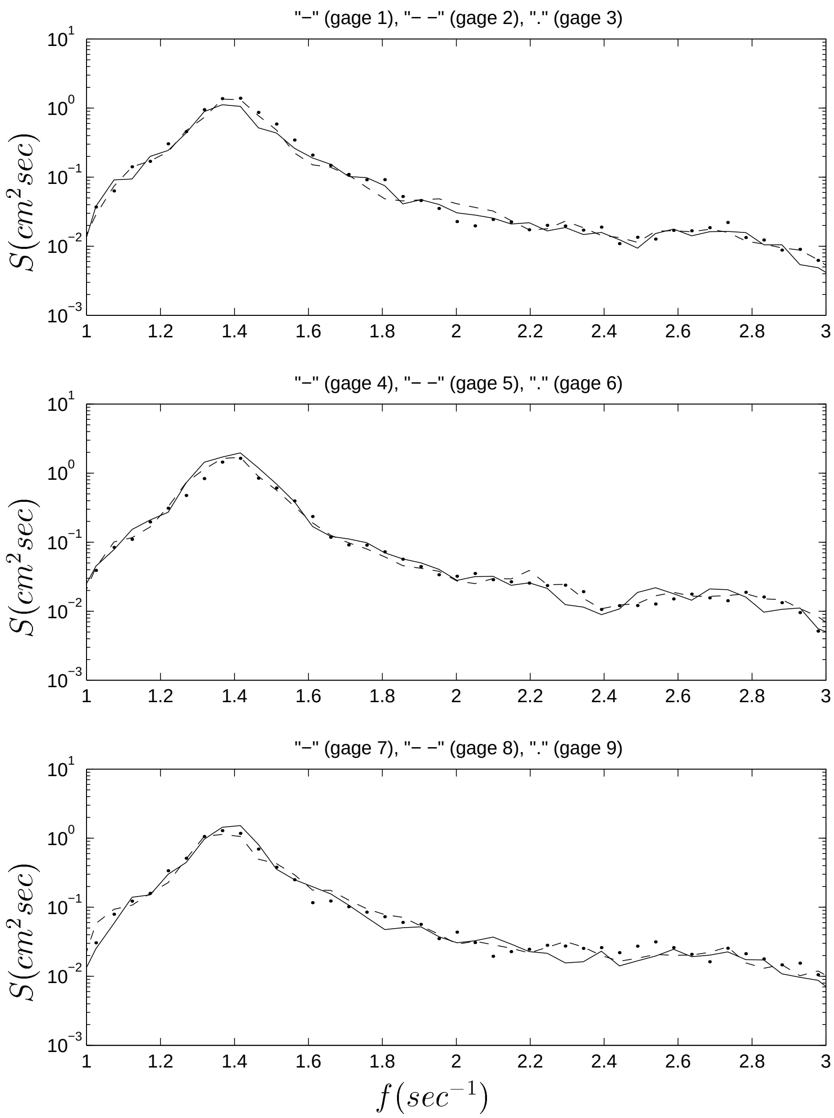

Figure D.48: Frequency spectra for Test 6 (position 6).

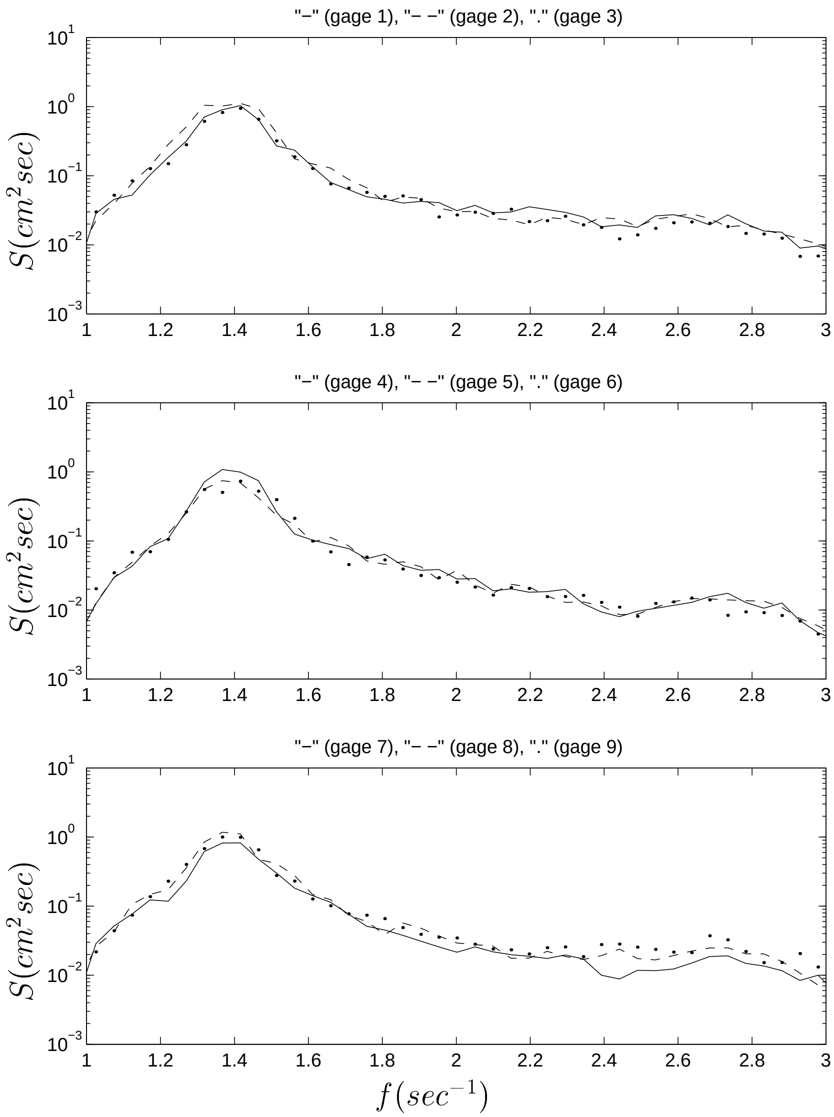

Figure D.49: Frequency spectra for Test 6 (position 7).

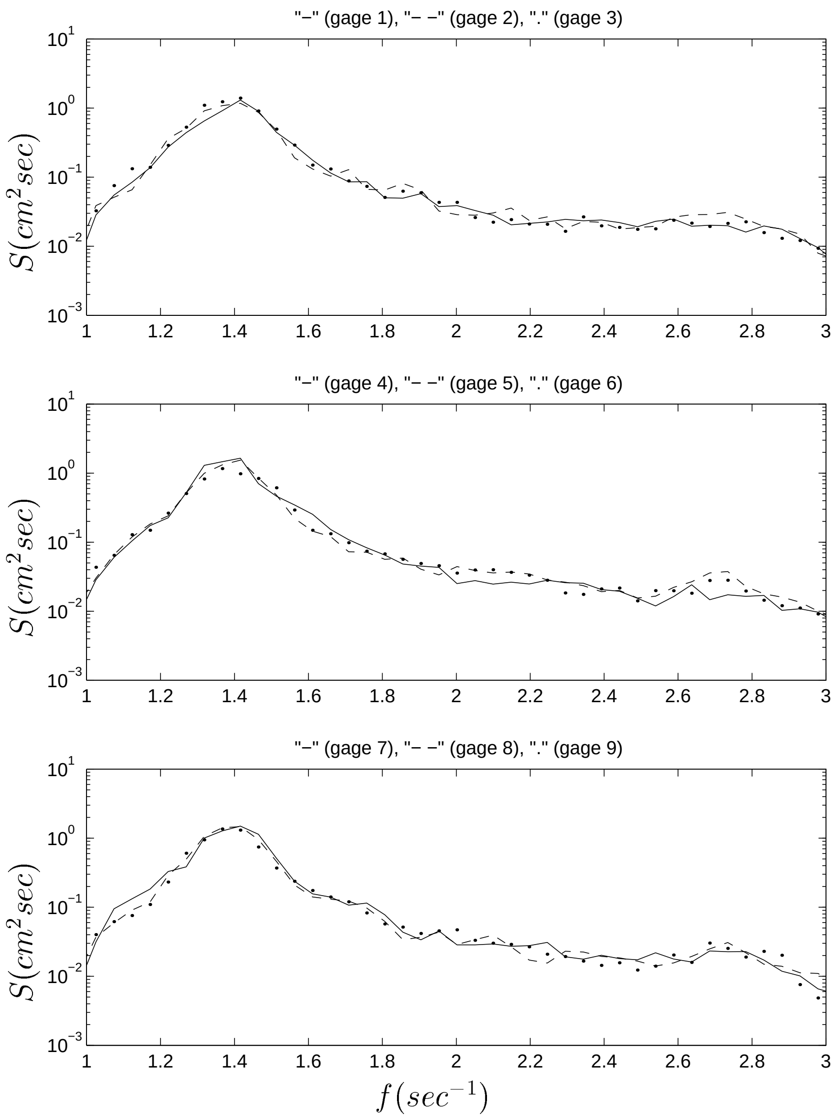

Figure D.50: Frequency spectra for Test 6 (position 8).

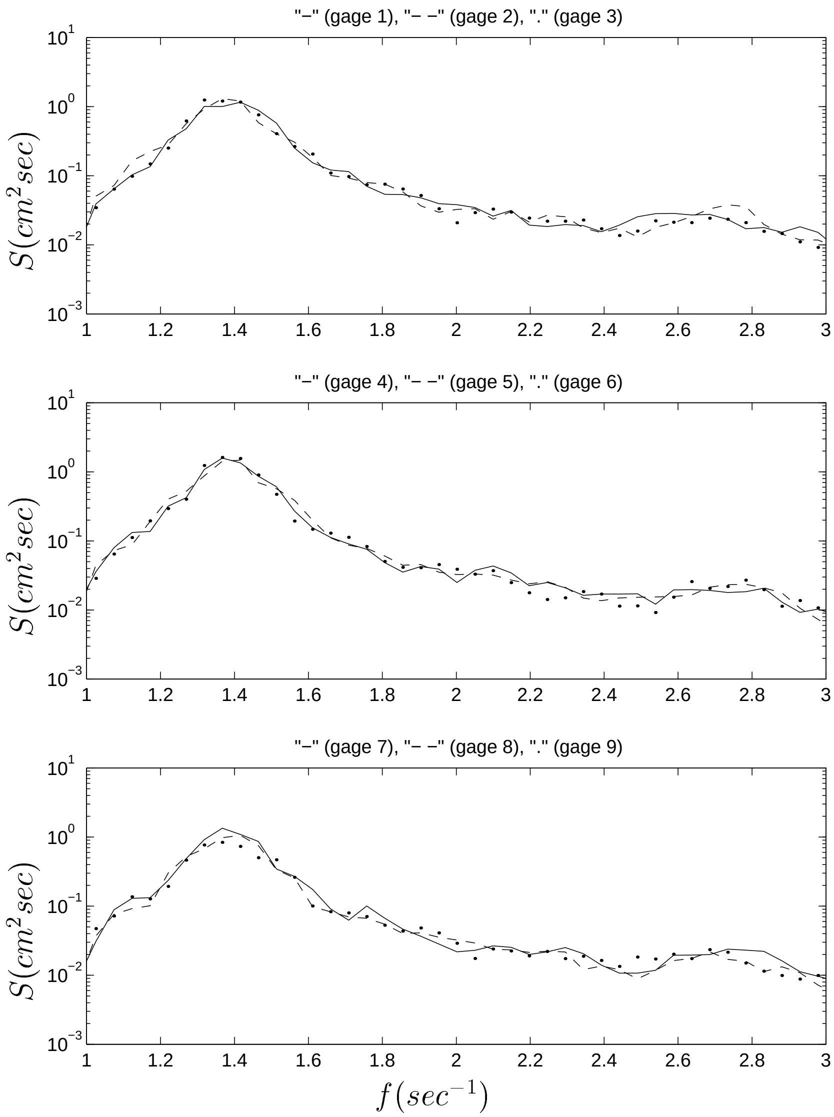

Figure D.51: Frequency spectra for Test 6 (position 9).

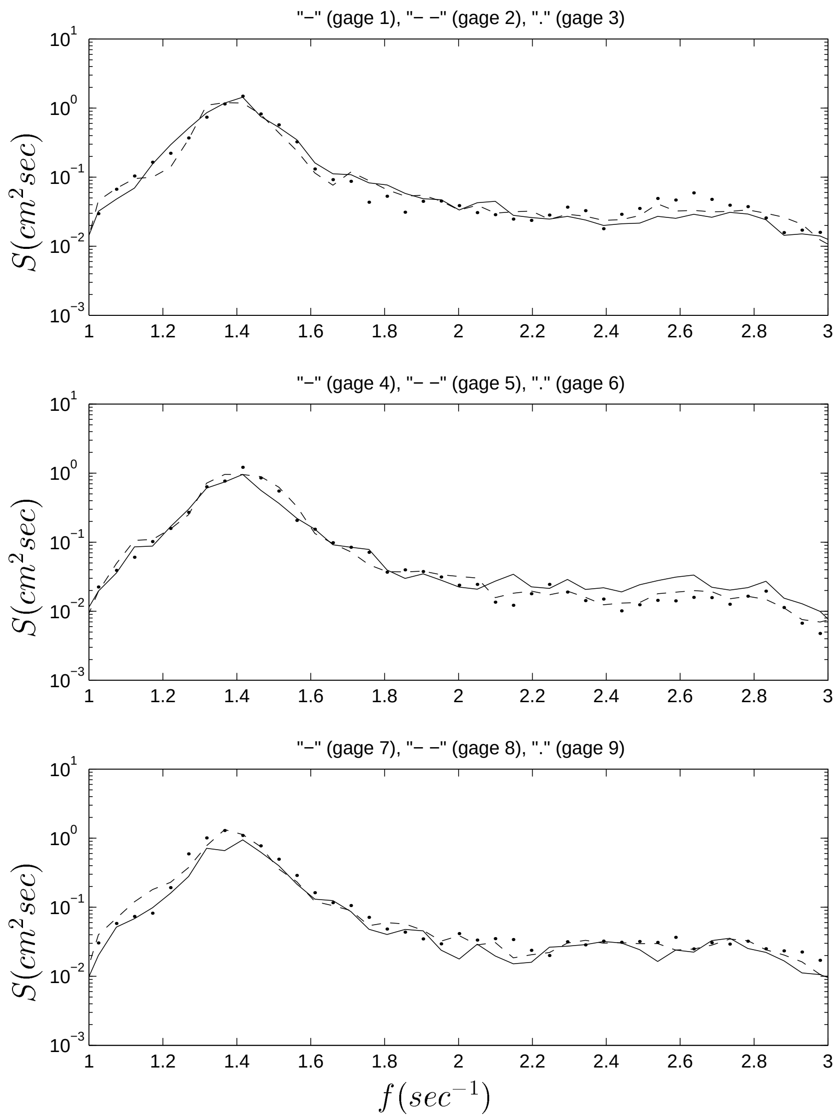

Figure D.52: Frequency spectra for Test 6 (position 10).

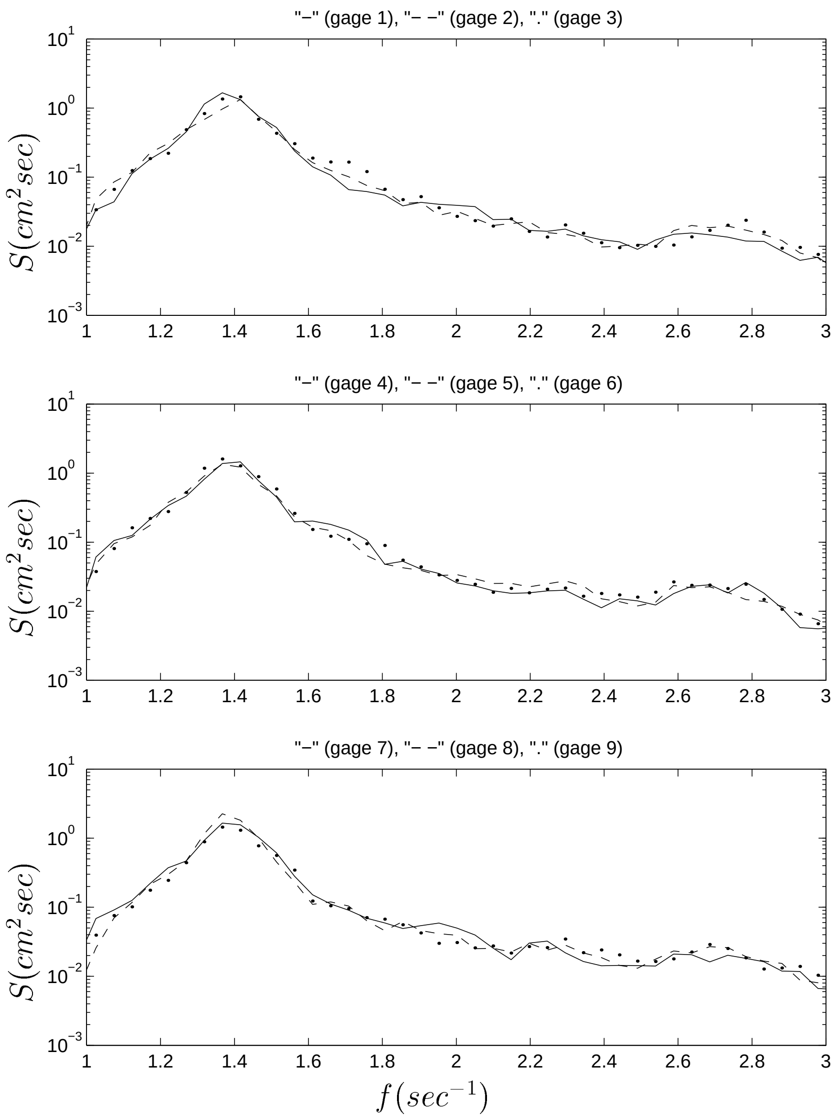

Figure D.53: Frequency spectra for Test 6 (position 11).

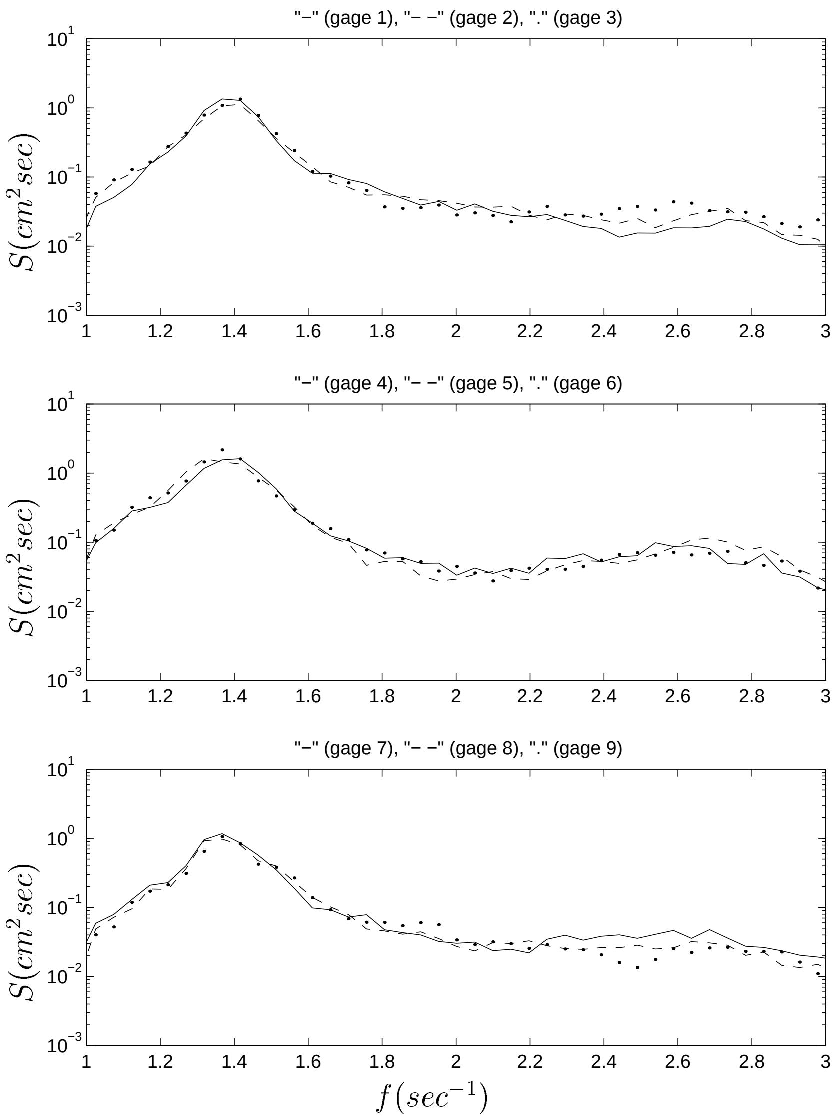

Figure D.54: Frequency spectra for Test 6 (position 12).

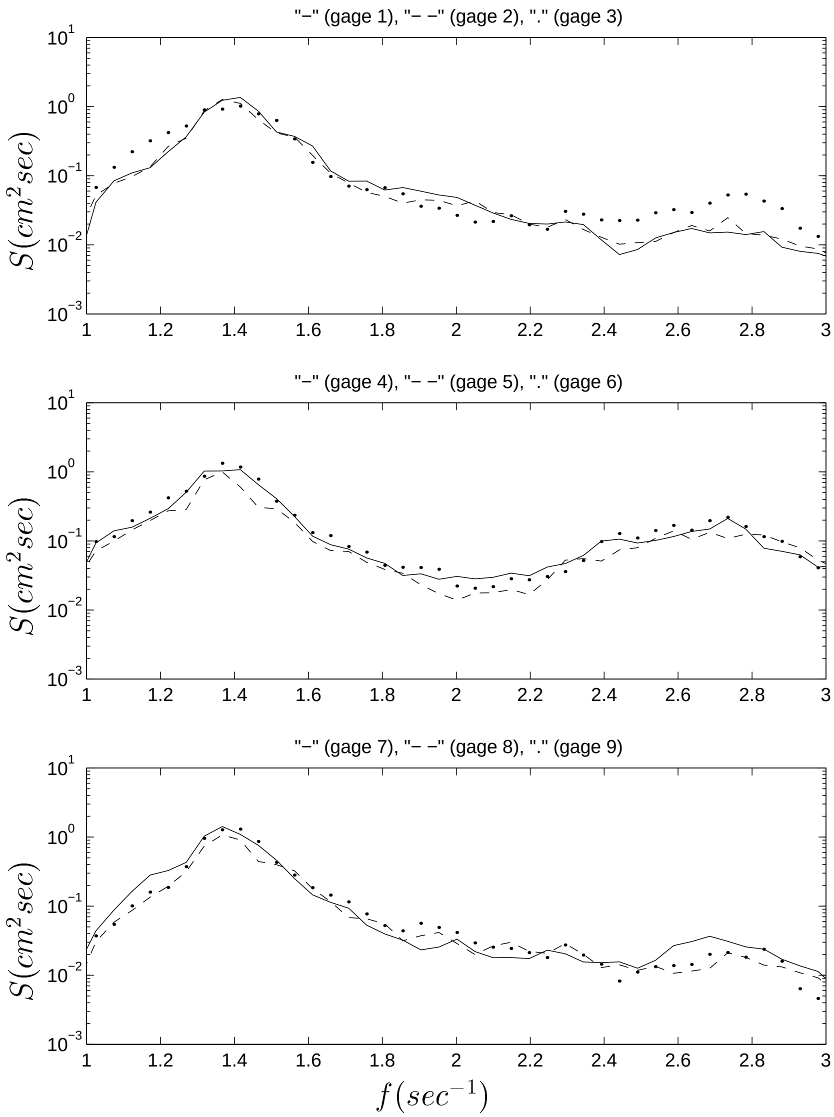

Figure D.55: Frequency spectra for Test 6 (position 13).

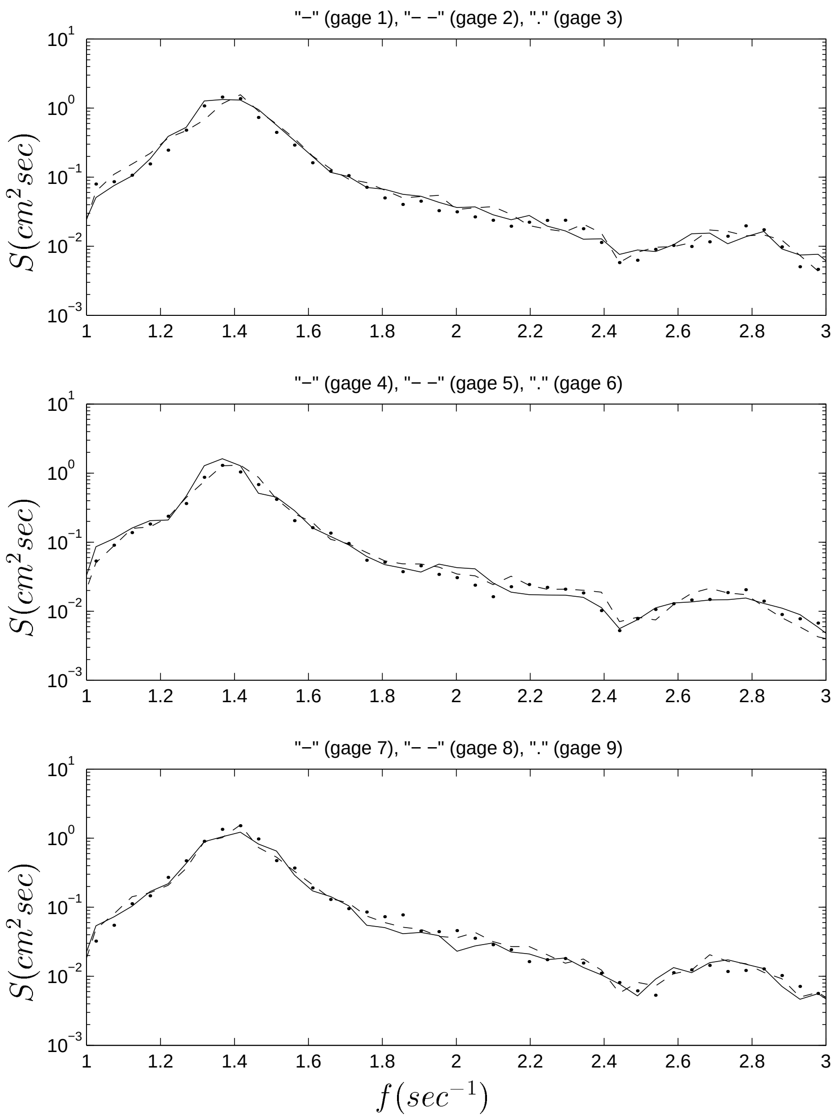

Figure D.56: Frequency spectra for Test 6 (position 14).

Appendix E

DIRECTIONAL SPECTRA PLOTS

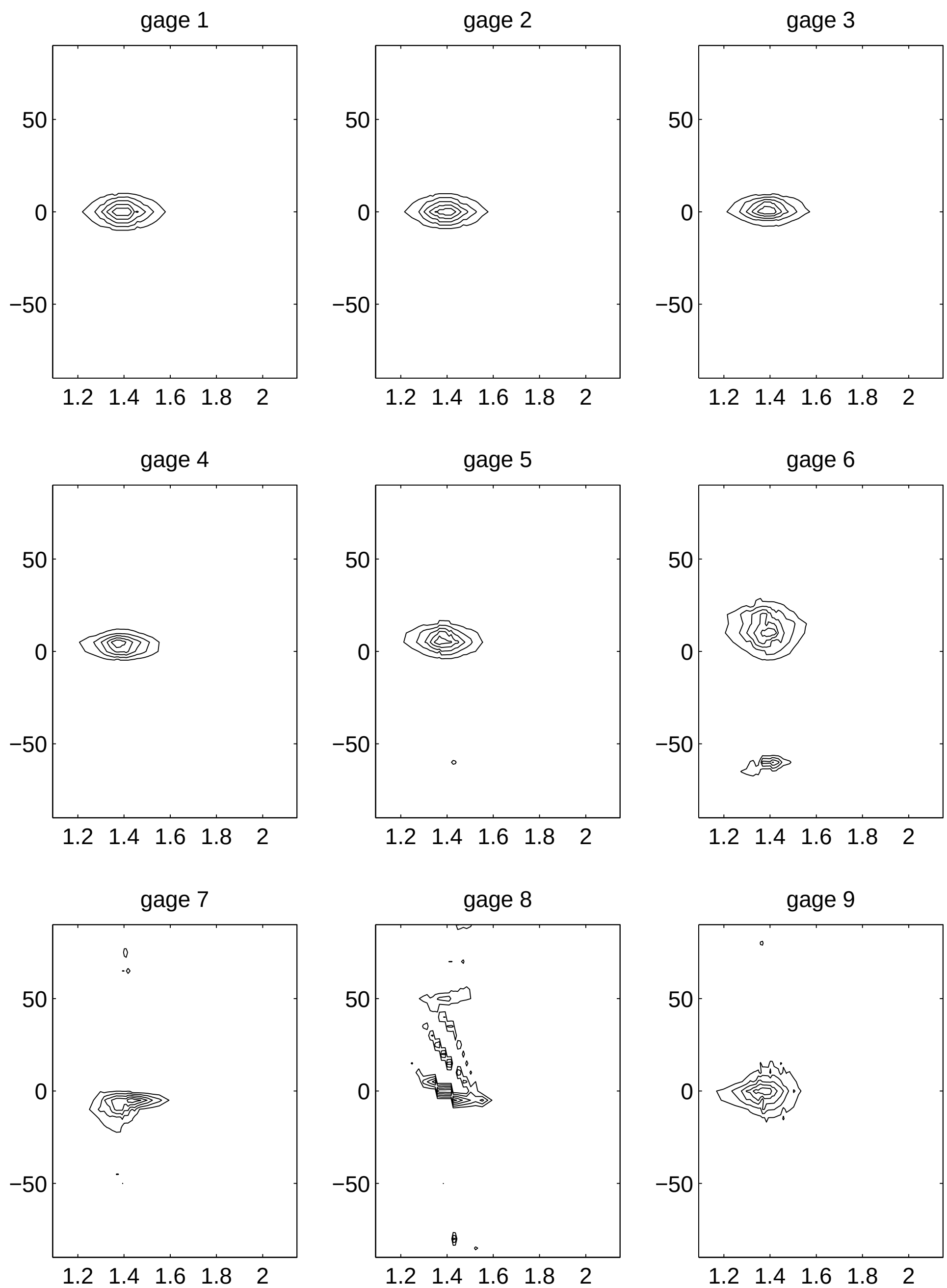

Figure E.1: Directional spectra for Test 3 (position 1).

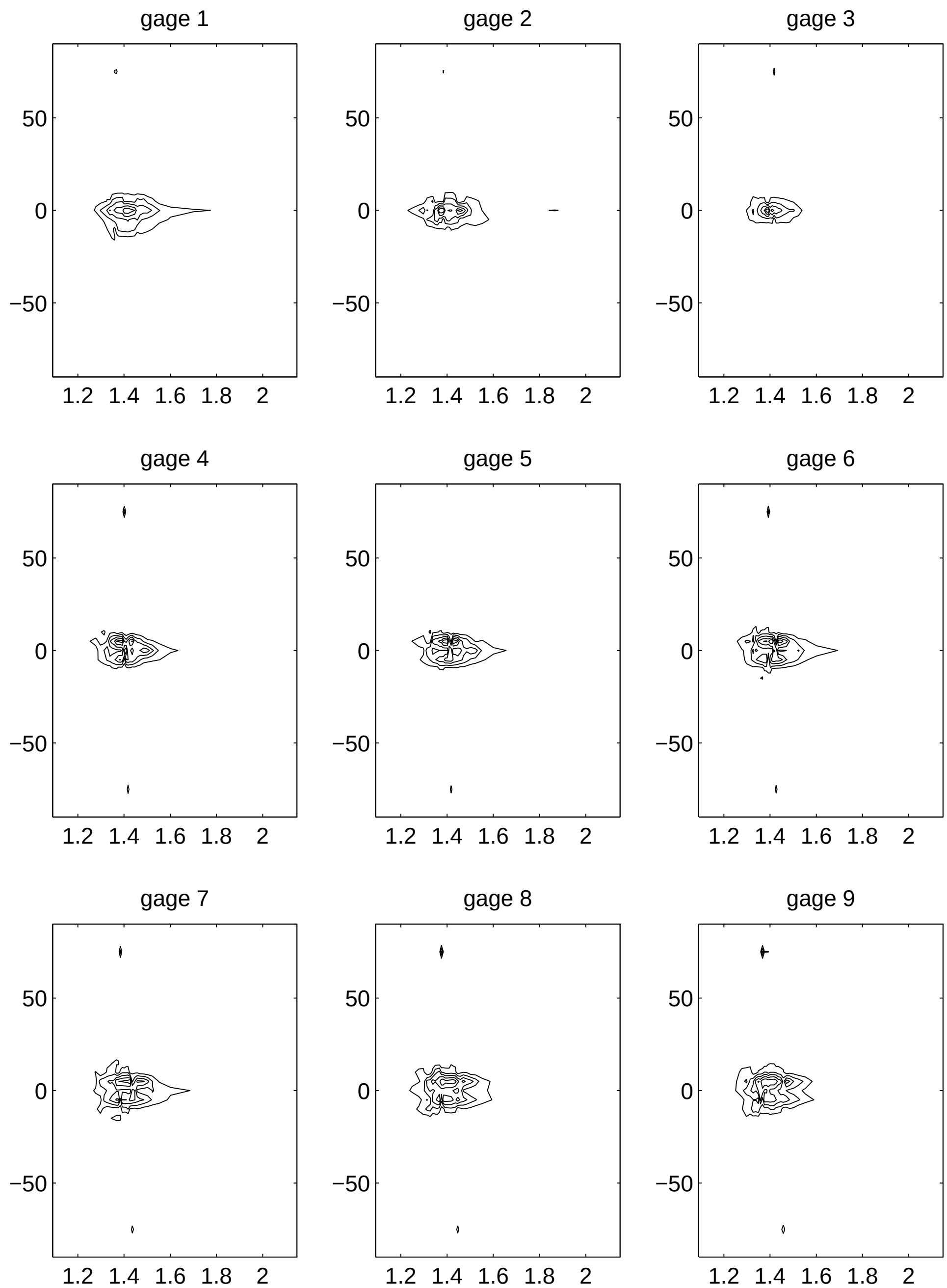

Figure E.2: Directional spectra for Test 3 (position 2).

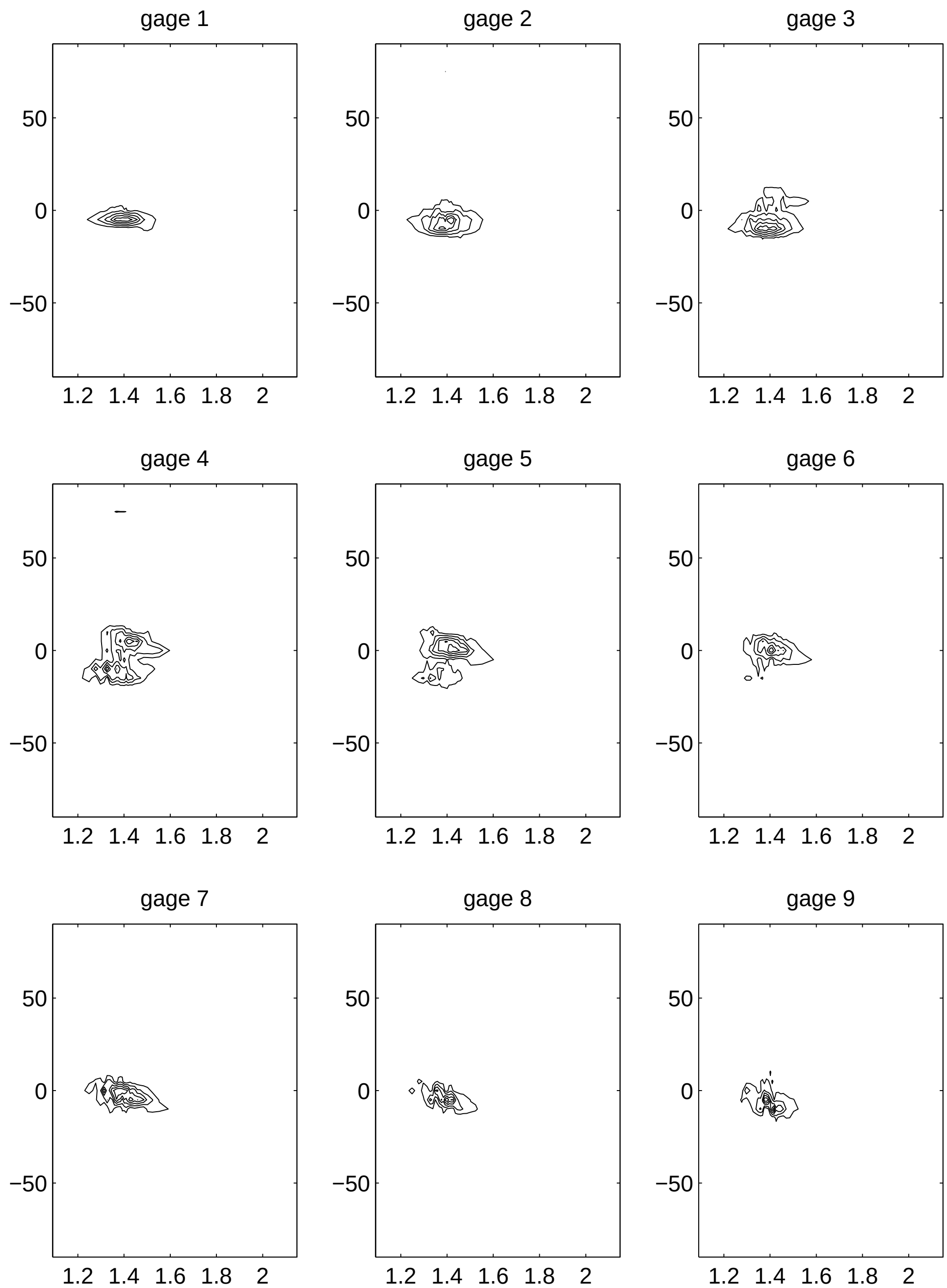

Figure E.3: Directional spectra for Test 3 (position 3).

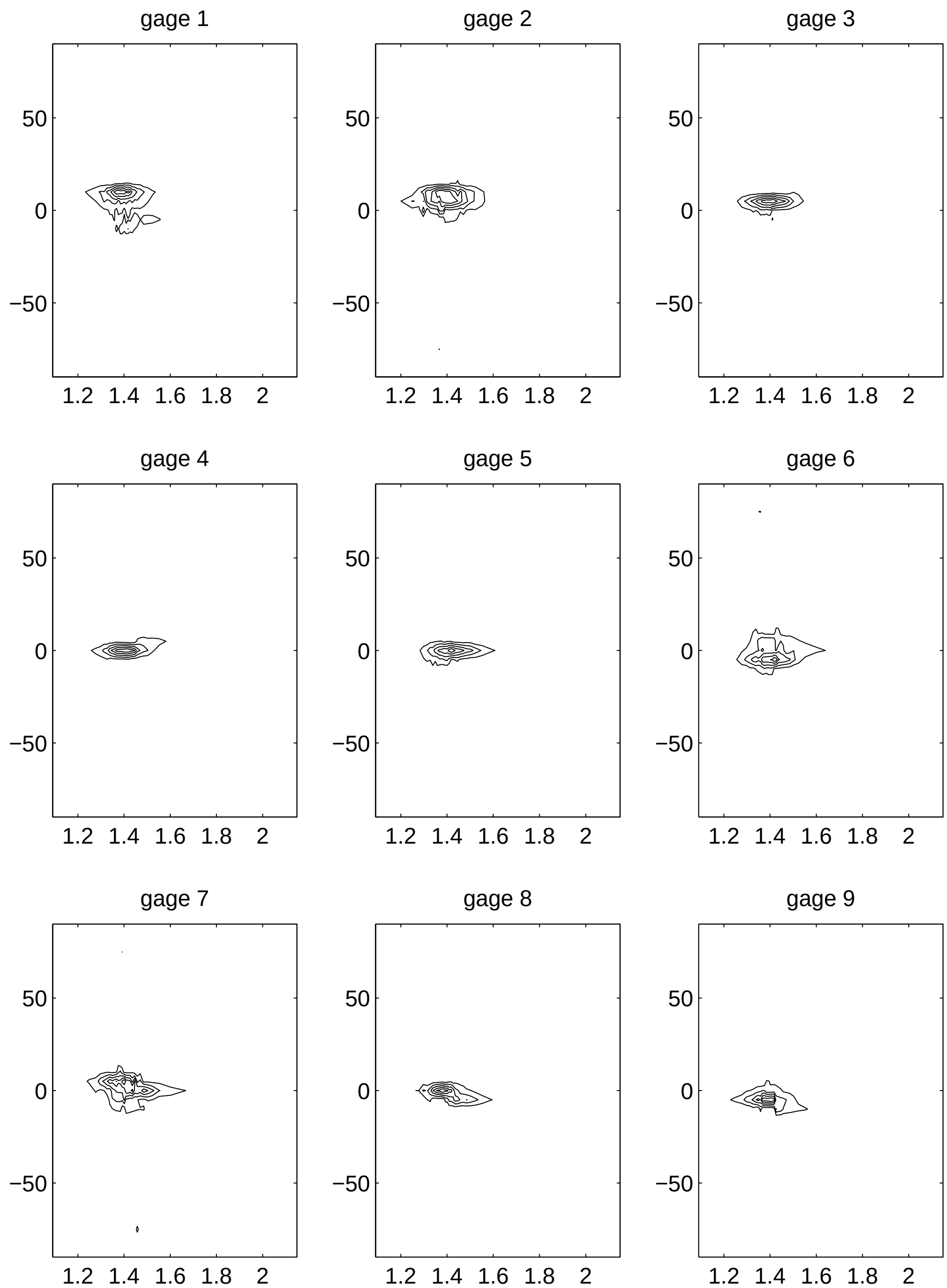

Figure E.4: Directional spectra for Test 3 (position 4).

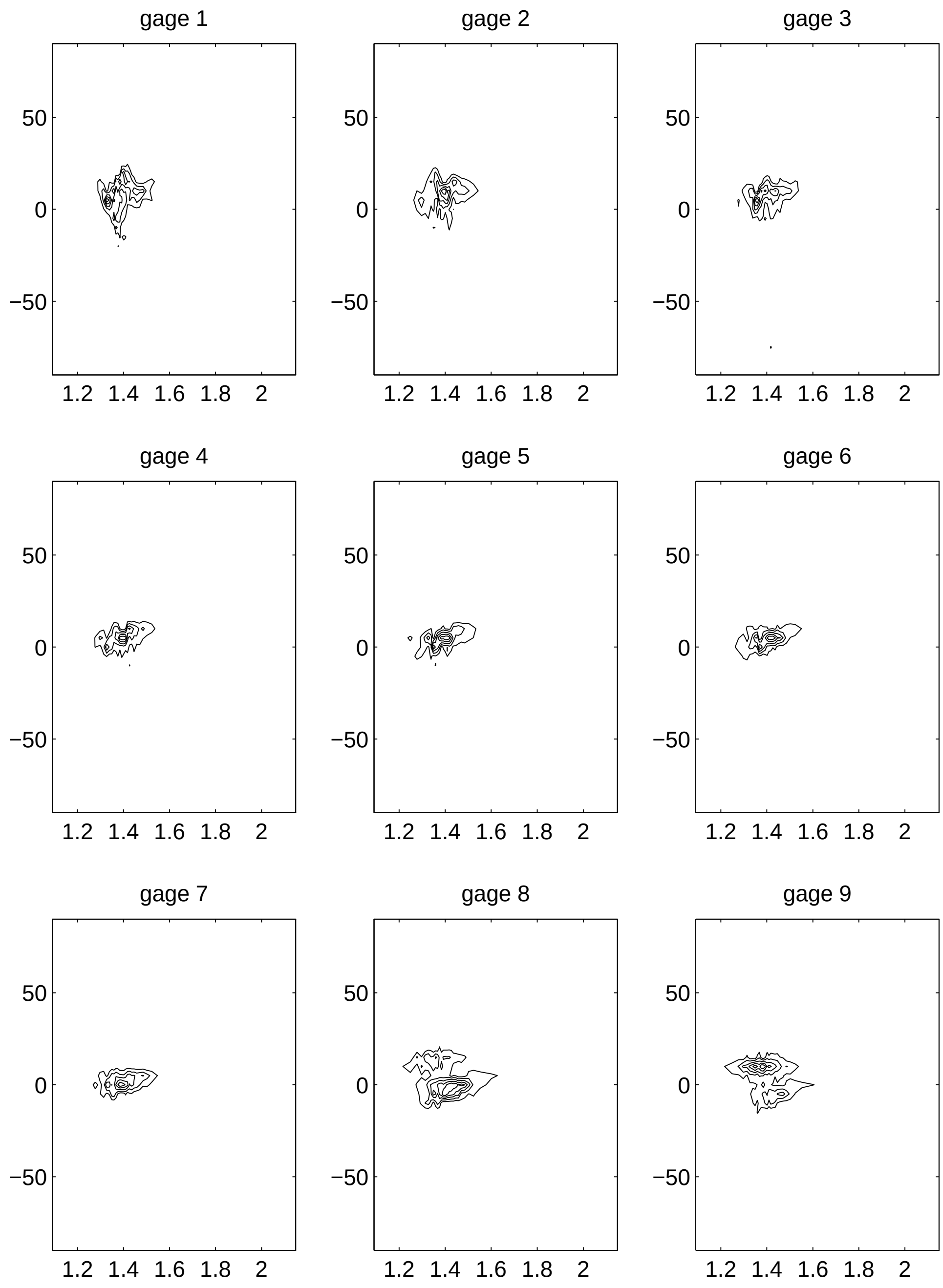

Figure E.5: Directional spectra for Test 3 (position 5).

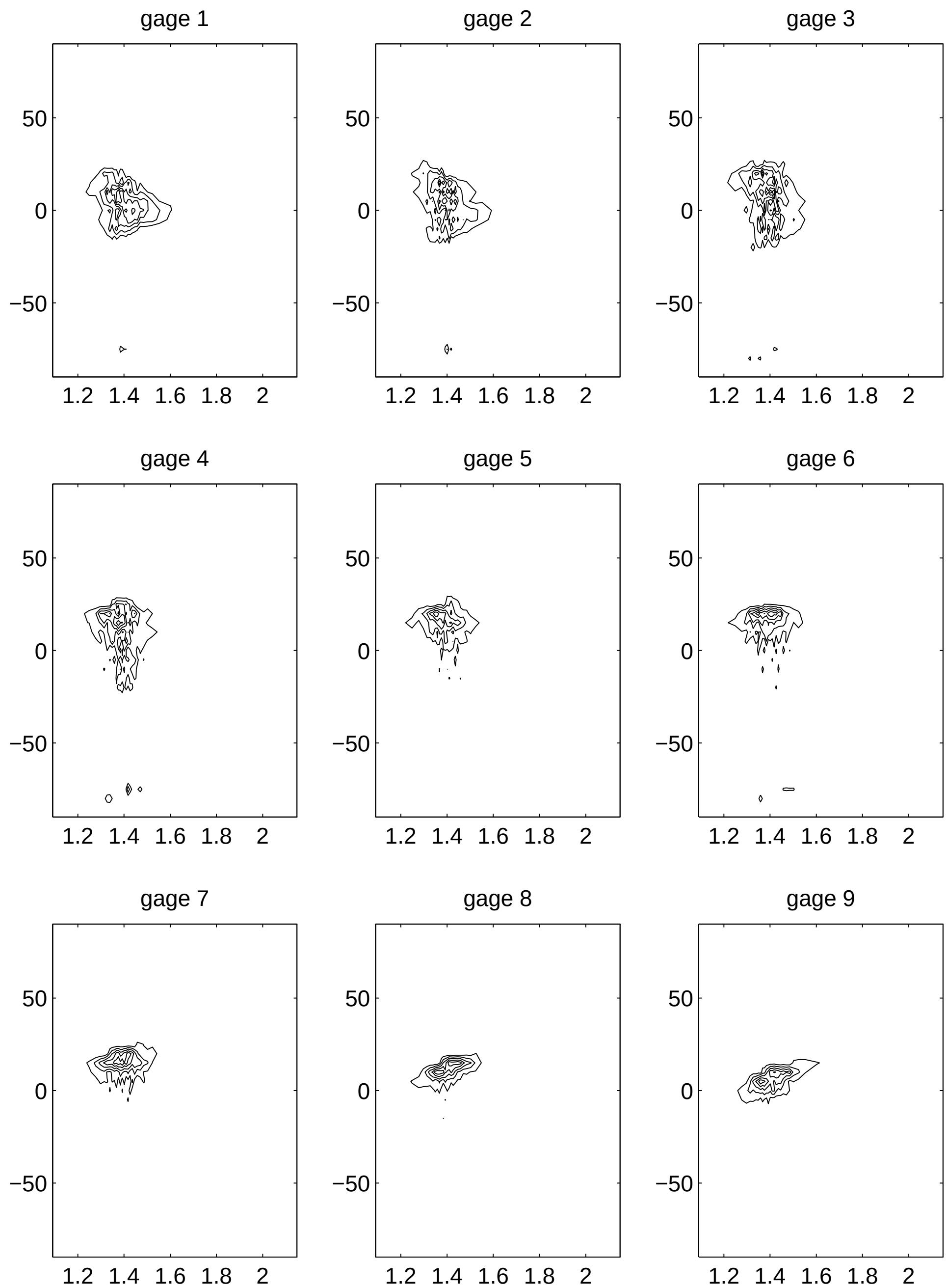

Figure E.6: Directional spectra for Test 3 (position 6).

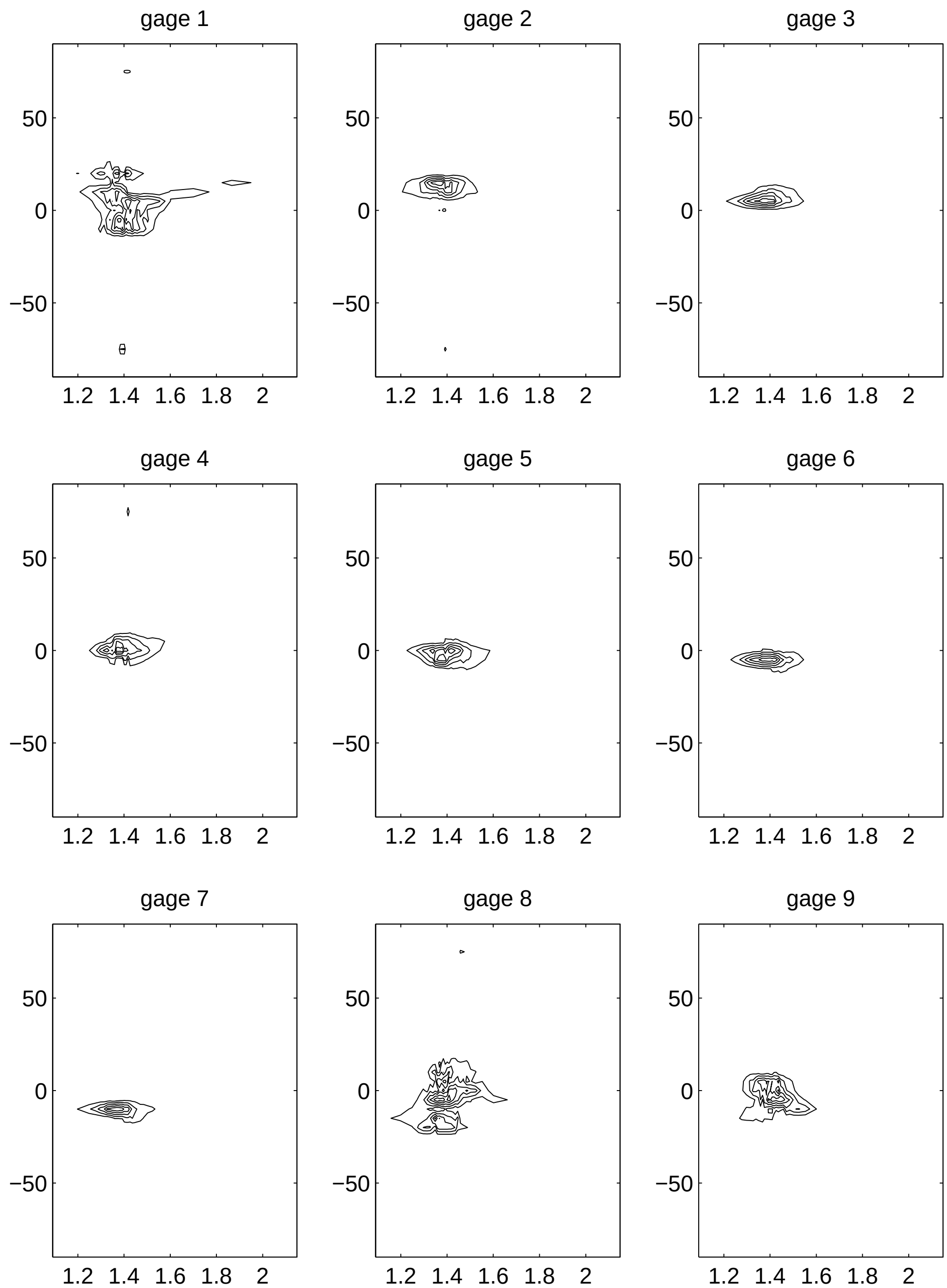

Figure E.7: Directional spectra for Test 3 (position 7).

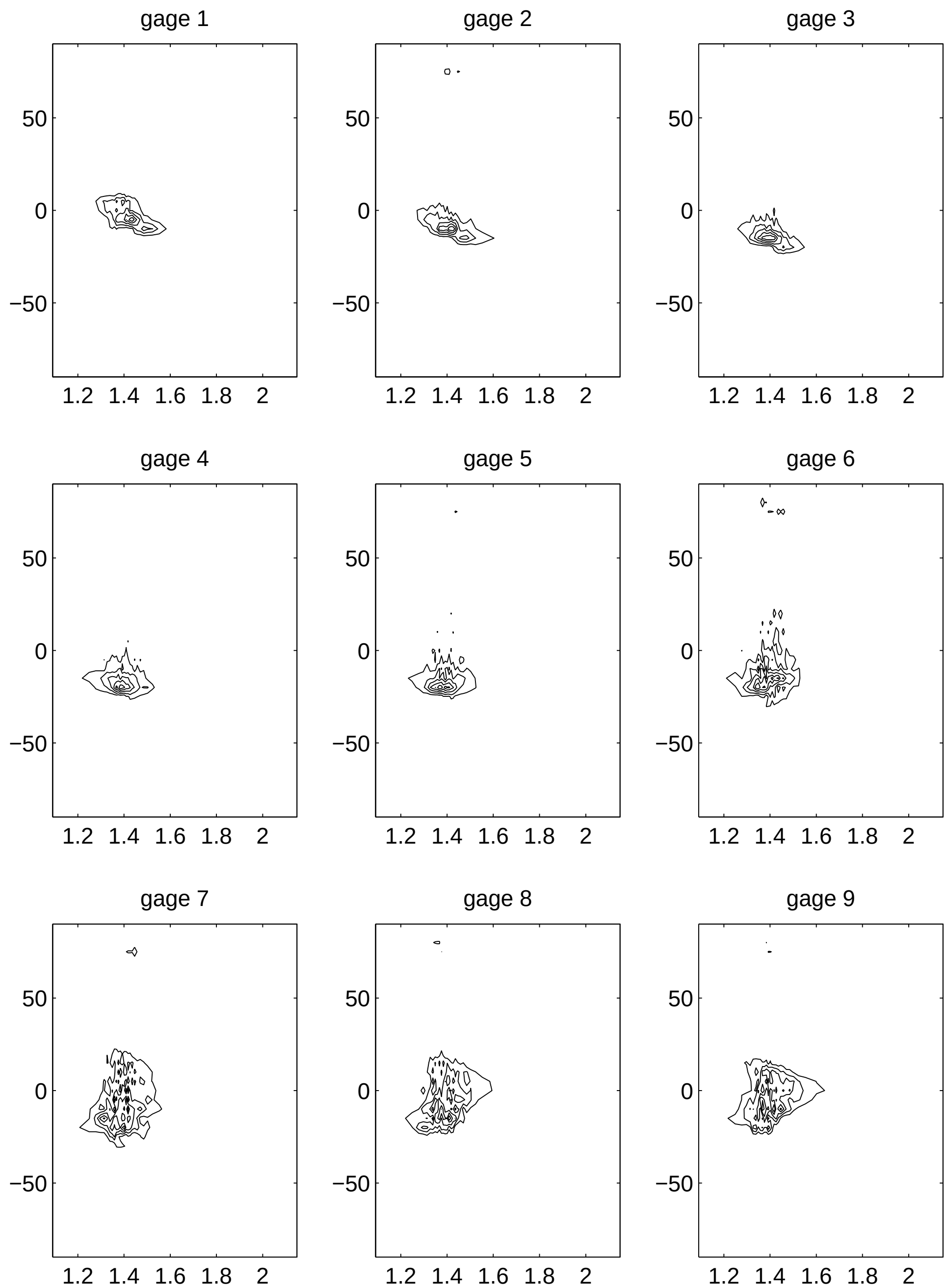

Figure E.8: Directional spectra for Test 3 (position 8).

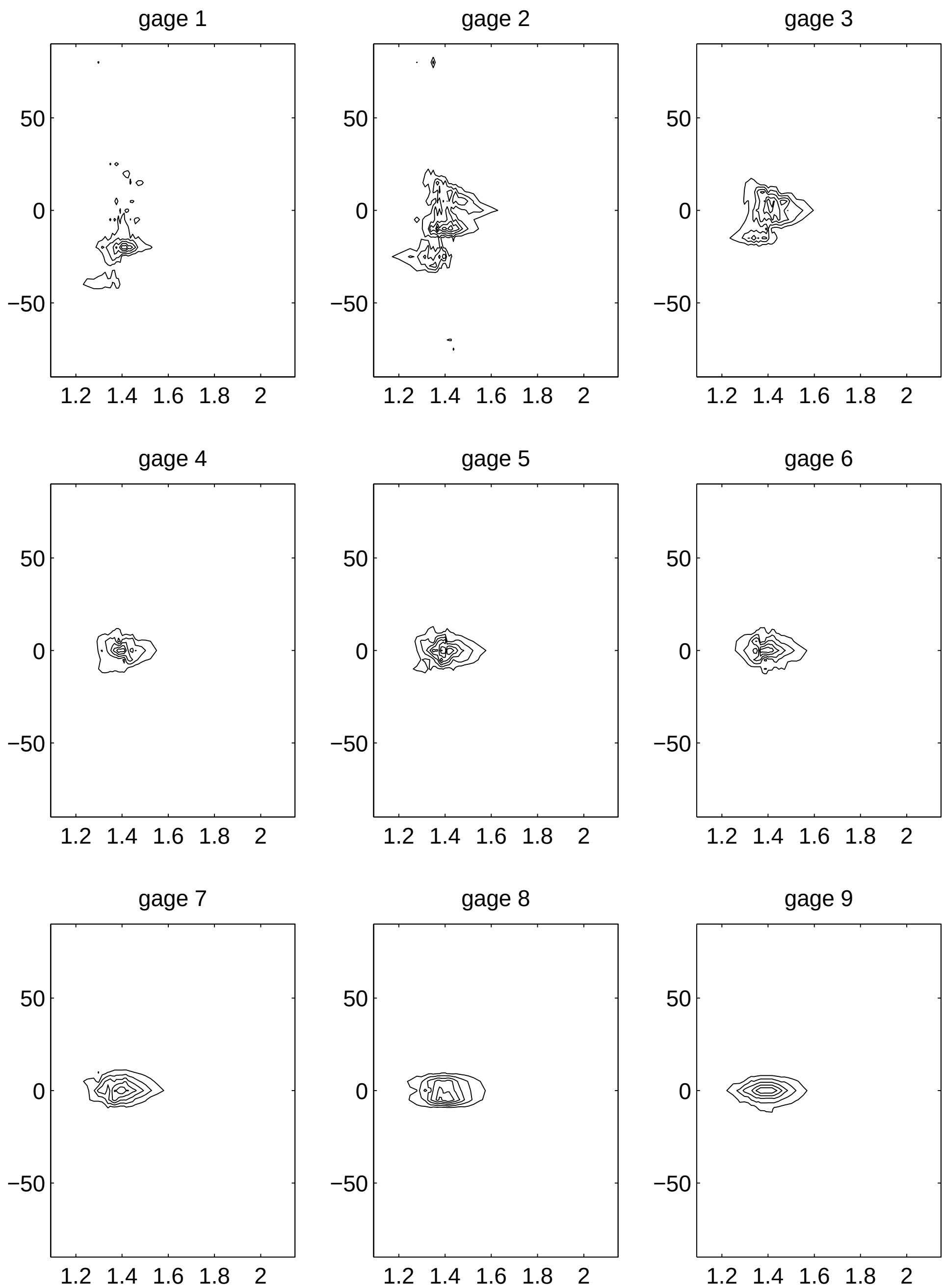

Figure E.9: Directional spectra for Test 3 (position 9).

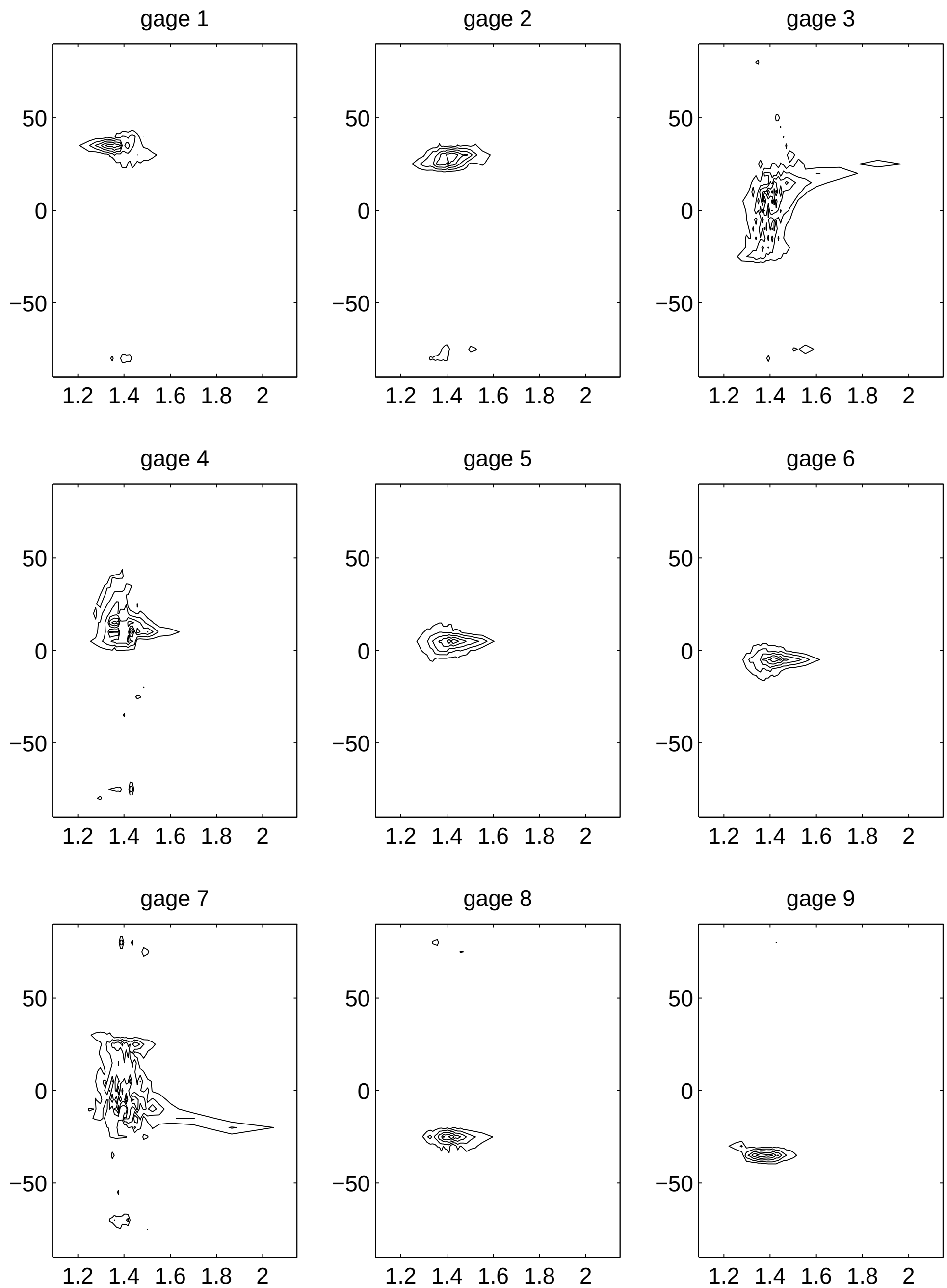

Figure E.10: Directional spectra for Test 3 (position 10).

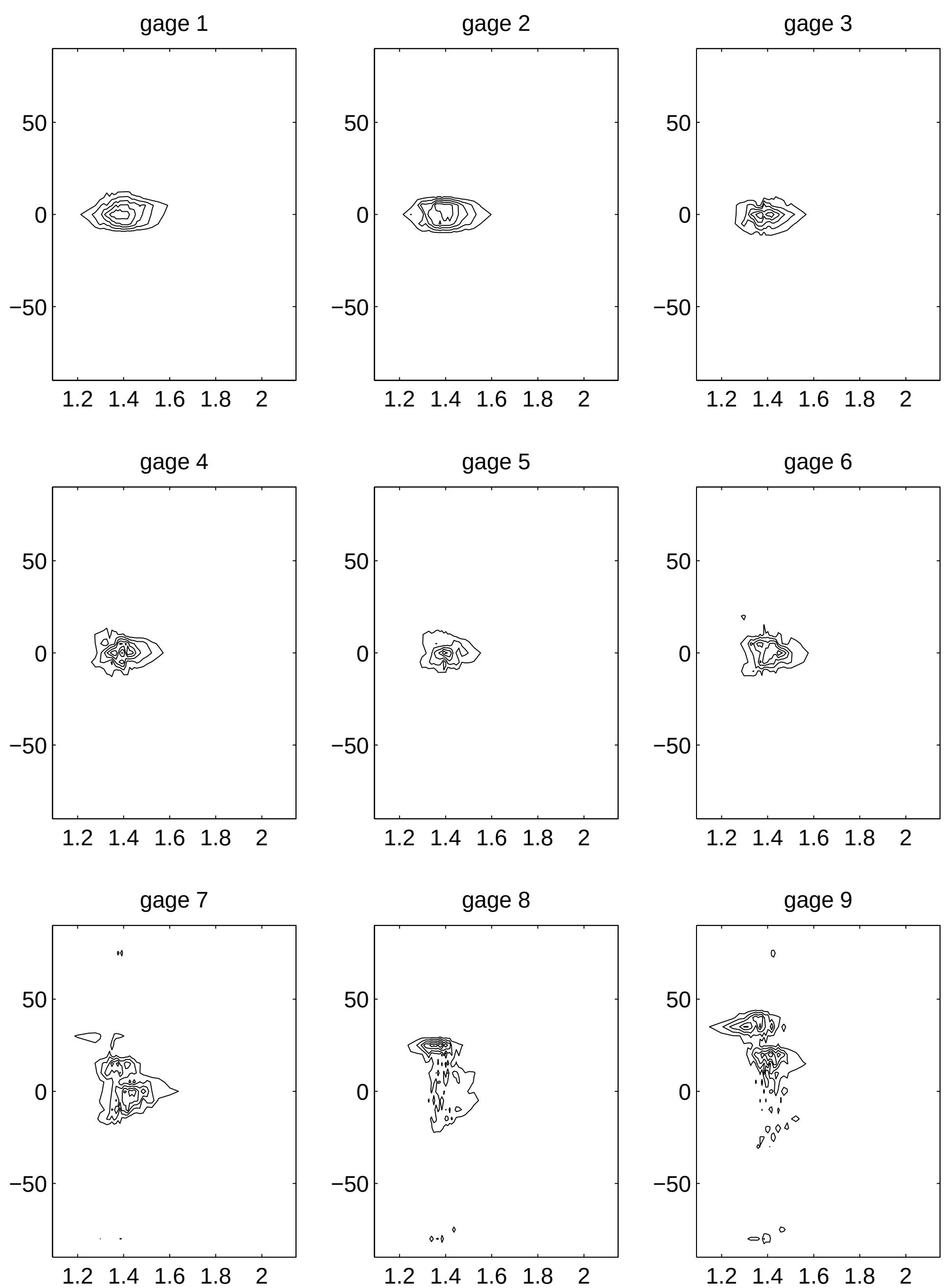

Figure E.11: Directional spectra for Test 3 (position 11).

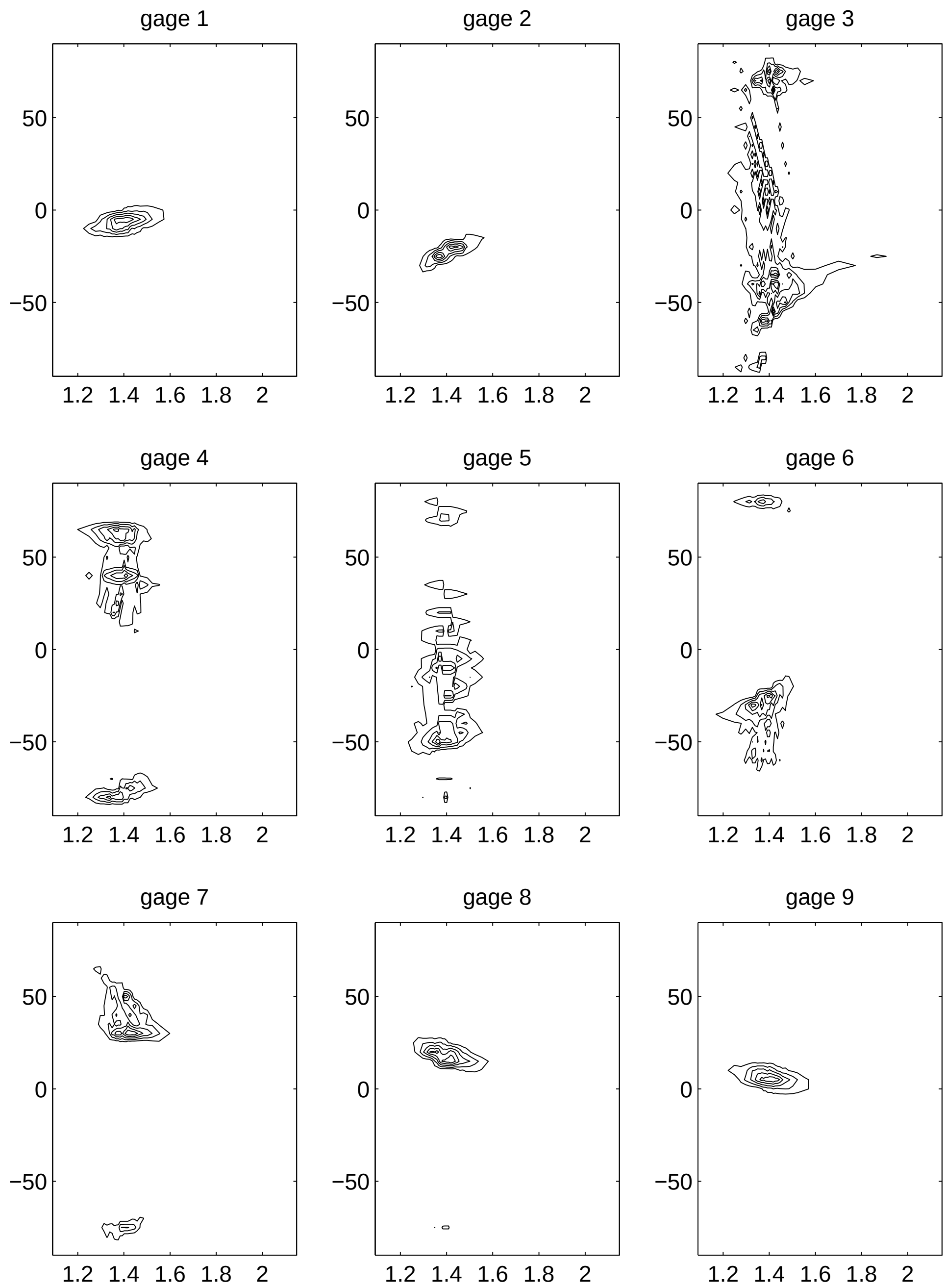

Figure E.12: Directional spectra for Test 3 (position 12).

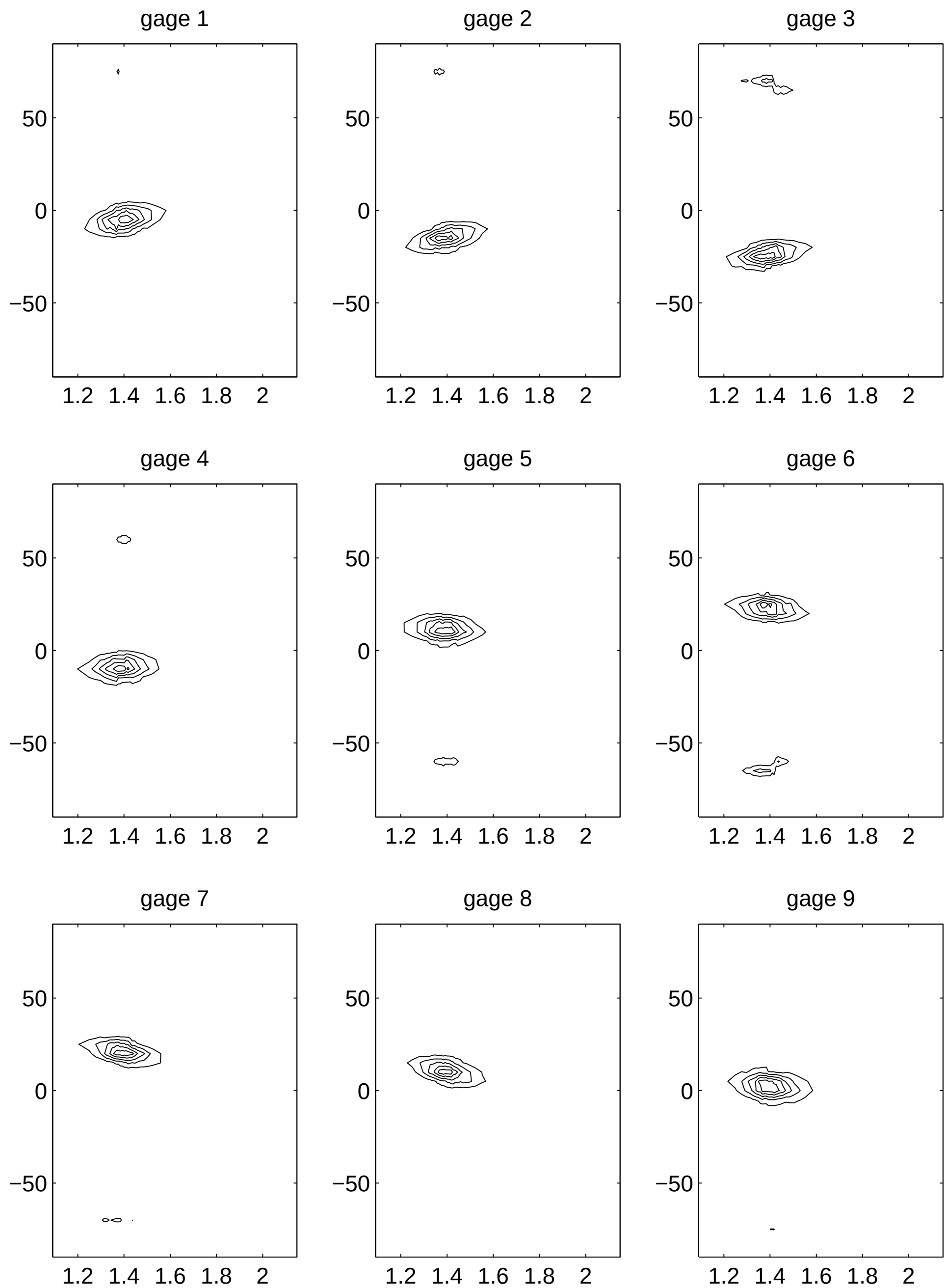

Figure E.13: Directional spectra for Test 3 (position 13).

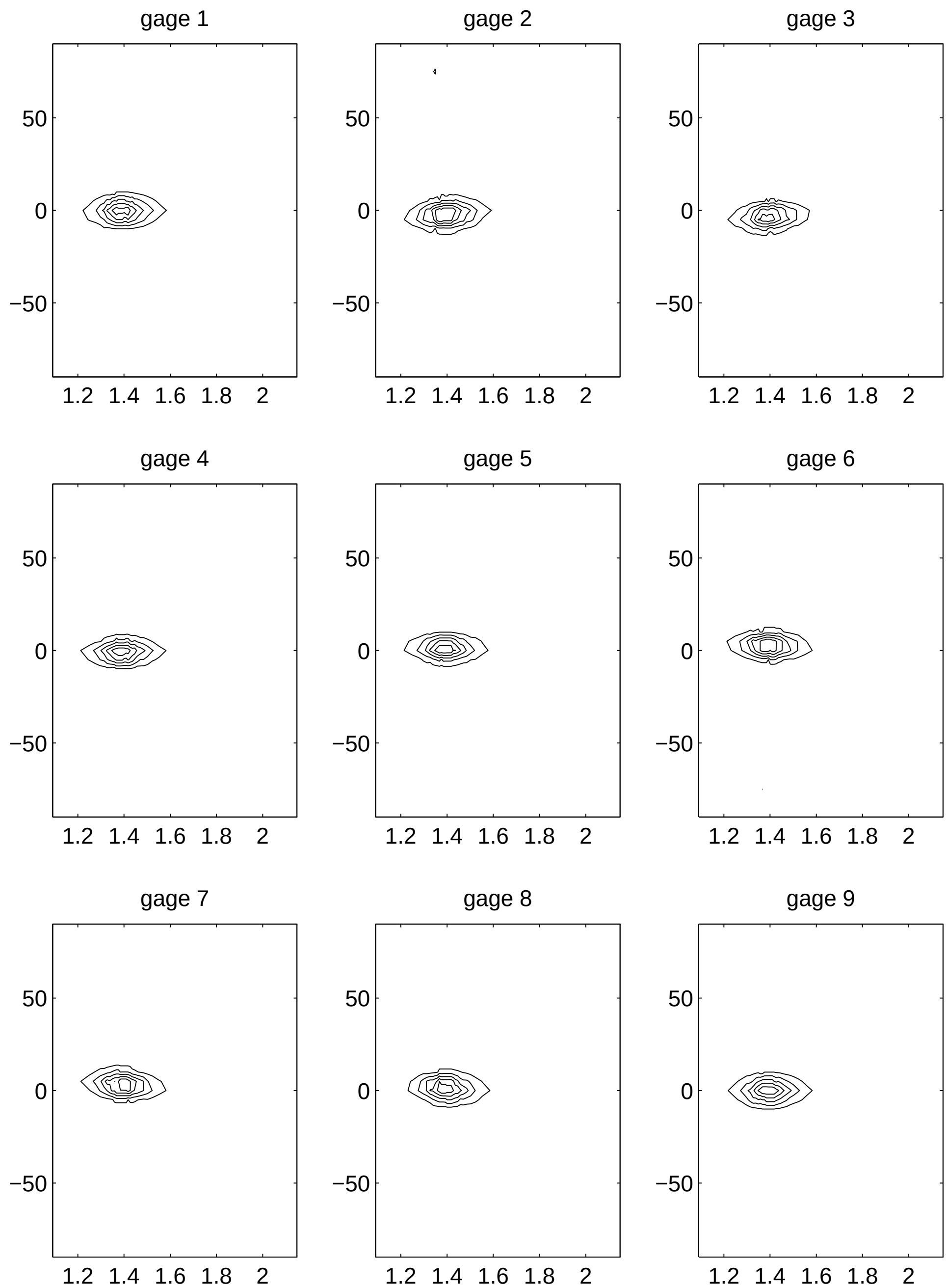

Figure E.14: Directional spectra for Test 3 (position 14).

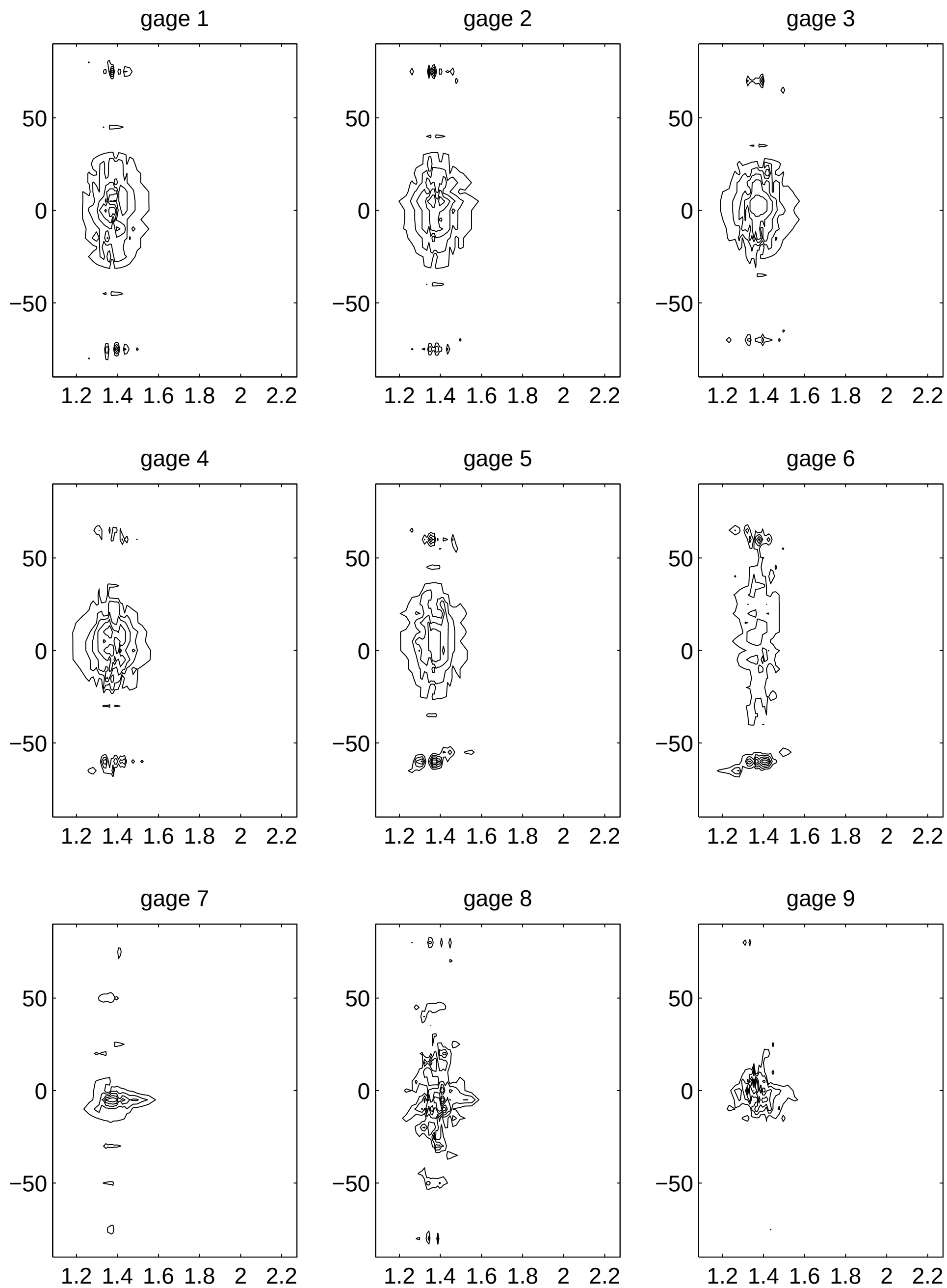

Figure E.15: Directional spectra for Test 4 (position 1).

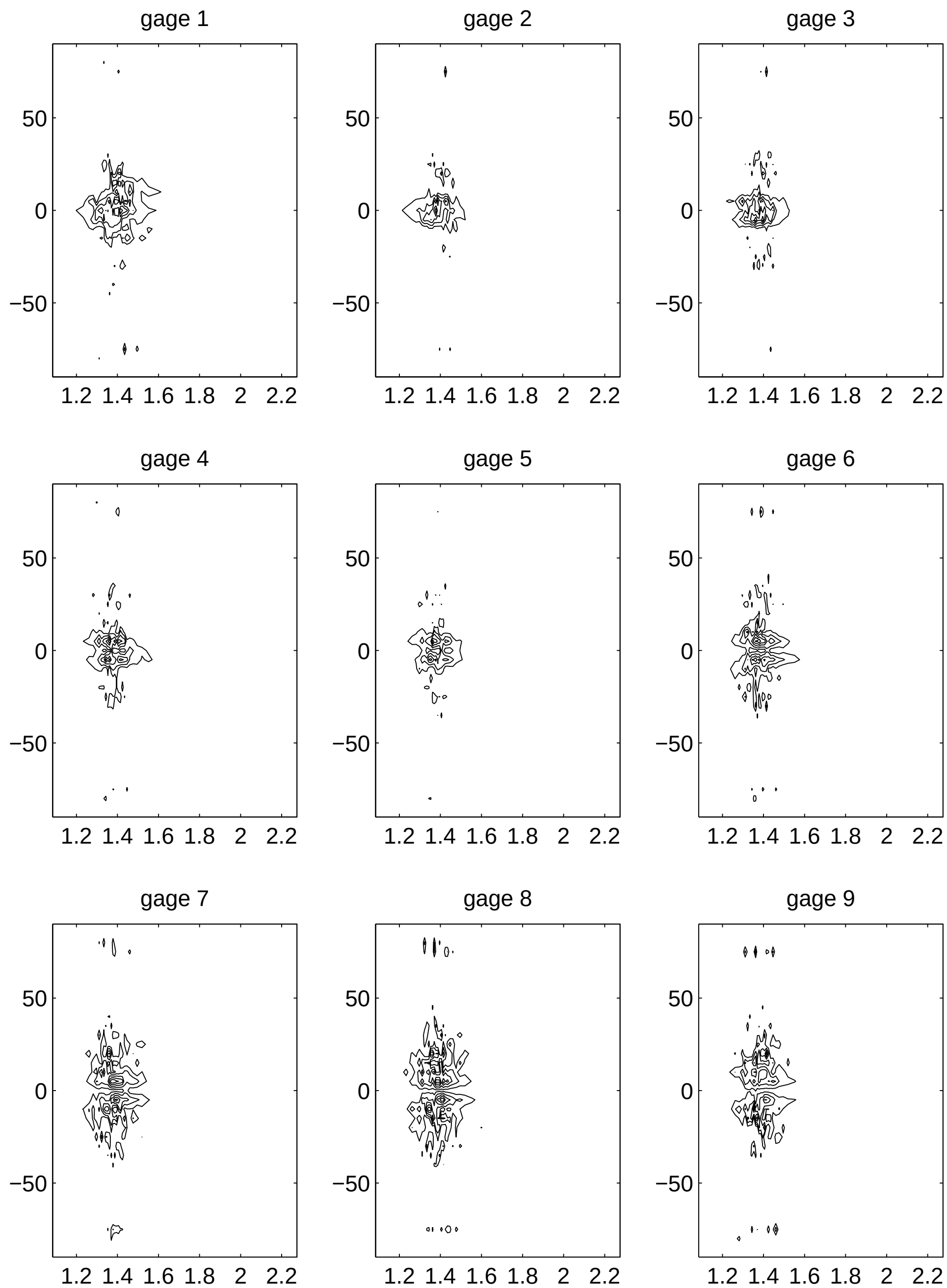

Figure E.16: Directional spectra for Test 4 (position 2).

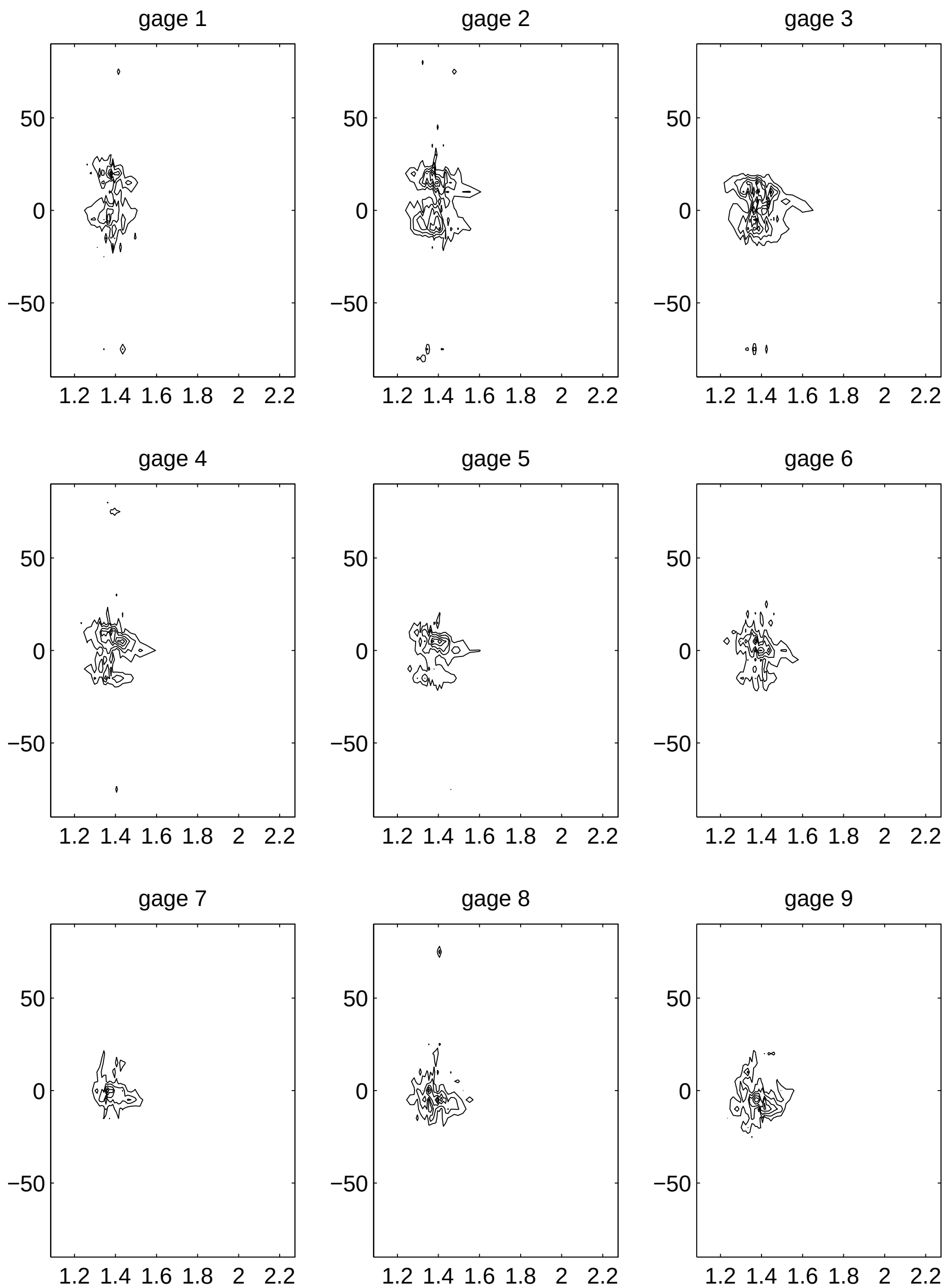

Figure E.17: Directional spectra for Test 4 (position 3).

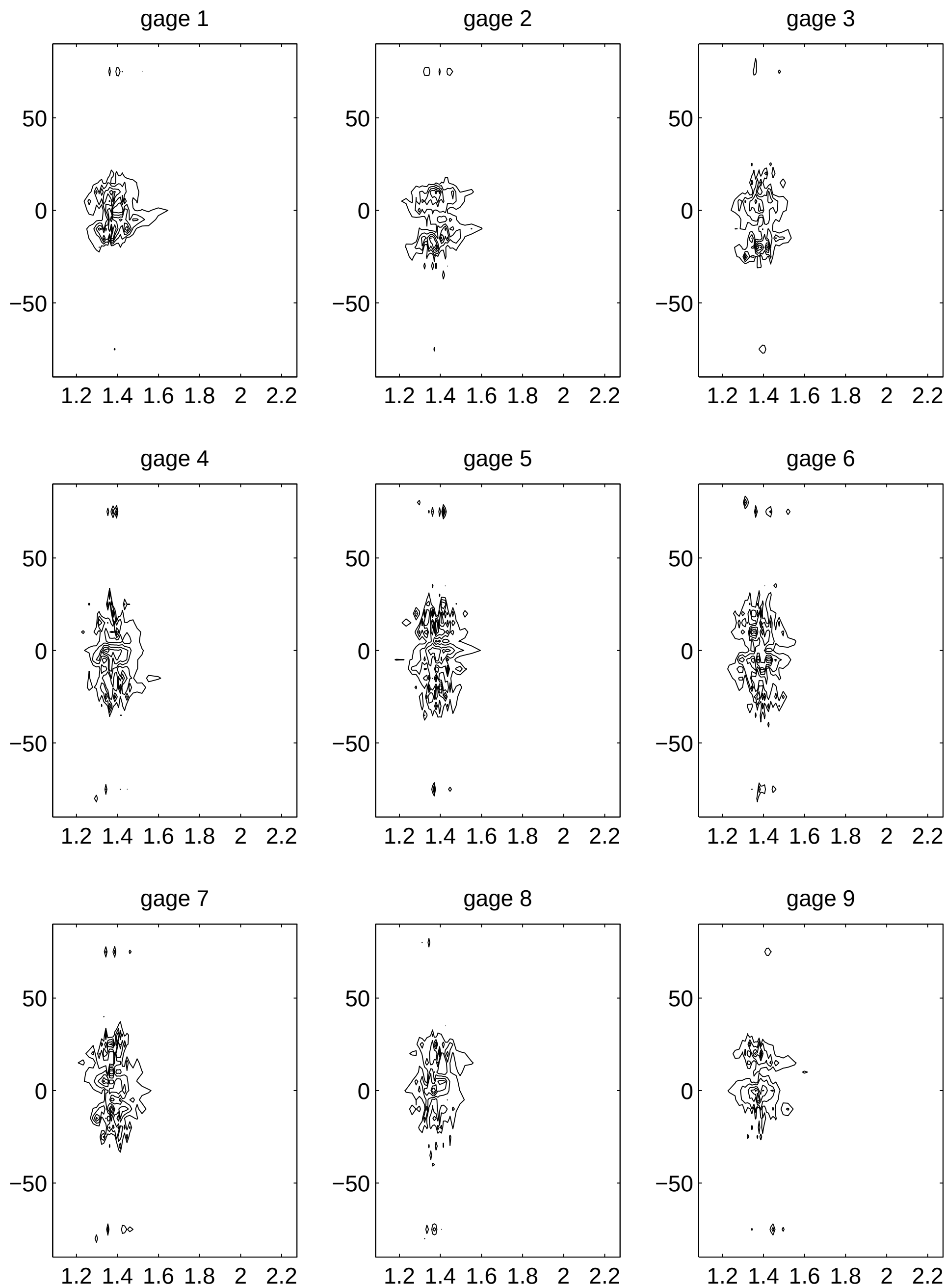

Figure E.18: Directional spectra for Test 4 (position 4).

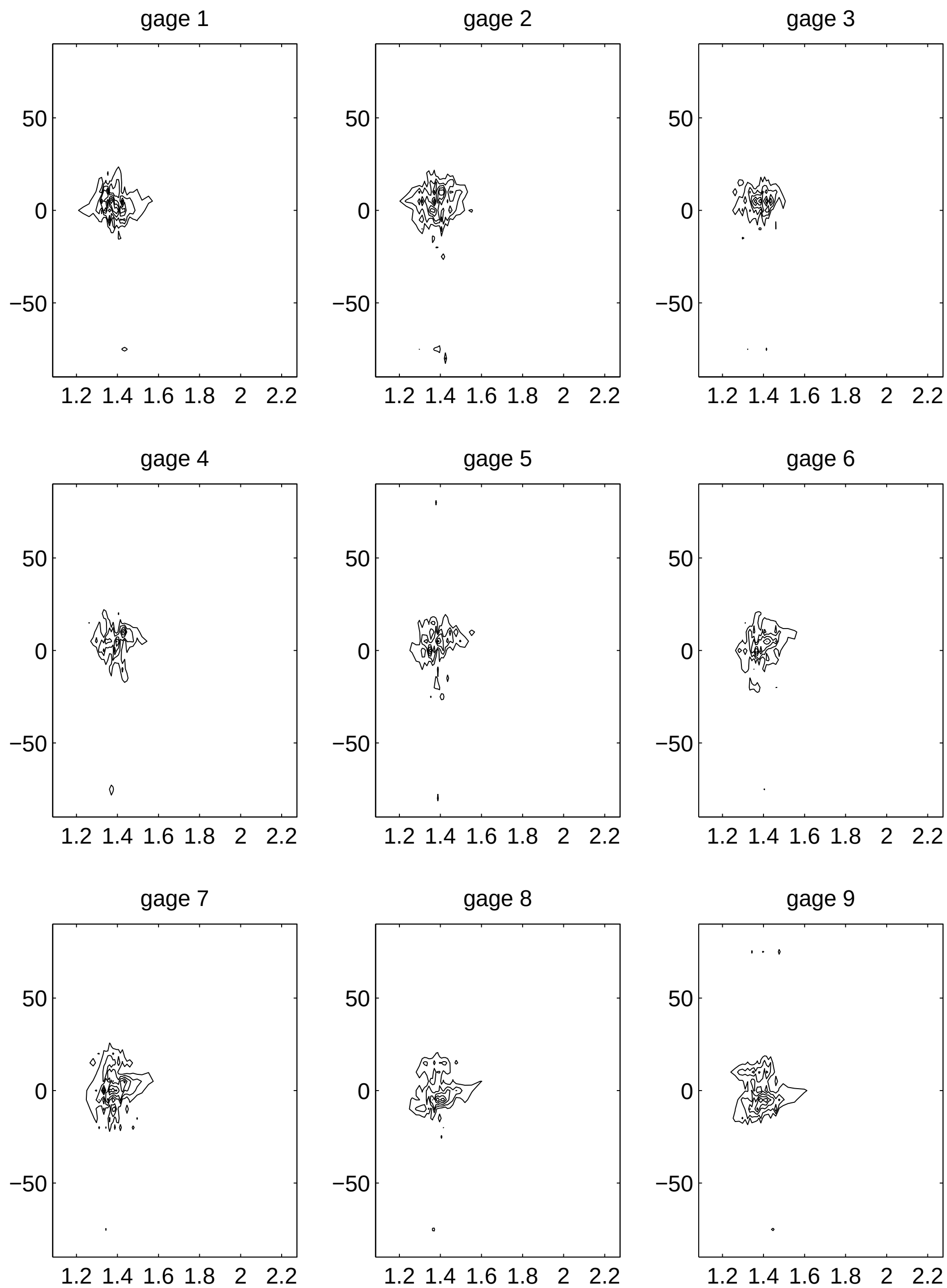

Figure E.19: Directional spectra for Test 4 (position 5).

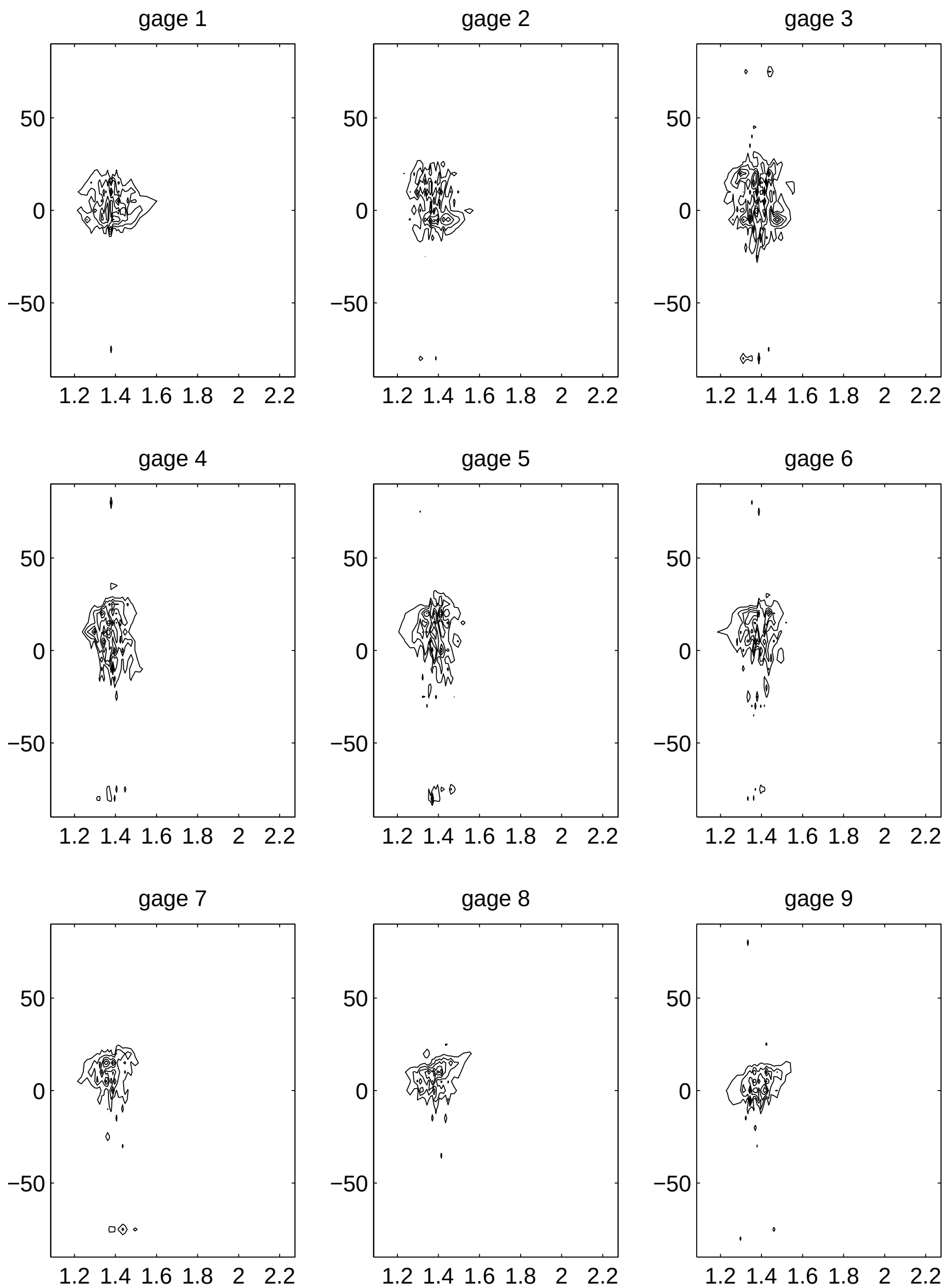

Figure E.20: Directional spectra for Test 4 (position 6).

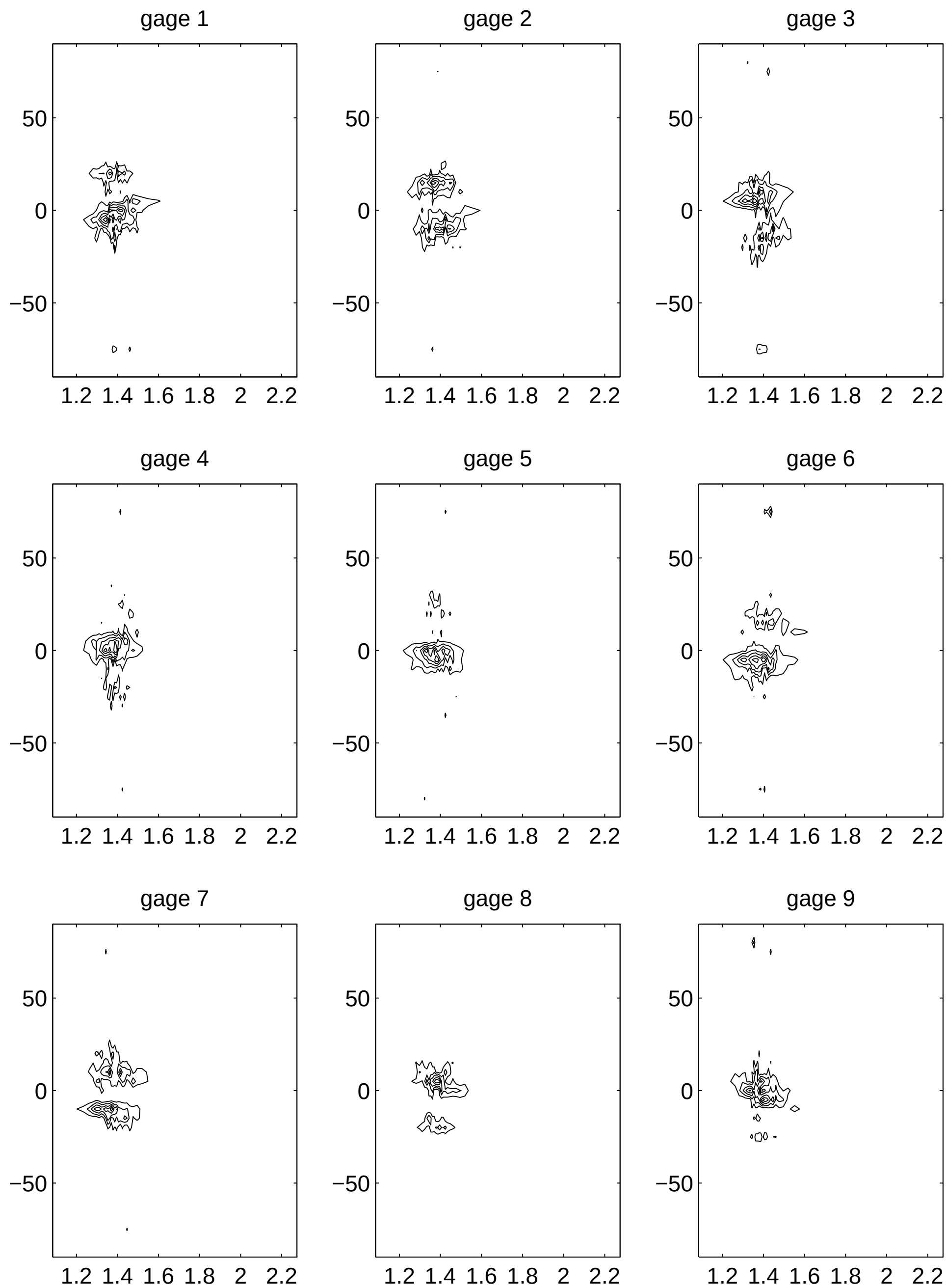

Figure E.21: Directional spectra for Test 4 (position 7).

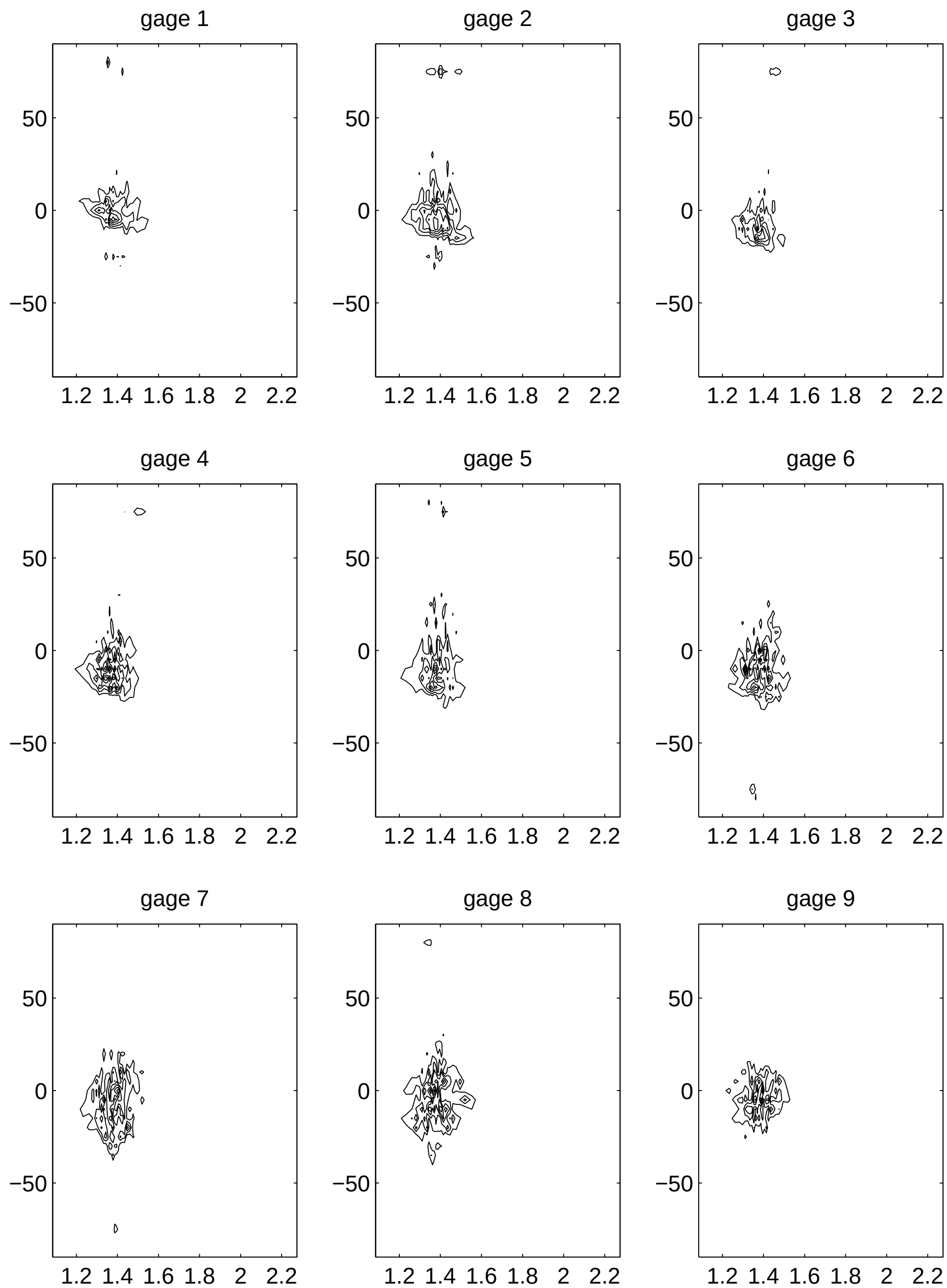

Figure E.22: Directional spectra for Test 4 (position 8).

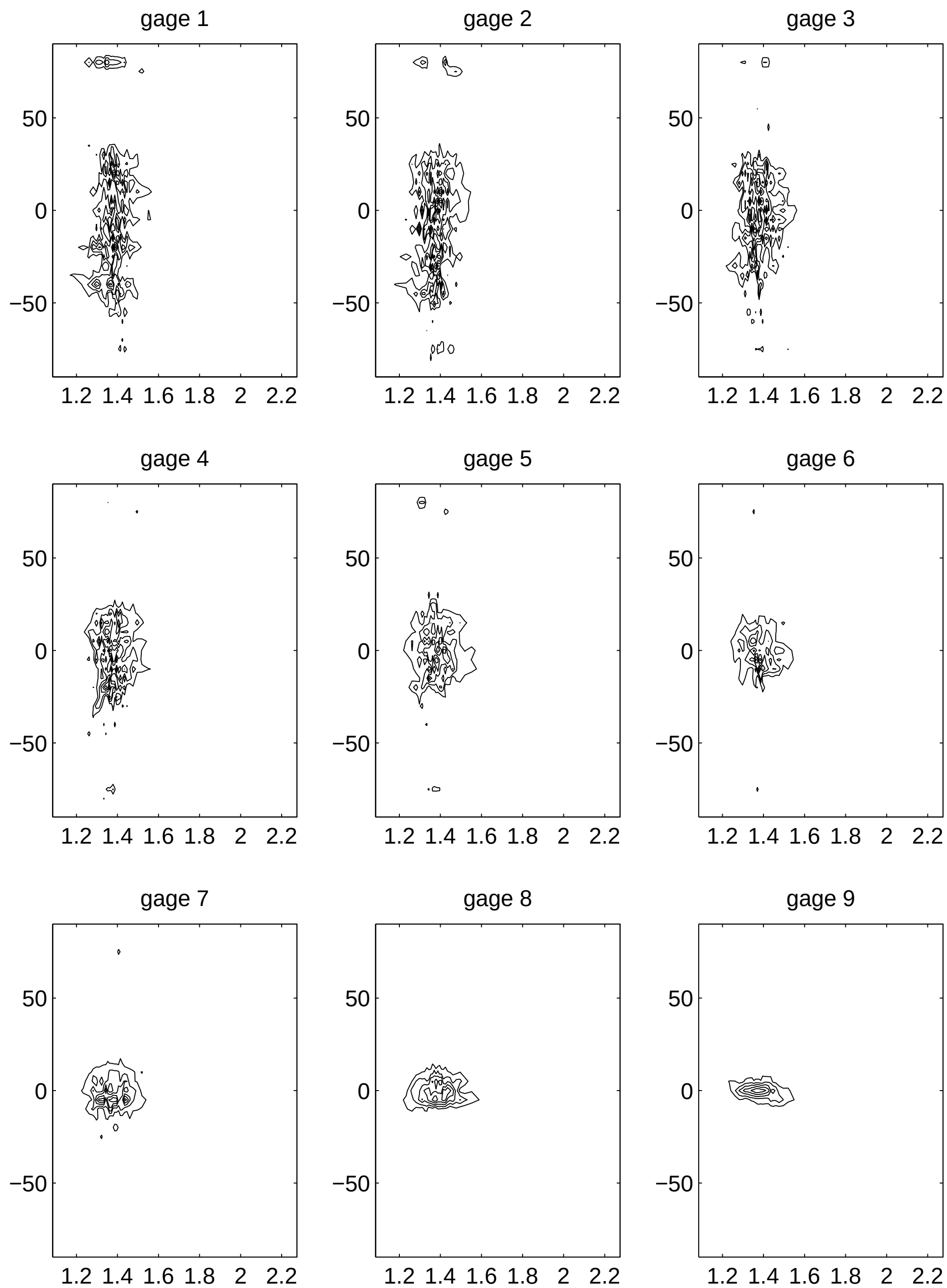

Figure E.23: Directional spectra for Test 4 (position 9).

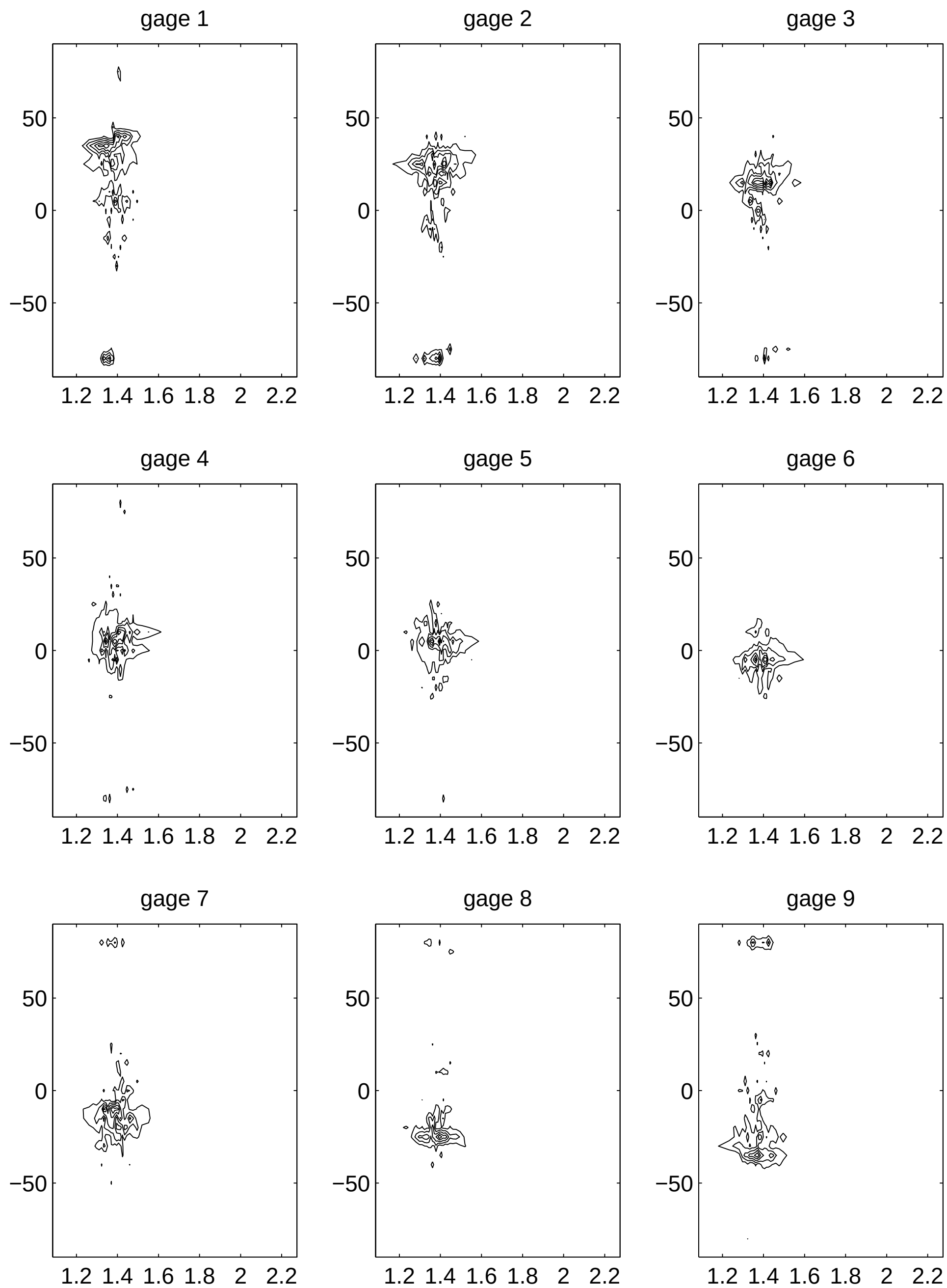

Figure E.24: Directional spectra for Test 4 (position 10).

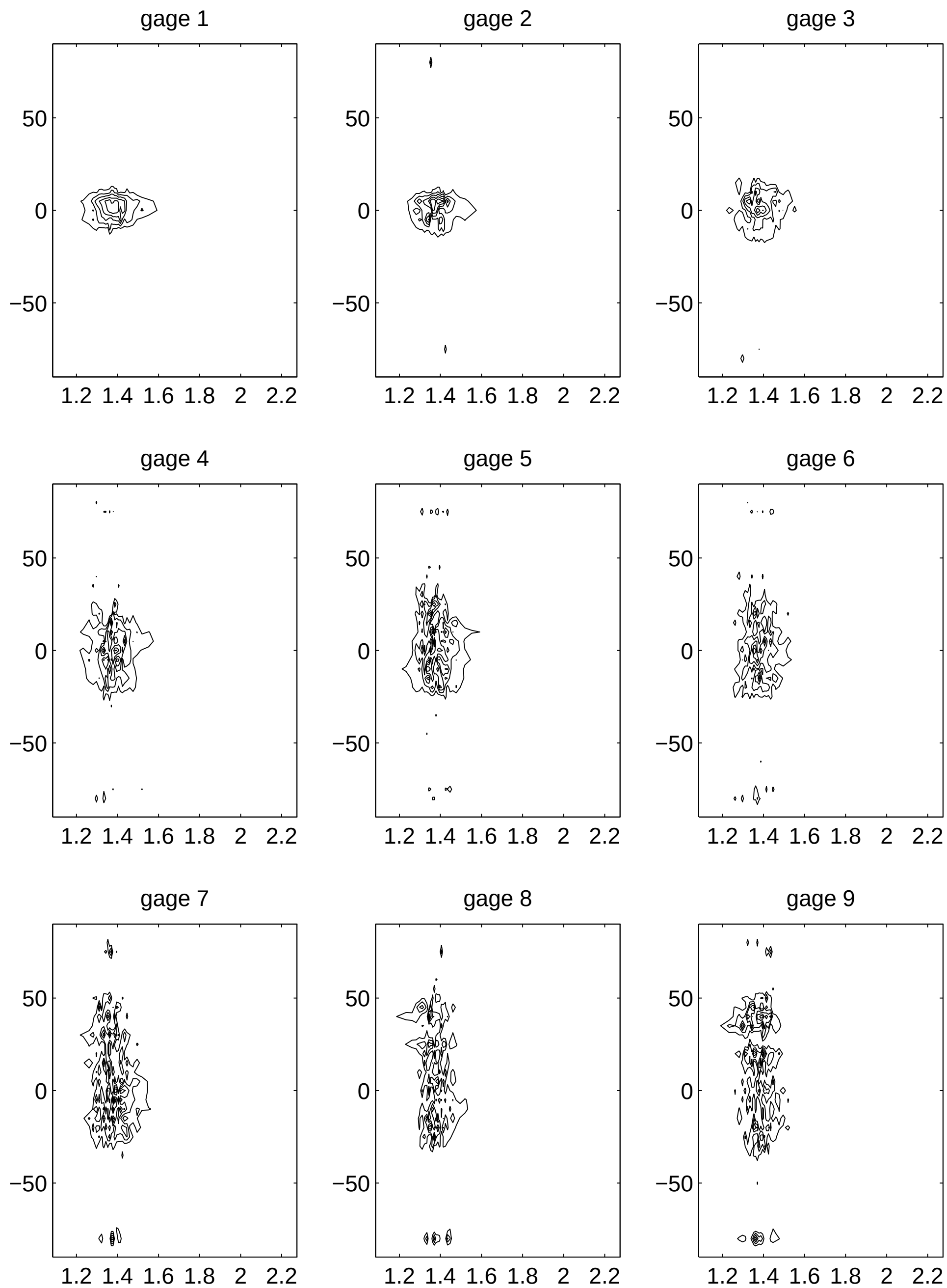

Figure E.25: Directional spectra for Test 4 (position 11).

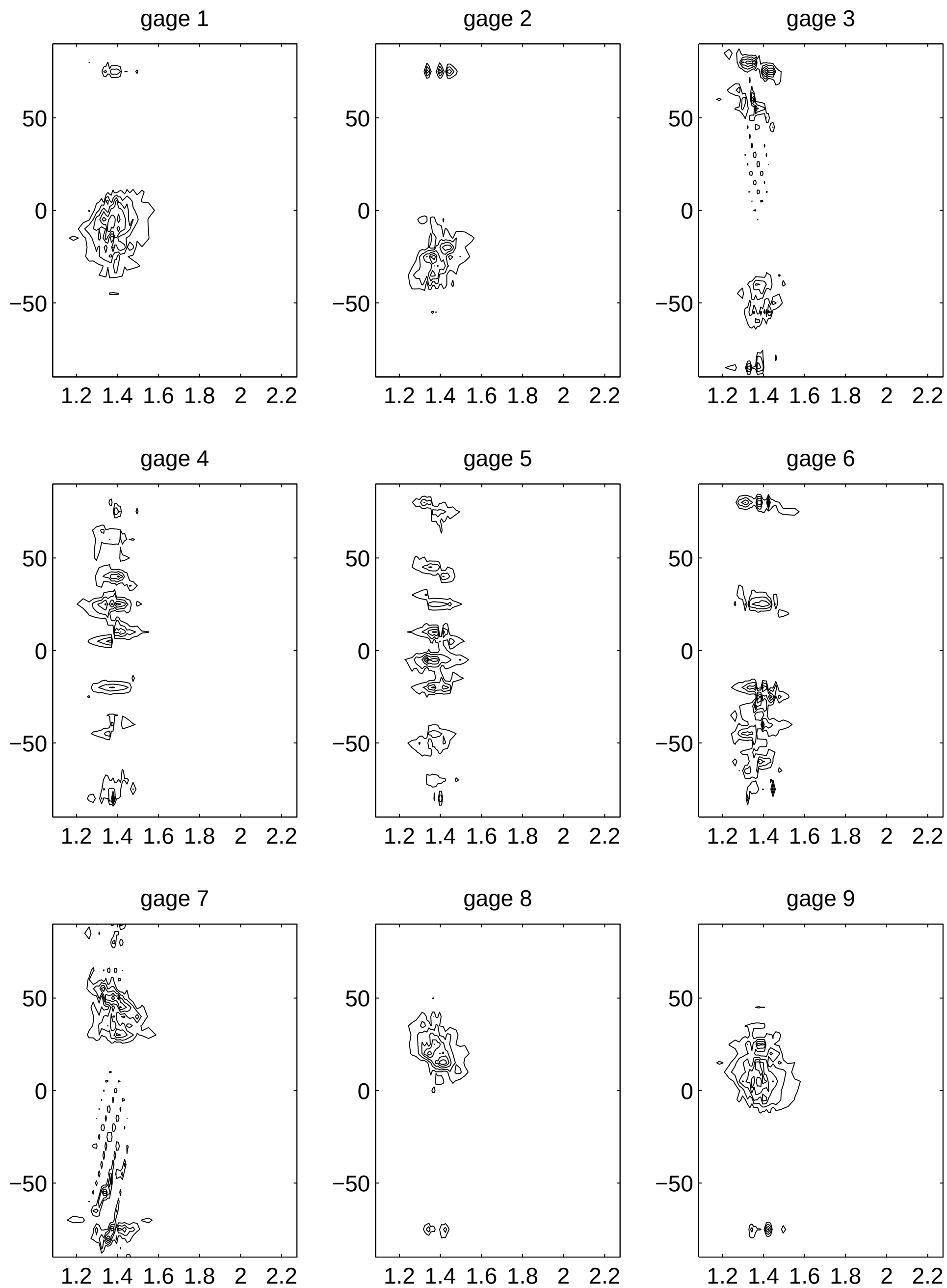

Figure E.26: Directional spectra for Test 4 (position 12).

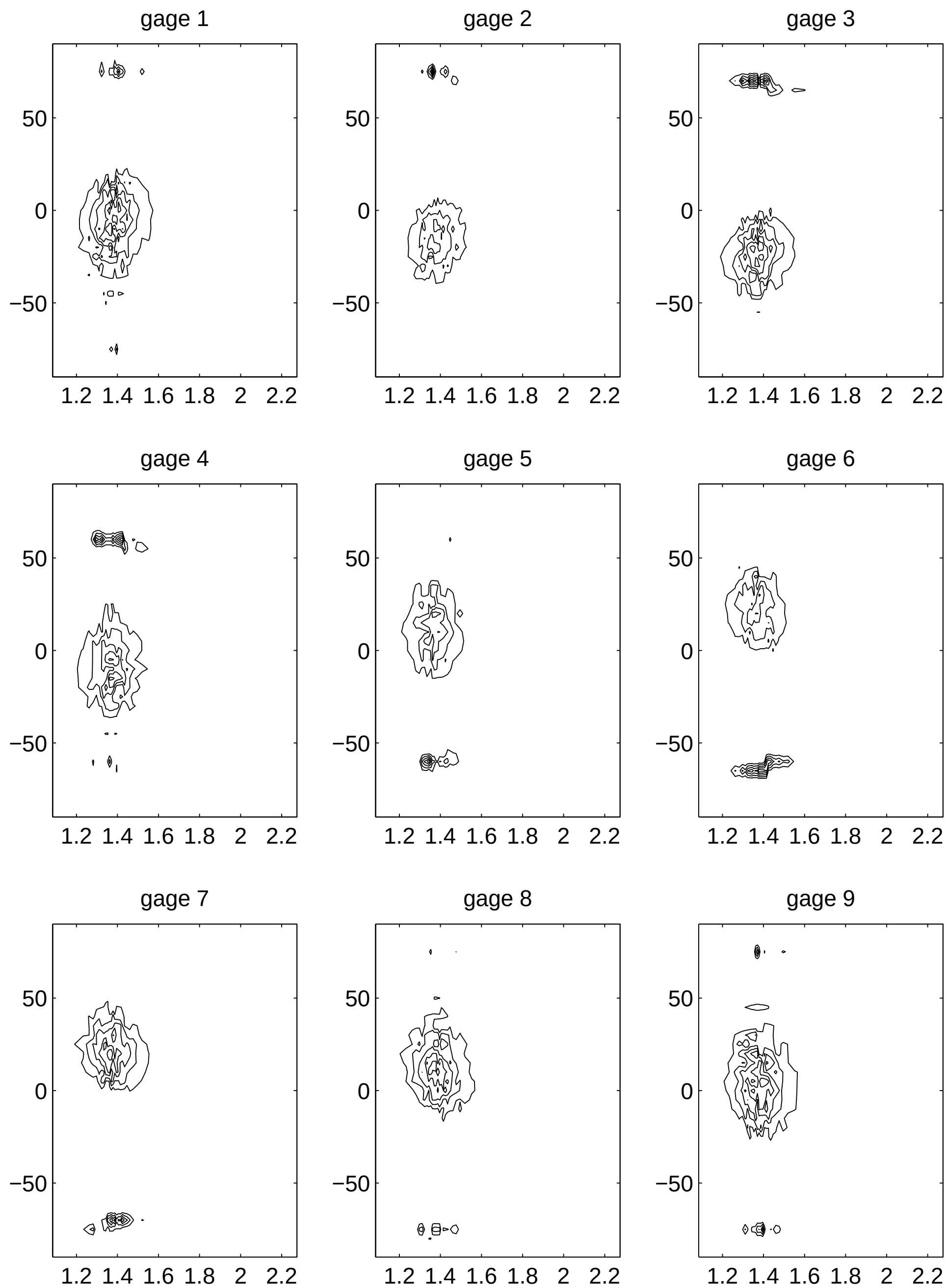

Figure E.27: Directional spectra for Test 4 (position 13).

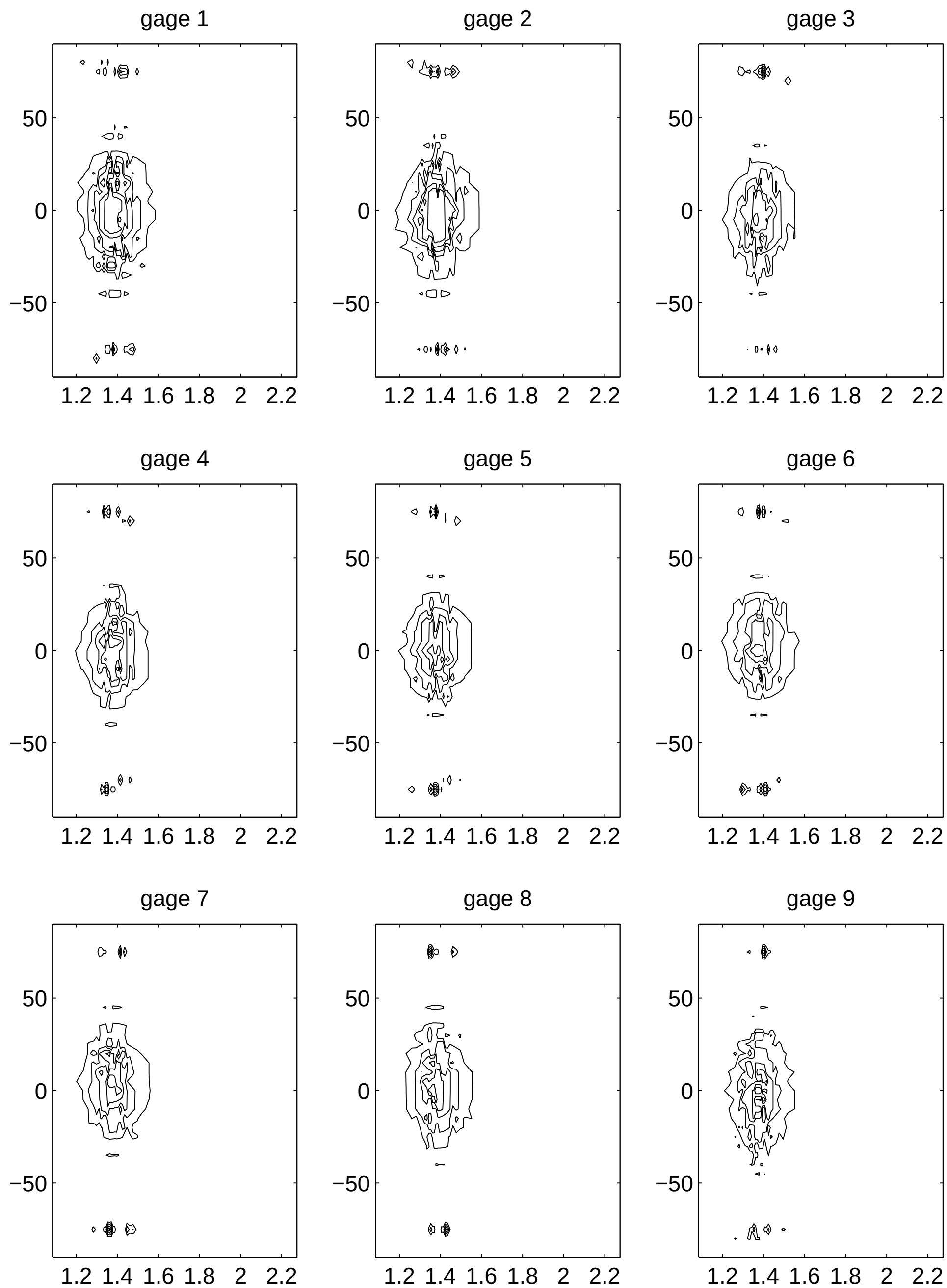

Figure E.28: Directional spectra for Test 4 (position 14).

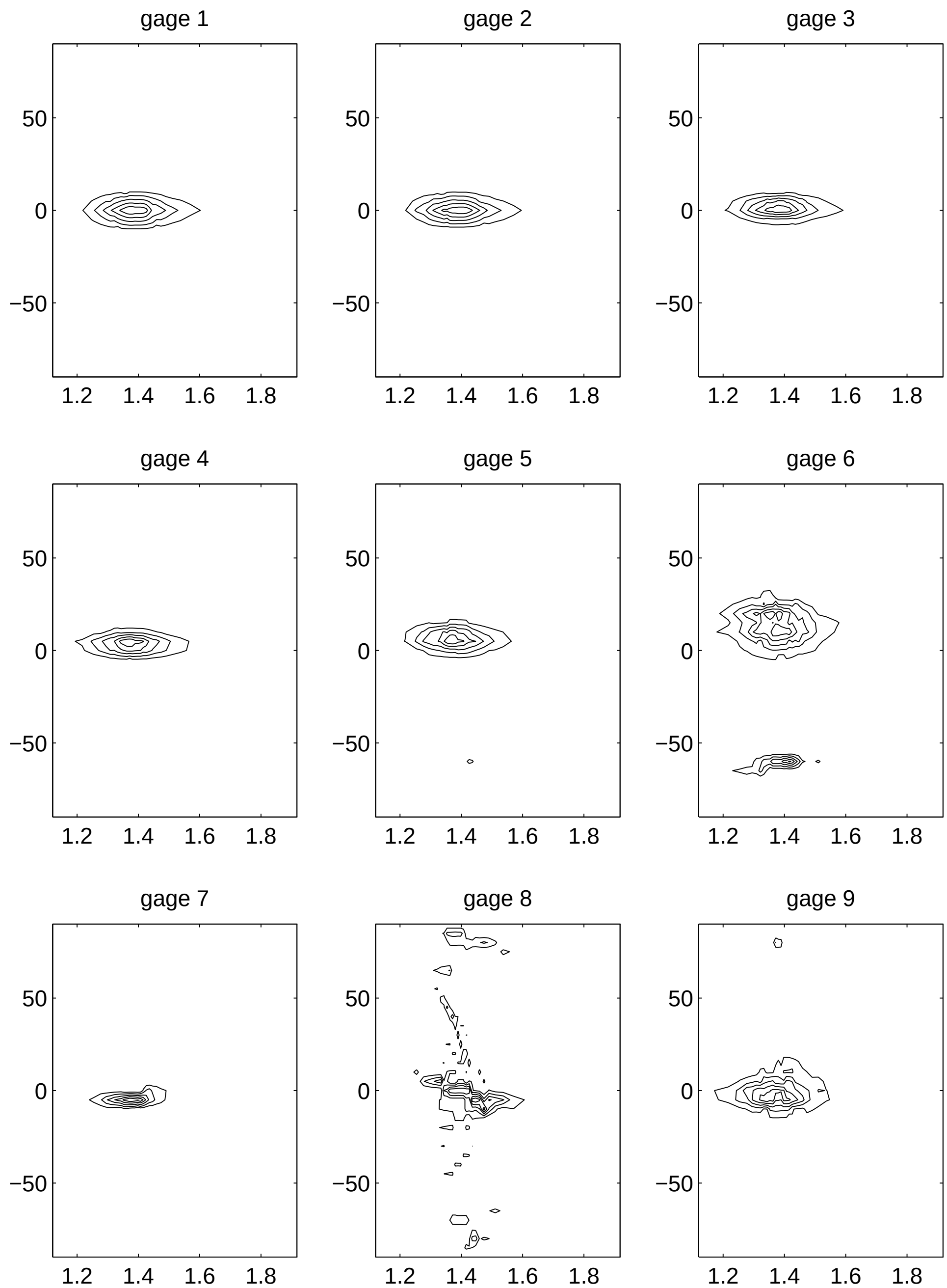

Figure E.29: Directional spectra for Test 5 (position 1).

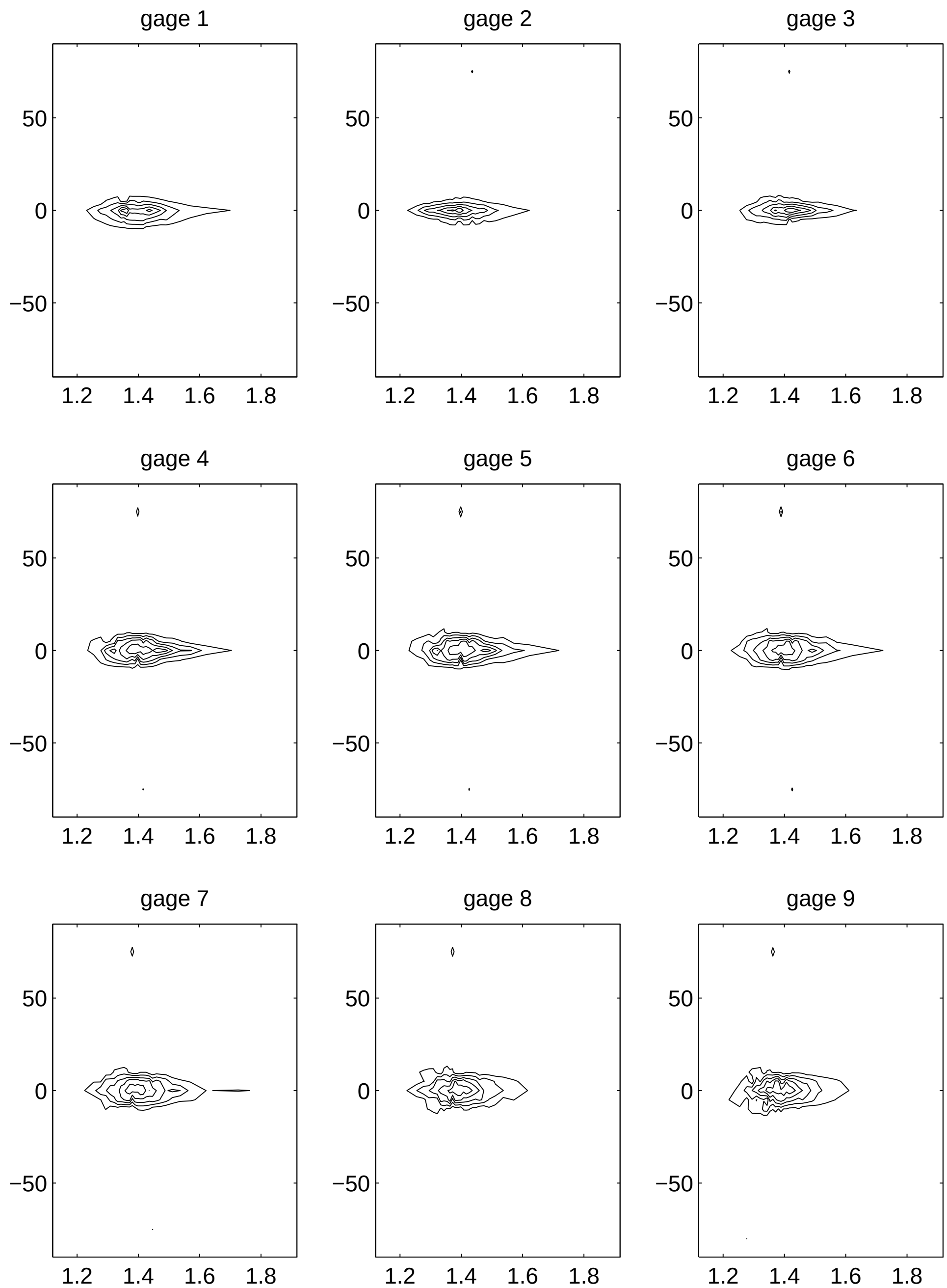

Figure E.30: Directional spectra for Test 5 (position 2).

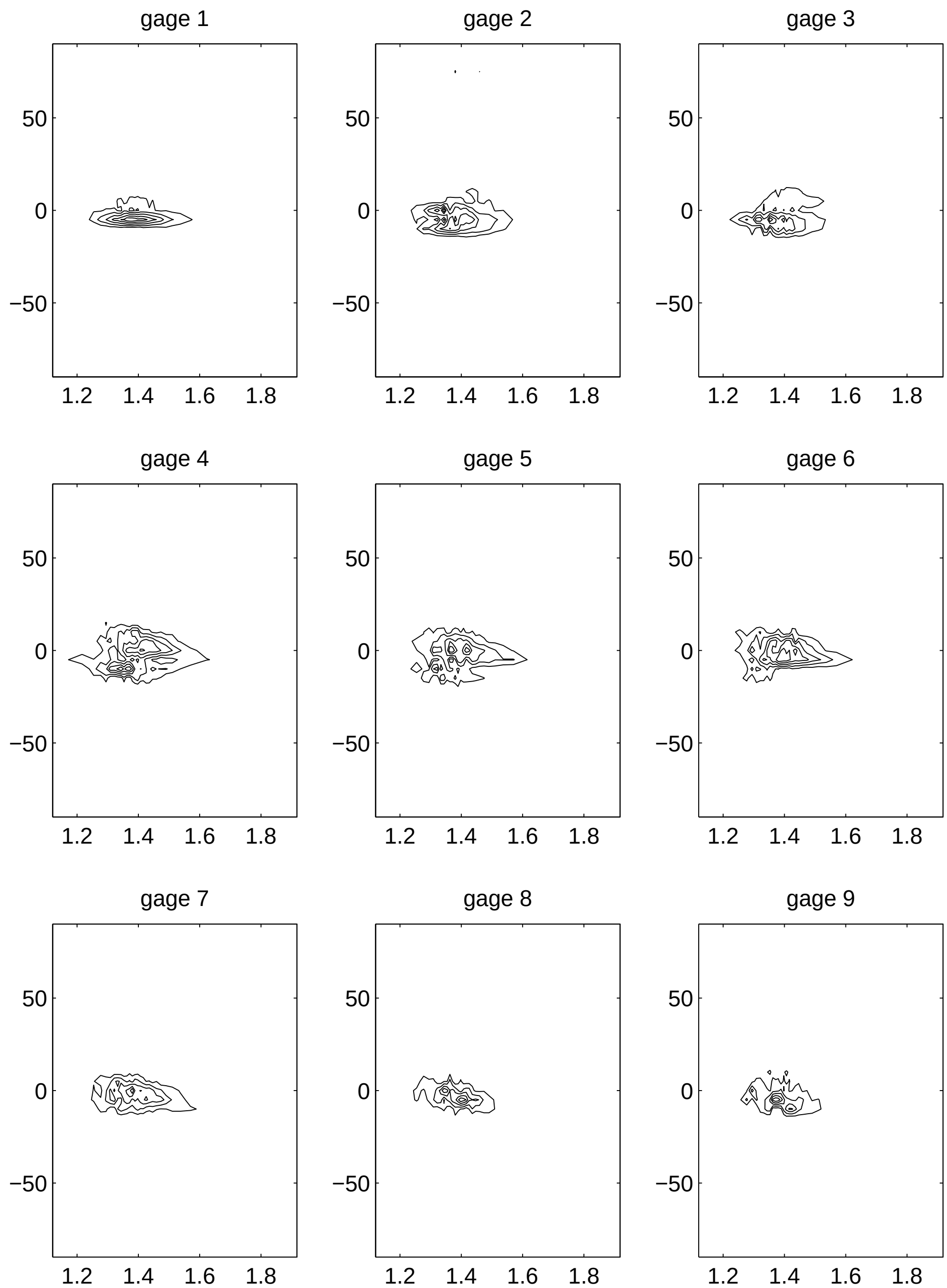

Figure E.31: Directional spectra for Test 5 (position 3).

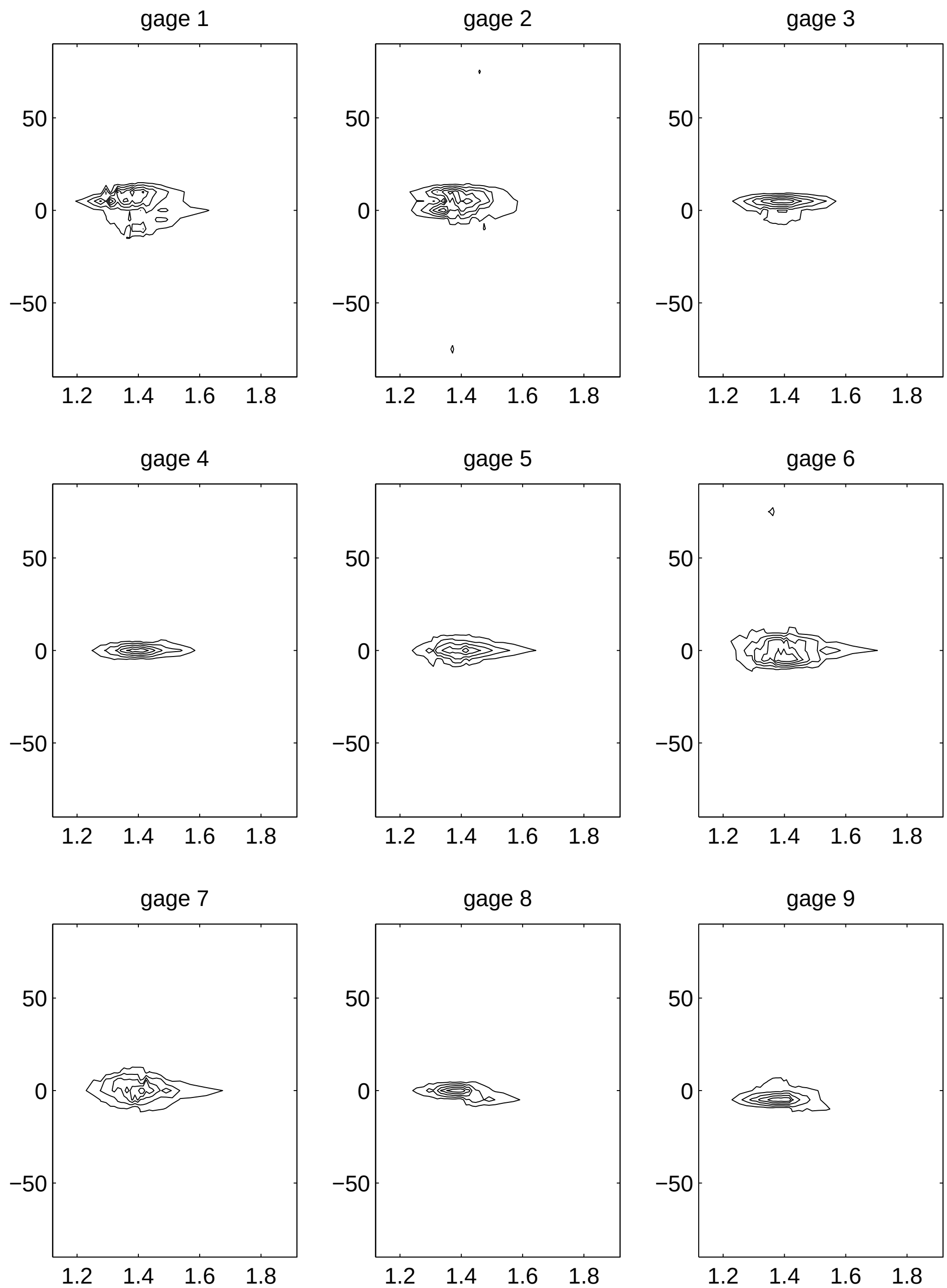

Figure E.32: Directional spectra for Test 5 (position 4).

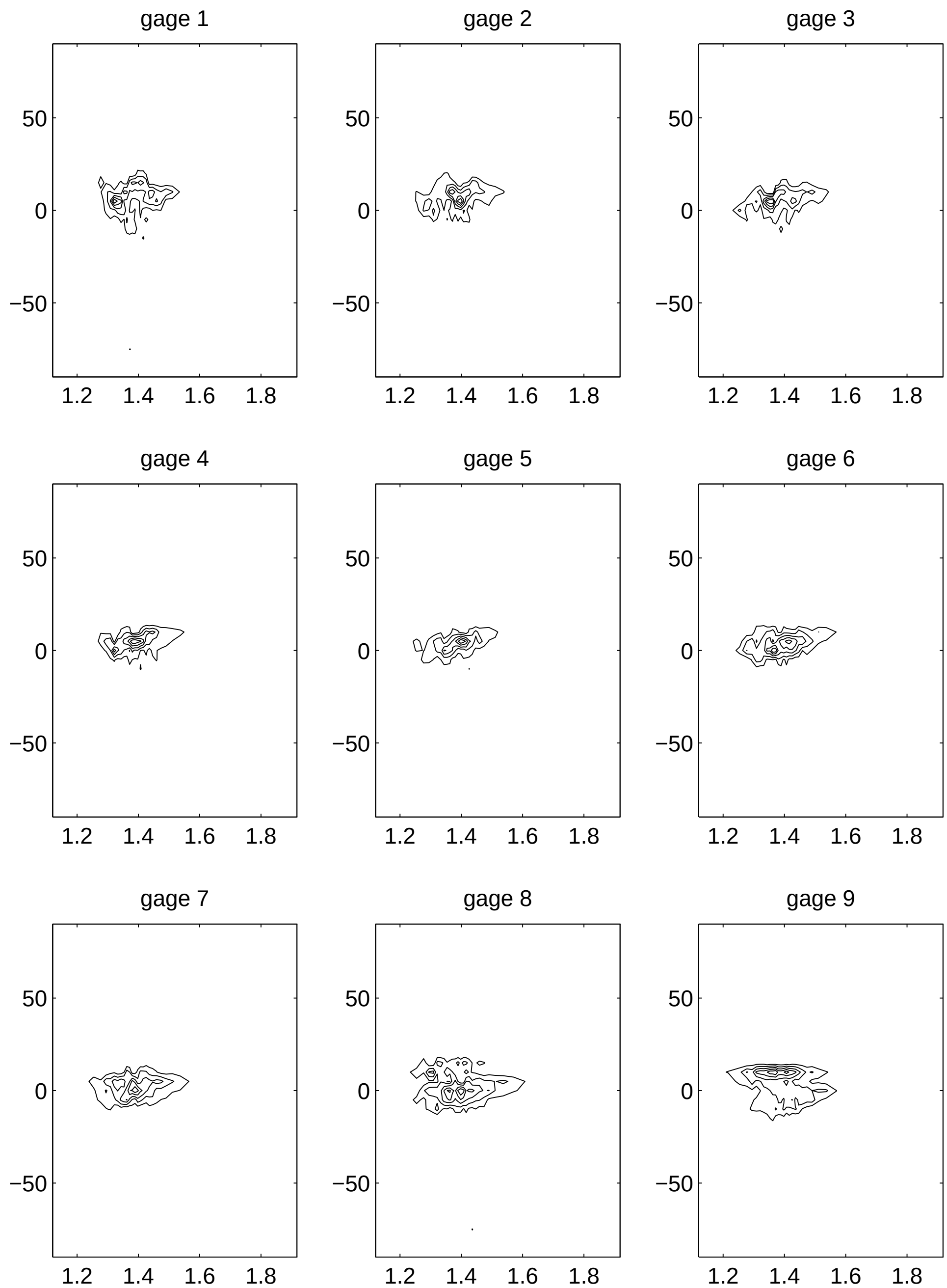

Figure E.33: Directional spectra for Test 5 (position 5).

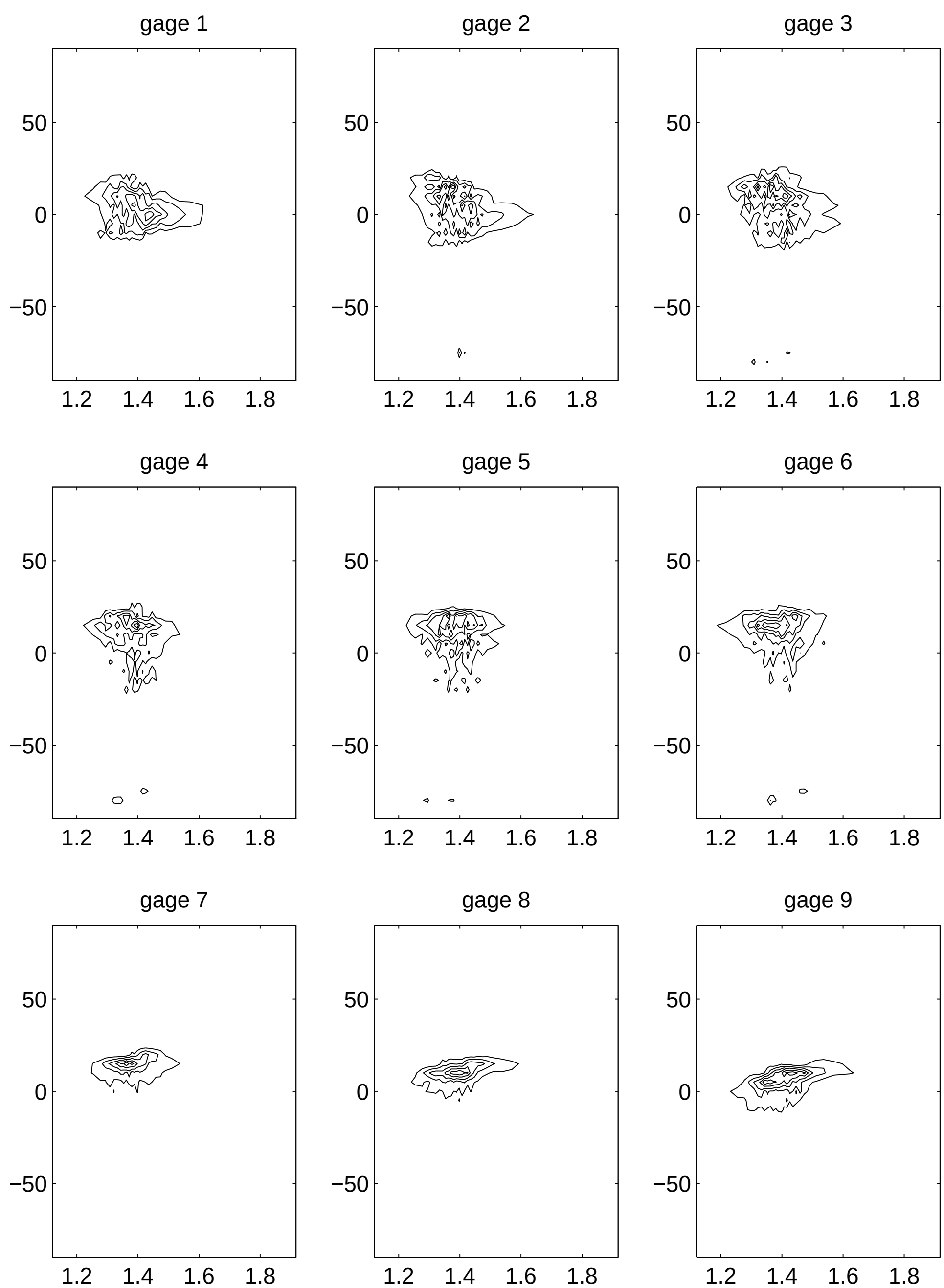

Figure E.34: Directional spectra for Test 5 (position 6).

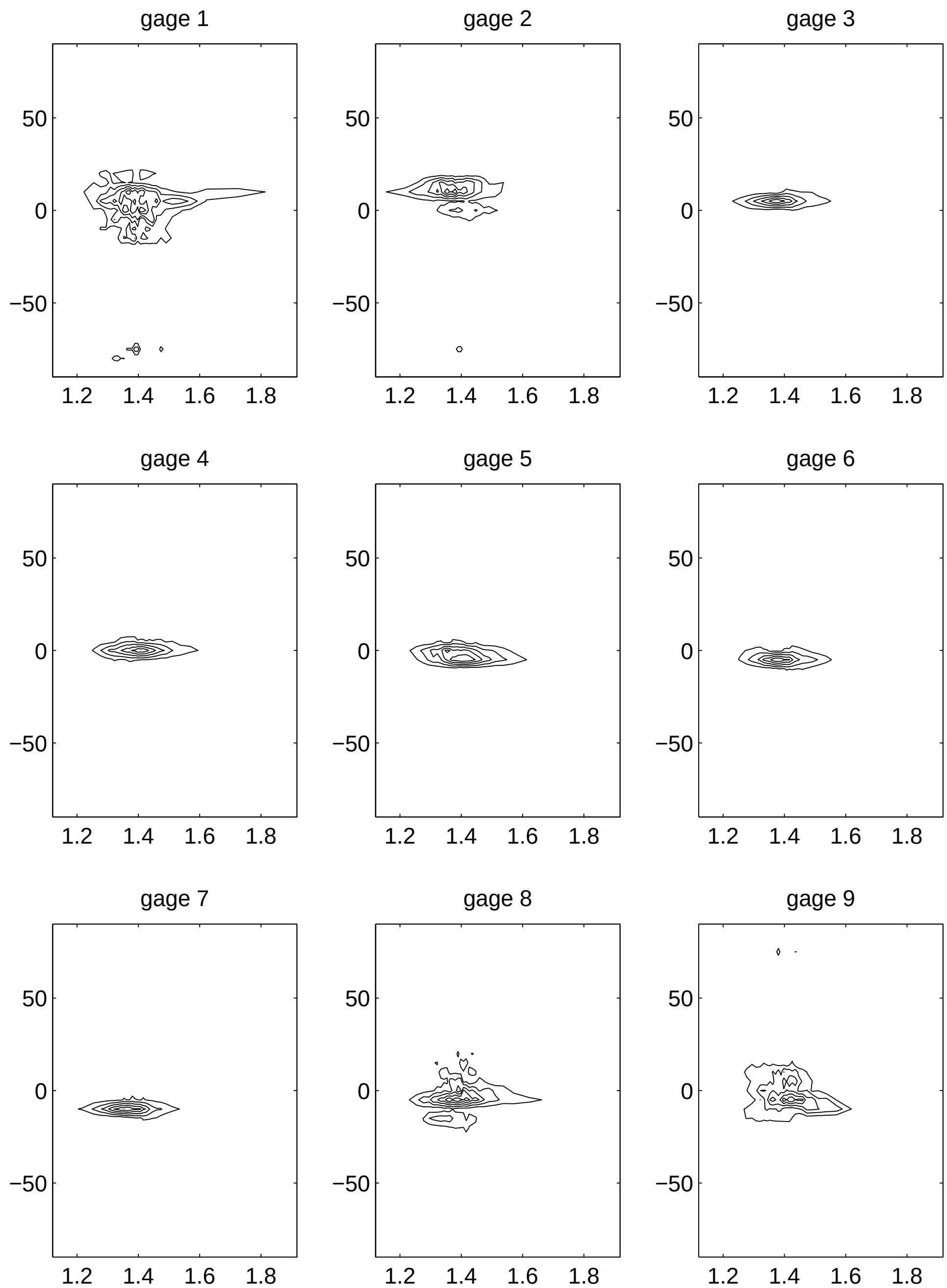

Figure E.35: Directional spectra for Test 5 (position 7).

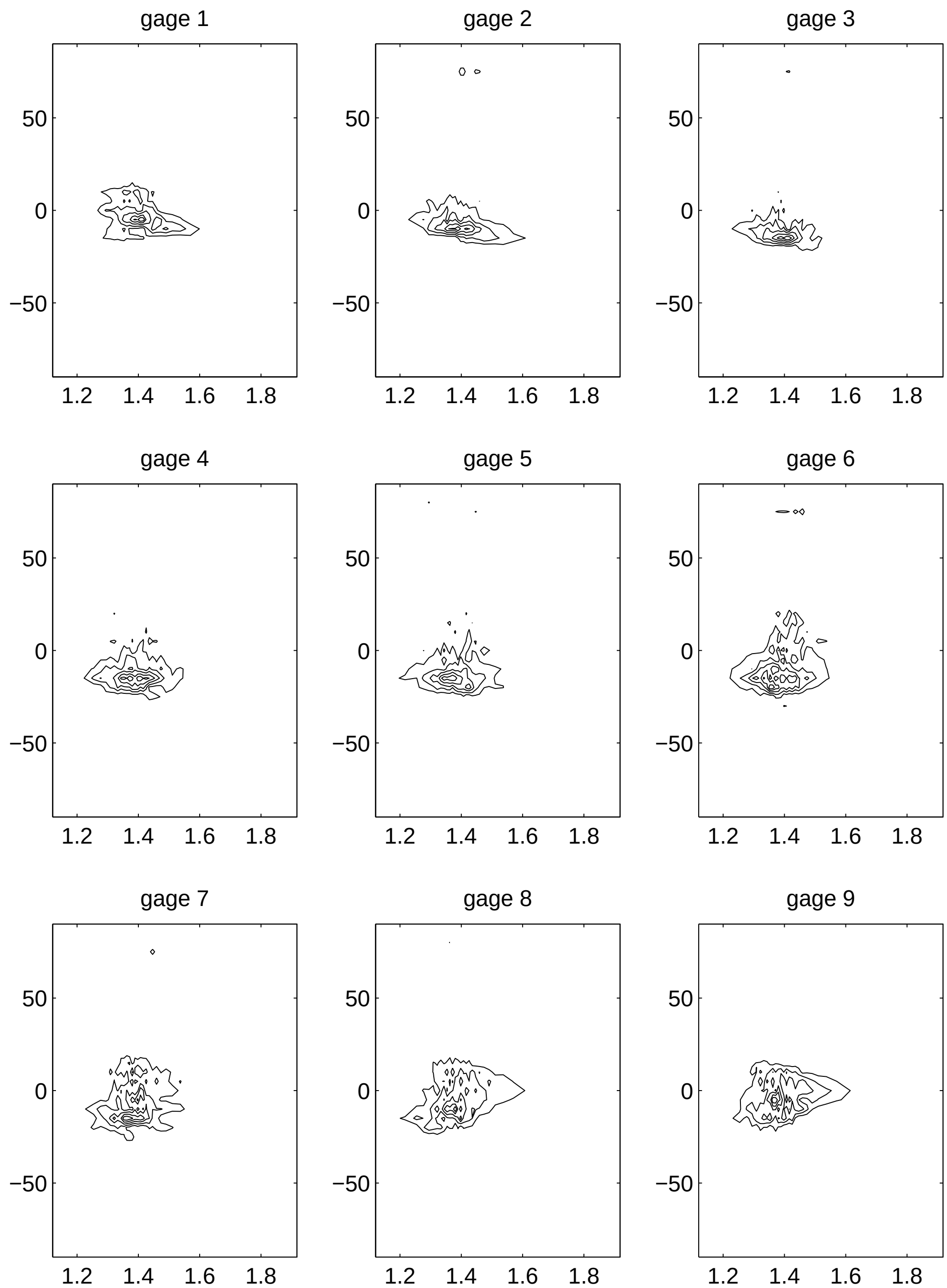

Figure E.36: Directional spectra for Test 5 (position 8).

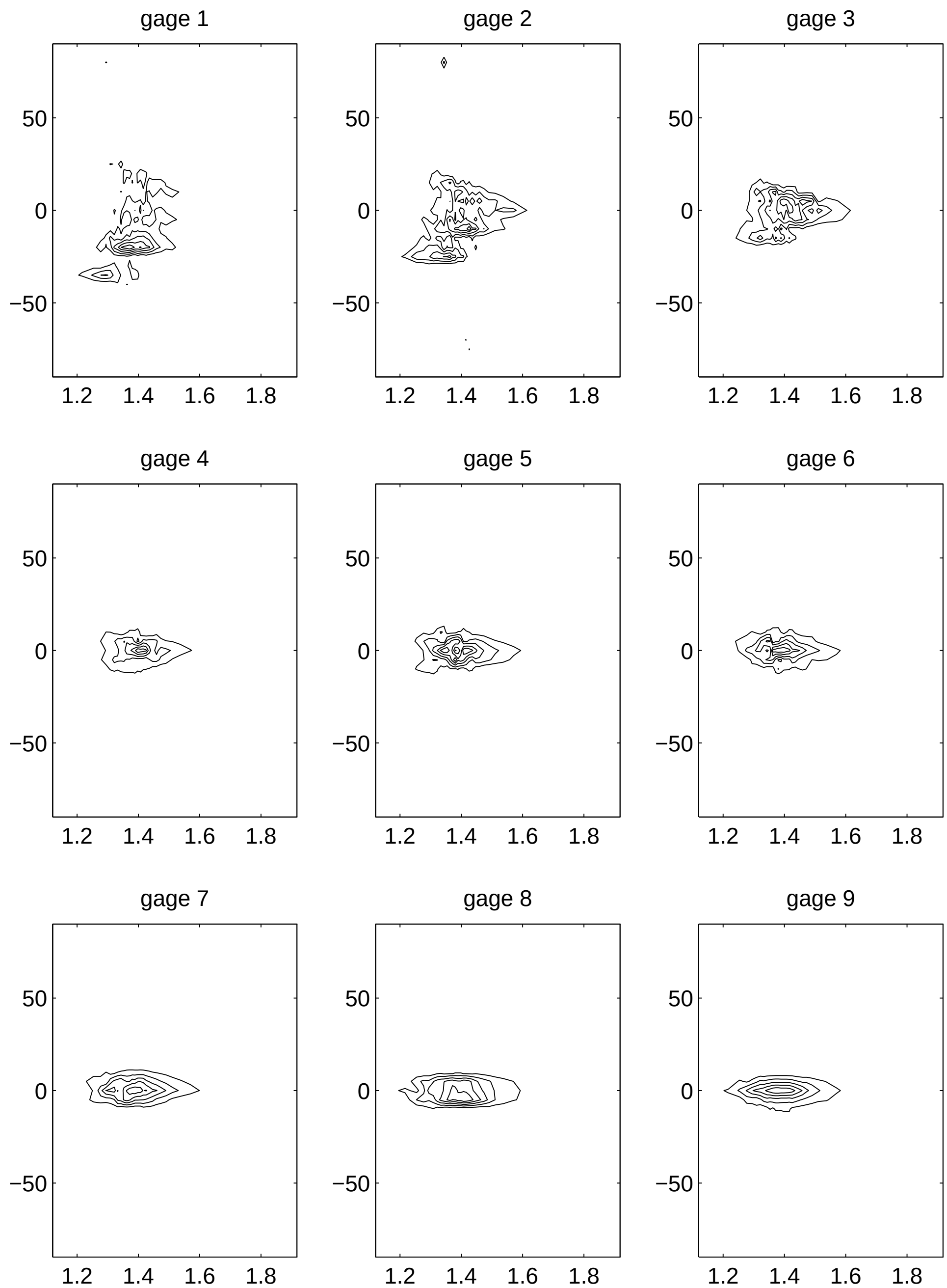

Figure E.37: Directional spectra for Test 5 (position 9).

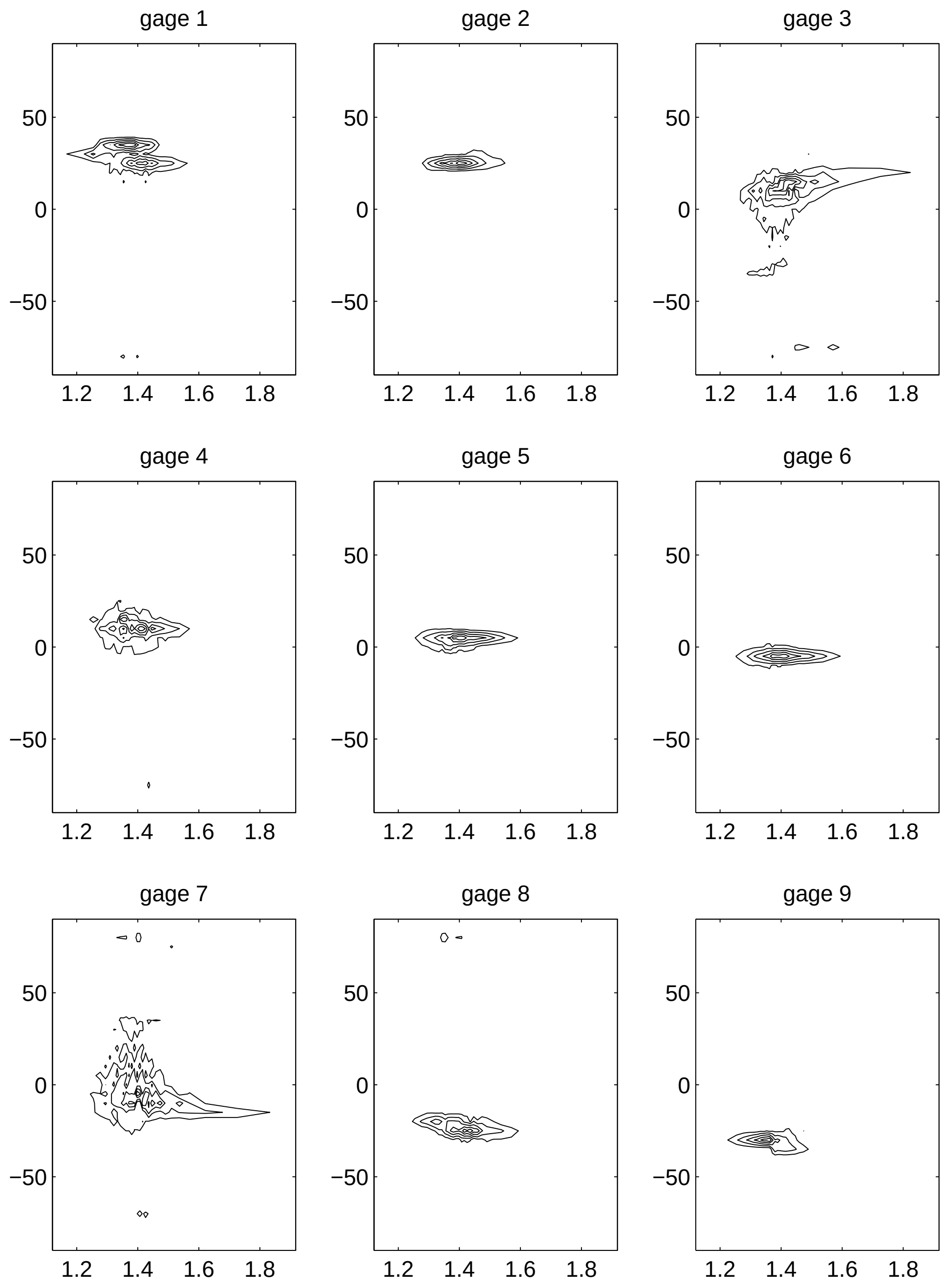

Figure E.38: Directional spectra for Test 5 (position 10).

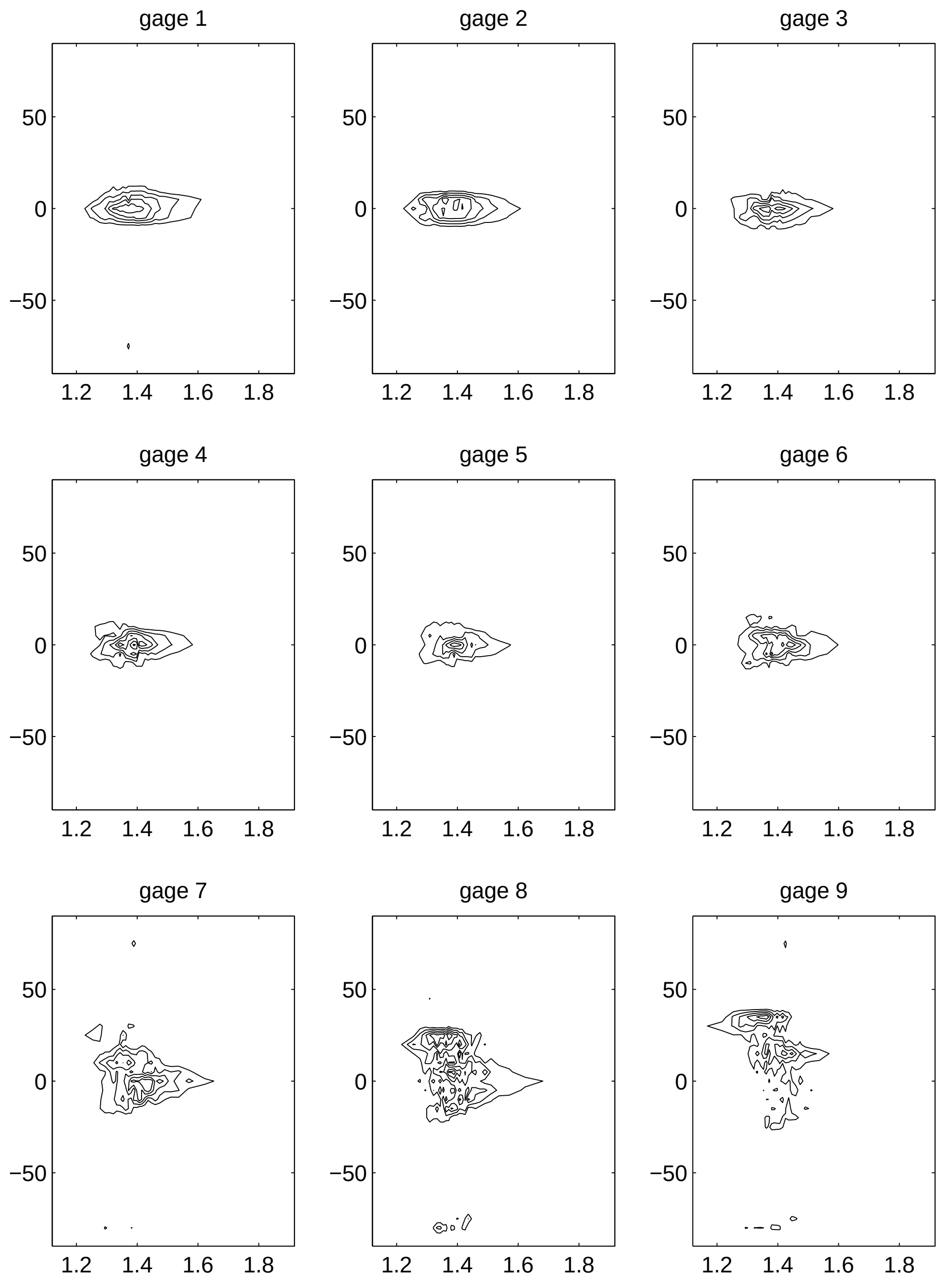

Figure E.39: Directional spectra for Test 5 (position 11).

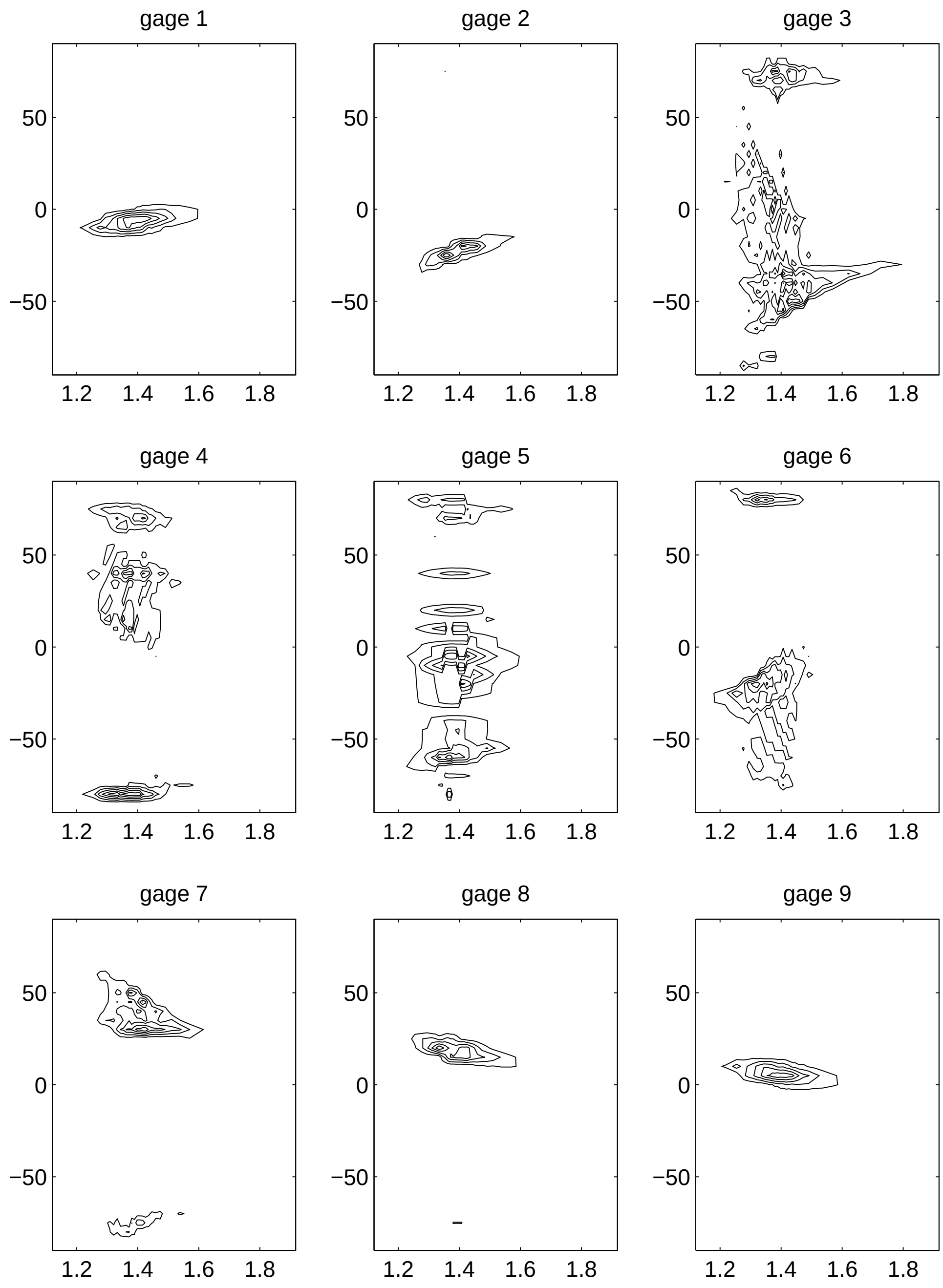

Figure E.40: Directional spectra for Test 5 (position 12).

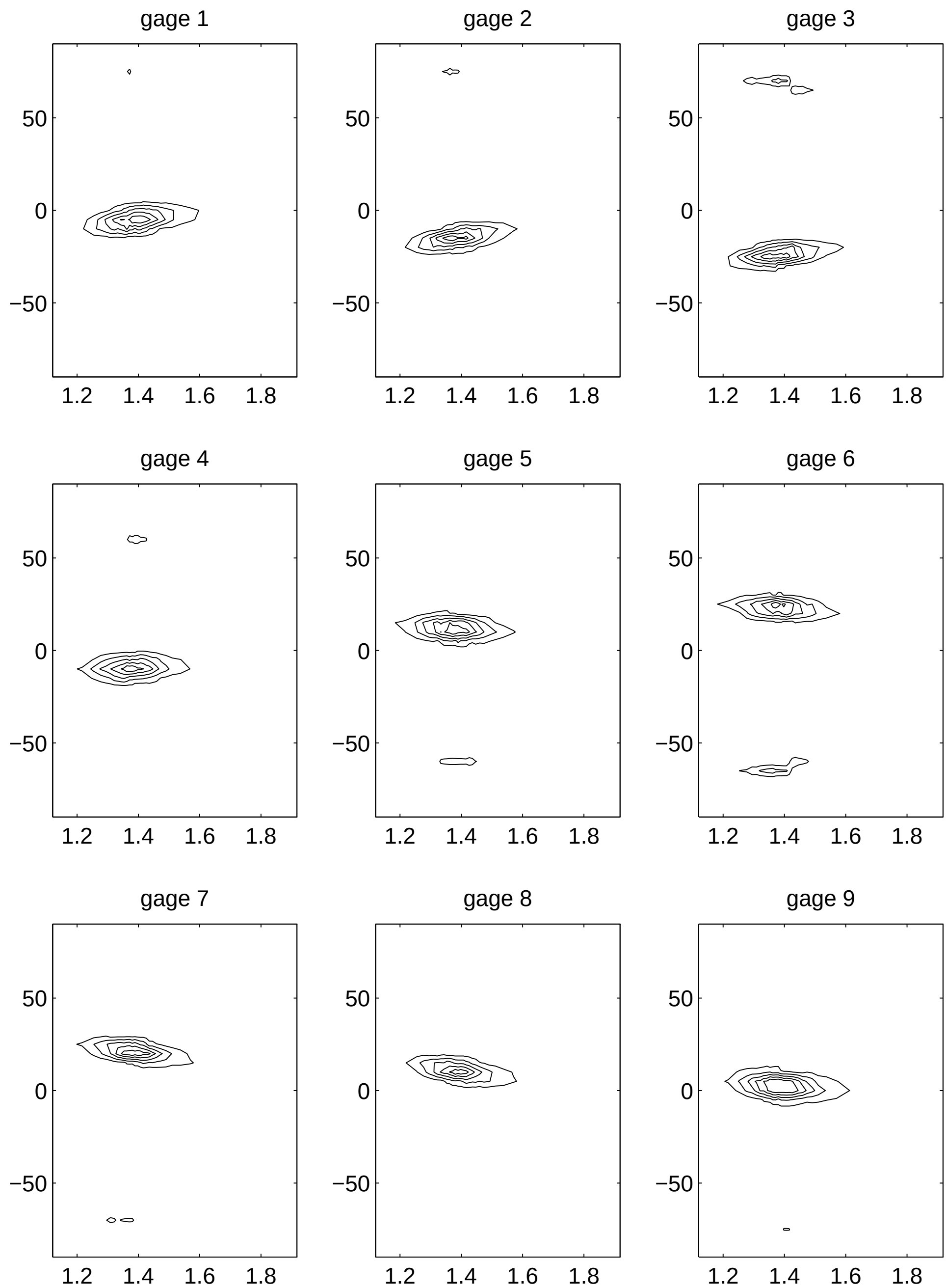

Figure E.41: Directional spectra for Test 5 (position 13).

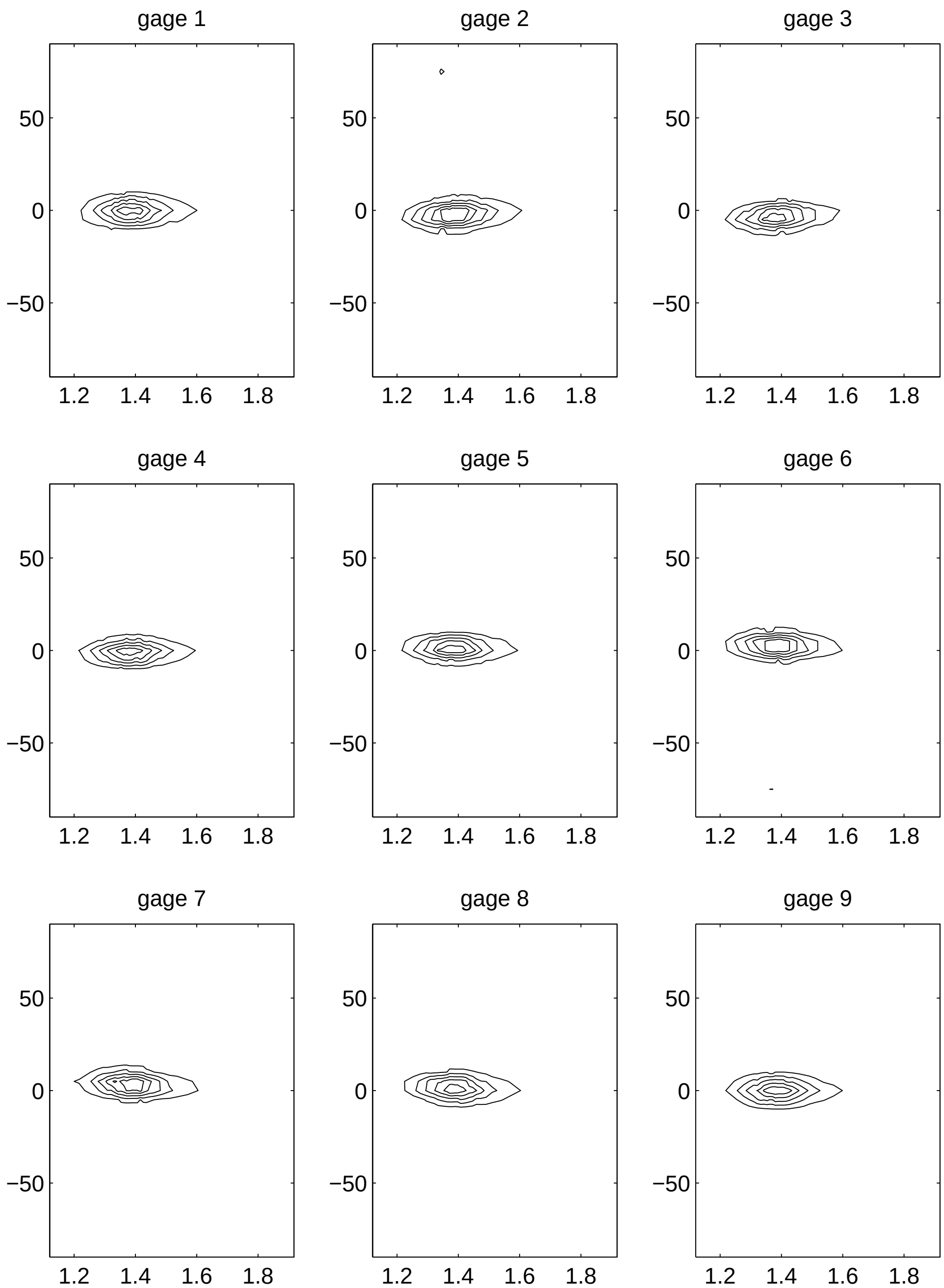

Figure E.42: Directional spectra for Test 5 (position 14).

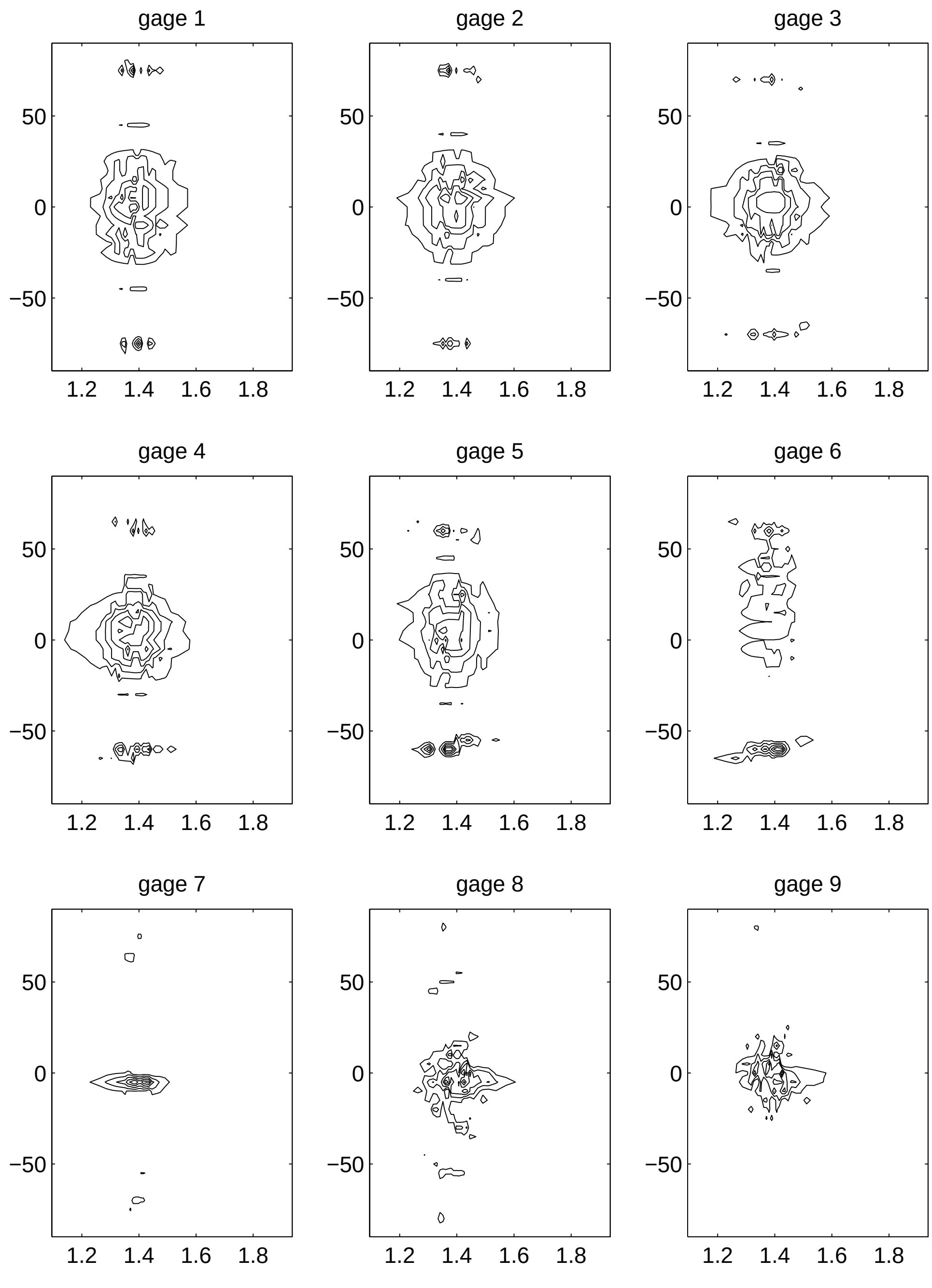

Figure E.43: Directional spectra for Test 6 (position 1).

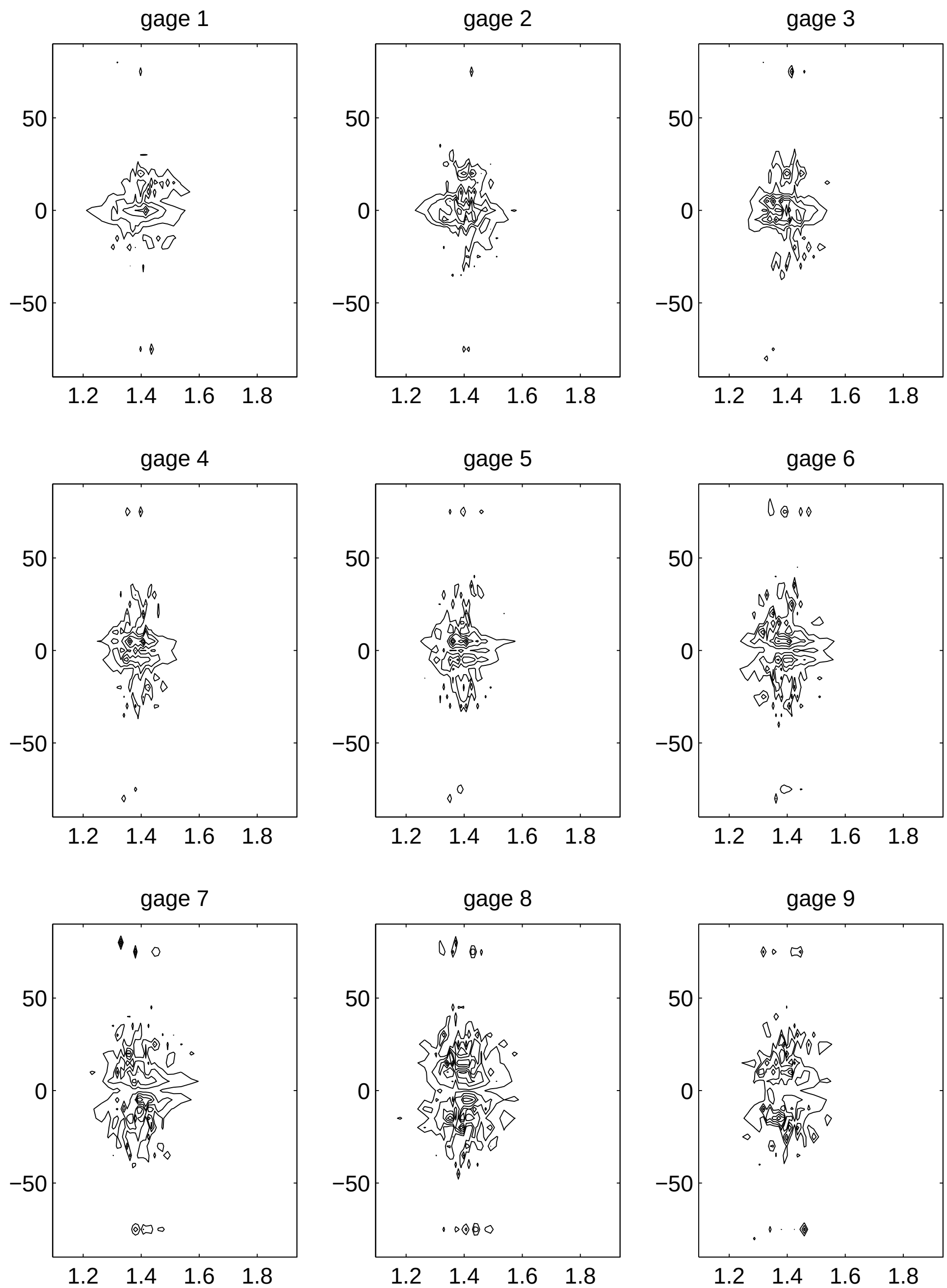

Figure E.44: Directional spectra for Test 6 (position 2).

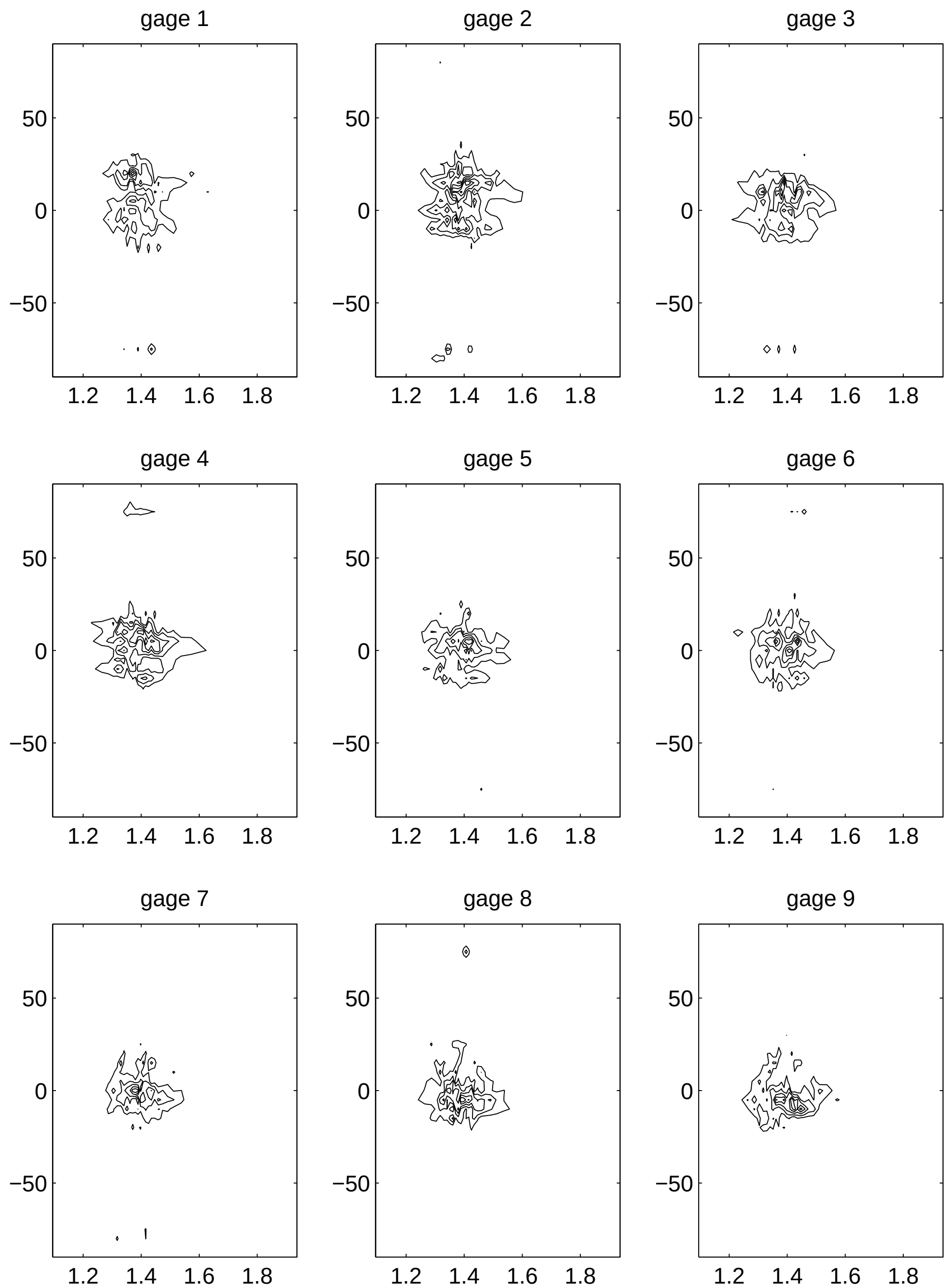

Figure E.45: Directional spectra for Test 6 (position 3).

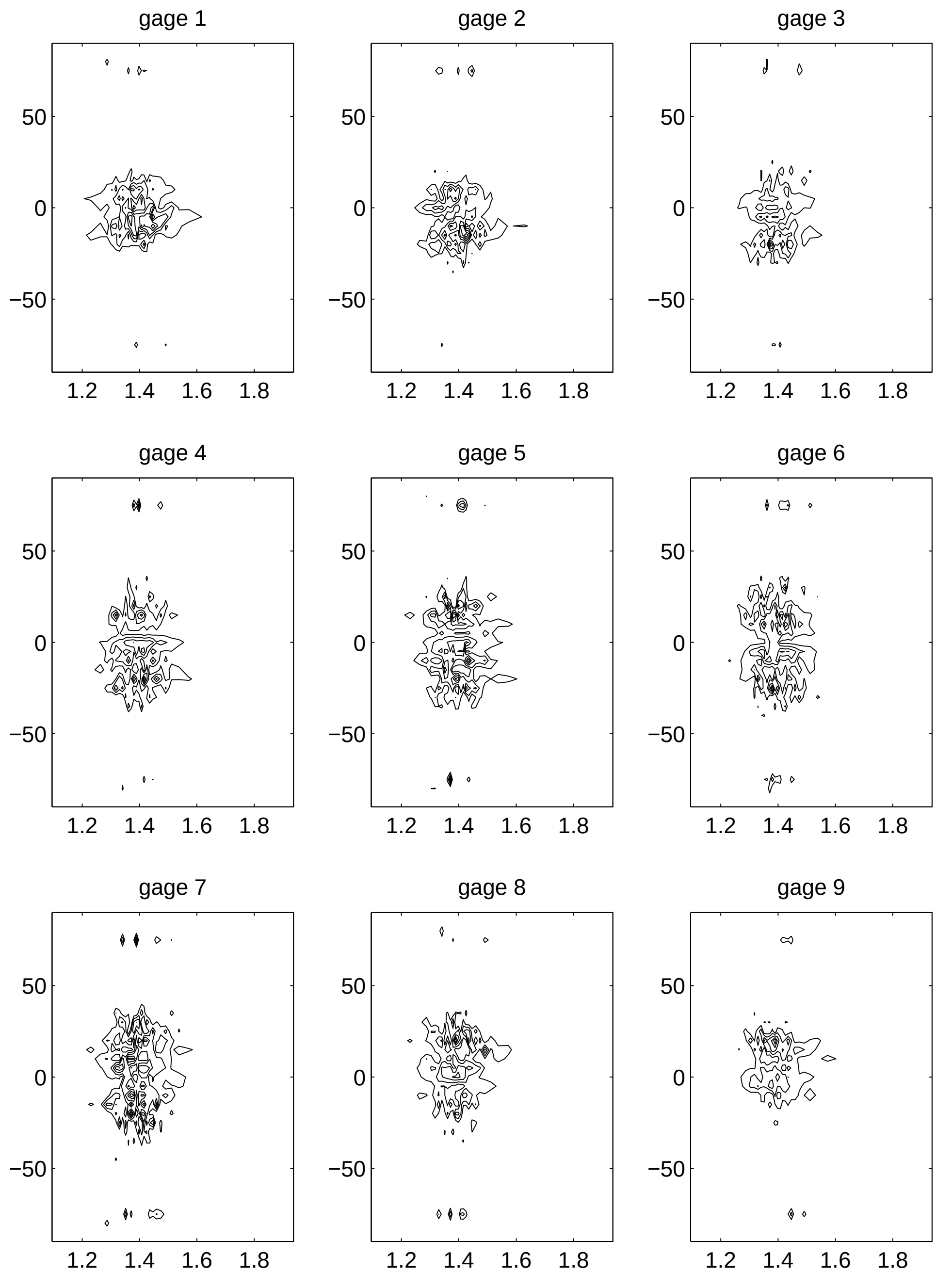

Figure E.46: Directional spectra for Test 6 (position 4).

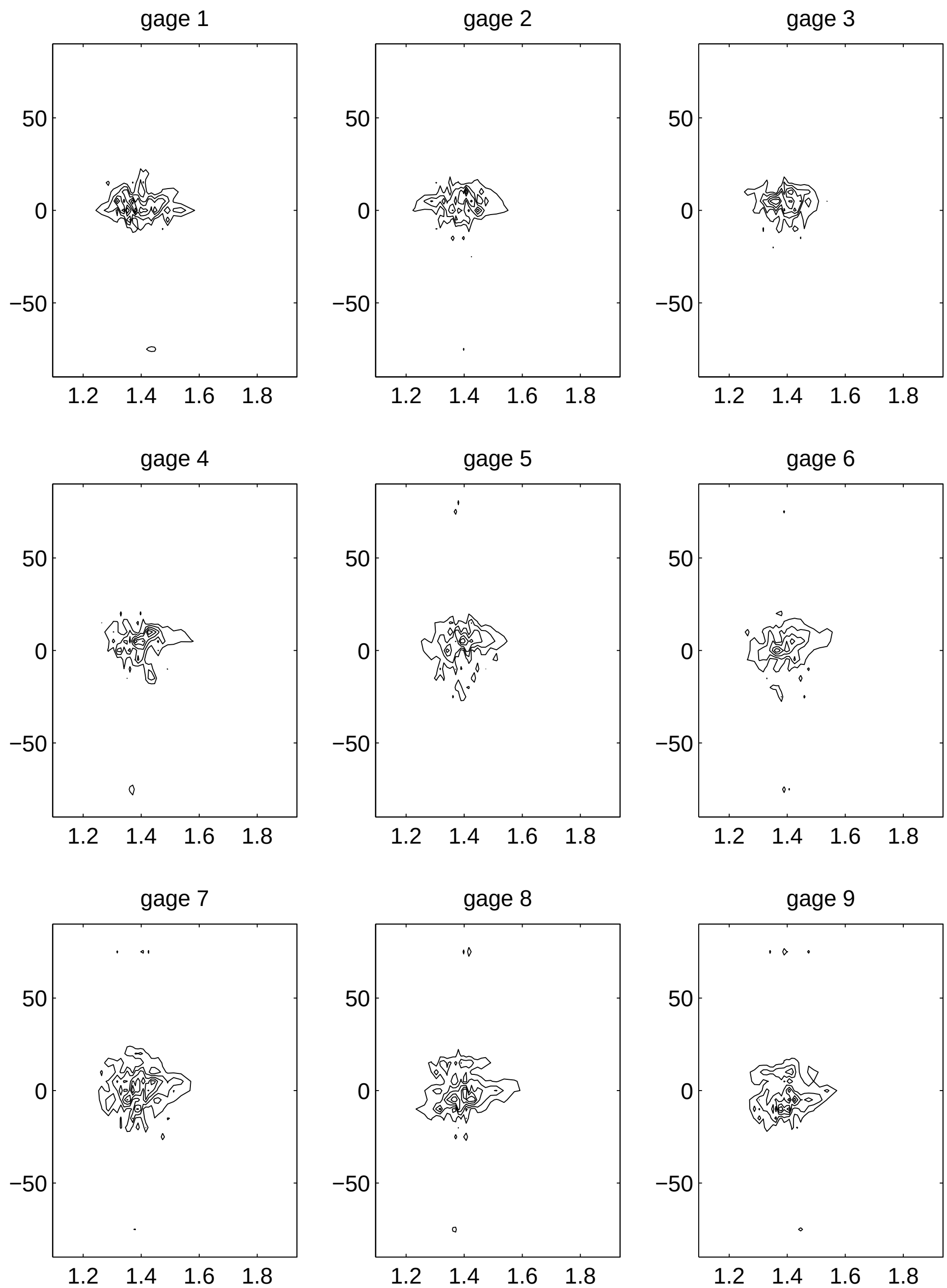

Figure E.47: Directional spectra for Test 6 (position 5).

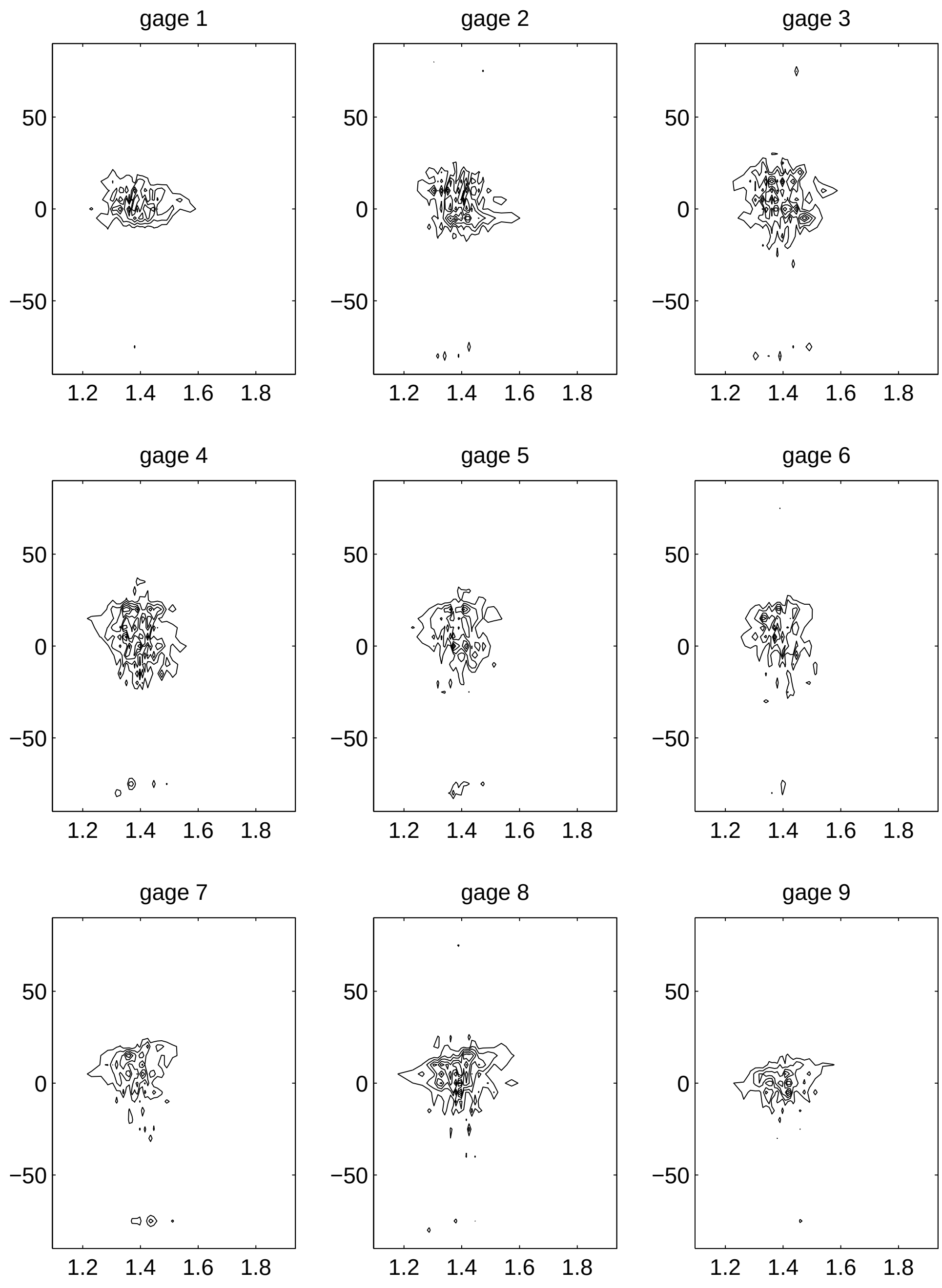

Figure E.48: Directional spectra for Test 6 (position 6).

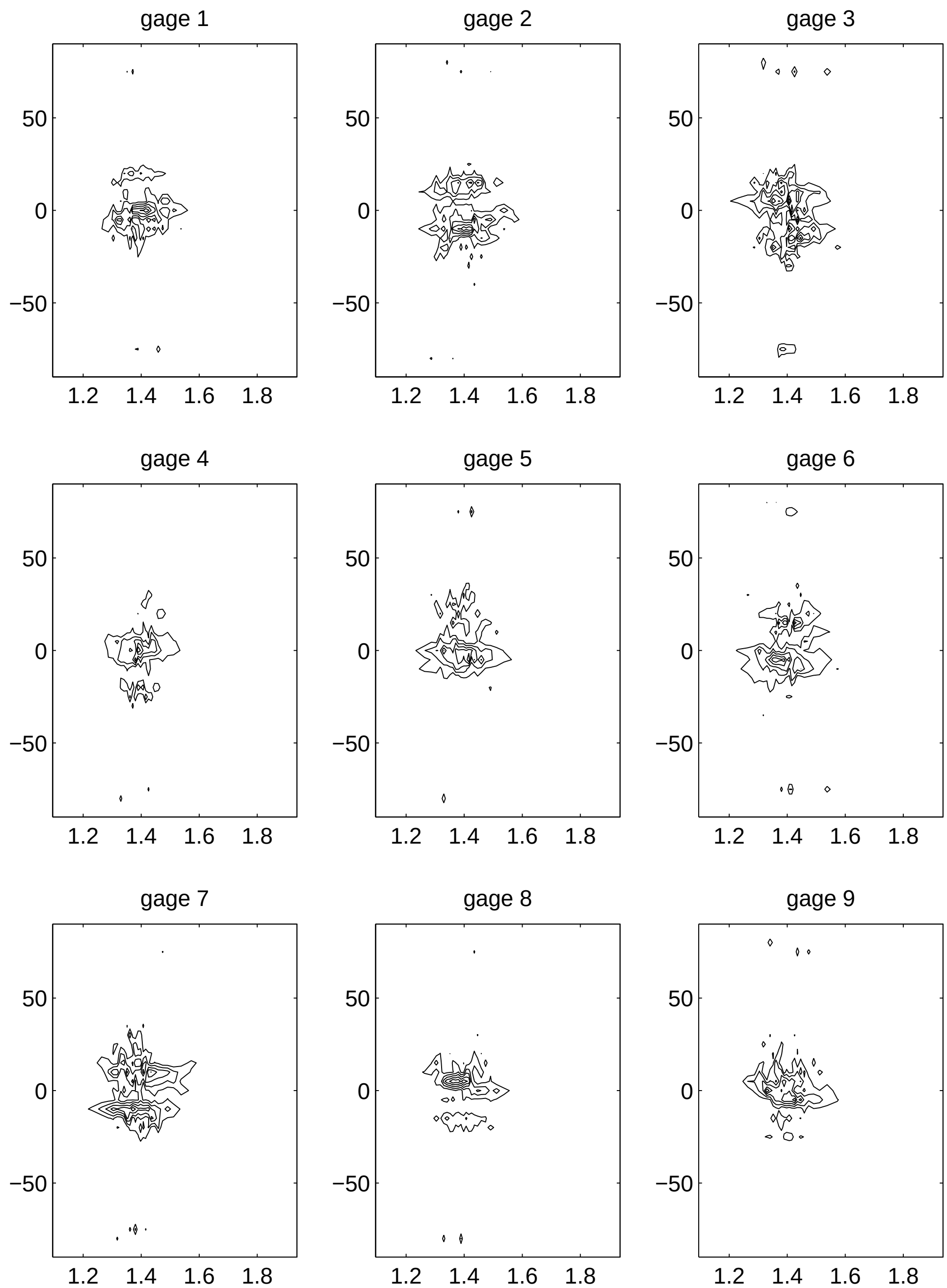

Figure E.49: Directional spectra for Test 6 (position 7).

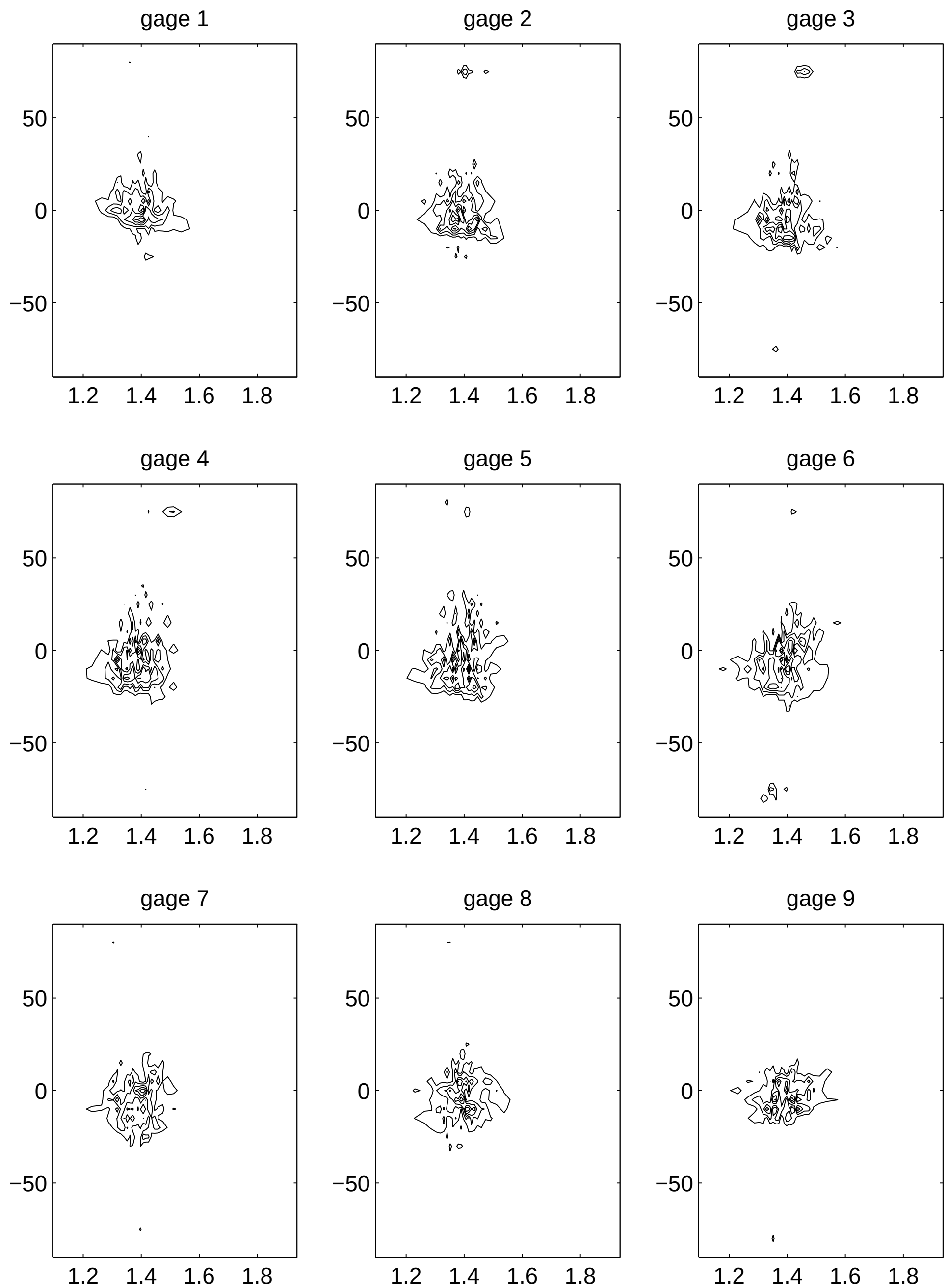

Figure E.50: Directional spectra for Test 6 (position 8).

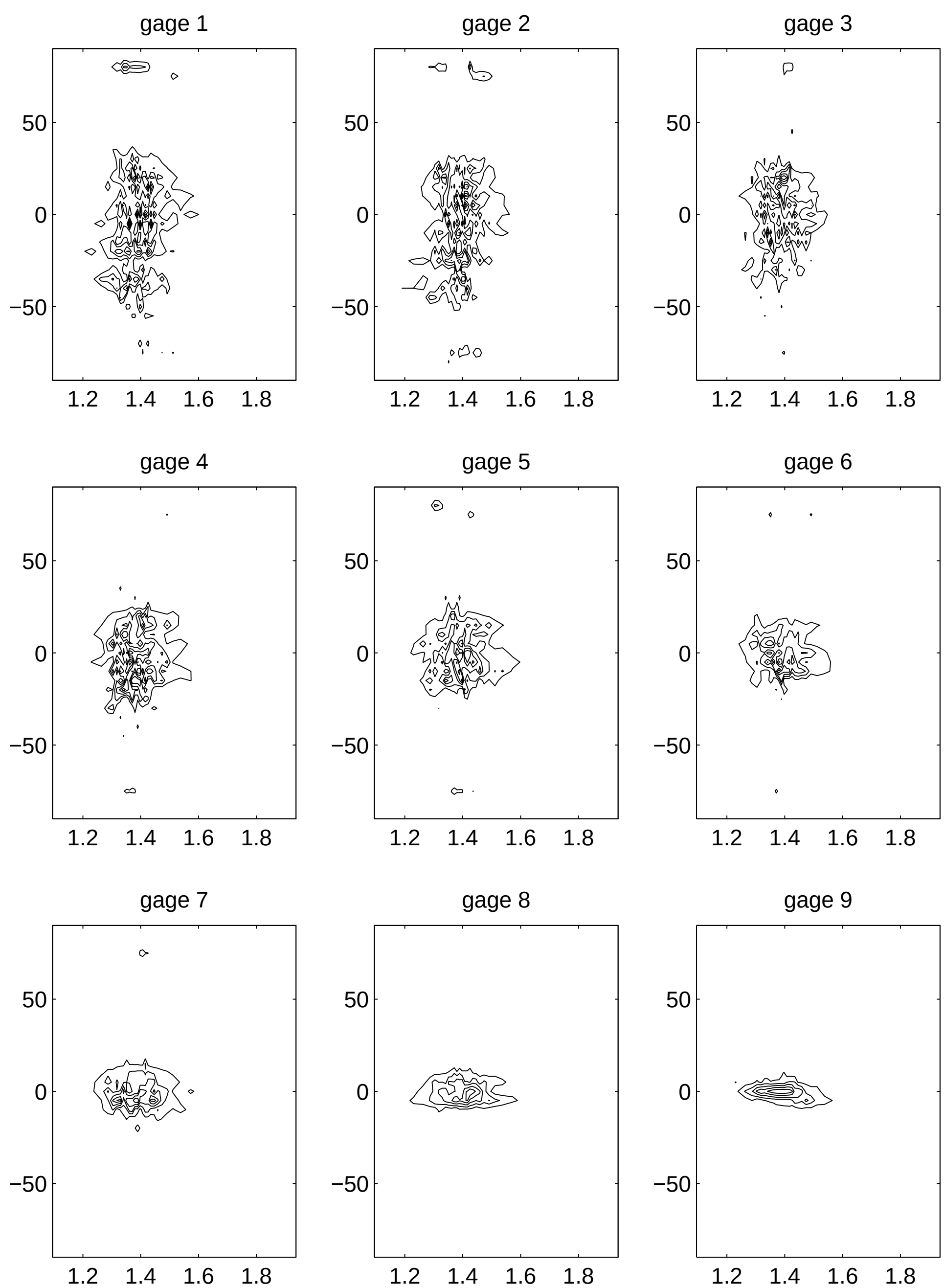

Figure E.51: Directional spectra for Test 6 (position 9).

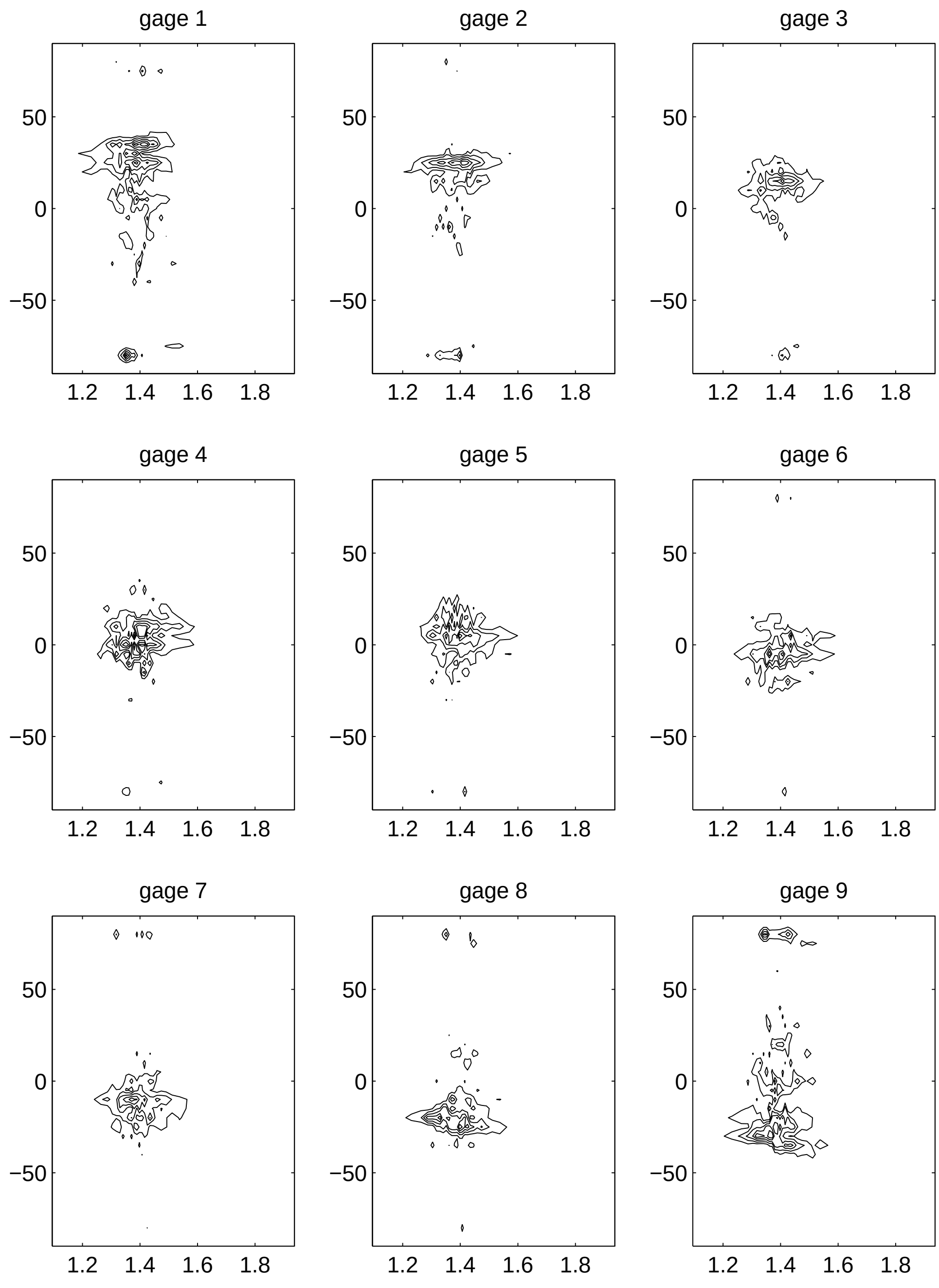

Figure E.52: Directional spectra for Test 6 (position 10).

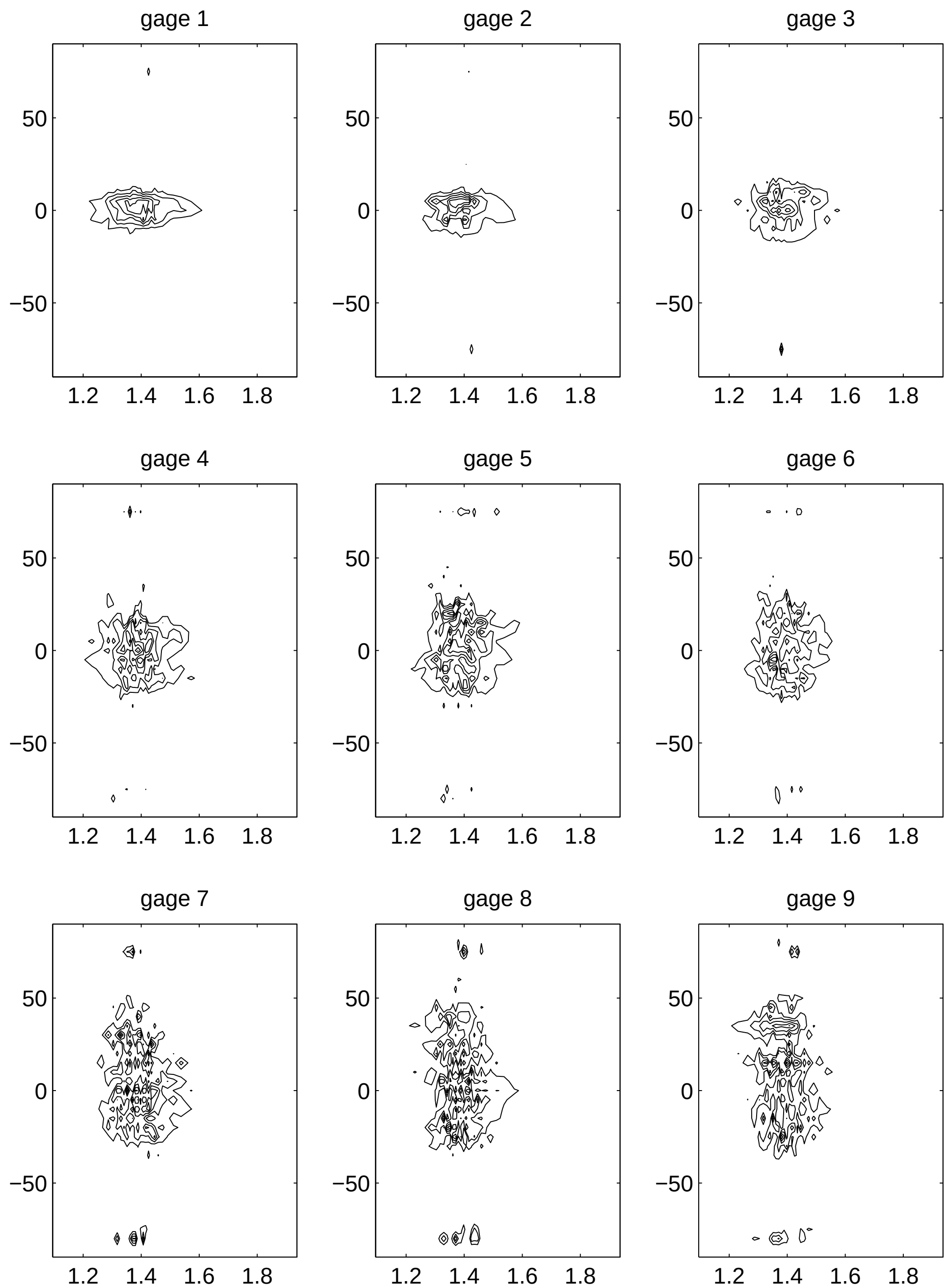

Figure E.53: Directional spectra for Test 6 (position 11).

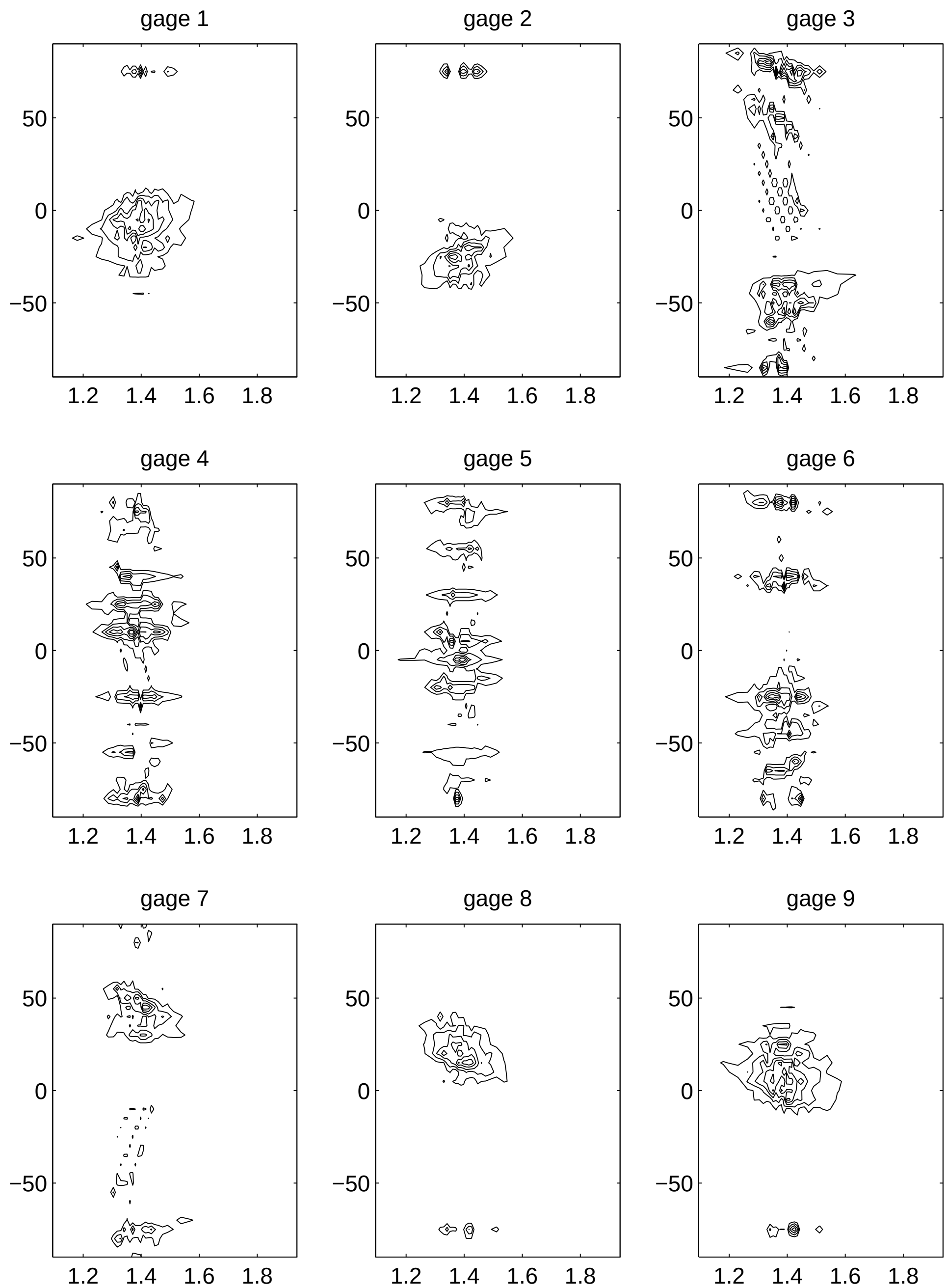

Figure E.54: Directional spectra for Test 6 (position 12).

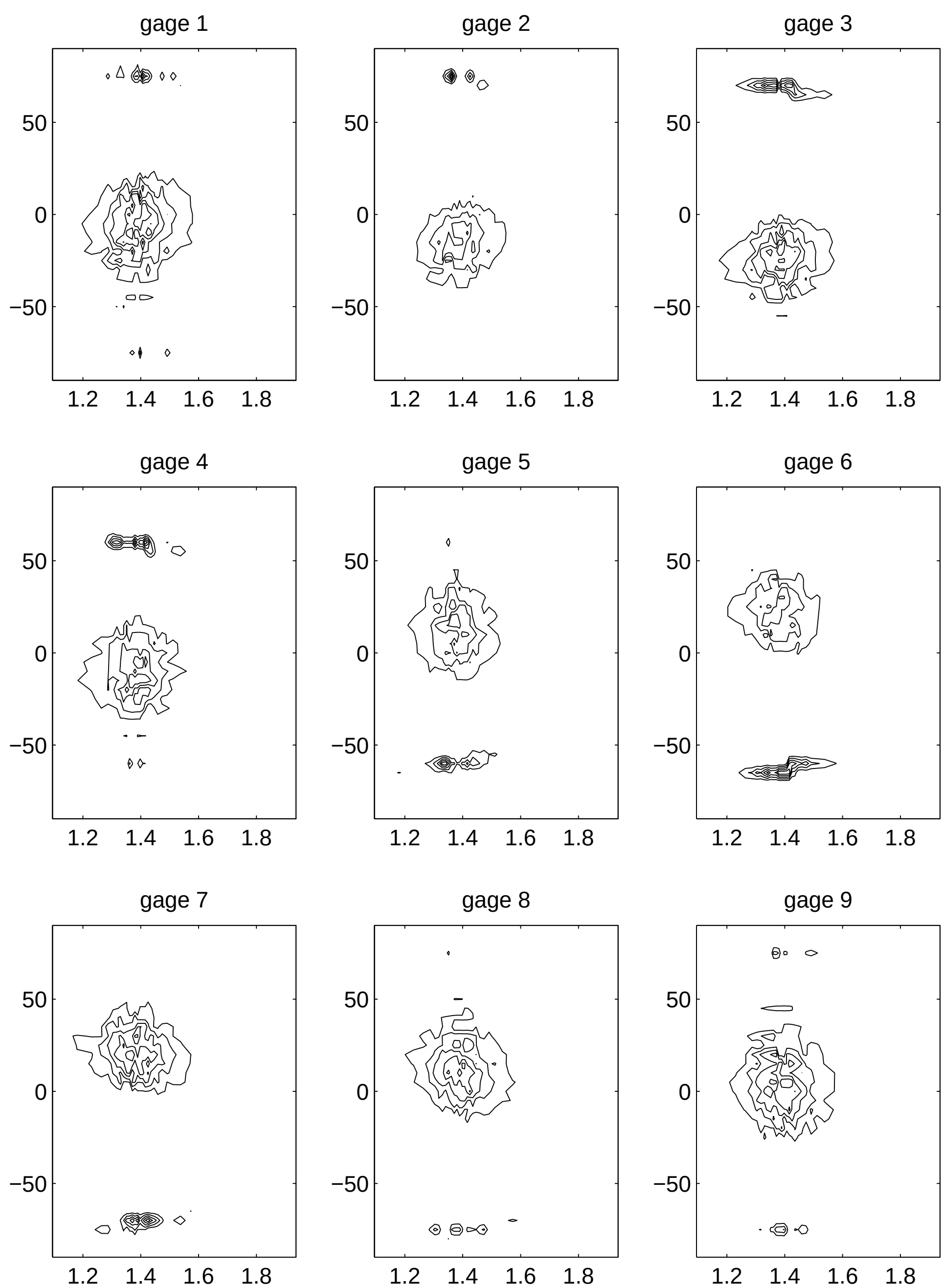

Figure E.55: Directional spectra for Test 6 (position 13).

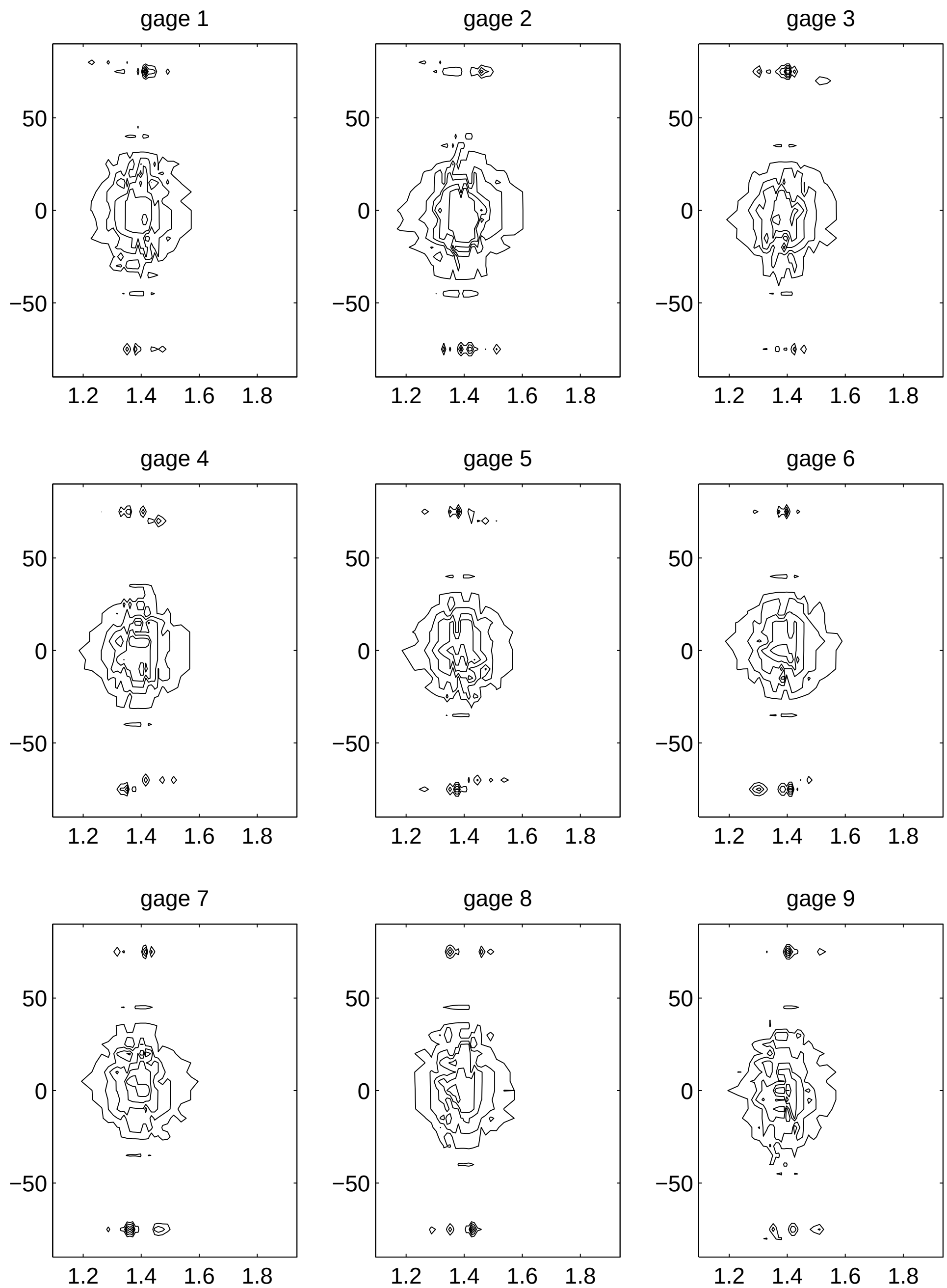

Figure E.56: Directional spectra for Test 6 (position 14).